DIATOMIC COLLISION MODELS
USED IN THE MONTE-CARLO DIRECT SIMULATION METHOD
APPLIED TO RAREFIED HYPERSONIC FLOWS

M N MACROSSAN

September 1983

A thesis submitted for the degree of Doctor of Philosophy
of the University of London
and the Diploma of Imperial College

Department of Aeronautics
Imperial College
Prince Consort Road
London SW7 2BY

ABSTRACT

Bird's Monte-Carlo direct simulation method is reviewed. Practical applications show that it is a powerful and accurate method for calculating the rarefied hypersonic flow of a diatomic gas about different body shapes. The methods by which it has been extended to the near continuum regime are discussed.

Diatomic collision models, in which the exchange of rotational-translational energy is combined with spherically symmetric scattering, are reviewed and developed. New scattering models are described; the 'linear inverse power' (LIP) model; the 'isotropic scattering' (ISO) model; and the 'variable diameter hard sphere' (VHS) model which has been proposed before under different names. The Morse potential, combining both repulsive and attractive forces, is considered and some difficulties encountered in its 'computer implementation' are overcome. Phenomenological energy exchange models are reviewed. The 'variable-ϕ' statistical exchange scheme, for which the rotational relaxation rate varies with temperature, is examined in detail. A new 'five-space' collision model is presented. Modifications to the phenomenological schemes are suggested in which the energy exchange is correlated to the scattering.

The structure of a one dimensional plane shock is calculated for a monatomic and diatomic gas. The flow of nitrogen about a blunt cylinder (Mach 20) and sharp and blunted cones (Mach 5 and 10) is calculated and details of the flowfields, the heat transfers and drag are given. Calculated density and rotational temperature profiles in the stagnation region ahead of the cylinder, the calculated drag and heat transfer are compared with independent experimental measurements.

These results show that the variable-ϕ scheme coupled with the Morse potential is the most versatile collision model but that the simpler models may be adequate in particular cases.

CONTENTS

page

LIST OF TABLES 7

LIST OF FIGURES 7

NOTATION 11

ACKNOWLEDGEMENTS 16

CHAPTER 1 INTRODUCTION 17

CHAPTER 2 THEORETICAL BACKGROUND AND REVIEW OF SIMULATION METHOD

2.0 Introduction 20

2.1 Kinetic Theory 20

2.1.1 The Boltzmann equation 20

2.1.2 Molecular collisions 21

2.1.3 Collision rates 24

2.1.4 The collision term in the Boltzmann equation 25

2.1.5 Equilibrium and approach to equilibrium 25

2.1.6 Moments of the Boltzmann equation 28

2.2 Approximate Solutions of the Boltzmann Equation 28

2.2.1 Chapman and Enskog's solution 28

2.2.2 B-G-K approximation 30

2.2.3 Numerical methods 30

2.3 The Monte-Carlo Direct Simulation Method 33

2.3.1 Description of method 33

2.3.2 Division of physical space 35

2.3.3 Weighting factors 36

2.3.4 Boundary conditions 36

2.3.5 Steady state solutions 37

2.4 Review of Monte-Carlo Direct Simulation Method 38

2.4.1 Probabilistic and deterministic simulation 38

2.4.2 The time-counter and collision rates 39

2.5 Other Monte-Carlo Direct Simulation Methods 42

2.6 The Random Walk Method 46

2.7 The Direct Simulation Method in the Near-Continuum Regime 48

CHAPTER 3 REVIEW OF COLLISION MODELS

3.0 Introduction 54

3.1 Intermolecular Potentials 56

3.1.1 The transport coefficients 56

3.1.2 The inverse power potential 57

3.1.3 Potentials which include a 'long range' attraction 61

3.1.4 Choosing a potential for the direct simulation method 65

3.2 Collision Models for Diatomic Molecules 67

3.2.1 Kinetic theory 67

3.2.2 Impulsive rotational-translational energy exchange 68

3.2.3 Quantum mechanical collision models 72

3.2.4 Phenomenological collision models 73

CHAPTER 4 COLLISION MODELS - I

4.0 Introduction 80

4.1 Two-body collision 80

4.2 The Collision integrals and Cut-off Cross-Sections 83

4.3 Inverse power molecules 85

4.4 Mean Free Paths 86

4.5 Cut-off Collision Cross-Sections 88

4.6 New Approximate Collision Models 93

CHAPTER 5 COLLISION MODELS - II

5.0 Introduction 101

5.1 Scattering Cross-Section for the Morse Potential 102

5.2 Statistical Exchange Schemes 105

5.3 Restricted Exchange 106

5.4 Empirical Derivation of Variable-ϕ Equation 110

5.5 Rotational Relaxation Tests for a Variable-ϕ Collision Model 113

5.6 Theoretical Derivation of Variable-ϕ Equation 119

5.7 Morse Potential with Variable-ϕ Energy Exchange 120

CHAPTER 6 A NEW COLLISION MODEL FOR POLYATOMIC MOLECULES

6.0 Introduction 122

6.1 Equilibrium 123

6.2 Geometry of 5 Dimensional Euclidean Space 125

6.3 Collision Model in 5 Space 127

6.4 Restricted Exchange 130

6.5 Detail Balance 135

CHAPTER 7 THE PLANE SHOCK

7.0 Introduction 139

7.1 Definitions 139

7.2 Method of Simulation 141

7.3 Computational Accuracy 142

7.4 Mean Free Path Across Shock 144

7.5 Comparison with Experiment 146

7.6 Diatomic Gas 152

CHAPTER 8 APPLICATIONS IN RAREFIED HYPERSONIC FLOWS

8.0 Introduction 157

8.1 Blunt Cylinder 157

8.1.1 Flowfield 157

8.1.2 Comparison with experiment 161

8.1.3 Heat transfer to blunt cylinder 167

8.2 Sharp Cones 171

8.2.1 Flowfield 171

8.2.2 Comparison with experiments 176

8.3 Blunt Cones 181

8.3.1 Flowfield 181

8.3.2 Comparison with experiments 181

8.4 Conclusion 188

CHAPTER 9 SUMMARY AND CONCLUSIONS 190

APPENDIX A COLLISION INTEGRALS 194

APPENDIX B THE COLLISION TIME COUNTER 198

APPENDIX C FIVE SPACE COLLISION MODEL 204

APPENDIX D EXECUTION TIMES OF EXCHANGE MODELS 209

APPENDIX E SHOCK THICKNESS 212

APPENDIX F CALCULATED HEAT TRANSFER AND DRAG 218

REFERENCES 227

LIST OF TABLES

page

4.1 Cut-off Deflection Angle 90

4.2 Error e% from equation (4.15) with $z_o = 3A^{(4)}$ 91

5.1 Relaxation data 111

7.1 Shock Thickness 147

A.1 Collision integrals for inverse power potential 195

A.2 Collision integral $Q^{(2)*}$ 196

A.3 Viscosity integral for Morse potential 197

D.1 Execution speeds for exchange schemes 210

E.7 (Reduction of experimental data) 217

Appendices E and F contain tables of shock thicknesses, heat transfer to a blunt cylinder and drag on sharp and blunted cones calculated using the Monte-Carlo direct simulation method.

LIST OF FIGURES

page

2.1 Collision represented in velocity space 22

2.2 Collision with fixed scattering centre 23

2.3 Probability of near-equilibrium distributions 26

2.4 Example results for near-continuum calculations 49

2.5 Example results for near-continuum calculations 51

3.1 Viscosity of Nitrogen and Theoretical Predictions 58

3.2 Shock Profiles 58

3.3 (a) Density Profiles for Flow over a Hollow Cylinder 60

3.3 (b) Density Profiles for Flow over a Hollow Cylinder 61

3.4 Inverse Power and Lennard-Jones Potentials 62

3.5 Viscosity of Nitrogen and Theoretical Predictions 64

3.6 Rotational Collision Number for Nitrogen 70

3.7 Collision in Velocity Space 76

4.1 Two-Body Collision in Centre of Mass Reference Frame 81

4.2 Deflection Angle for Inverse Power Potential 91

4.3 Deflection Angle Curves. Inverse Power and LIP Approximation 96

4.4 Deflections for Three Collision Models 98

5.1 Morse Potential Deflection Angle 102

5.2 Deflections for Morse and Inverse Power Potentials 104

5.3 Constant ϕ Relaxation Test 108

5.4 Relaxation Rate for Constant ϕ 109

5.5 Rotational Relaxation Time for Nitrogen 111

5.6 Near-Equilibrium Distribution of Molecular Speed for Two Variable-ϕ Collision Models 114

5.7 Temperature Relaxation for Variable-ϕ Model 115

5.8 Two Variable-ϕ Equations 117

5.9 Variation of Z_R for Variable-ϕ Models 118

6.1 Cylindrical Coordinates for Increasing Number of Dimensions 126

6.2 Temperature History: Pseudo Hard Sphere in 5 Space 130

6.3 Stability Test (a) Molecular speed distribution 131

6.4 Stability Test (a) Internal energy distribution 131

6.5 Stability Test (b) Deflection Angle from LIP model 132

6.6 Collision in Velocity Space 133

6.7 Stability Test (c) Restricted Exchange 134

6.8 Equilibrium Distribution of Collision Energy in Simulation 136

6.9 Stability Test (d) Modified Collision Probability 138

7.1 The Plane Shock 140

7.2 Typical shock Profiles 140

7.3 Successive Shock Profiles 143

7.4 Density and Temperature Shock Profiles - VHS Model 145

7.5 Density Profile for VHS Model compared with Experiment 146

7.6 Shock Profiles for Two Collision Models 148

7.7 Shock Thickness for Argon 150

7.8 Asymmetry of Density Profiles for Argon 151

7.9 Density and Temperature Profiles for Mach 5 Shock:Nitrogen 153

7.10 Shock Thickness Δ for Nitrogen 154

7.11 Calculated Shock Thickness δ for Diatomic Gas 155

8.1 Density Contours Ahead of Blunt Cylinder 158

8.2 (a) Density Profiles Ahead of Blunt Cylinder 159

8.2 (b) Temperature Profiles ahead of Blunt Cylinder 159

8.3 Number of Collisions Along Streamlines 160

8.4 Computed Density Profiles Ahead of Blunt Cylinder
Compared with Measured Profiles 162

8.5 Density Profiles for Two Collision Models 164

8.6 (a) Streamwise Rotational Temperature Profiles
Near Stagnation Line Ahead of Blunt Cylinder 166

8.6 (b) Streamwise Translational Temperature Profiles
Near Stagnation Line Ahead of Blunt Cylinder 166

8.7 Variation of Heat Transfer Across Front Face of Cylinder 167

8.8 Correlation of Calculated Heat Transfer to
Front Face of Blunt Cylinder Using Cheng's Parameter K_r^2 169

8.9 Heat Transfer to Blunt Cylinder Compared with Experiments 170

8.10 Density Contours - Sharp Cones 172

8.11 Flowfield Temperature About Sharp Cone 173

8.12 Flowfield Temperature About Sharp Cone 174

8.13 Temperature Profiles - Sharp Cone 175

8.14 Cone Drag vs. Freestream Knudsen Number 177

8.15 Hot and Cold Wall Cone Drag 180

8.16 Density Contours - Blunt Cones 182

8.17 Flowfield Temperature About Blunt Cone 183

8.18 Flowfield Temperature About Blunt Cone 184

8.19 Pressure and Stress on Blunted Cone 185

8.20 Drag on Blunt Cones 186

8.21 Pressure, Stress on Blunted Cone for Two Collision Models 187

C.1 Collision Co-ordinate Systems 204

E.1 Asymmetry of Calculated Shock Profiles (Monatomic Gas) 214

E.2 Asymmetry of Density Profiles for Nitrogen 216

F.1 Heat Transfer to Blunt Cylinder -
Correlation with Wall Mean Free Path 222

F.2 Cone Drag vs. Wall Mean Free Path (Variable Cross-Section) 225

NOTATION

a	Range factor in the inverse power potential (equation 3.3)
$A(g)$	Collision cross-section = $\pi b_o^2(g)$
$A^{(\ell)}(\alpha)$	Dimensionless collision integral for the inverse power potential (equation 4.7)
b	Collision miss distance, i.e. the trajectory separation
b^*	= b/σ
$b_o(g)$	Maximum miss distance in collision at relative speed g
c	Thermal speed of molecule
$\langle c \rangle$	Mean thermal speed in an equilibrium gas = $(8RT/\pi)^{\frac{1}{2}}$
c_w	Mean speed of molecules emitted from a thermally accommodating surface = $(9\pi RT_w/8)^{\frac{1}{2}}$
Cd	Drag coefficient
C_h	Stanton number (equation 8.1)
d	Hard sphere molecular diameter
D	Diameter of base of model
e_{cm}	Centre of mass collision energy = $e_t + e_I$
e_I	Total internal energy of two colliding molecules
e_t	Centre of mass translational collision energy = $\frac{1}{2}m^*g^2$
$e(z_o,2)$	Error in theoretical viscosity cross-section for Q_o based on z_o (equation 4.15)
$f(v)$	Velocity distribution function
$f_o(c)$	Equilibrium distribution (equation 2.10)
$\underset{\sim}{g}, \underset{\sim}{g}'$	Relative velocity of molecules before and after collision
g, g'	= $\lvert\underset{\sim}{g}\rvert$, $\lvert\underset{\sim}{g}'\rvert$
g^*	= $g/(4RT')^{\frac{1}{2}}$

g_{max}, g_{min}	Maximum and minimum relative speeds for which the deflection angle for the Morse potential is stored
H	Enthalpy
k	Boltzmann's constant
K_{bf}	Dimensionless parameter $\propto \lambda_{bf}/D$ (equation 8.3)
K'_{bf}	(Equation F.2)
$\bar{K}$	(Equation F.1)
K_i	Constant defining Q_i
Kn_D, Kn_r	Knudsen number based on model diameter (λ/D) or radius (λ/R)
K_r^2	Cheng's rarefaction parameter (equation 8.2)
m	Molecular mass
m_1, m_2	Masses of colliding molecules
m*	Reduced mass of colliding molecules = $m_1 m_2/(m_1 + m_2)$
M	Mach number = $(2/\gamma)^{\frac{1}{2}}S$
n	Number density of molecules
n_s	Number density of simulators in simulation units
n_o	Freestream number density of simulators in simulation units
N	Number of simulators in a cell
p	Fluid pressure or number of molecules represented by each unit weight simulator particle (equation B.1)
$\dot{q}$	Heat transfer rate
Q	Schmidt's asymmetry factor for a shock profile (equation 7.2)
$Q^{(2)}(g)$	Collision integral (equation 4.2)
$Q^{(2)*}(g)$	Dimensionless collision integral (equation A.6)
Q_i, Q_o	Collision cross-section (equations 4.8, 4.17)
$\underset{\sim}{r}$	Position vector
r	Molecular separation measured centre to centre

r_{min}	Distance of closest approach
r_n, r_b	Nose and base radii of a blunted cone
R	Radius of base of blunt cylinder or gas constant k/m
Re	Reynolds number $\rho UD/\mu$
R_f	Uniformly distributed random fraction
s_j	Random fraction selected from the beta distribution
S	Speed ratio $U/(2RT)^{\frac{1}{2}}$
S_w	Wall speed ratio (equation 8.3)
$t, \hat{t}$	Time, dimensionless time (simulation units)
T	Temperature
T'	Potential well depth temperature for the Morse and Lennard-Jones (6-12) potentials = 91.5 K for nitrogen
$\bar{T}$	Dimensionless temperature in shock (equation 7.1)
T_e	Equilibrium temperature
T_R	Rotational temperature
T_t	Translational temperature
$\hat{T}$	$= T/T_\infty$
U	Fluid velocity
U(r)	Intermolecular potential
$\underset{\sim}{v}$	Velocity
$\underset{\sim}{v}_{cm}$	Collision centre of mass velocity
w	Relative weighting factor (equation B.1)
(x,r)	Cylindrical coordinates
z	Dimensionless impact parameter (equation 4.4)
z_o	Maximum value of z in collisions
Z_R	Rotational relaxation number (equation 5.8)

α	Inverse power exponent (equation 3.3)
β	Range factor for the Morse potential = 14.798 for nitrogen
$B(i,j)$	The beta function $\int_o^1 x^{i-1}(1-x)^{j-1}dx$
γ	Ratio of specific heats = $(\xi+5)/(\xi+3)$
$\Gamma(j)$	The gamma function $\int_o^\infty x^{j-1} \exp(-x)dx$
δ	Shock thickness (figure 7.2)
Δ	Shock thickness (figure 7.2)
δt_m	Decoupling interval
Δt_c	Collision time increment per collision (equations 2.14, B.1)
ε	Angle specifying the orientation of the collision plane
θ	Cylindrical coordinate angle
Θ	Collision rate (equation 2.6)
λ	Mean free path between molecular collisions (equation 2.7)
λ_i	Mean free path in an equilibrium gas based on Q_i (equation 4.10)
$\lambda_\infty, \lambda_1$	Nominal mean free path in the freestream based on viscosity (equations 4.11, 4.12, B.3)
λ_{bf}	Body to freestream mean free path
λ_{12}	Mean free path across a shock (equation 7.3)
λ_m	Mean free path λ_{12} based on the momentum cross-section
λ_μ	Mean free path λ_{12} based on the viscosity cross-section
μ	Viscosity
$\underset{\sim}{v}$	Velocity
ξ	Number of degrees of freedom for storing internal energy = 2 for a diatomic molecule
ρ	Fluid density
$\bar{\rho}$	Dimensionless density in a shock (equation 7.1)
σ	Zero point of the Morse and Lennard-Jones (6-12) potentials = 3.681 Å for nitrogen

τ	Exponential decay time; specifically the rotational relaxation time
τ_{eff}	$= 3/5\ \tau$
$\underset{\sim}{v}$	Velocity
ϕ	Fraction of energy redistributed in collisions or fraction of inelastic collisions or χ_{max}/π
χ	Angle of deflection in a two body collision (figure 4.1)
χ_{max}	Maximum 'deflection' for 5-space restricted exchange scheme
$\Omega^{(2,2)}$	Collision integral (equation 4.3)
$\Omega^{(2,2)*}$	Dimensionless collision integral for the Morse and Lennard-Jones (6-12) potentials (equation A.7)

Subscripts

1,2	Conditions on up and downstream sides respectively of a shock or refers to the two molecules in a collision
fm	Free molecular (collisionless) conditions
o	Stagnation conditions
∞	Freestream conditions or the long time conditions in a relaxation calculation
w	Wall or body conditions

ACKNOWLEDGEMENTS

I thank Dr J K Harvey for supervising this research and for his invaluable help and encouragement. His many suggestions have been of great assistance in the preparation of this thesis.

I thank also Mia Retrot for helping with the proof reading.

This work was supported by the Ministry of Defence under research agreement number AT-2037-084 and by the Science and Engineering Research Council under agreement number GR/B/67025.

CHAPTER 1

INTRODUCTION

At high altitudes the density of the atmosphere is so much less than at the earth's surface that the gas can no longer be regarded as a continuum. Re-entry flight through the upper atmosphere has focused attention on the importance of rarefied hypersonic flows but because of the low density the methods of conventional aerodynamics are inadequate. The molecules of the freestream flow impinging on the vehicle interact with molecules reflected from the body surface. The average momentum and thermal energy of each group of molecules are vastly different. If the speed is high and the density low it is unlikely that there will be sufficient collisions between particles as they pass the vehicle to ensure that the gas is close to equilibrium. Thus the Navier-Stokes equations of continuum mechanics no longer apply and the flow must be studied at the molecular level. The fundamental equation describing the flow is the integro-differential Boltzmann equation which has remained intractable to analytical and conventional numerical solution for complicated flowfields of engineering interest.

The Monte-Carlo direct simulation method introduced by G. A. Bird (1963 1965) has often been used to obtain statistical 'solutions' to these problems. The behaviour of the gas is simulated at the molecular level, using a computer to follow the motion and collisions of particles. Energy and momemtum are redistributed by molecular collisions and are carried through the flow as the molecules move. A mathematical description of the collisions between molecules is

required. A number of collision models are available from the kinetic theory of gases and most calculations for monatomic gases have used simple representations of the force between molecules. For diatomic molecules the problem is more difficult, since the exchange of energy between translation and rotation of the molecules must be considered. Nevertheless a number of approximate methods suitable for the simulation method have been developed.

It has not been universally acknowledged that Bird's direct simulation method provides a rigorous statistical solution of the Boltzmann equation and this question is discussed in chapter 2. The 'construction' of the method is such that it is difficult to demonstrate its validity. By the same token it is difficult to show that it is clearly wrong and no fatal objection has been raised. Since the method is computationally efficient, compared to the proposed alternatives, it is useful to test its performance in practical applications. Bird (1976) gives a general summary of the method and a collection of results, primarily for monatomic gases, which show that the method works well. Experimental measurements of the heat transfer, the pressure and the shear on bodies immersed in a flow, may be compared with the results of calculations. However, in the calculations these 'integrated quantities' are generally not sensitive to fine details of the flow and the scatter of the experimental results limits their usefulness for detailed verification of the method. A great deal of experimental work at Imperial College has been concerned with testing both the accuracy of the simulation method for diatomic gases and the accuracy of the diatomic collision models (Jeffery 1975; Davis 1978; Dominy, Macrossan and Harvey 1981). The

predictions using the simulation method are compared with detailed surveys of representative flowfields in the Imperial College hypersonic nitrogen wind tunnel for which the freestream conditions are determined accurately (Jeffery 1975).

We examine, with two different objectives, the various collision models which have been proposed. Firstly, we show how collision models may be simplified and still remain useful in many applications. Secondly we show how the present more accurate collision models can be improved with little or no increase in computing cost. The development of these models has been somewhat haphazard and full advantage has not been taken of the presently available methods. We also present a new collision model for polyatomic gases.

In the final part of this thesis a number of the collision models are tested in different applications. The one dimensional plane shock for a monatomic and diatomic gas is studied using a number of the new collision models. The rarefied hypersonic flows of a diatomic gas about a blunt cylinder, a sharp cone and a blunted cone are used to test other collision models. Density and rotational temperature profiles, calculated for freestream conditions matching as closely as possible the experimental conditions obtained by R. G. Dominy in the Imperial College nitrogen wind tunnel, are compared with the measured values. The calculated heat transfer to the blunt cylinder and the drag on the sharp and blunted cones are compared with published experimentally determined values. We are thus able to determine the limitations and advantages of various collision models.

CHAPTER 2

THEORETICAL BACKGROUND AND REVIEW OF SIMULATION METHOD

2.0 Introduction

In this chapter some results from kinetic theory are presented which are relevant to the Monte-Carlo direct simulation method. The theory is presented for idealised atoms having only translational energy but no 'internal' structure and no internal energy. The extension to molecules having energy stored by the rotation of the internal structure is indicated when diatomic collision models are considered in detail.

The basic flow equation of kinetic theory is the Boltzmann equation. A number of methods for finding solutions or approximate solutions to this equation are considered before considering the direct simulation method. A number of criticisms of the method and some recent attempts to extend the method to continuum fluid mechanics are considered.

2.1 Kinetic Theory

2.1.1 The Boltzmann equation

In kinetic theory the gas is described by the velocity distribution function $f(\underset{\sim}{v},\underset{\sim}{r})$, where $f(\underset{\sim}{v},\underset{\sim}{r})\, d\underset{\sim}{v}$ is the fraction of molecules which have velocity vectors in the range $\underset{\sim}{v}$ to $\underset{\sim}{v} + d\underset{\sim}{v}$ (called 'molecules of class $\underset{\sim}{v}$'). The distribution function is normalised so that

$$\iiint f \, dv_1 \, dv_2 \, dv_3 = 1 \qquad (2.1).$$

The average of any quantity Q that depends on the velocity of a molecule is often needed. This average will be denoted $\langle Q \rangle$ and is given by

$$\langle Q \rangle = \int Q\, f(\underset{\sim}{v})\, d\underset{\sim}{v} \qquad (2.2)$$

The average number of molecules of class $\underset{\sim}{v}$ in a volume $d\underset{\sim}{r}$ surrounding the end point of the vector $\underset{\sim}{r}$ is $nf(\underset{\sim}{v},\underset{\sim}{r},t)\, d\underset{\sim}{v}\, d\underset{\sim}{r}$ where n is the local number density of the molecules in the volume $d\underset{\sim}{r}$. The Boltzmann equation

$$\partial nf/\partial t + v_i\, \partial nf/\partial r_i + F_i\, \partial nf/\partial v_i = \{\partial nf/\partial t\}_{coll} \qquad (2.3)$$

(where a repeated subscript is summed from 1 to 3) describes the change in the distribution function. The term $v_i\, \partial nf/\partial r_i$ accounts for the convection of molecules out of the volume $d\underset{\sim}{r}$. The term $F_i\, \partial nf/\partial v_i$ accounts for the change of the distribution of velocities in $d\underset{\sim}{r}$ by the acceleration of an external force $\underset{\sim}{F}$. The term $\{\partial nf/\partial t\}_{coll}$ accounts for the change in velocities in $d\underset{\sim}{r}$ by the action of collisions.

2.1.2 Molecular collisions

The range of the intermolecular force, which is approximately the size of the molecule, is many times smaller than the average spacing of molecules in gases at normal temperatures and pressures. The chance of three molecules simultaneously colliding is consequently negligible and the collision term is evaluated for collisions between two molecules only. The average distance travelled by a molecule between collisions, the mean free path λ, is many times the molecular size so that, in the absence of external forces, the typical trajectory of a molecule is a series of straight lines with changes of directions occurring abruptly over a distance approximately equal to the molecular size. If we denote the average spacing of the molecules as δ and the diameter of the molecules as d, then for air at standard temperature and pressure (Vincenti and Kruger 1965; p 25)

$$\lambda : \delta : d = 170 : 10 : 1.$$

The ratio of mean spacing to molecule size of 10:1 is virtually the limit of the expected validity of the 'dilute gas' assumptions for which the Boltzmann equation is valid.

Consider the collision between two molecules with velocities $\underset{\sim}{\nu}$ and $\underset{\sim}{\upsilon}$ relative to a laboratory frame of reference which is

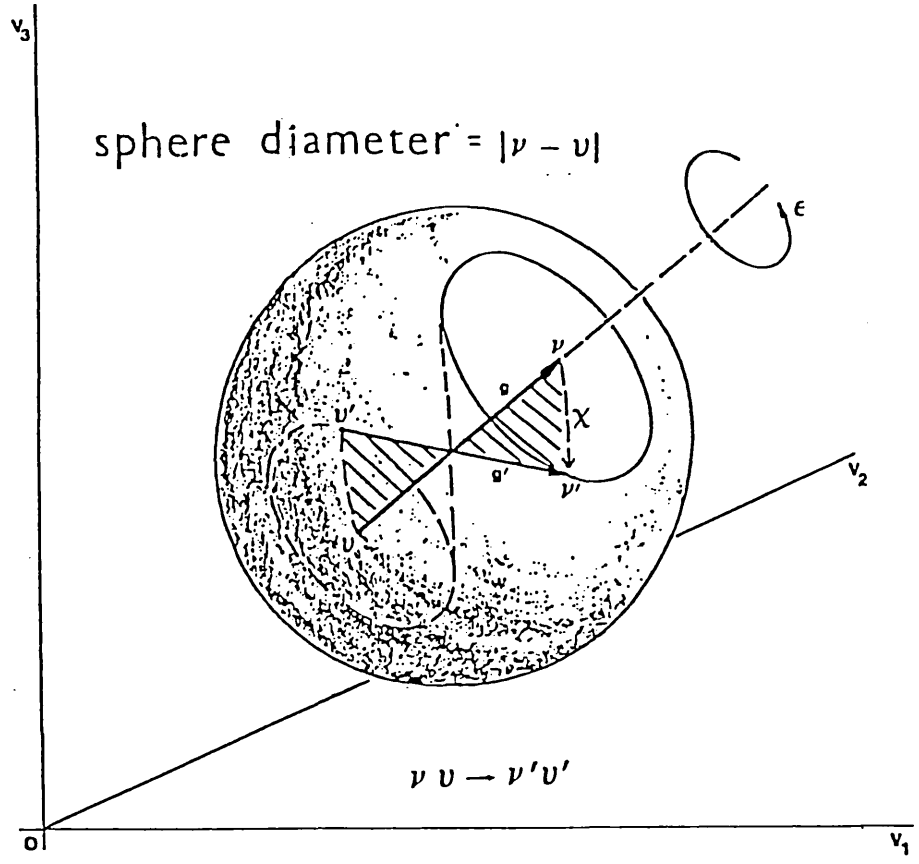


Fig. 2.1 COLLISION REPRESENTED IN VELOCITY SPACE

represented in velocity 'space' in figure 2.1. The energy of these two particles is

$$\tfrac{1}{2}\, m\, \underset{\sim}{v}_{cm} \cdot \underset{\sim}{v}_{cm} + \tfrac{1}{4}\, m\, \underset{\sim}{g} \cdot \underset{\sim}{g}$$

where $\underset{\sim}{v}_{cm} = \tfrac{1}{2}(\underset{\sim}{\nu} + \underset{\sim}{\upsilon})$ is the centre of mass velocity and $\underset{\sim}{g} = \underset{\sim}{\nu} - \underset{\sim}{\upsilon}$ is the relative velocity of the collision. The term $\frac{1}{4}m\underset{\sim}{g}.\underset{\sim}{g}$ is the centre of mass collision energy. Providing the collision duration is negligible, the conservation of momentum requires that the centre of mass velocity be unchanged by the collision, even in the presence of

an external force, and that the post-collision velocities relative to $\underset{\sim}{v}_{cm}$ be oppositely directed. Energy is conserved if the relative speed g is not changed by the collision. The conservation laws are satisfied if the post-collision relative velocity $\underset{\sim}{g}'$ is the diameter of the sphere in velocity space centred on $\underset{\sim}{v}_{cm}$.

The plane, in both velocity and physical space, containing the pre- and post-collision relative velocities is called the 'collision plane'. It is determined by the initial orientations of the trajectories of the molecules and is defined by an angle ϵ relative to some reference plane. The 'deflection angle' χ between $\underset{\sim}{g}$ and $\underset{\sim}{g}'$ is a function of g and the minimum distance between the initial trajectories of the molecules. This distance, which would be the distance of closest approach if there were no intermolecular force, is called the 'miss distance' and is denoted by b. The values ϵ and b are known as the 'geometric impact parameters' defining the collision. Figure 2.2 shows the collision in the frame of reference in which the

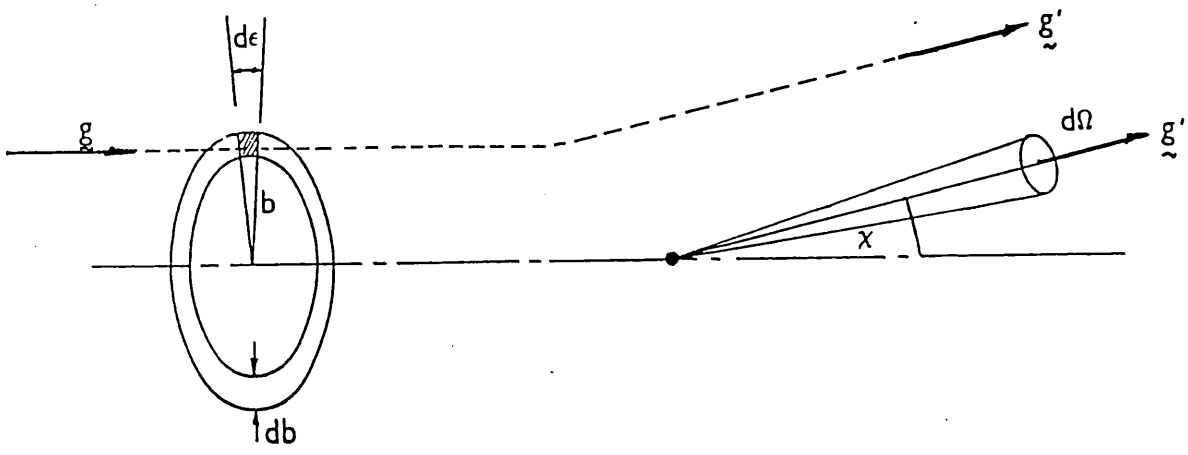


Fig. 2.2 COLLISION WITH FIXED SCATTERING CENTRE

'target' molecule is initially at rest. There is a miss distance b_o beyond which the deflection can be considered to be negligible and the molecules pass each other without interfering. We leave to later the problem of finding this miss distance for realistic representations of the intermolecular force but note that it will in general be a function of the relative velocity. For very high relative velocities molecules may pass quite close to each other without the intermolecular force 'having time' to give an appreciable deflection.

2.1.3 Collision rates

The total number of collisions between molecules of class $\underset{\sim}{v}_1$ and molecules of class $\underset{\sim}{v}_2$ per unit time per unit volume of gas is

$$N\ (\underset{\sim}{v}_1, \underset{\sim}{v}_2) = n^2\ f(\underset{\sim}{v}_1)\ f(\underset{\sim}{v}_2)\ g\ A(g)\ d\underset{\sim}{v}_1\ d\underset{\sim}{v}_2 \qquad (2.4)$$

where

$$A(g) = \int_0^{b_o}\int_0^{2\pi} b\ d\epsilon\ db = \int_A dA$$

is the total 'collision cross-section' at relative velocity $\underset{\sim}{g}$. Dividing equation (2.4) by $nf(\underset{\sim}{v}_1)\ d\underset{\sim}{v}_1$ shows that the collision rate per molecule of each class is the same when $gA(g)$ is constant. This simplification was discovered by Maxwell and $A(g) \propto 1/g$ is called a 'Maxwell collision cross-section'.

The total number of collisions per unit time per unit volume of gas is

$$N_c = \tfrac{1}{2}\ n^2\ \langle gA(g)\rangle \qquad (2.5)$$

where

$$\langle gA(g)\rangle = \iint^{gA(g)} f(\underset{\sim}{v}_1)\ f(\underset{\sim}{v}_2)\ d\underset{\sim}{v}_1\ d\underset{\sim}{v}_2$$

The product $f(\underset{\sim}{v}_1)\ f(\underset{\sim}{v}_2)$ is the joint distribution function for the two velocities in a collision and $\langle gA(g)\rangle$ is the average volume swept out by the collision cross-section moving with speed g. The number of collisions for a single molecule in unit time is

$$\Theta = n \langle gA(g) \rangle \tag{2.6}$$

The inverse of this collision rate is the mean time between collisions or the 'mean collision interval'. The mean free path

$$\lambda = \langle c \rangle / (n \langle gA(g) \rangle) \tag{2.7}$$

is defined in a frame of reference in which the mean velocity of the gas is zero. The velocities in this frame are denoted c and $\langle c \rangle$ is the mean 'thermal speed' of the molecule.

2.1.4 The collision term in the Boltzmann equation

The collision term in the Boltzmann equation consists of the difference between a 'sink' term representing the rate of scattering out of the velocity element $d\underset{\sim}{v}$ and a 'source' term representing all collisions which give a final velocity of $\underset{\sim}{v}_1$ for one of the collision partners. The source collisions are accounted for by counting the 'inverse' collisions ($\underset{\sim}{v}_1' \; \underset{\sim}{v}_2' \rightarrow \underset{\sim}{v}_1 \; \underset{\sim}{v}_2$), the existence of which for atomic collisions is assured by the three symmetry properties of the laws of motion (Huang 1963; p. 63). All replenishing collisions are the inverse of some depleting collision. For spherically symmetric molecules the impact parameters b and ϵ are the same as for the 'forward' collision. It may be shown that $d\underset{\sim}{v}_1 \, d\underset{\sim}{v}_2 = d\underset{\sim}{v}_1' d\underset{\sim}{v}_2'$ (Chapman and Cowling 1952; Sec. 3.52) so the nett loss out of class $\underset{\sim}{v}_1$ by forward and inverse collisions is

$$n^2 \left\{ f(\underset{\sim}{v}_1') \, f(\underset{\sim}{v}_2') - f(\underset{\sim}{v}_1) \, f(\underset{\sim}{v}_2) \right\} g \, dA \, d\underset{\sim}{v}_1 \, d\underset{\sim}{v}_2$$

and the collision term in the Boltzmann equation is

$$\{\partial nf/\partial t\}_{\underset{=}{coll}} \iint n^2 \left\{ f(\underset{\sim}{v}_1') \, f(\underset{\sim}{v}_2') - f(\underset{\sim}{v}_1) \, f(\underset{\sim}{v}_2) \right\} gdA \, d\underset{\sim}{v}_2 \tag{2.8}$$

2.1.5 Equilibrium and approach to equilibrium

For a spatially homogeneous volume of a dilute gas in the absence of any external force the Boltzmann equation is

$$\partial_t^n f/\partial t = n^2 \iint \left\{ f(\underset{\sim}{v}_1') f(\underset{\sim}{v}_2') - f(\underset{\sim}{v}_1) f(\underset{\sim}{v}_2) \right\} gdA \, d\underset{\sim}{v}_2$$

where n is constant. It may be shown (e.g. Bird 1976; p. 50) by substituting for the collision term in the expression for $\partial H/\partial t$, where H is the Boltzmann H-function $\int f \ln f \, d\underset{\sim}{v}$, that $\partial H/\partial t$ is never positive. Therefore H always decreases and it may also be shown that $\partial H/\partial t$ is zero only when

$$f(\underset{\sim}{v}_1') \, f(\underset{\sim}{v}_2') = f(\underset{\sim}{v}_1) \, f(\underset{\sim}{v}_2) \qquad (2.9).$$

It follows that the number of collisions $(\underset{\sim}{v}_1 \, \underset{\sim}{v}_2 \rightarrow \underset{\sim}{v}_1' \, \underset{\sim}{v}_2')$ per unit time is equal to the number of collisions $(\underset{\sim}{v}_1' \, \underset{\sim}{v}_2' \rightarrow \underset{\sim}{v}_1 \, \underset{\sim}{v}_2)$ and the collision term in the Boltzmann equation is zero (the equilibrium condition). Equation (2.9) is 'the detail balance condition' and is necessary to establish equilibrium.

Boltzmann's H-theorem is the kinetic equivalent of the second law of thermodynamics. How the result may be reconciled with the time reversal symmetry of the equations of motion for individual collisions has been a matter of some contention since it was published and Tolman (1938) gives a long discussion of the issue. Briefly we note that an important assumption was made in the derivation of the collision term. It was assumed that the velocity distribution function for the group of molecules which collide in the small interval δt is the same as the distribution function for all the molecules. The probability that the velocities of the collision partners will be $\underset{\sim}{v}_1$ and $\underset{\sim}{v}_2$ is taken as the joint probability $\propto f(\underset{\sim}{v}_1) \, f(\underset{\sim}{v}_2) \, d\underset{\sim}{v}_1 \, d\underset{\sim}{v}_2$. This is known as the assumption of 'molecular chaos' and may be expressed by saying that the pre-collision velocities and positions are uncorrelated. The result that H never increases must be interpreted as the most probable behaviour of the gas. When the assumption of molecule chaos is not satisfied the H function may increase for a time. However, the collisions 'shuffle' the points in velocity space and achieve molecular chaos after a few mean collision intervals.

The most general solution of equation (2.9) is (Vincenti and Kruger 1965; p. 44)

$$f_o(\underset{\sim}{c}) = (m/2\pi kT)^{\frac{3}{2}} \exp(-mc^2/2kT) \qquad (2.10)$$

where k is Boltzmann's constant. The probability of the state of the gas (composed of many millions of molecules) may be illustrated as in

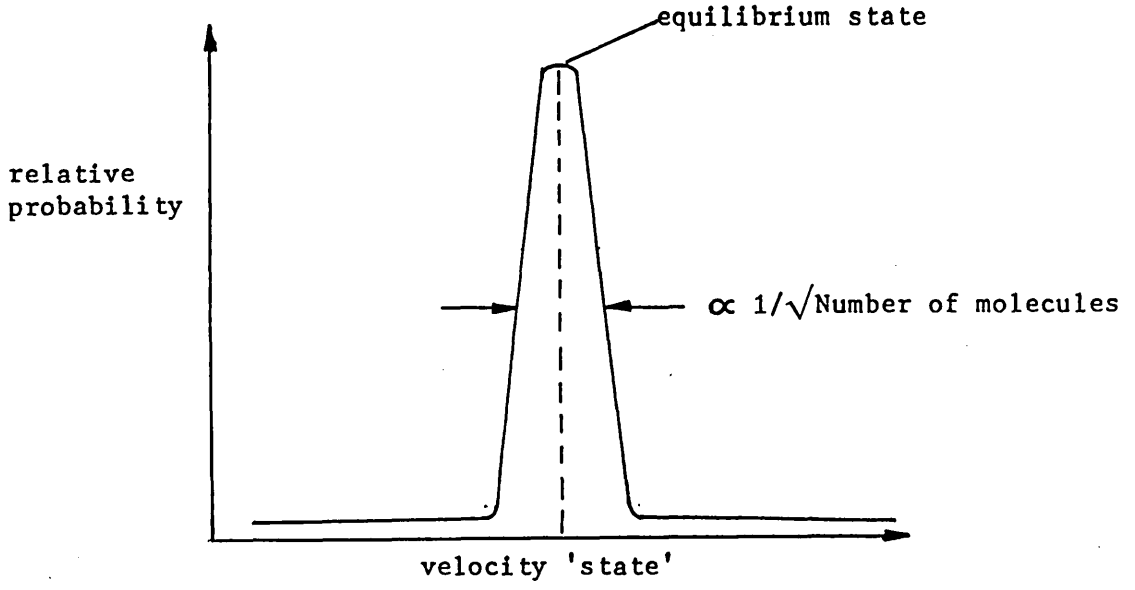


Fig. 2.3 PROBABILITY OF NEAR EQUILBRIUM DISTRIBUTIONS (HUANG 1963)

figure 2.3. There are some 'essentially equilibrium' distributions that are very little different from f_o and which have a probability almost as high. From any initial state the gas will, if undisturbed, come to a near equilibrium state and it is overwhelmingly probable that it will stay close to this state (Huang 1963; p. 83).

The kinetic temperature is defined at equilibrium as $T = T_t = \langle e_t \rangle / 3k$, where $\langle e_t \rangle$ is the mean translational energy per molecule. The amount of energy stored in each of the three degrees of freedom of translational is kT.

2.1.6 Moments of the Boltzmann equation.

The Boltzmann equation may be multiplied by any quantity Q which is a function of $\underset{\sim}{v}$ only and the resulting equation may be integrated over all velocity. After some manipulation of the convection and acceleration terms (Vincenti and Kruger 1965; p. 347), the result is

$$\partial n\langle Q\rangle/\partial t + \partial n\langle v_i Q\rangle/\partial r_i - n\langle F_i \partial Q/\partial v_i\rangle = \triangle(Q) \qquad (2.11)$$

where

$$\triangle(Q) = \int Q \{\partial nf/\partial t\}_{coll} \, d\underset{\sim}{v}.$$

Equation (2.11) is a continuity equation for Q with $\triangle(Q)$ being a source term. It may be shown that $\triangle(Q)$ is zero when Q is the mass, momentum or energy of the colliding molecules. With these substitutions for Q, equation (2.11) reduces to the the flow equations derived in continuum mechanics from the conservation of mass, momentum and energy. The average momentum and energy transported across an arbitrary surface in the gas by the molecular motion may be evaluated using the velocity distribution function. Hence the pressure tensor, the viscous stress tensor, and the heat flux vector may be calculated. For the equilibrium distribution of velocities the heat flux and viscous stress are zero and the equations reduce to those of equilibrium flow (Vincenti and Kruger 1965; p. 345).

2.2 Approximate Solutions of the Boltzmann Equation

2.2.1 Chapman and Enskog's solution

The Boltzmann equation may be expressed in dimensionless variables by dividing velocities by local reference speed u, distances by a characteristic length L required for an appreciable change in nf, time by L/u, forces by u/L, n by a local reference density n_r and f by 1/u. The collision term may be made dimensionless by dividing the collision frequency ngdA by a reference collision frequency Θ. Denoting the

dimensionless variables by a caret over the symbol (e.g $\hat{n} = n/n_r$), the Boltzmann equation becomes

$$\zeta \left[\partial \hat{n}\hat{f}/\partial \hat{t} + \hat{v}_i \partial \hat{n}\hat{f}/\partial \hat{x}_i + \hat{F}_i \partial \hat{n}\hat{f}/\partial \hat{v}_i \right] = \{ \partial \hat{n}\hat{f}/\partial \hat{t} \}_{coll}$$

where $\zeta = u/L\Theta$. Each individual reference quantity should be chosen so the dimensionless variables are at most of the order unity. The parameter ζ is a measure of the departure from equilibrium since when it is zero the collision term is zero. The reference collision frequency is approximately equal to $\langle c \rangle / \lambda$ (see equation (2.7)) so

$$\zeta = (1/\Theta) \; / \; (L/u) \approx u/\langle c \rangle \; \lambda/L.$$

Thus the departure from equilibrium is proportional to:

(a) the ratio of a characteristic time between collisions and a time for the flow to traverse the characteristic length

or (b) the ratio of the mean free path between collisions and the characteristic length, called the Knudsen number.

Notice that λ is defined in the frame of reference moving with the stream velocity ($\approx u$) which accounts for the factor $u/\langle c \rangle$.

The Chapman-Enskog method (Chapman and Cowling 1952; p. 191) expresses the distribution function for small departures from equilibrium as an expansion about the equilibrium distribution

$$\hat{f} = \hat{f}_o \; (1 + \zeta \psi_1 + \zeta^2 \psi_2 \; ..)$$

By substituting the expression for f into the Boltzmann equation, and equating terms in like powers of ζ , integral equations for successive approximations to the distribution function are obtained and the viscous-stress tensor and the heat flux vector can be evaluated. If terms in ζ^2 and higher order are ignored, the Navier-Stokes equations can be derived with expressions for the viscosity μ and the thermal conductivity K derived from the collision integral in the Boltzmann equation. This provides a link between these 'bulk' properties and the intermolecular force. The expressions for the viscosity and heat flux

can be approximated as a rapidly converging series of polynomials, and the first approximation is usually taken as sufficiently accurate (Hirschfelder, Curtiss and Bird 1954).

2.2.2 The B-G-K Approximation

Bhatnagar, Gross and Krook (1954) proposed that the collision integral in the Boltzmann equation be replaced by an approximation that retains many features of the collision integral. The most frequently used approximation is

$$\{\partial nf/\partial t\}_{coll} = (n/\tau)(f_o - f) \qquad (2.15)$$

where f_o is the equilibrium distribution expressed in terms of the local mean velocity and local temperature and $1/\tau$ is a local collision frequency that is proportional to density and may depend on temperature but not on molecular velocity. The sink term in the Boltzmann equation is replaced by $-nf/\tau$ so the collision frequency $1/\tau$ replaces the correct collision frequency. The source term in the Boltzmann equation is approximated by an expression for velocities selected from the local equilibrium distribution f_o rather than from the outcome of collisions.

If the left hand side of the B-G-K equation is considered as a time derivative alone the equation reduces to

$$dnf/dt = (n/\tau)(f_o - f)$$

which describes a relaxation of f towards f_o in a 'relaxation time' τ.

2.2.3 Numerical methods

The conventional numerical method for solving the full Boltzmann equation for $f(\underset{\sim}{v})$ would be the finite difference technique. The distribution function can be represented at each point of a network in

phase space ($\underset{\sim}{v}$ and $\underset{\sim}{r}$) and the integro-differential equation must be solved for each velocity class. The collision integral would be replaced by summations which extend over all velocity space at each point in physical space. Since each term in each sum is itself summed over all impact parameters this presents a prohibitive computing task.

By replacing the collision integral with the B-G-K approximation the computing task can be reduced. Liepmann, Narasimha and Chahine (1962) and Chahine (1963) have found solutions for the distribution function through a plane shock wave for the B-G-K model equation. They use an iterative procedure which works from an assumed shock structure obtained from the Navier-Stokes equations. They found a difference between the Navier-Stokes solution and the B-G-K solution in the low density side of the shock profile.

Another method is to replace the full integration of the collision term by a Monte-Carlo 'integration' (Nordsieck and Hicks 1967). A statistical sampling technique based on the collision probability is used to give a reduced group of summations representing the collision integral. Various least squares techniques are needed to ensure the conservation laws are not violated as a result of the round off errors arising from the statistical sampling of the collision integral. The distribution function must first be estimated and the calculations approach the final solution through an iterative process. The method has been applied to the shock structure problem over a number of years and extended from the hard spheres to Maxwell cross-sections (Yen, Walters, Ng and Flood 1974). Yen and Tcheremissine (1981) have tested a number of different forms of the Monte-Carlo integration and estimate the error in the collision term to be less than 2%.

The collision integral is also simplified in the 'test particle Monte-Carlo method' (Haviland 1963) which has been applied to the shock structure problem. In addition this method replaces the finite difference solution of the convection problem by a direct simulation. An initial distribution function is stored at discrete points in phase space and a large number of test particles are selected from this distribution. The trajectory of each test particle is calculated and the time spent in each 'cell' in phase space is used to build up a new distribution function at that cell. In each cell of physical space the particle has an appropriate probability of colliding with a 'target' particle which has a velocity selected from the target distribution stored separately in that cell. Since the relative orientation of the trajectories of the test and target particles are not known the geometric impact parameters for each collision are selected from the distribution of these parameters in collisions in the real gas. After many trajectories have been calculated the distribution function built up from these replaces the target distribution and the process is repeated until the target and final distributions coincide to a required accuracy.

The numerical methods which store the distribution function become unwieldly when applied to problems of 'engineering' interest. The phase space becomes extremely large for two dimensional flow geometries and the velocity space is unlimited. The cutoff in velocity space must be well placed to avoid 'conservation errors', which arise when high velocities are ignored, and an initial estimate of the flow is required which can be a disadvantage. All this tends to make the methods inflexible. A more 'physical' approach to the problem is the direct simulation Monte-Carlo technique which avoids some of the computing difficulties associated with a direct solution for $f(\underset{\sim}{v})$.

2.3 The Monte-Carlo Direct Simulation Method

2.3.1 Description of method

The direct simulation Monte-Carlo method introduced by G. A. Bird (1963 1965) simulates the behaviour of a gas by a combination of deterministic and probabilistic techniques. The physical space of the flowfield is divided into a number of 'cells' and the distribution of velocities in the gas is represented by the set of velocities of a many-orders-of-magnitude smaller number of particles distributed amongst these cells. We use the phrase 'simulator particle', 'simulator' or 'particle' to indicate the 'atoms' of the 'simulation gas', the positions and velocities of which are stored in the computer. The position and velocity of each particle can be considered to be the average position and velocity of a large number of molecules in the real gas. The time evolution of the positions and velocities of the 'simulators' is followed by decoupling the collision and convection effects. During convection, collisions are ignored and the particles are moved for a time δt_m which is small compared to the mean free time between collisions. The trajectories are straight and the velocities remain unchanged. If an external force were included it would curve the trajectories and alter the velocities during the convection calculation.

At the end of the convection the particles are frozen in position and 'collisions' are calculated in which only the velocities of the particles are altered. Since each particle represents a large number of real molecules distributed throughout the cell the positions of the particles can be ignored and any pair of particles within the cell may be selected to collide. The geometric impact parameters , b and ϵ ,

are randomly selected for each collision. According to the principle of molecular chaos the initial relative trajectories are uniformly distributed over each differential area b db de of the collision cross-section (see figure 2.2). Hence b and ϵ are chosen by

$$b^2 = R_f\, b_o^2 \quad \text{and} \quad \epsilon = 2\,\pi\, R_f' \tag{2.12}$$

where the R_f and R_f' are different random fractions uniformly distributed in the range (0,1). The velocity of each particle is altered by the collision and the new velocities are determined from the deflection angle and the orientation of the collision plane. The deflection angle is calculated from the assumed intermolecular force as a function of the relative velocity and the miss distance.

The 'shuffling' of the velocities in a cell by collisions tends to bring the distribution towards the local equilibrium. In order that the correct departure from equilibrium is maintained the collision rate for each class of collisions should match the Boltzmann collision rate given by (2.4). This collision rate is proportional to $f(\underset{\sim}{v}_1)d\underset{\sim}{v}_1\, f(\underset{\sim}{v}_2)d\underset{\sim}{v}_2$ and $g\, A(g)$. The first term is the probability that two molecules selected at random will have velocities $\underset{\sim}{v}_1$ and $\underset{\sim}{v}_2$ and it is generated by selecting possible collision partners at random from the cell. The second term is the volume swept out by the collision cross-section moving with speed g. This probability is achieved in the simulation method using von Neumann's acceptance-rejection technique. Let $(gA)_{max}$ be the maximum value of the function gA(g) calculated for each possible collision pairing in the cell. A pair of particles k and l are chosen at random as possible collision partners. A collision is calculated if

$$g_{kl}\; A(g_{kl})\; /(gA)_{max} > R_f \tag{2.13}$$

where g_{kl} is the relative speed of the collision pair. If the pair is rejected another pair is selected at random and the procedure is

repeated until a pair is selected.

The total number of collisions in a cell of volume V in the interval δt_m is found from equation (2.5) and is

$$N_{COLL} = \tfrac{1}{2} n^2 \langle gA(g) \rangle V \delta t_m$$

where n is the local number density. Each particle represents many molecules, however and each calculated collision represents many collisions. The number of 'simulated' collisions may be expressed by a similar expression in 'simulation' units independently of the number of real molecules represented by each particle (Pullin 1974). One way to achieve the correct collision rate would be to determine the number of collisions in each time step by calculating the average $\langle gA(g) \rangle$ over all the pairings in the cell. If $N = nV$ is the number of particles in the cell the average $\langle gA(g) \rangle$ must be calculated over $N(N-1)/2$ collision pairings. Bird (1963) avoided this lengthy calculation by adding a time increment

$$\Delta t_c = 2/[\, N\, n\, g_{kl}\, A(g_{kl})\,] \qquad (2.14)$$

to a cell time-counter for each collision. He then calculated collisions at each time step until the time-counter exceeded the total elapsed convection time. If the collision pairs are selected so that the probability of collision is proportional to $g_{kl} A(g_{kl})$ then it may be shown that over a large number of collisions the collision rate is correct (Bird 1970b).

2.3.2 Division of physical space

When a flow is one or two dimensional in physical space, i.e. the gradients of flow properties are zero in two or one directions respectively, the cells may be considered to be of arbitrary or unit width in these directions. The three velocity components of each particle are always stored and used in the collision calculations but

only the position of the molecule in the direction of flow gradients is required. Axisymmetric flows are a special case of two dimensional flows. It is only necessary to store the cylindrical coordinates (x,r), where x is parallel to the axis and r is the distance from the axis. All particles with the same (x,r) coordinates are considered to be in the same cell since each particle represents a large number of molecules uniformly distributed around the axis at that x-location.

2.3.3 Weighting factors

In order to keep the sample sizes in cells approximately equal each particle in a cell may represent a different number of molecules than that represented by each particle in another cell. The relative numbers of molecules represented by each particle is the relative weighting factor. In axisymmetric flows it is convenient to make the weighting factor for each cell proportional to the radial position of the cell to compensate for the increase in volume of cells with the radial position. When a particle moves to a cell with a different weighting factor it suffers an appropriate chance of either being 'removed' from the simulation or being 'duplicated' to represent more molecules.

2.3.4 Boundary conditions

The boundaries of the physical space of the simulation may be a body surface or an arbitrary surface within the flow. At a solid surface a scattering law must be defined and two often used simple laws are:

(i) 'Diffuse reflection' by which an impacting molecule is accommodated to the temperature of the surface. It is immediately emitted and the velocity components for the reflected particle are chosen from the distribution of these

velocities amongst the molecules of a gas (at equilibrium at temperature T_w) which cross a plane surface in one direction.

(ii) 'Specular reflection' for which the velocity component normal to the surface is reversed.

Maxwell originally proposed that surface reflection be modelled by specifying that a fraction of the molecules hitting a surface be considered to be diffusely reflected and the remaining fraction be specularly reflected. For most engineering standard surfaces completely diffuse reflection is appropriate.

When particles cross the other boundaries within the flow they may be lost from the simulation. If a mirror image symmetry exists in the flow a boundary may be specified as specularly reflecting and the reflected particle represents a particle entering the simulation from the 'mirror image' gas on the other side of the boundary. At most boundaries, however, the state of the gas outside the simulation region must be specified. At each time step a flux of new particles enters the simulation across these boundaries with velocity components selected from the specified distribution. For convenience an equilibrium distribution is usually specified with a particular temperature and mean velocity. The upstream boundaries are usually chosen sufficiently far from the body so that they may be considered to be at the freestream condition. The downstream boundaries will not in general be at equilibrium but for flows with high Mach numbers these boundaries have little influence upstream and providing they are sufficiently downstream may be arbitrarily set.

2.3.5 Steady state solutions

The calculations are time dependent. To obtain a quasi-steady solution the calculation has to be continued to the point where all

the initial transients have died away. This point can be identified by monitoring the total number of particles in the simulation, the total collision rate, and the heat transfer and drag on the body, all of which will tend towards statistical fluctuations about their 'steady' values. After 'steady' conditions are reached the sample sizes for any flow properties are built up by time averages. Alternatively the simulation may be repeated, using a different sequence of random numbers, to build up ensemble averages at any instant after the beginning of the simulation. For these calculations the precise details of the initial conditions are more or less irrelevant. A uniform undisturbed flow into which the body is suddenly 'injected' is often used for convenience. During the initial phase it is possible to monitor the flow conditions just inside the downstream boundaries and to adjust the specified boundary conditions although this has little effect on the overall flow.

2.4 Review of Monte-Carlo Direct Simulation Method

2.4.1 Probabilistic and deterministic simulation

Alder and Wainwright (1958) have proposed a 'molecular dynamics method' in which the evolution of a gas of hard spheres was followed. In this method the intermolecular distance between all possible collision partners is checked to determine if a contact has been made. The Monte-Carlo method has some computational advantage over this method since this lengthy task is avoided by randomly selecting collision partners from particles within a small cell. The particles must first be sorted into cells but this task is linearly proportional to the number of particles in the simulation.

If the Monte-Carlo method is considered merely as a development of a deterministic method it appears at first to be a weakness that

the positions of the particles are ignored during collisions. It is apparently this procedure, however, which makes the method so successful. Using anthropomorphic language we say that in a deterministic calculation each particle can only 'know' about the other particles in the vicinity by actually colliding with them. To 'know' as much about the distribution of nearby velocities as completely as a molecule in a gas there must be a large number of adjacent particles which are possible collision partners. The advantage of the random selection procedure is that it allows each particle to 'know' about the velocity distribution over all the particles in the cell so that the same 'information' is available with many fewer simulator particles. As in the test particle method the velocity distribution is altered by a representative subset of all the collisions considered in the Boltzmann collision term. In effect a reduced 'integration' is substituted for the full collision term. Bird (1970b) has argued that as long as the collision partners are selected with the appropriate probability and at the approriate rate so that the 'sink' term in the Boltzmann equation is correctly simulated then the source term arises automatically as the outcome of the collision calculation. Since the terms in the Boltzmann equation are statistically represented he argues that the 'quasi-steady' distribution of velocities in a cell, either time averaged or ensemble averaged, represents a statistical solution of the Boltzmann equation.

2.4.2 The time-counter and collision rates

The accuracy of the time-counter method for establishing the collision rate is the most often questioned part of the method. Macpherson (1969 1971), for example, presents a method of selecting the collision partners and setting the collision rate based on a complete survey of the initial velocity distribution. He also makes

the most likely collisions occur first. Bird (1981) does not think that a temporal ordering of the collisions is appropriate to a statistical (as opposed to a deterministic) simulation.

Another criticism is that the cell time-counters are always ahead of the total elapsed time in the simulation. It is possible that a collision in one time step will advance the time-counter so that no collisions are calculated at all during the next step. For a large number of molecules the error is very small but Macpherson (1969) gave a possible modification to keep the time-counters more in step with the elapsed convection time. Larsen (1976) gave a more natural and less time consuming modification. The last collision for each cell at each time step, which would take the cell time-counter past the flow time, is not always calculated. If the collision is rejected the cell time-counter is left lagging the elapsed convection time and slightly more collisions must be calculated at the next step. Bird (1981) does not accept this modification and says the error introduced by the Larsen's modification, which is an error in the distribution of relative velocities, is more serious. He maintains that the error in the time-counter method can be kept small for reasonable numbers of particles in the cell. In multi-dimensional flows the number of molecules in a cell can be small and consequently the general purpose program at Imperial College includes Larsen's modification. The generally good results suggest that the time-counter method with this modification is reasonable although it is always preferable to increase the number of particles.

Desphande, Subba Raju and Ramani (1979) argue that when using the acceptance-rejection technique it is necessary to know the maximum possible value of the relative speed in each cell at each time step to

ensure that the distribution of relative velocity in collisions is correct. If the maximum value is not known it must be set as a large value in which case the selection procedure is too time consuming. Alternatively if it is set at a low value, which must be increased if a larger relative velocity is found, the distribution of relative velocities in the collisions is not correct for that time step. Given that the complete range of relative velocities at each time step must be reviewed they argue that the correct collision rate should be calculated since this requires little extra effort.

In all the simulations a period of adjustment is allowed during which the updating of the maximum relative velocity of collision in each cell will take place. As disturbances build up in the flow we would expect that the maximum relative velocity would be quickly found and be rarely altered from then on. It must be accepted, however, that there always remains the possibility that a larger relative velocity will be found and the collision rates will be temporarily distorted. If this happens then the simulation method cannot be guaranteed to be a solution of the Boltzmann equation. It is not clear that the resulting disturbance in the velocity distribution function in the cell can be separated from the statistical fluctations arising from the small sample sizes.

Bird (1981) has reviewed a number of proposed methods of establishing the collision rate. He is reluctant to increase the computing time in the interests of a nebulous increase in accuracy. Bird (1983) has compared the time-counter method with some of the alternatives. By calculating the drag on a slender cone in Mach 5 flow he shows that there is virtually no difference between the methods and

that the simulation results agree with experimental values. In practice it appears that local departures from the correct Boltzmann collision rate have little effect on the average flux of particles onto the bodies in the flow. If comparisons of detailed surveys of the flow are made it may be that local differences can be found. It is difficult to judge the small effects of the different methods of setting the collision rate because of the errors associated with the finite cell sizes and the reduced description of the velocity distribution. The theoretical collision rates are derived assuming a constant density and a constant velocity distribution function within each cell. In practice there will be gradients across the cells which give rise to unquantifiable errors.

2.5 Other Monte-Carlo Direct Simulation Methods

Belotserkovskiy and Yanitsky (1978) were not satisfied with the representation of the collision term in the Boltzmann equation by Bird's method. They say it is a 'fairly crude' representation of the correct collision rate, that it is 'derived from heuristic considerations' and it 'does not have a rigorous mathematical foundation'. They, on the other hand, consider the relaxation process as a Markov chain process (a random walk) and work in terms of a probability of the change in state arising from collisions, where the state is defined by the 3N dimensional vector specifying the N velocities in the cell. The original papers are in the Russian language but it appears that the change in the velocities at the collision stage is, like most modifications to Bird's method, determined from a complete survey of all the possible collision partners in the cell. They give no indication of computing times but say that their method works well with much smaller numbers of particles than Bird's and so saves on memory. It may be that working

with a smaller number of particles will reduce the computing time sufficiently to make it a viable alternative to Bird's method.

Nanbu (1980a) also was not satisfied with the justification of the simulation method given by Bird. He offers no specific criticism of the Bird technique other than that it is not derived directly from the Boltzmann equation and hence cannot be confidently claimed to be a solution of the equation. Watanabe and Nanbu (1982) make a distinction between a solution of the Boltzmann equation and a process like Bird's method which they say is consistent with the Boltzmann equation. This is a fine philosophical point, since it could be said that the actual behaviour of the gas itself is consistent with the Boltzmann equation yet, because of the assumptions in the equation itself, not an exact solution. As we have seen the monotonic decrease in Boltzmann's H-function derived from the Boltzmann equation (a solution of the equation) is not a perfectly valid description of the behaviour of the gas. Belotserkovskiy and Yanitsky (1978) say that any method, like theirs or Bird's, which calculates collisions amongst the particles in a cell will automatically create correlations amongst the velocities so these methods must depart from a solution to the Boltzmann equation in some degree. Provided that a statistical 'solution' and a statistically 'consistent process' can be distinguished it is safer to have a method which can be shown to be a solution of the Boltzmann equation within a specified accuracy.

Nanbu (1980a 1980b 1980c) has developed a collision scheme working directly from the Boltzmann equation. His method is to express the local velocity distribution function directly in terms of the velocities of the particles in the cell. Knowing this pre-collision distribution of velocities he can make the probability of a

post-collision state depend on the complete information for the cell more reliably than through the selection of collision partners in Bird's method. In fact his method of selecting the collision partners is virtually the same, without the temporal ordering, as that used by Macpherson (1971). The distinguishing feature of Nanbu's method is that the velocities of single particles are altered by colliding with a 'dummy' collision partner. The dummy particle is chosen from the particles in the cell with the velocities they had at the beginning of the collision phase. The velocity of the dummy partner is not changed by the collision. This reduces the correlation between pre-collision velocities compared with Bird's method and so Nanbu's method will presumably always be closer to a 'solution' of the Boltzmann equation. Energy and momentum in the cell cannot be conserved directly but only on average. It requires slightly more memory since the dummy particles' pre-collision velocities must be saved at each time step as well as the progressively updated post-collision velocities. A more serious limitation is that it requires more computing time, apart from the time to survey the complete set of relative velocities, since twice as many collisions must be calculated at each time step.

During collisions the velocity distribution changes by an amount df_n to a new distribution $f_{n+1} = f_n + df_n$. Both Nanbu and Belotserkovskiy-Yanitsky start from this statement of the problem and determine the form of df_n, which they make depend on the form of the distribution before the collisions begin. Similarly the proposed alternatives to the time counter method determine the collision rate from the initial distribution of velocities in the cell. A theoretical defence of Bird's method of establishing the collision rate could be that, since the collision pairs are selected from a distribution of velocities in the cell which is being progressively updated, it tends

to depend on the average of the pre- and post-collision velocity distribution. This average might be expected to be more representative of the state of the gas than the velocity distribution at the start of the collision calculation. The initial distribution, arising from the collisionless convection phase, may not be considered more representative of the local distribution of velocities than the post-collision distribution. Although it seems unsound that the same particle may be included in two collisions while another is not selected at all it can be justified. Collision partners are selected with a probability depending on their relative velocity. After one collision the velocities of each collision partner are most likely to be brought towards the mean value. It will be unlikely that one of these is selected again but if it is then, provided the cell population is reasonably large, this is a reflection of its appropriate collision probability.

Nanbu has applied his method so far only to relatively simple relaxation problems (Nanbu and Watanabe 1981; Nanbu 1981b). He (Nanbu 1980a) obtains excellent agreement with a recently discovered solution of the Boltzmann equation for a relaxing distribution function (Krook and Wu 1977). He has also investigated the effects of correlation resulting from small sample sizes within cells (Nanbu 1981a, 1982b) and near surfaces (Nanbu 1982c). The condition that the pre- collision velocities of particles are statistically independent will depend on the sample sizes. He is able to derive analytical expressions for the correlation coefficients and his extensive tests confirm the analytical predictions. The general result is that when the velocities in a cell are 'refreshed' by convection or by independent velocities accommodated to a diffusely scattering surface the correlation is diminished. When these refreshing effects are absent, for example in a

relaxation calculation with a closed set of particles, then the correlation will increase. The necessary sample sizes tend to be larger than those found satisfactory with Bird's method. It seems that the statistical 'conservation' of energy and momentum is responsible for this. It is obviously extremely useful to have an independent method to compare with Bird's method. While computational efficiency can be expected to become less important as computing power increases it seems unlikely that Nanbu's method will replace Bird's unless a gross deficiency in Bird's method could be demonstrated. The quicker method will always be applied first to more and more complicated problems.

2.6 Random Walk Method

The criticisms and suggested modifications to the direct simulation method so far discused have all been concerned with the collision phase of the calculation. The convection part of the calculation (or the simulation of the corresponding terms in the Boltzmann equation) has usually been considered obvious. Belotserkovskiy and Yanitsky (1978) extend the statistical techniques to the convection part of the calculation. The convection is considered as a random walk process in which each particle has a certain probability that it will be in a new cell at each time step. This probability depends on the velocity of the particle, the time step and the cell size. The idea appears startling at first but could be considered a logical extension of the general method. If before the molecules were moved at each time step they were randomly redistributed throughout the cell the effect would be much the same. Since we assume that the flow gradients across the cell are small when we choose collision partners without regard to position it seems we cannot object in theory to this procedure. Less memory is required

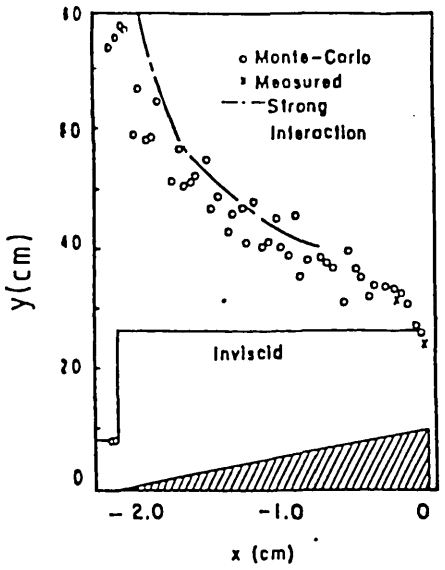
since the cell containing a particle is stored (as in the present schemes) but not the particle's position vector (as opposed to the present schemes). For one dimensional flows with a constant cell size the method is reasonably simple. Nanbu (1982d) shows that the expectation for a particle's position (cell) is identical to that in a deterministic calculation (assuming no density gradient across cells) but that the variance increases with time. For highly directed flows he shows that the variance in the random walk method will generally remain small and suggests that it may be used for supersonic or hypersonic flows but does not recommend it.

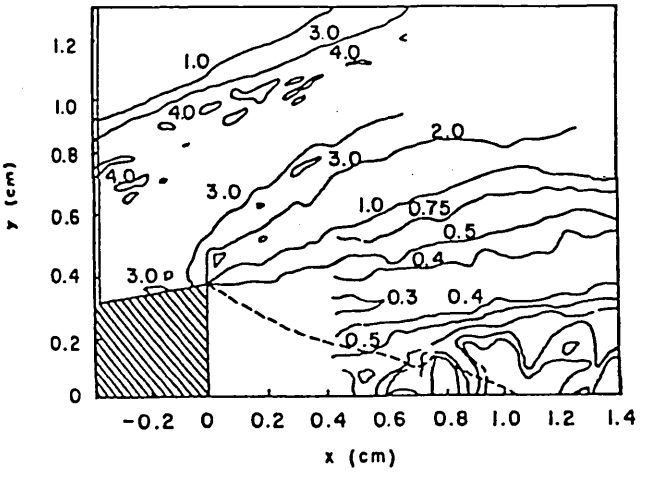
It is not immediately obvious that the method can be easily extended to multi-dimensional flows with varying cell sizes. For each cell, the probabilities that a particle will end in adjacent cells would have to be stored. These probabilities would be derived from an assumed uniform density distribution in the cell and an isotropic velocity distribution. They would have to be modified for each particle depending on its particular velocity. The new cell for the particle would then be selected from this modified probability distribution. The present method which determines the new cell containing a particle after it has moved also requires some cross-referencing information. If the decoupling interval is kept small so that particles may only move to adjacent cells then no more memory may be required than at present (considering the saving on the particle co-ordinates). It is possible that a number of intricate computing problems arising from the 'cell-searching' algorithm (Macrossan 1981) might be avoided. The random walk technique could provide a quick alternative to the present solutions to these problems which have tended to increase the computing time. It may be that the technique is more appropriate to the 'vectorising' and 'parallel processing' of

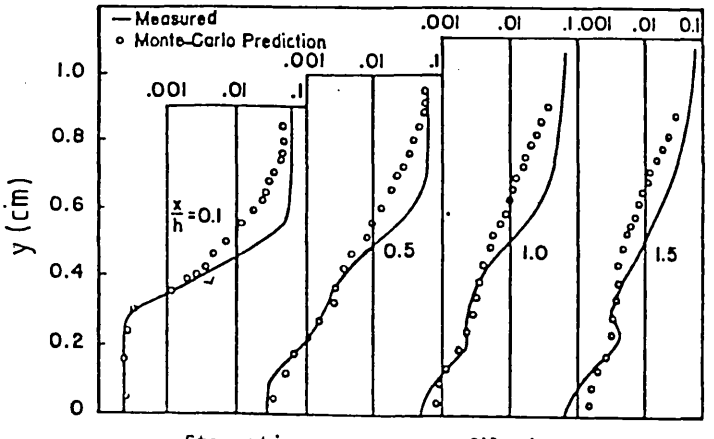
modern large computers. The complex logic of the presently used searching algorithm usually thwarts most optimising techniques on these machines. For very large three dimensional flows Bird (1979) has found that the methods which have proved satisfactory for the two dimensional calculations were limited by the memory requirements. He had to revert to the earlier but less flexible technique of dividing the flow field into regular cells and separately describing the boundary surfaces analytically. If the random walk method can be extended to two dimensional flows with variable cell sizes it may be more easily extended to three dimensions.

2.7 The Direct Simulation Method in the Near-Continuum Regime

Bird (1973) has suggested that his direct simulation method can be extended into the continuum regime even though the decoupling interval would have to be larger than the mean collision interval. He suggests that although the fine details of the flow field will not be correct many qualitative features of the flow might be correct. If this is so the limit on the cell size will not be the mean free path, which approaches zero, but the scale length of flow gradients. The calculations are extremely time consuming in these collision dominated flows. Merkle, Behrens and Hughes (1981) note that the direct simulation method is unsuitable for parallel processing on large computers. They have followed Bird's recommendation that the method is more suited to long calculations with small dedicated computers. They calculate the Mach 6 flow over a sharp wedge with a 10° half angle. Figure 2.4 shows some of their results. The calculated surface pressures on the body are in reasonable agreement with (very sparse) experimental values. Behind the body the results show many of the fine details of a complex re-circulating flow. The pressure behind the wedge is in reasonable agreement with measured values showing the same





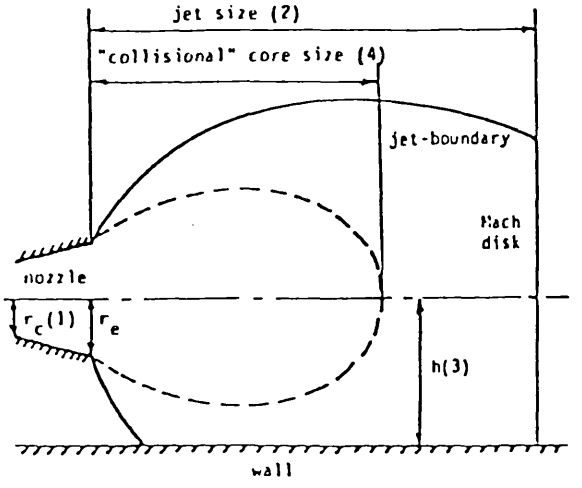


Stagnation pressure profile in wake.

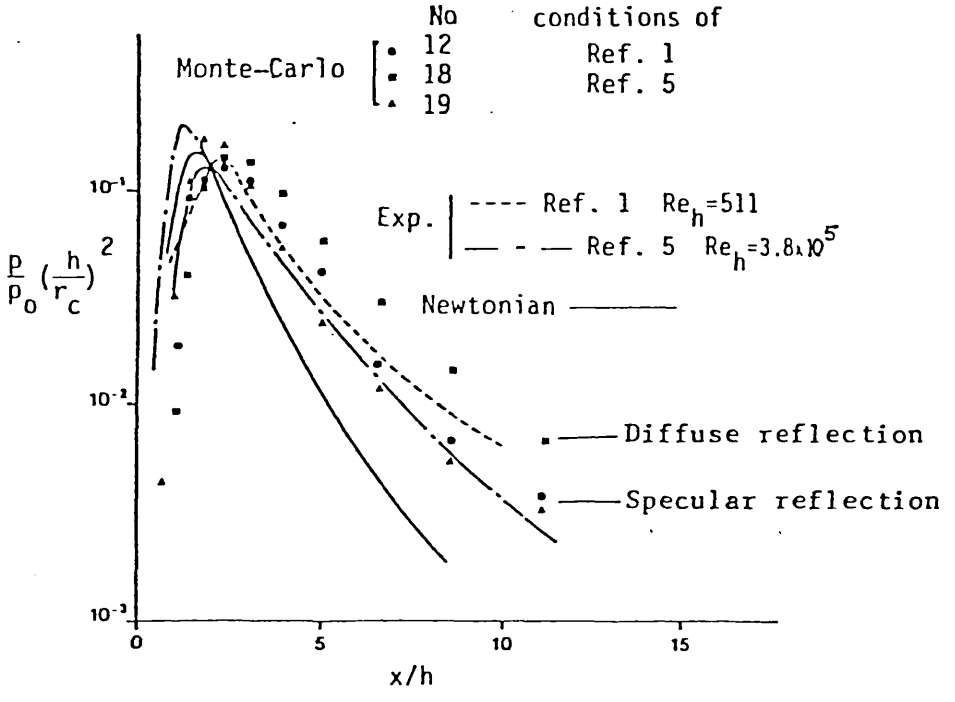
Fig. 2.4 EXAMPLE RESULTS FOR NEAR-CONTINUUM CALCULATIONS (MERKLE, BEHRENS AND HUGHES 1981)

two orders of magnitude increase transverse to the flow.

Lengrand, Raffin and Allègre (1981) used an interesting method suggested by Bird (1973) to reduce the computational load. Since after a few mean collision intervals the state within a cell can be considered to be at or near equilibrium they limit the number of collisions calculated in each cell. The limit is set at three times the number of particles in the cell (an average of 6 collisions per particle) which reduces enormously the computational time. Since non-equilibrium effects are ignored or reduced they suggest that the results should approach the inviscid limit, particularly when boundary layers are suppressed by specifying specularly reflecting surfaces. This is similar in some respects to a method devised by Pullin (1980) to obtain an inviscid solution with the direct simulation method. At the end of each convection phase the velocities within the cell are distributed according to the local equilibrium distribution determined from the total momentum and energy within the cell. The method is not entirely satisfactory because it is difficult and time-consuming to preserve both momentum and energy while selecting the velocities from a prescribed distribution. Using collisions to drive the molecules towards equilibrium automatically conserves momentum and energy and may be a faster method. Lengrand et al. (1981) got promising results for surface pressure on a plate parallel to the flow axis of an under-expanded jet. Figure 2.5 shows the pressure on the plate compared with experiments and a Newtonian approximation. It is not clear from all their results whether it is best to suppress the boundary layers by assuming specular reflection from surfaces. Diffuse reflection generates a thickness of boundary layer which will depend more on the decoupling interval than any real effects. Most interesting is the discovery that the results were less sensitive to



Flow geometry and characteristic lengths.



Comparison of calculated pressure distribution with experiment (h/r_c = 20, p_∞ = 0).

Fig. 2.5 EXAMPLE RESULTS FOR NEAR-CONTINUUM CALCULATIONS

(LENGRAND, RAFFIN AND ALLÈGRE 1981)

variations in cell sizes and number of particles in cells than is generally the case in the transition or rarefied regime.

The continuum calculations have used the hard sphere collision model since the details of the collision process are expected to be unimportant and the collision dynamics are simple for this model. It is possible that ~~the~~ the computing time may be reduced even further by modifying the method slightly. One of the most time consuming parts of the calculations is the acceptance-rejection technique of selecting collision partners. If the collisions are considered to be merely a redistributing mechanism then it is not important that the collision rate at each particular relative velocity is correct. The selection algorithm for Maxwell cross-sections is particularly simple since the collision partners can be chosen at random without considering the relative velocity. There is the disadvantage that the relaxation rate will be slightly slower. The distribution of speeds in collisions in an equilibrium gas is given by equation (6.7) and the distribution for a relaxing gas would be only slightly different from this. A hard sphere cross-section gives a slightly quicker relaxation towards equilibrium since there is a higher proportion of larger relative velocities in collisions and the extremes of velocities in a cell are eliminated faster.

If the collision partners are selected at random the collision algorithm should be much more efficient and the extra collisions needed to achieve the same relaxation might be easily accomodated. The molecules (or 'pointers' to each molecule in a cell) can be shuffled before the collisions begin. Pairs of molecules can then be selected as collision partners in a pre-determined pattern and the process continued until each particle has suffered the required number of

collisions. Since, once the particles are shuffled, the collision partners are known in advance the technique is perfectly suited to vector or parallel processing.

The particularly simple collision dynamics of the hard sphere molecule can still be used in combination with the selection procedure approriate to the Maxwell cross-section. The equilibrium distribution is the most probable distribution and should result from any 'shuffling' of the velocities which conserves energy and momentum. This combination of collision probability independent of relative velocity and hard sphere collision dynamics is a particular case of a diatomic collision model proposed by Borgnakke and Larsen (1973 1975) which would be particularly appropriate for these continuum calculations. We will consider this collision model in more detail when we review the diatomic collision models.

Although a few collisions are usually all that are necessary to establish approximate equilibrium this is not always so. For example when the higher speeds are underpopulated the relaxation can take much longer. Bird (1963) found that it can take as many as 15 collisions per molecule for the higher speeds to come to the equilibrium values. The reason for this is of course that the post-collision speeds can at most be half the relative speed of collision different from the centre of mass speed. It might appear that the cutoff of 6 collisions per particle used by Lengrand et al was too low. However, it is unlikely that the single peaked distributions of thermal speeds within a cell will arise in these simulations. When the distribution is multi-peaked the average relative speed of collision will be larger and the relaxation to 'virtual equilibrium' should take place in a few collision times. The number of collisions needed to bring various initial distributions to equilibrium could be found by experiment.

CHAPTER 3

REVIEW OF COLLISIONS MODELS

3.0 Introduction

In the classical kinetic theory the atoms of a monatomic gas are considered to be structureless 'points', interacting only through an intermolecular force. Diatomic molecules will have not only energy of translation but also energy stored in rotation. The observed specific heats for diatomic molecules indicated that energy, which is equally shared amongst all the possible degrees of freedom, is stored in rotation about two axes. Thus it is assumed that the individual atoms have no structure and the molecules are two-dimensional 'dumbbells' moving in three-dimensional space. When diatomic molecules collide they may exchange energy between 'internal' rotation and 'external' translation. These collisions are termed 'inelastic' collisions by analogy with the inelastic collisions of two macroscopic bodies in which some of the translational energy is converted to internal heat energy. When pairs of molecules collide some 'internal' energy may be released and converted to translational energy and these are also called 'inelastic' collisions.

Although the collision between molecules should be described by the methods of quantum mechanics the correspondence principle states that the quantum and classical descriptions will coincide when the energy of the molecules is much greater than the difference between the energies of stable quantum states. This will be so except for relatively small mass molecules or very low relative velocities in collisions. It can be shown that the deflections calculated in classical mechanics approach those calculated in the quantum theory (see for example Wu and Ohmura 1962). For our purposes classical methods will be adequate although some collisions in any simulation will be of sufficiently low energy to invalidate the classical

approach.

Although a good qualitative description of the intermolecular force in the classical limit can be obtained from quantum mechanics there are so many mathematical difficulties, for any but the simplest atoms, that an exact specification cannot be given (Hirschfelder, Curtiss and Bird 1954). It is usual to represent the intermolecular force as the derivative dU/dr of a suitably chosen potential U(r), where r is the distance between the molecules. The potential will contain a number of adjustable constants indicating the range of the force (the molecular 'size') and the strength of the force. The constants are determined by comparing the observed behaviour of gases with the predicted behaviour of particles obeying the classical laws of motion and interacting according to the chosen potential. The viscosity, heat transfer and diffusion can be derived from the Chapman - Enskog theory and depend on the scattering characteristics. Although the results can only be expected to apply to monatomic or structureless molecules, the viscosity predictions derived from spherical potentials can be fitted to the viscosity of a large number of diatomic gases and even to some polyatomic gases (Hirschfelder et al. 1954).

If a diatomic molecule is represented by two centres of force separated by a small inter-atomic distance, classical calculations show that the collision trajectories are only slightly different than those derived from a symmetrical potential (Lordi and Mates 1970; Pullin 1974). This justifies a technique first used in the direct simulation method by Bird (1970c) in which the collision calculation for diatomic molecules is divided into two parts by treating the molecular inelasticity as an energy transfer superimposed upon the spherical scattering. The perturbations to the trajectories arising

from the exchange of internal energy are ignored. The amount of energy transferred from translation to rotation ΔE is calculated independently according to an appropriate exchange model. To conserve energy the relative speed of the molecules is changed to

$$g' = (g^2 - 4\Delta E/m)^{\frac{1}{2}} \qquad (3.1).$$

Before considering the various inelastic energy exchange models, we review the spherically symmetric potentials which have been used in simulations to represent both monatomic and diatomic molecules. We pay special attention to the properties of nitrogen when reviewing the collision models, since nitrogen is a simple gas having properties close to those of the atmosphere.

3.1 Intermolecular Potentials

3.1.1 The transport coefficients

For a given potential the coefficients of diffusion, viscosity and heat transfer of a gas composed of these model molecules can be determined by the methods devised by Chapman and Enskog. The first approximations to the transport coefficients are (Hirschfelder et al. 1954)

$$\begin{aligned} &\text{diffusion coefficient} && \Upsilon = 3\ kT\ /16\ \rho\Omega^{(1,1)} \\ &\text{viscosity} \quad " && \mu = 5kT/8\,\Omega^{(2,2)} \\ &\text{heat transfer} \quad " && K = 5\mu c_v/2m \end{aligned} \qquad (3.2)$$

where $\Omega^{(\ell,s)}(T)$ is a collision integral derived from the scattering (see equation 4.3). It is a function of the temperature T and the constants in the potential. Within the limits of the simulation method itself we would expect that the same expressions would represent the transport properties of the 'simulation gas'. Given good experimental data for these coefficients the constants in the potential can be determined. Ideally the constants derived from heat transfer or diffusion measurements would agree with those derived from viscosity

measurements. In practice the constants are usually derived from the more reliable viscosity measurements and the resulting theoretical values of heat transfer and diffusion are in reasonable agreement with the experimental values (Hirschfelder et al. 1954).

3.1.2 The inverse power potential

The potential most often used in simulations is the inverse power repulsive potential

$$U(r) = a/r^{\alpha} \tag{3.3}$$

The inverse fourth power potential (the 'Maxwell molecule') and the hard sphere molecule, for which the force acts only when the intermolecular distance is equal to the sphere diameter, are two special cases and may be considered the 'soft' and 'hard' limits of the inverse power potential. For $\alpha = 1$ (the Coulomb force $\propto 1/r^2$) the field is so extensive that we cannot say that these particles collide in the sense that there is an abrupt change in the direction of the trajectories.

The theoretical viscosity of gas composed of 'inverse power molecules' is

$$\mu = \frac{5(mkT/\pi)^{\frac{1}{2}} \quad (2kT/\alpha a)^{\frac{2}{\alpha}}}{8\, A^{(2)}(\alpha)\ \Gamma(4-2/\alpha)} \tag{3.4}$$

where $A^{(2)}(\alpha)$ is a dimensionless collision integral related to $\Omega^{(2,2)}$ (Chapman and Cowling 1952), and which is defined in equation (4.7). The viscosity of nitrogen taken from NACA TN 3271 (Wooley 1956) is shown in figure 3.1. The quoted viscosities are within 2% of a great number of experimental values and the size of the data points in the figure approximately represent this range. The theoretical viscosity for inverse power molecules is a straight line on this log-log plot and the figure shows a line chosen to match the high temperature data. The slope of this line gives $\alpha = 13.51$ and the intercept determines the

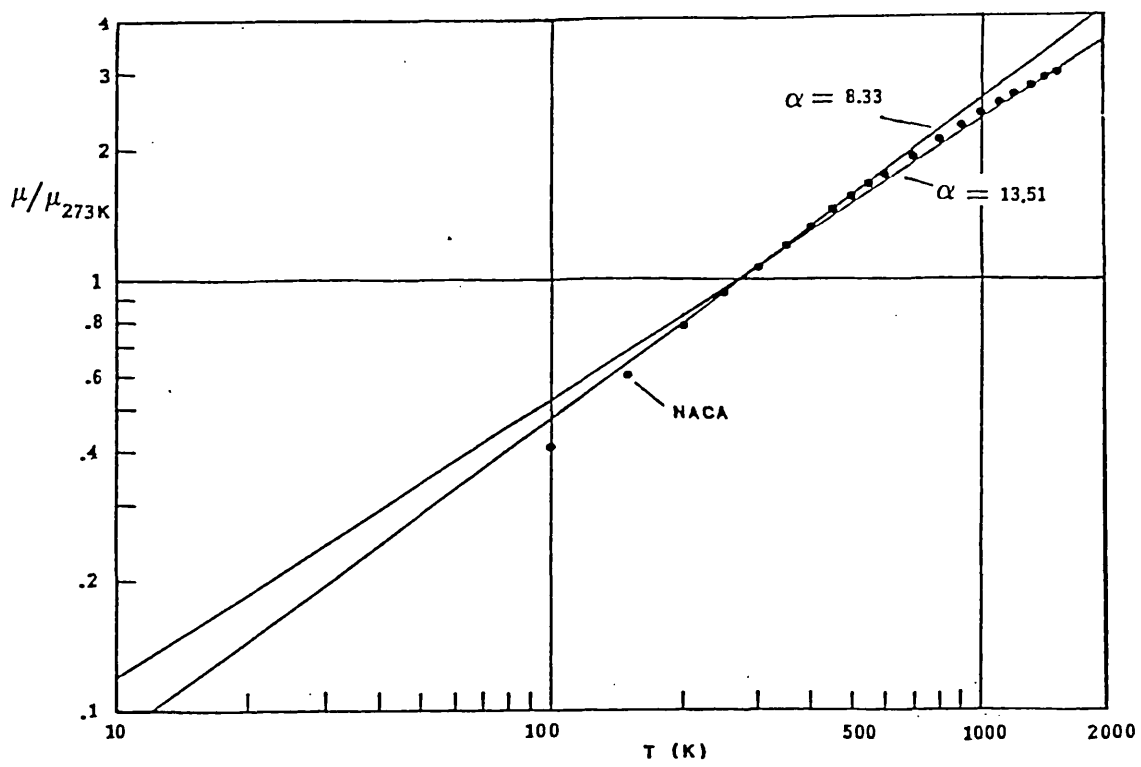
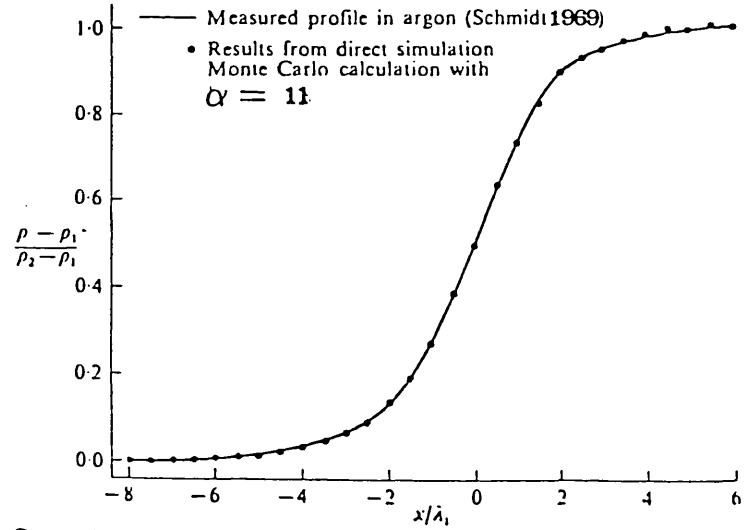


Fig. 3.1 VISCOSITY OF NITROGEN AND THEORETICAL PREDICTIONS

constant 'a' in equation (3.3). It is apparent from the figure that inverse power molecules are able to match the experimental viscosity data over only a limited range of temperatures. In any particular simulation the temperatures can be such that there will be some regions of the flow where the viscosity of the simulation gas is different from the real gas.



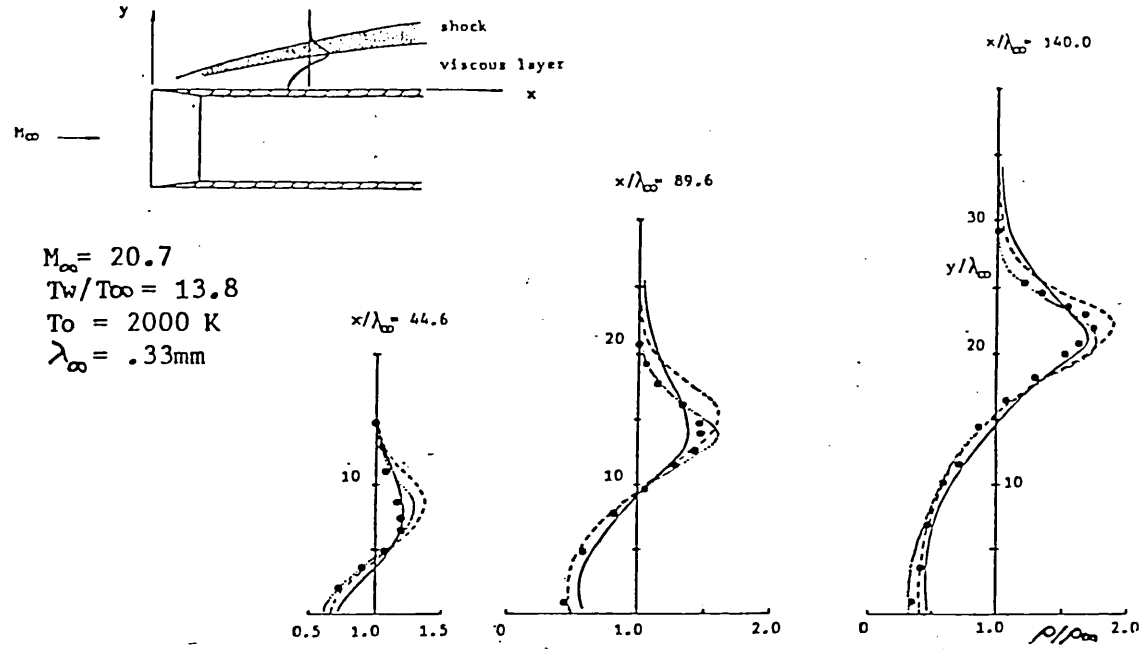
Comparison of experimental and numerical density profiles for a normal shock wave of Mach number $(Ma)_\infty = 8$.

Fig. 3.2 SHOCK PROFILES (BIRD 1976)

Bird (1970a) has calculated the structure of a plane shock in a monatomic gas using the inverse power potential in the direct simulation method. He was able to determine the exponent for which the calculated density profile was closest to the profiles measured in argon by Schmidt (1969) and these results are shown in figure 3.2. He suggested that this may be a way to determine the appropriate exponent for a particular gas when the viscosity measurements are not so reliable. The temperature range across a shock is limited though and a different exponent may be appropriate at different temperatures.

Pullin, Davis and Harvey (1977) have used the inverse 13.5 th power potential to calculate the stagnating flow ahead of a blunt cylinder and obtained good results. Davis (1978) compared the results of simulations of the flow over a flat plate with experiments performed in the Imperial College nitrogen tunnel (Harvey, Jeffery and Uppington 1971). This tunnel has a stagnation temperature from about 1500K to 2000K, and it was thought that the viscosity at this high temperature was the important property of the gas which should be modelled correctly. Thus he used $\alpha = 13.5$. However, for the complex flow in the boundary layer around a low temperature surface it might be that it is more important that the viscosity is correct for a lower range of temperatures somewhere between the surface temperature and the stagnation temperature. It was for this reason that Pullin (1974) used a more sophisticated collision model (considered later) to study the rarefied hypersonic flow over a flat plate.

In fact Davis (1978) found that the inverse power potential was not very succesful in the viscous layer around the outer surface of a hollow cylinder (the axisymmetric equivalent of the flat plate flow).

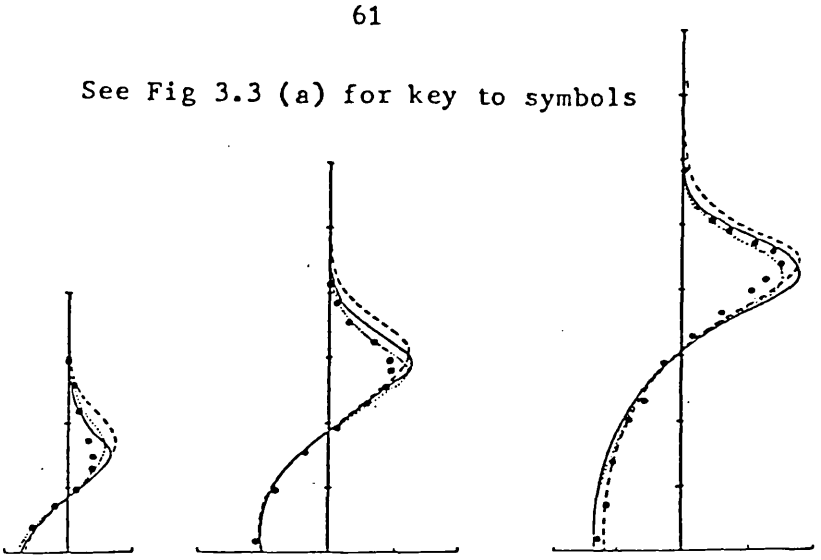


●Experimental results. Computed results:– – – – – variable-ϕ, Morse potential; ·····hybrid, Morse potential; ——— variable-ϕ, inverse power potential

Fig. 3.3 (a) DENSITY PROFILES FOR FLOW OVER A HOLLOW CYLINDER

Figure 3.3 (a) shows the density profiles calculated by Davis (1978) with the inverse power and other collision models and it is clear that the viscous layer beneath the shock is poorly represented by the inverse power model. The position of the density peak however agrees well with the experiment. If the density profiles calculated with the inverse power potential are normalised against a larger mean free path, as is shown in figure 3.3 (b) then the structure of the viscous sub-layer is well matched to experimental values but the position of the density peak is not. Neither choice matches the size of the peak very well. The different normalisation amounts to selecting a larger value of the constant a (the molecular 'size') in equation (3.3). The calculations are not truly dimensionless, however, since the radius of the hollow cylinder is effectively changed by the new normalisation. More importantly the calculations included the effects of energy transfer from rotation to translation at a rate depending on the simulation collision rate. Since the 'size' of the molecule is increased by the new normalisation, the collision rate and the energy

See Fig 3.3 (a) for key to symbols



Inverse power curves for larger mean free path = 46 mm

Fig. 3.3 (b) DENSITY PROFILES FOR FLOW OVER A HOLLOW CYLINDER

transfer rate are altered. The difference in the density profiles can not be attributed solely to the change in the viscosity.

For this and many applications where the 'crucial' temperature is lower, different values of 'a' and α might be appropriate. Figure 3.1 also shows a low temperature fit with the data given by Bird (1981). The value of α is 8.33 and the line passes through the experimental point at 273 K. If the temperatures within the flow are everywhere in the range 100 K - 400 K we would expect this choice of constants to be best. Appendix B gives the values of 'a' derived for both the high and low temperature fits with the viscosity of nitrogen.

3.1.3 Potentials which include a 'long range' attraction

The law of 'corresponding states' postulates that all gases will obey the same equation of state in terms of the dimensionless variables p/p_C, T/T_C and V/V_C where p_C, T_C and V_C are the pressure, temperature and volume at the critical point where both $(dp/dV)_T$ and

$(d^2p/dv^2)_T$ are zero (Hirschfelder et al. 1954). The principle is reasonably well established empirically. For molecules interacting via spherical potentials it implies that the potential can be expressed as $U(r) = e\,\kappa(r/\sigma)$ where e is a scaling factor for the potential strength, σ is a scaling factor for the range of the potential and $\kappa(r/\sigma)$ is the same function for all gases (Hirschfelder et al. 1954). The inverse power potential is a poor representation of the postulated universal function κ, since the exponent is different for different gases and different ranges of temperature.

There are many theoretical reasons to suppose that molecules attract each other as they approach before they begin to repel each other. These 'van de Waals' forces, which account for the cohesion of molecules in liquids, can also account, in part, for the deviations from the perfect gas equation. A number of potentials incorporating such an attractive component have been studied. A rather crude model, the 'square well' potential, adds a constant attractive potential with a finite range outside a hard sphere molecule, while the Sutherland potential adds an inverse power attractive component. For a sixth power of repulsion the Sutherland viscosity prediction can be fitted to a large number of monatomic and diatomic gases. More realistic and

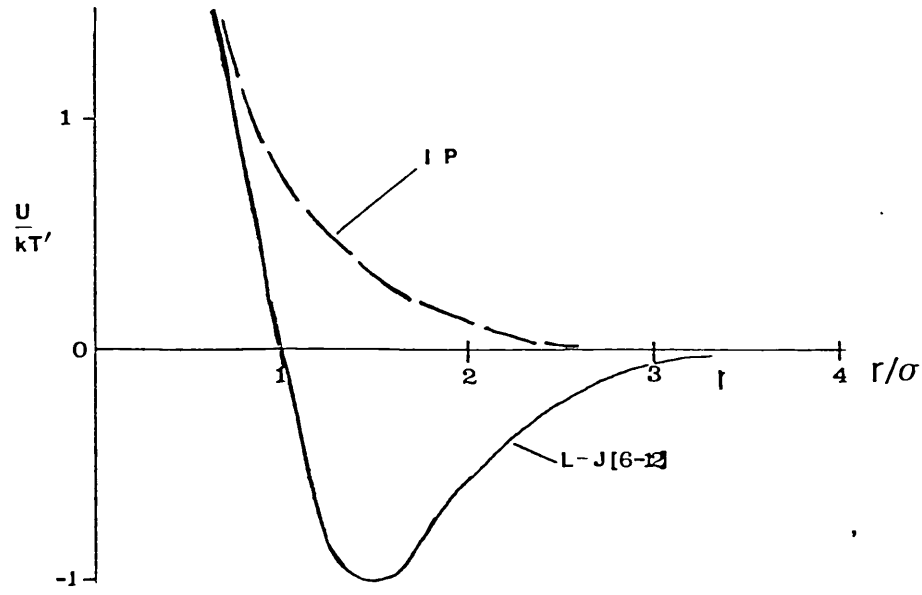


Fig. 3.4 INVERSE POWER AND LENNARD-JONES POTENTIALS

extensively studied is the Lennard-Jones potential

$$U(r) = 4kT' \left\{ c(\sigma/r)^n - d(\sigma/r)^m \right\}$$

which combines attractive and repulsive forces in a 'soft' molecule. Figure 3.4 shows the general shape of the Lennard-Jones potential compared with the inverse power potential. The separation at which the potential changes from positive to negative is a rough measure of the diameter of the molecule and T' determines the depth of the potential well.

The viscosity for these molecules is given by

$$\mu = \frac{5(m \pi kT)^{\frac{1}{2}}}{16 \pi \sigma^2 \Omega^{(2,2)*}} \qquad (3.5)$$

where $\Omega^{(2,2)*}$ is a dimensionless collision integral derived from $\Omega^{(2,2)}$ (see appendix A). An analytical solution for the collision integral for general values of m and n cannot be obtained so these must be specified in advance. At high temperatures where the majority of collisions are at high relative velocities the attractive part of the potential is less important and the model behaves like an inverse n th power molecule. Roughly speaking this is because the fine details of the intermolecular force have little time to effect the molecular trajectories. At low temperature however the attractive component is important. The most generally useful values of m and n are m = 6 and n = 12 (with c and d = 1). Values of the collision $\Omega^{(2,2)*}$ integral as a function of the reduced temperature $T^* = T/T'$ are given by a number of authors (Hirschfelder et al. 1954; Monchick and Mason 1961). The values of σ and T' can be chosen to fit the experimental data for a particular gas. The viscosity of nitrogen up to 600 K quoted by Wooley (1956) and shown in figure 3.1 is in fact the theoretical prediction derived for the Lennard-Jones potential with σ = 3.681 Å and T' = 91.5 K. Figure 3.5 shows that for high temperatures the

Lennard-Jones viscosity is slightly greater than the experimental values.

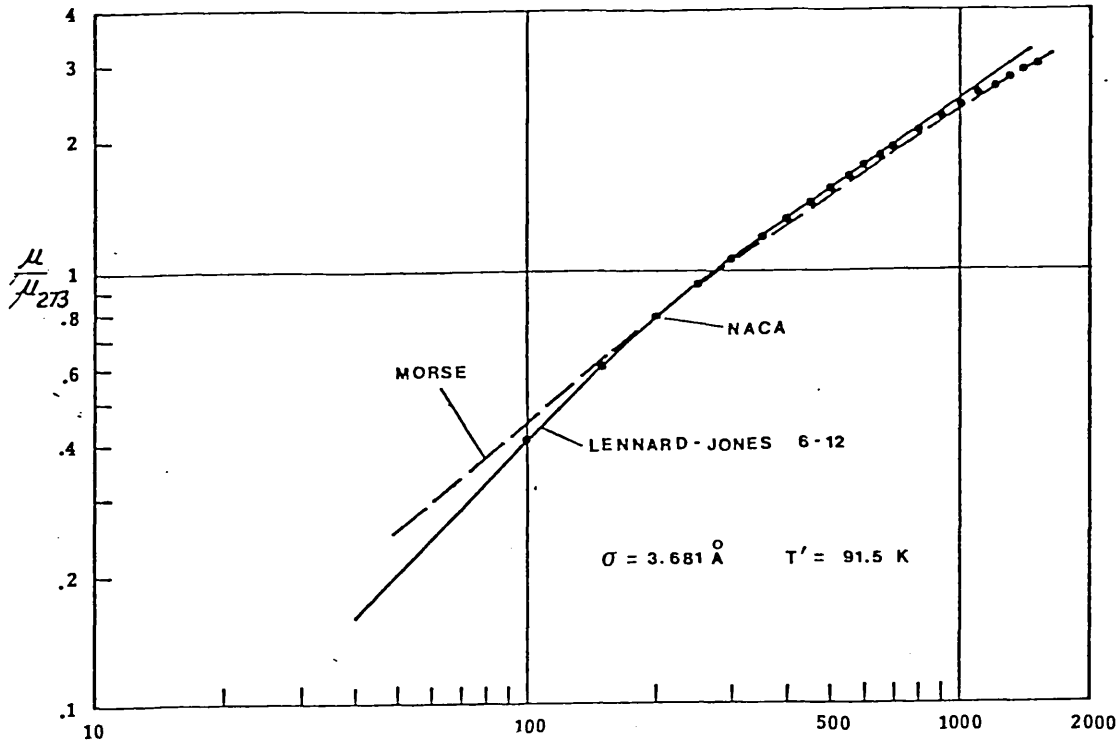


Fig. 3.5 VISCOSITY OF NITROGEN AND THEORETICAL PREDICTIONS

A potential which has been shown to be better than the Lennard-Jones for a number of monatomic gases is the Buckingham exp-6

$$U(r) = kT'/(1-6/\beta)\{ 6/\beta \exp(-\beta(r/\sigma - 1)) - (\sigma/r)^6 \}$$

which replaces the inverse power repulsion in the Lennard-Jones potential with an exponential repulsion. It is found that this potential can satisfy the law of corresponding states over a greater range of temperatures than can the Lennard-Jones potential (Keeler, Van Theil and Alder 1965). Sturtevant and Steinhilper (1974) have used the Lennard-Jones (6-12) and the Buckingham exp-6 potentials in Monte-Carlo calculations of shock structure. Both potentials gave good results and although they were not able to conclude that either potential gave a better fit with the experimental data they were able to determine the values of σ and T' which gave the best fit for each potential.

A similar potential was proposed by Morse (1929) to represent the binding energy between hydrogen atoms. The form of the potential was suggested by theoretical analysis of atomic bonding according to quantum mechanics. In a form corresponding to the Lennard-Jones potential, the Morse potential is

$$U(r) = 4kT' \{ \exp(-\beta(r/\sigma - 1)) - \exp(-\frac{\beta}{2}(r/\sigma - 1)) \} \qquad (3.6).$$

The potential changes sign where $r = \sigma$ and T' is the depth of the potential well. The constant β determines the range of the potential (choosing β is similar to choosing the indices m and n for the Lennard-Jones potential) and the value can be determined to give good viscosity predictions (Parker 1959). The appropriate value of β for nitrogen is 14.798.

The collision integral $\Omega^{(2,2)*}$ for this potential has been calculated by Pullin (1974) and these results are tabulated in appendix A. Although slightly different values of T' and σ might give a better fit for the viscosity data for nitrogen we have followed Pullin in taking the same values of T' and σ used with the Lennard-Jones potential. The viscosity derived for the Morse potential is shown in figure 3.5 and fits the experimental values over a wider range of temperatures than the inverse power potential can. The Morse potential was used in the direct simulation method by Pullin (1974) to calculate the leading edge flat plate flow. Davis (1978) obtained the better set of results, shown in figure 3.3 (a), when he used the Morse potential.

3.1.4 Choosing a potential for the direct simulation method

A particular potential must be chosen for the simulation calculations by considering the accuracy required and the computational efficiency. The inverse power potential has been most often used because of the relative ease with which the collision

problem can be solved. By a careful choice of the constants α and 'a' it can give good results. The appropriate constants to use can be determined from the viscosity. This ensures that this property of the simulation gas matches that of the real gas but, it must be remembered, this is a minimum condition that a collision model must satisfy. Since viscosity is a near equilibrium property there is no guarantee that a model which reproduces the viscosity of a real gas near equilibrium will behave like the real gas when the flow conditions are far from equilibrium.

It is possible to construct an infinite number of approximate collision models which have the same variation of viscosity with temperature as the inverse power potential (see chapter 4). The diffusion and heat transfer coefficients, derived from equation (3.2), will in general be different for each model and we find that in spite of this each gives reasonable predictions of shock profiles. Sturtevant and Steinhilper (1974) concluded that the Lennard-Jones and the Buckingham exp-6 potential give little improvement over the inverse power potential when calculating the shock structure. Although a plane one dimensional shock could be considered a severe test of non-equilibrium performance of these collision models it is still a restricted and idealised flow compared with the complex flows around bodies of various shapes. It is a matter of experiment to determine whether the approximate collision models can adequately simulate a gas in these conditions.

The main reason for preferring a realistic potential is that it is more likely to match reliably the behaviour of a real gas for a wider range of conditions, without adjusting the constants defining the potential. The realistic potentials also provide a standard of

comparison for the simpler collision models. The Morse potential has suffered slightly in the past because of an unsatisfactory limitation on the range of relative velocities in collisions which could be in practice be calculated. This problem can be overcome (see chapter 5). The Morse potential extends further than the inverse power potential when both are adjusted to give the same high temperature viscosity. Thus more collisions must be calculated, making the Morse potential more time-consuming. When combined with an inelastic exchange model the scattering calculation is only a fraction of the time required to calculate each collision and so the proportional time penalty is reduced to about 15%.

The cross-section for the Morse potential is smaller than for the Lennard-Jones potential so there is a practical advantage in using it rather than the Lennard-Jones or exp-6 potentials. The high temperature viscosity of nitrogen is slightly better reproduced with the Morse potential and it is only below about 100 K that the differences between the potentials is great (see figure 3.5). At low temperatures we must accept that the classical potentials will be in error so there is little incentive for using the Lennard-Jones (or the exp-6) potential rather than the Morse potential.

3.2 Collision Models for Diatomic Molecules

3.2.1 Kinetic theory

For diatomic molecules the Boltzmann collision term needs to be modified to include the exchange of energy between translation and internal energy. The state of each molecule is represented by its velocity v_i and its quantum number i for internal energy. A collision between two molecules (v_i, i) and (v_j, j) will give post-collision states (v_k, k) and (v_l, l). A differential collision cross-section is denoted $I_{ij}^{kl}\, dA$. The modified collision term is

$$\Sigma_{jkl} \int\int (f'_k \; f'_l \; - f_l \; f_j) \; g_{lj} \; I^{kl}_{ij} dA \; dv_j .$$

The derivation depends on the existence of inverse collisions and the equality $g_{lj} \; I^{kl}_{lj} \, dv_l \; dv_j = g'_{kl} \; I^{ij}_{kl} \, dv'_k \, dv'_l$ (Hirschfelder et al. 1954). Boltzmann's H-theorem holds and in the classical limit the Maxwell-Boltzmann equilibrium distribution function is

$$f \, d\underset{\sim}{v} \, de_R = (m/2\pi kT)^{\frac{3}{2}} \exp(-mv^2/2kT) \, d\underset{\sim}{v} \, (1/kT) \exp(-e_R/kT) \, de_R$$

The internal energy of rotation e_R is independently distributed $\propto \exp(-e_R/kT)$. In accordance with the principle of equipartition of energy each degree of freedom stores kT/2 of the total energy. A 'rotational' temperature is defined as $T_R = \langle e_R \rangle / k$ where $\langle e_R \rangle$ is the mean rotational energy of the gas. At equilibrium $T_R = T_t$.

3.2.2 Impulsive rotational-translational energy exchange

Early representations of molecules with internal rotational energy were based on simple classical representation of molecules. Bird has used 'rough sphere' molecules which exchange translational and rotational energy in collisions by the action of a 'friction force' as well as the normal force at the point of contact. This force is assumed to be such that it reverses the relative velocity of the points of contact. Energy may be exchanged between translation and rotation about three axes so the molecule inadequately represents a diatomic molecule with two internal degrees of freedom. Jean's' 'loaded sphere' model has the required two degrees of internal freedom. This is a hard sphere with its centre of mass slightly displaced from the geometric centre. The mass distribution is symmetric about an axis passing through the geometric centre and the centre of mass, and the energy of rotation about this axis can not be altered by the collision. Thus there are two active degrees of rotational energy. This was used by Melville (1972) to determine shock profiles for diatomic gases with the direct simulation method.

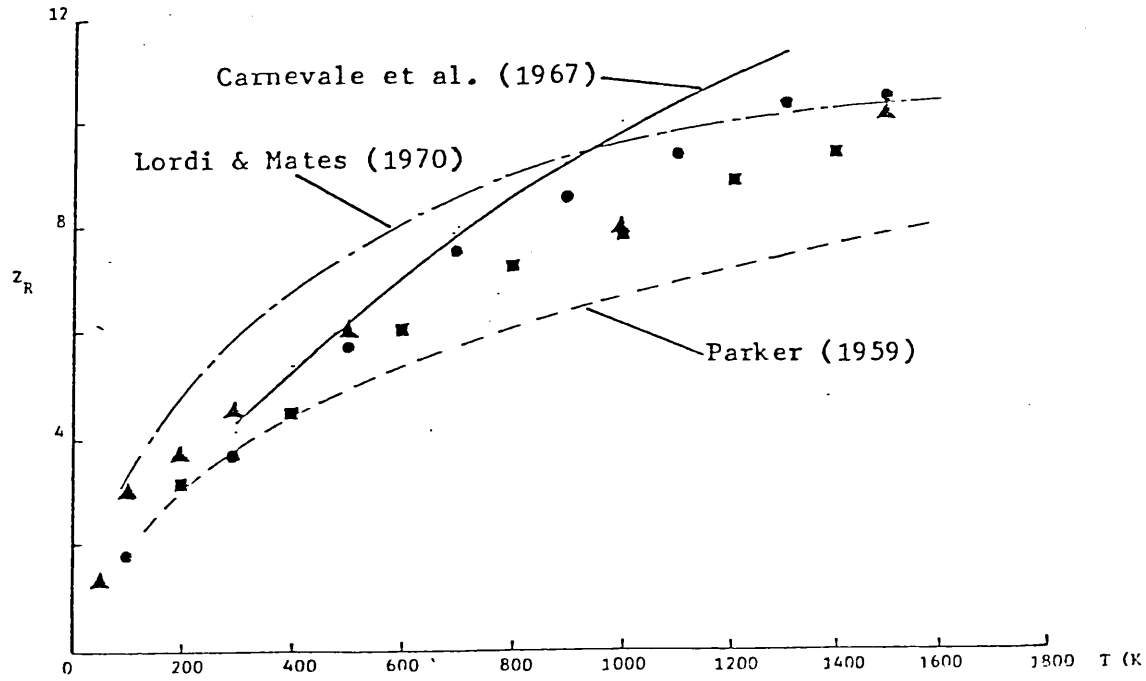
A more realistic representation of a diatomic molecule was used by Parker (1959) to study the exchange of energy between rotation and translation. Parker's molecule was made up of two masses rigidly connected to make a 'dumbbell'. Two centres of repulsion were located along the line connecting the masses but did not coincide with the centres of the masses. A spherically symmetrical short range attractive force acting between the 'dumbbells' along the line joining their centres was included. Parker simplified the calculations by assuming that the rotations of each molecule were co-planar. The non-coincidence of the centres of repulsive force with the centres of mass compensated in some measure for this unrealistic assumption. Parker determined the average rate of transfer of energy into rotation when the rotational energy was zero before the collision.

If the energies stored by a molecule in each degree of freedom are not equal the differences are reduced by the action of collisions as the gas approaches equilibrium. It is assumed in the phenomenological description that the average rate of energy transfer depends on the difference between the translational and rotational energy and this difference decays exponentially. For a gas in which the translational temperature is held constant the rotational temperature will differ from the translational temperature according to the equation

$$(T_R - T)/T = \exp(-t/\tau) \qquad (3.7)$$

where t is time and τ is the decay constant called the 'relaxation time'. If a collision rate is assumed the relaxation time can be converted to a number of collisions Z_R called the 'rotational collision number'. From his results for the rate of transfer of rotational energy into initially non-rotating molecules Parker found that Z_R increased with temperature, that is that the average energy transferred from translation to rotation in each collision decreased

as the energy of the collisions increased. This is not perhaps a surprising result since the duration of these high relative velocity collisions is short and the rotational coupling between the centres of repulsion has less time to act. The variation of Z_R with temperature was measured by Carnevale, Cary and Larsen (1967) and their results for nitrogen are compared with some theoretical predictions in figure 3.6.



Monte-Carlo results: ● variable-ϕ, inverse power; ▲ hybrid Morse, potential; ■ variable-ϕ Morse potential

Fig. 3.6 ROTATIONAL COLLISION NUMBER FOR NITROGEN

Neyland (1967), Brau and Jonkman (1970) and Lordi and Mates (1970) have all extended Parker's analysis to initially rotating molecules. The Z_R (T) curve calculated by Lordi and Mates is shown also in figure 3.6. The experimental results fall between the Parker's and Lordi and Mates' predictions at low temperatures but are above both for high temperatures. Lordi and Mates' result is based on an approximate solution of the energy exchange which was invalid for miss distances $b > \sigma$. The complete calculations indicated that the energy exchanged

ΔE decreased rapidly for $b > \sigma$ although collisions arising from outside this miss distance produced a substantial deflection. The error in ignoring the contributions to the average internal energy transferred by collisions outside this cross-section was small. Parker's analysis also included an assumption of collision rate based on this same constant collision cross-section which may be termed the 'inelastic cross-section' for this model.

The collision number is not measured directly but through a relaxation time which is converted to Z_R by assuming a collision rate based on the viscosity of the gas. As we shall see, for most potentials the assumed collision rate derived from the viscosity includes only about half of all those collisions which produce an appreciable deflection. It is not exactly the same as the constant cross-sections assumed by Parker and Lordi and Mates. Since the theoretical and experimental curves in figure 3.6 are reasonably close it can be assumed that the 'viscosity' collision rate does include all those 'inelastic' collisions which transfer an appreciable amount of energy between translation and rotation. A 'cutoff cross-section' for inelastic collisions is incorporated into many of the diatomic collision models which we will consider. Collisions arising from outside this cross-section are treated as perfectly elastic collisions in which the rotational energy is frozen.

Macpherson (1971) has applied the complete solution for the trajectories of Parker's model in the Monte-Carlo method to determine the structure of one-dimensional shocks. Even for this relatively simple problem the technique is so time consuming that the results were meagre although they did demonstrate an overshoot of translational temperature. This same effect was found by Melville (1972) for calculations with the loaded sphere. This increase of

temperature above the Rankine value behind the shock is a direct consequence of the relatively slow exchange of energy between translation and molecular rotation compared to the transit time through the shock.

Pullin (1974) developed an approximate solution for Parker's diatomic molecule. However it was unable to satisfy detail balance sufficiently well to produce acceptably near equipartition at equilibrium. It does have the advantage however that the energy transferred depends partly on both the relative velocity and the miss distance, that is, there is some correlation between the amount of deflection in a collision and the amount of energy exchanged. The approximate method broke down for large miss distances and the inelastic cross-section $\pi \sigma^2$ was used. It was also found that the approximate method was unsatisfactory for low energy collisions and various modifications were made (Pullin 1974).

3.2.3 Quantum mechanical collision models

At present it is unlikely that this classically exact modelling of the exchange can be applied usefully to more complicated flowfields. Quantum mechanical collision models have been tried. Deiwert and Yoshikawa (1975), who were concerned with low temperature (~10 K), were able to use a semi-classical method based on the Pearson-Hansen model (1974). This employs point centres of repulsion for the collision dynamics and the Schrödinger equation for a rigid rotator harmonic oscillator to compute the rotational energy transition probabilities. Simplifying semi-empirical assumptions had to be incorporated to make the model tractable for Monte-Carlo calculations. Reasonable equipartition is achieved up to temperatures of 320 K but thereafter it breaks down.

Itikawa and Yoshikawa (1975) have developed a more realistic quantum mechanical model based on the inverse power potential. Well behaved relaxation tests are obtained by optimising against the exponent of the intermolecular potential. Although an advance on Deiwert's model, it is extremely time consuming and it is unlikely that bulk properties, such as viscosity, will be adequately predicted by this method of chosing the power law exponent. Neither paper makes reference to the variation of Z_R with temperature.

3.2.4 Phenomenological collision models

The principal disadvantage of the classical and quantum mechanical models is that they are either unacceptably artificial or too demanding of computing time. Alternative methods have been proposed by Bird (1970c) and Borgnakke and Larsen (Borgnakke and Larsen 1973 1975; Larsen and Borgnakke 1974; Larsen 1976). The complex inelastic collision dynamics are avoided and each post-collision state is not correctly related to the pre-collision state. The idea is to make the distribution of the post-collision states over a large number of collisions reflect that in the real gas through a phenomenological calculation of the energy exchange. For example, in Bird's energy sink method the rotational energy is compared with the appropriate equilibrium value for a collision at that relative velocity. A fraction of rotational energy is transferred to the translational energy such that the final state is closer to equilibrium than before. This guarantees macroscopic equilibrium but because there are no inverse collisions the model cannot satisfy the principle of detail balance.

Borgnakke and Larsen have proposed statistical collision models similar to Biird's energy sink model. In the first, the 'two-class'

exchange scheme, individual collisions are either elastic (in which translational energy is conserved) or inelastic (in which energy is exchanged freely between translation and rotation). The fraction ϕ of the total collisions that are treated inelastically is specified and the effect of the combination of the two types of collision is that the translational and rotational energies relax towards the local equilibrium with a rate proportional to $1/\phi$.

For the inelastic collision the total centre of mass energy is divided into post-collision translational and rotational energy according to the local equilibrium distribution of these quantities. This is interpreted as analogous to the B-G-K modification of the collision term in the Boltzmann equation where the source term arising from the outcome of collisions is derived from the local equilibrium distribution. Borgnakke and Larsen apply this condition not only to the magnitude of the translational energy after collision but also to the direction of the post-collision relative velocity vector. They make the distribution of this direction isotropic with respect to the centre of mass of the collision. Over a large number of collisions between hard spheres in which the geometric impact parameters are randomly selected the direction of the post-collision relative velocity is also distributed isotropically. In other words Borgnakke and Larsen have assumed that the molecules are hard spheres even though the collision partners are chosen with a probability appropriate to the variable cross-section of the inverse power molecule.

The remaining collisions are treatedly elastically and correspond to monatomic collisions. The post-collision relative velocity is again uniformly distributed over each element of solid angle. Borgnakke and Larsen give example calculations with both hard sphere and 'Maxwell'

cross-sections and refer to 'pseudo-Maxwell' collision dynamics. In effect they have defined a modified collision model different from the classical potentials. A number of authors have independently proposed this same collision model. Erofeev and Perepukhov (1979) have used what they called the 'pseudo-power potential' and refer to Russian language papers dated 1976 and 1977 which describe the method. It seems clear from their brief description that their method corresponds to the elastic (or monatomic) part of Borgnakke and Larsen's method. Krook and Wu (1977) found a particular solution of the Boltzmann equation for a general monatomic collision model which corresponds in a particular case to the pseudo-Maxwell collision dynamics of Borgnakke and Larsen.

Borgnakke and Larsen have not discussed the effect of substituting the hard sphere deflections for the softer inverse power deflections. The rates of transfer of momentum and the viscosity are different from that derived from the inverse power. It turns out that theoretical viscosity for these molecules will match the inverse power viscosity if the collision cross-section is made smaller. We later consider this collision model along with some other approximate alternatives all based on the variation of collision cross-section derived from the inverse power potential. Bird (1981) has presented the model in a dimensional form calling it the 'variable diameter hard sphere (VHS) model'.

Two conditions are necessary to make a collision model satisfy the principle of detail balance; the inverse of each collision must be possible and the rate of the forward and inverse collisions at equilibrium must be equal. The two class scheme satisfies the principle of detail balance (Pullin 1975) but it goes much further. To satisfy the principle it is not necessary that the post-collision

direction of the relative velocity be uniformly distributed or that the post-collision rotational energies be distributed according to the equilibrium condition.

Consider first how the principle is satisfied for a monatomic gas even though the direction of the post-collision vectors $\underset{\sim}{g}'$ are not distributed isotropically. The collision between particles with

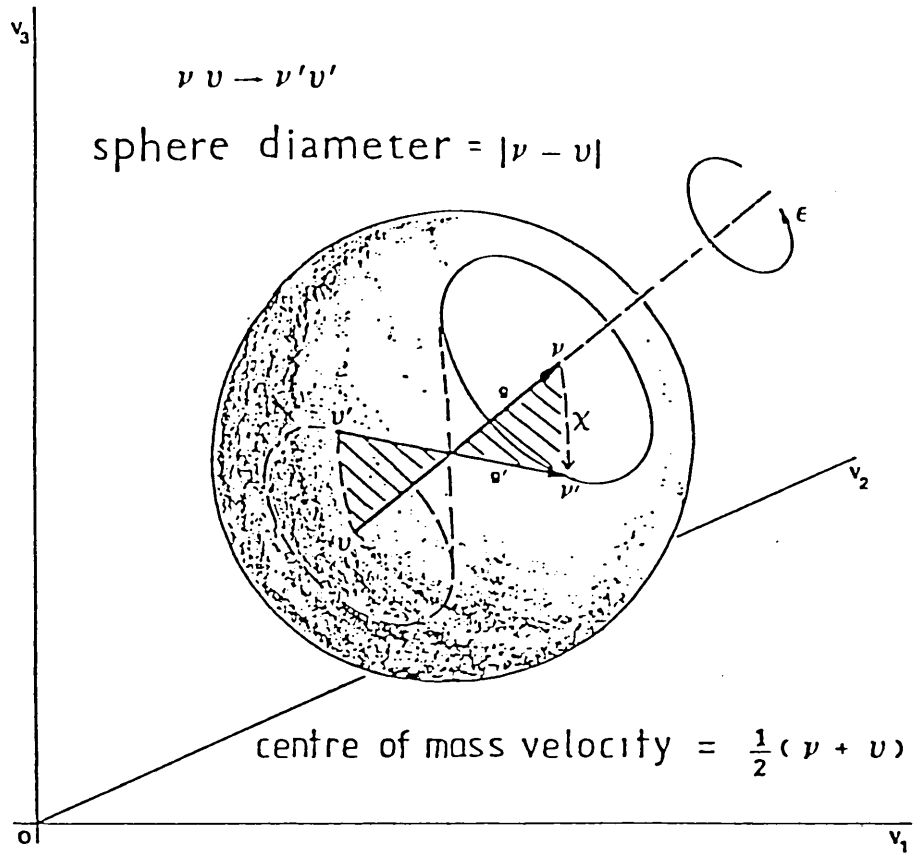


Figure 3.7 COLLISION IN VELOCITY SPACE

initial velocities $\underset{\sim}{\nu}$ and $\underset{\sim}{\upsilon}$ is represented in velocity space in figure 3.7. The points representing the post-collision velocities ($\underset{\sim}{\nu}'$, $\underset{\sim}{\upsilon}'$) are distributed over the sphere in velocity space. Since the distribution of these points is axisymmetric about the direction of $\underset{\sim}{g}$ and since at equilibrium the number of collisions with relative velocity $\underset{\sim}{g}$ is the same as the number of collisions with $\underset{\sim}{g}'$ (i.e. $g = g'$) the inverse and forward collision rates are equal. For 'soft'

potentials the post-collision points will be more closely spaced around the original points ($\underset{\sim}{v}'$, $\underset{\sim}{v}$). To apply the isotropic condition to the outcome of individual collisions as Borgnakke and Larsen have done is too strict a condition. Using their analogy we might say that the Boltzmann collision term is much less restrictive than the B-G-K approximation. Krook and Wu (1977) derive an expression for the relaxation rate of the velocity distribution function (in a particular case) for Maxwell collision probability and an arbitrary deflection law. The relaxation is slower for a soft potential than for the hard sphere scattering.

Pullin (1975) has shown how the argument must be modified when internal energy is exchanged ($g' \neq g$). It turns out that the two class scheme will still satisfy the principle of detail balance when the deflections are calculated using the inverse power potential.

Pullin used the two class scheme to replace his earlier modifications to his approximate classical model (Pullin and Harvey 1976). For low energy collisions, for which the classical scheme was unsatisfactory, he substituted the two-class statistical scheme. The high energy collisions were calculated using the approximate classical method providing its effect was to drive the translational and rotational energy fractions towards local equilibrium. If this was not the case the collision was recalculated using the statistical scheme. It was hoped that those classical collisions which were retained would ensure a 'realistic' correlation of pre- and post-collision energies. The variation of $Z_R(T)$ for this 'hybrid' model was shown in figure 3.6. The results of calculations using this model have already been shown in figures 3.3 (a) and 3.3 (b). Most of the success of the model could be attributed to the improved viscous modelling of the Morse potential compared with the inverse power potential but there is some

indication that the classical exchange scheme was a contributing factor (Davis 1978).

Pullin's classical model incorporated an inelastic cross-section smaller than the total collision cross-section and this was justified by the more exact calculations with Parker's molecule. The hybrid model is itself a 'two class' scheme with the difference that there was a correlation between the deflection angle and the exchange of internal energy. The two class scheme itself could retain this sort of correlation between deflection angle and energy exchange. For any chosen potential an inelastic collision cross section can be defined equal to a fraction ϕ of the total cross-section. For that fraction ϕ of collisions arising from inside the inelastic cross-section (which will correspond to large angles of deflection) the statistical exchange scheme can be used. This makes the collision calculation slightly more complicated than in the original two class scheme since it is more time consuming to determine the components of the post-collision relative velocity which are not distributed isotropically. Bird (1981) considers the simplicity of the variable hard sphere collision calculations to be its main advantage. However, the method proposed is only about 5% slower than the method originally proposed by Borgnakke and Larsen. This penalty might be considered an acceptable 'price' to pay to ensure that the velocity components relax at a rate appropriate to a soft potential and that there is some correlation between deflection angle and energy exchange.

Like the distribution of the direction of the post-collision relative velocity vector which does not have to be isotropic, the distribution of the post-collision energies of translation and rotation need not be derived from the equilibrium distribution. In their second collision model Larsen and Borgnakke (1974)

limit the amount of energy which can be exchanged between translation and rotation. A fraction $1 - \phi$ of the total centre of mass energy is frozen and does not take part in the exchange, while the remaining energy is redistributed. These redistributed energies are then added to the frozen values of translational and rotational energies to obtain the total post-collision energies. The method is an improvement over the two class scheme since a more realistic collision is calculated each time.

Pullin (1975 1978) has analysed in detail the construction of statistical exchange schemes with particular regard to their ability to satisfy the H-theorem. He has shown that this model fails to satisfy the principle of detail balance although the error is small. He gives a version of the restricted exchange scheme which does satisfy detail balance and relaxes towards equilibrium in much the same way. The computing time is approximately doubled and because of this it has not often been used in simulations. This model is discussed further in chapter 5 and is used in simulation calculations in chapter 7.

The most serious criticism of these statistical exchange schemes is that Z_R does not vary with temperature. Pullin and Davis (Davis 1978) proposed that the value of ϕ should be allowed to be different for each collision in such a way as to reproduce in relaxation simulations the experimentally determined variation of Z_R . This was called the 'variable-ϕ ' collision model and it is examined in more detail in chapter 5.

CHAPTER 4

COLLISION MODELS - I

4.0 Introduction

In this chapter the inverse power potential is studied in detail. The two body collision is reviewed in slightly more detail than in Chapter 2. The relation between the Chapman-Enskog collision integrals and the collision cross-section is emphasised. We show how a number of 'scattering models' can be constructed based on this potential. All these have the same theoretical viscosity and the same variation of collision cross-section with relative velocity of collision. The exchange of energy between internal and external modes is not considered so these models may be used in calculations for monatomic gases. The energy exchange models are considered separately in subsequent chapters.

4.1 The Two-Body Collision

The collision between two molecules is best studied in a frame of reference moving with the velocity of the centre of mass of the two molecules. If m_1 and m_2 are the molecular masses then the velocities of the molecules relative to the centre of mass are

$$\underset{\sim}{v}_1' = \frac{m_2}{m_1+m_2}\,\underset{\sim}{g} \quad \text{and} \quad \underset{\sim}{v}_2' = \frac{-m_1}{m_1+m_2}\,\underset{\sim}{g}$$

The collision kinetic energy relative to the centre of mass is $\frac{1}{2}m^*g^2$, where the reduced mass is $m^* = \frac{m_1 m_2}{m_1+m_2}$. Consider the plane which contains the line joining the centres of the molecules and their initial relative velocity. For a spherically symmetric potential the mutual force of interaction lies along the line of centres so there is no component of force which can deflect the molecules out of this plane. In the centre of mass frame the trajectories of the molecules are confined to this 'plane of collision' and the angle of deflection is the angle in this plane between the pre- and post-collision relative

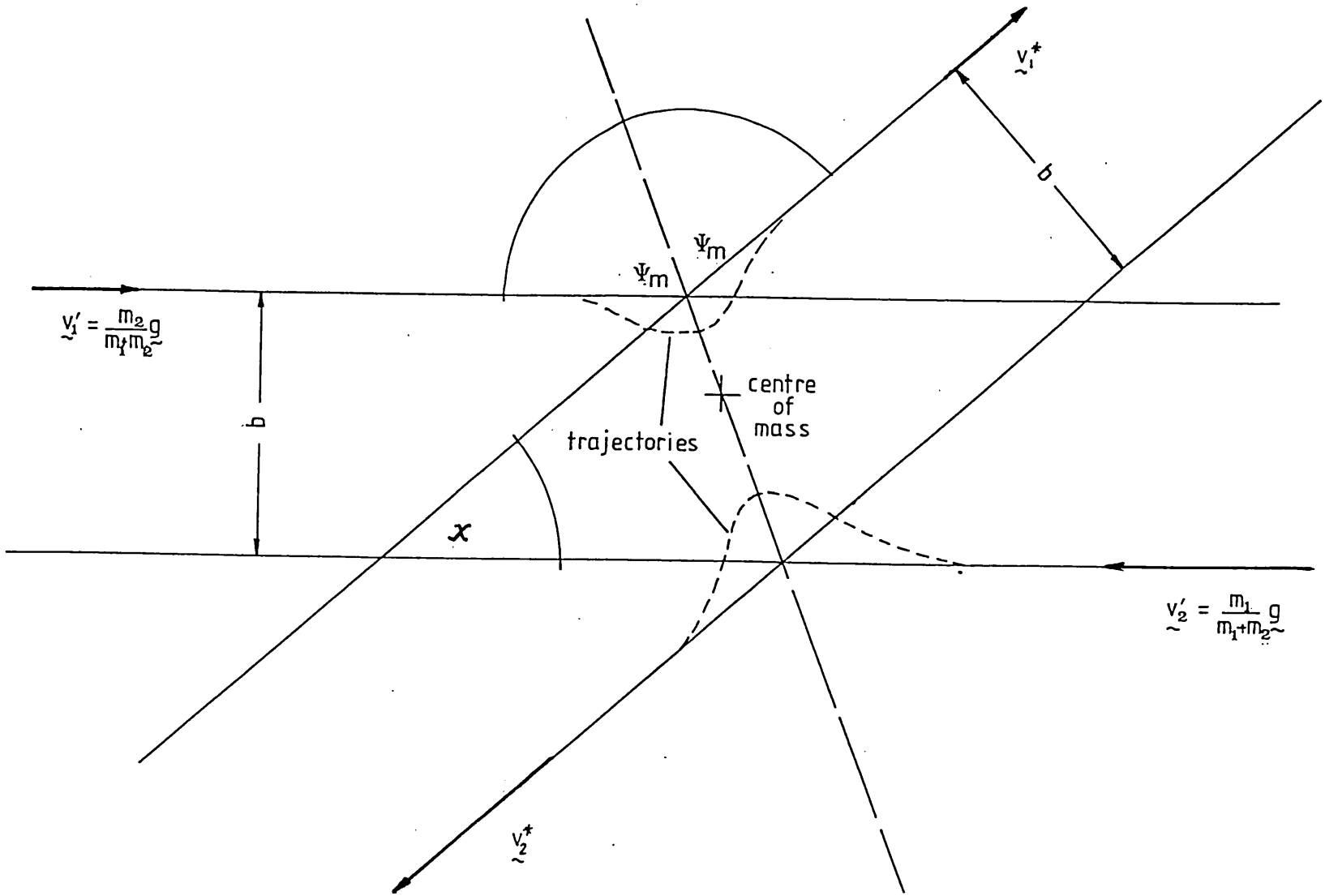


Fig. 4.1 TWO-BODY COLLISION IN CENTRE OF MASS REFERENCE FRAME

velocities. Figure 4.1 shows typical trajectories in this collision plane. The diagram is similar to those in the books by Hirschfelder et al. (1954), Figure 1.5-2, and Bird (1976), Figure 2.2, which treat the two body collision in greater detail.

In the accelerated frame of reference attached to the line joining the centres, the molecules move in the apparent or effective potential

$$e(r) = U(r) + \tfrac{1}{2}m^*g^2(b/r)^2$$

which includes an extra 'inertial ' or 'centrifugal' potential, $\tfrac{1}{2}m^*g^2(b/r)^2$ (Hirschfelder et al. 1954). If Ψ is the angle between the line of centres and the initial relative velocity it can be shown that

$$dr/d\Psi = -(r^2/b)\,[1-e(r)/\tfrac{1}{2}m^*g^2]^{\frac{1}{2}}$$

At the point of closest approach ($r=r_{min}$) this derivative is zero, that is

$$1-e(r_{min})/\tfrac{1}{2}m^*g^2 = 0$$

which is the point where the collision energy is balanced by the effective potential energy. The angle of deflection is related to the angle Ψ_m at the point of closest approach by $\chi=\pi-2\Psi_m$ (see Figure 4.1). Since $\Psi_m = \int_{\infty}^{r_{min}} d\Psi$, we have

$$\chi = \pi - 2b \int_{r_{min}}^{\infty} \frac{dr/r^2}{[1-e(r)/\tfrac{1}{2}m^*g^2]^{\frac{1}{2}}} \qquad (4.1)$$

The post-collision velocities in the laboratory frame of reference can be determined from the angle of deflection and the orientation of the collision plane (see Appendix C).

4.2 The Collision Integrals and Cut-off Cross-Sections

For a given speed ~~and~~ the angle of deflection in a collision decreases as the distance b increases. The collision cross-section was introduced in Chapter 2 and is

$$A(g) = 2\pi \int_0^{b_o(g)} b \, db$$

Unfortunately, for the classical potentials which extend to infinity the deflection angle is finite for all values of b. The collision cross-section and the collision rate are infinitely large. This contradicts the assumptions of the simulation method that the trajectory of a molecule is a series of straight lines with abrupt changes of direction at collisions, and that each collision involves only two molecules. In spite of this we would expect, because the potentials fall off rapidly at large distances, that the error would be small. According to the uncertainty principle of quantum mechanics, however, the angle of deflection will become undefined at large miss distances (Vincenti and Kruger 1965, p. 360) which we may interpret for our purposes as showing that the potentials do not extend infinitely. There is a theoretical justification for defining a cut-off collision cross-section (Bird 1976) and this must also be done to find solutions to the Boltzmann equation itself. The following reflections may help to find a logical way of establishing a cut-off for the classical potentials.

We would expect that not all collisions are equally important in determining the bulk behaviour of the gas. In particular the 'grazing'

collisions which deflect the trajectories an insignificant amount cannot affect the bulk properties of the gas. To find a theoretical cross-sectional area we can weight each elemental annulus $2\pi bdb$ of the cross-section according to the relative importance of the collisions at that miss distance. A suitable weighting function should make the integral $\int_0^\infty$weight (b) b db converge to a finite 'effective' cross-section. For example, we could use the deflection angle itself as the weighting function to obtain

$$A_\chi(g) = 2\pi \int_0^\infty \chi(g,b) b \, db$$

This integral, which we might call the 'deflection cross-section', emphasizes the small values of b and gives a very small cross-section. Probably more important than the deflection itself is the transfer of momentum from one molecule to the other in a collision. It can be inferred from Figure 4.1 that the momentum of each molecule, in the direction of the initial relative velocity, is changed in each collision by an amount proportional to $(1-\cos\chi)$. Weighting the areas by this amount we get

$$A = 2\pi \int_0^\infty (1-\cos\chi)\, b \, db$$

which is called the 'momentum cross-section'. It is a special case of an integral which arises in the Chapman-Enskog transport theory, i.e.

$$Q^{(\ell)}(g) = 2\pi \int_0^\infty (1-\cos^\ell \chi)\, b \, db \qquad (4.2)$$

The transport co-efficients are derived from the cross-sections $Q^{(\ell)}$ through the integrals

$$\Omega^{(\ell,s)}(T) = (kT/2\pi m^*)^{\frac{1}{2}} \int_0^\infty \gamma^{2s+3} Q^{(\ell)}(g) \exp(-\gamma^2) d\gamma \qquad (4.3)$$

where $\gamma^2 = \frac{1}{2}m^*g^2/kT$ (Hirschfelder et al. 1954). Note that the integrals $\Omega^{(\ell,s)}$ are proportional to a weighted average of the cross-sections $Q^{(\ell)}(g)$ over all values of relative speed g. The diffusion integral $\Omega^{(1,1)}$, for example, is a particular weighted average of the momentum cross-section. Since the viscosity integral $\Omega^{(2,2)}$ is derived from $Q^{(2)}(g)$, the latter is known as the 'viscosity cross-section'. The 'higher' cross-sections, those with $\ell > 2$ in Equation (4.2), appear in the higher approximations to the transport properties (Hirschfelder et al. 1954). When we define a cut- off cross-section for our model molecules we should ideally retain the same dependence on the relative velocity as for one (or all, if possible) of these weighted cross-sections.

4.3 Inverse power molecules

The great analytical advantage of the inverse power potential is that the deflection angle may be expressed as a function of a single dimensionless 'impact parameter' z defined by

$$z = b(m^*g^2/\alpha a)^{1/\alpha} \qquad (4.4)$$

The expression for the deflection angle in Equation (4.1) can be reduced to

$$\chi(z) = \pi - 2\int_0^{b/r_{min}} [1-(b/r)^2-2/\alpha(b/rz)^\alpha]^{-\frac{1}{2}} d(b/r) \qquad (4.5)$$

and the cross-sections in Equation (4.2) are

$$Q^{(\ell)}(g) = 2\pi A^{(\ell)}(\alpha a/m^*g^2)^{2/\alpha} \qquad (4.6)$$

where $A^{(\ell)}$ is a dimensionless collision integral given by

$$A^{(\ell)} = \int_0^\infty (1-\cos^\ell \chi) z \, dz \qquad (4.7)$$

Values for the integrals $A^{(1)}$, $A^{(2)}$, $A^{(3)}$ and $A^{(4)}$ for many values of α have been evaluated and are given in Appendix A to four decimal places. These agree where appropriate with the smaller sets given by Chapman and Cowling (1952), Section 10.3, and by Nanbu and Watanabe (1981), (except in one instance mentioned in the Appendix).

4.4 Mean Free Paths

It is useful to evaluate the collision rate from Equation (2.6), and the mean free path from Equation (2.7), in a gas at equilibrium at temperature T, based on the collision cross-section

$$Q_i = K_i \pi (a\alpha/m^* g^2)^{2/\alpha} \qquad (4.8)$$

where K_i is a constant. It is necessary to find the average

$$\langle g Q_i \rangle = \iint_{-\infty}^{\infty} f_o(\underset{\sim}{V}_1) \, f_o(\underset{\sim}{V}_2) \, g Q_i \, d\underset{\sim}{V}_1 d\underset{\sim}{V}_2$$

where f_o is the equilibrium velocity distribution. The method is given by Bird (1976, Section 4.3) and the result for the collision rate is

$$\Theta = n K_i \pi (2a\alpha/m)^{2/\alpha} \, \Gamma(2-2/\alpha) \, (4kT/m)^{\frac{1}{2}-2/\alpha} \qquad (4.9)$$

where we have substituted $m^*=\frac{1}{2}m$ which is appropriate for a gas of identical molecules of mass m. The required mean free path is

$$\lambda_i = \frac{(2kT/a\alpha)^{2/\alpha}}{\sqrt{2}\, n\pi K_i \Gamma(2-2/\alpha)} \qquad (4.10)$$

A nominal mean free path is often quoted which is based on the viscosity of a gas. The viscosity cross-section $Q^{(2)}$ for hard spheres is $2/3\,\pi d^2$ (i.e. $A^{(2)} = 1/3$ for $\alpha=\infty$, see Appendix A)and $\Omega^{(2,2)}$ may be calculated to derive the theoretical viscosity for a hard sphere gas;

$$\mu = \frac{5\pi}{16} d^2 (kT/\pi m)^{\frac{1}{2}} \qquad \frac{5(\pi m k T)^{1/2}}{16\pi d^2}$$

The mean free path from Equation (2.7) for hard sphere molecules with a collision cross-section πd^2 is

$$\lambda = 1/[\sqrt{2} n \pi d^2]$$

(Bird 1976, Equation 1.47) which may be combined with the expression for viscosity to get

$$\mu = \frac{5\pi}{32} mn \langle c \rangle \lambda \qquad (4.11)$$

We follow Pullin (1974) and Bird (1976) in using this expression to define a nominal mean free path for any potential based on the measured viscosity of the gas. From simple considerations of momentum transfer it can be shown that

$$\mu = \tfrac{1}{2} m\, n\, \langle c \rangle\, \lambda\ .$$

Some experimental work which quotes a mean free path or assumes a collision rate uses the simpler expression. The difference in the two expressions is small enough that it may usually be ignored. Combining Equation (4.11) with the expression for the viscosity for inverse power molecules (3.4) we get the nominal mean free path for the inverse power potential

$$\lambda = \frac{\sqrt{2}\ (2kT/\alpha a)^{2/\alpha}}{\pi n\ A^{(2)}(\alpha)\Gamma(4-2/\alpha)} \qquad (4.12)$$

The ratio of the 'actual' mean free path (4.10) to the nominal mean free path (4.12) is

$$\lambda_i/\lambda = \frac{A^{(2)}(3-2/\alpha)(2-2/\alpha)}{2\ K_i} \qquad (4.13)$$

If K_i is equal to a $2\ A^{(2)}$ then the cut-off cross-section is equal to the viscosity cross-section. The free paths λ_i and λ are then based on different weighted averages of the viscosity cross-section for all g and their ratio is

$$(3-2/\alpha)(2-2/\alpha)/4.$$

For hard spheres ($\alpha=\infty$) the ratio is 3/2 which expresses the fact that the viscosity cross-section is only 2/3 the collision cross-section.

4.5 Cut-off Collision Cross-Sections

The usual cut-off cross-section in simulations for these molecules is based on the value of the deflection angle (Bird 1976). Collisions are calculated only if the deflection is greater than a small angle. Since χ is a function of z this means that the cut-off is based on a maximum value of impact parameter, say z_o, which

corresponds to a maximum value of b. The cut-off cross-section which establishes the collision rate in the simulations (or the real gas molecules if they also behaved this way) is thus

$$Q_o = 2\pi \int_0^{b(\chi=\chi_o)} b \, db$$

or, using Equation (4.4)

$$Q_o = \pi \, z_o^2 \, (a\alpha/m^*g^2)^{2/\alpha} \qquad (4.14)$$

which has the same variation with g as the $Q^{(\ell)}$. Since b^2 is randomly chosen for each collision the impact parameter is chosen by

$$(z/z_o)^2 = R_f.$$

It is important to select the cut-off cross-section as small as possible since the collision rate (and hence computation time) increases as the cross-section increases. Moreover the extra collisions, in numbers proportional to $d(z^2)$, are for even smaller values of the deflection angle and so less important in the calculation.

A possible method for establishing z_o , other than by arbitrary choice, is to set $z_o^2 = 2A^{(\ell)}$ so that Q_o is exactly equal to one of the $Q^{(\ell)}$. Since the viscosity cross-section for the hard sphere molecule is only 2/3 the actual cross-section, a cross-section equal to 3/2 $Q^{(2)}$ would be a more logical value. Appendix A shows that for hard sphere molecules $A^{(4)} = A^{(2)}$ ($\therefore$ $Q^{(4)}=Q^{(2)}$) so the cross-section 3/2 $Q^{(4)}$ will be πd^2 . The cut-off deflection angles for the various cross-sections based on multiples of the $Q^{(\ell)}$ cross-sections are shown below.

Table 4.1 Cut-off Deflection Angle (radians)

α	$z_o^2 = 2A^{(1)}$	$2A^{(2)}$	$2A^{(3)}$	$2A^{(4)}$	$3A^{(2)}$	$3A^{(4)}$
3	.7258	.6482	.4879	.4563	.4315	.2872
4	.7330	.7004	.5062	.4935	.4382	.2786
5	.7288	.7545	.5133	.5216	.4386	.2662
6	.7203	.7924	.5152	.5447	.4368	.2528
7	.7103	.8242	.5144	.5647	.4338	.2395
8	.6996	.8521	.5121	.5826	.4307	.2267
9	.6890	.8764	.5090	.5984	.4273	.2142
10	.6789	.8978	.5053	.6131	.4239	.2026
11	.6689	.9168	.5014	.6263	.4204	.1913
12	.6594	.9339	.4975	.6384	.4172	.1807
13	.6537	.9492	.4931	.6485	.4138	.1700
14	.6414	.9633	.4874	.6599	.4109	.1609
32	.5338	1.091	.4284	.7695	.3669	.0519
∞	0	1.459	0	1.287	0	0

These large values of cut-off angle for the soft potentials show that not all collisions which give an appreciable deflection arise from inside these theoretical cross-sections. The cut-off cross-sections in the simulations will have to be larger than these nominal cross-sections.

Probably more important than the absolute value of the deflection angle itself, at least for classical calculations, is the error in the contribution to the momentum or viscosity cross-sections caused by ignoring deflections ~~greater~~ smaller than the cut-off angle. We can define this error as

$$e(z_o, \ell) = 1 - \frac{\int_0^{z_o} (1-\cos^{\ell}\chi) z \, dz}{A^{(\ell)}} \qquad (4.15)$$

Figure 4.2 shows the deflection angle and $\sin^2\chi$ as a function of z for the inverse 13.51th power potential. The area under this latter curve is equal to $2A^{(2)}$ and the error in the viscosity (i.e. for $\ell=2$ in Equation (4.15)) arising from the cut-off is proportional to the area under the curve for $z > z_o$.

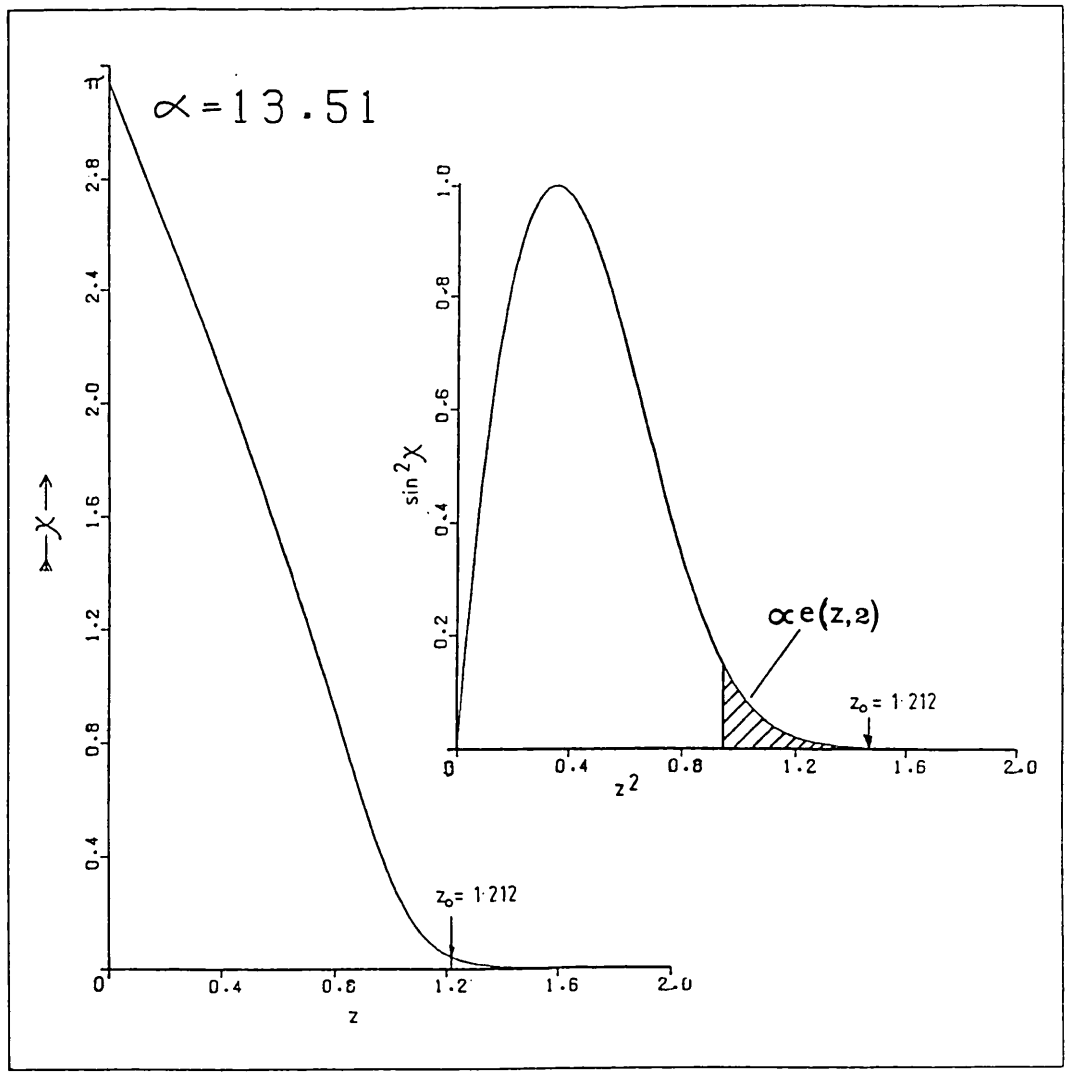


Fig 4.2 DEFLECTION ANGLE FOR INVERSE POWER POTENTIAL

Considering only the largest cut-off cross-section ($z_o^2 = 3A^{(4)}$) the contribution to the momentum transfer and the viscosity cross-sections for those collisions outside the cut-off are

Table 4.2 Error e% from Equation (4.15) with $z_o^2 = 3A^{(4)}$

α	$\ell=1$	$\ell=2$	α	$\ell=1$	$\ell=2$
3	6.00	10.5	9	.60	1.39
4	3.38	6.50	10	.45	1.09
5	2.14	4.40	11	.36	.87
6	1.46	3.14	12	.28	.70
7	1.05	2.36	13	.22	.57
8	.78	1.79	14	.19	.45

These values of error are not very large for the useful values of $\alpha > 8$ but the cut-off angle in simulation computations has usually been chosen as a smaller angle than those above. We can compare these errors (with $\ell = 2$ say) for those arising from the cut-off angles that have been used. For example, Bird (1976) sets the cut-off angle as .032 (e=.05%) for the inverse 8th power potential. For α=13.5 Pullin et al. (1977) have used 0.1 (e=.15%). Nanbu (1980) has tested the effect of cut-off angle (using his slightly different simulation scheme) and found that for relaxation calculations using inverse 4th power molecules there was no difference in the speed distribution function for cut-off angles of .0175 (1°, e = .1%) and .035 (2°, e = .28%). He has also used a cut-off angle of .175 (10°, e = 3.16%) and found, comparing the equilibrium moments up to 4th order, that there was little difference between these results and those for the 1° or 2° cut-off angle (Nanbu 1982a). This result suggests that the cut-off based on $z_o^2 = 3A^{(4)}$ for which the errors in Table 4.2 are less than the 3.16% in Nanbu's calculations might be reasonable. For simulations where there are large departures from equilibrium it seems safer, however, to choose a smaller deflection angle. With 8th and 12th power molecules Nanbu and Watanabe (1981) have used a cut-off angle of .035 (2°, e= .06% and .03%) and they recommend this value. Since the error is not constant for a fixed

cut-off angle for different values of α it would be sensible to choose a maximum allowable error rather than a cut-off angle. Considering all the above it seems that a maximum error based on the viscosity integral equal to .1% would provide a safe upper limit to the deflection angle. The corresponding error in the momentum cross-section is even lower. In all calculations with the inverse 13.51 power potential we have used a cut-off deflection of .05 radians (2.75°) which corresponds to $z_o = 1.212$ and an error of .06% in the theoretical viscosity.

It is impractical to solve Equation (4.5) for χ for each collision and approximate methods must be used. Bird (1976) gives a polynomial for $\chi(z)$ for an 8th power, Nanbu and Watanabe (1981) use a polynomial fitted to calculated values of $\chi(z)$. The method at Imperial College has been to store the function $\chi(z)$ for 200 intervals of z from 0 to z_o. The curve in Figure 4.2 is made up from only 100 straight segments in this interval and it is clear that a linear interpolation is very accurate.

4.6 New Approximate Collision Models

It can be seen in Figure 4.2 that the curve for the deflection angle for the inverse 13.51th power potential is reasonably close to a straight line up to quite a large value of z. Since the collisions above a certain value of z are assumed to be unimportant (and excluded by quantum restrictions) an approximation to the inverse power molecule is proposed in which the deflection curve is replaced by a straight line

$$\chi = \pi(1-z/z_o) \qquad (4.16)$$

where z is given by Equation (4.4) and α and a are constants which define the collision model. Clearly this model, which we have called the 'linear inverse power' (LIP) model has some computational advantages. Notice that it has a cut-off deflection angle of zero and has a finite cross-section given by

$$Q_o = z_o^2 \pi (a\alpha/m^*g^2)^{2/\alpha} \qquad (4.17)$$

Can we expect that this model, will reproduce the relevant bulk behaviour of the gas as well as the inverse power potential, even though the scattering does not arise from any classical potential?

The Chapman-Enskog theory shows that the transport properties depend on the potential only through the collision integrals, that is, through the distribution of scattering angles in collisions. The collision integrals account for the average behaviour of the molecules over all collisions and the fine details are apparently unimportant in this theory which considers small departures from equibrium. That the model might work well was suggested by the following experience. While calculating the structure of a plane shock using the inverse 13.51th power potential, we accidently selected the deflection angle, when χ (the correct deflection angle) was in the range $\pi/2$ to π, as $\chi' = \pi - \chi$. Instead of the deflection being in the range 0 to π, it was restricted to the range 0 to $\pi/2$. Surprisingly this 'accidental' collision model, which is much further removed from a real potential than our approximate model, gave results that looked perfectly reasonable and similar to other calculations using the correct potential. Since $\cos\chi' = -\cos\chi$ in the range $\pi/2 < \chi < \pi$ the cross-sections $Q^{(\ell)}$ (ℓ=2,4 ..) are identical for the two models but the 'odd' cross-sections $Q^{(\ell)}$ (ℓ=1,3 ...) are not. The ratio of the momentum cross-section for this model, $Q^{(1)'}$,

to the momentum cross-section of the inverse power potential

$$R(\alpha) = Q^{(1)'}/Q^{(1)} \quad (\text{for } Q^{(2)'} = Q^{(2)}_{I.P.})$$

is a measure of the difference between collision models which have the same theoretical viscosity. In this case the 'momentum ratio' was approximately 0.60. This suggests that collision models with the same theoretical viscosity might give similar results even though their momentum cross-sections are different. This is a reassuring conclusion since the form of the potential has always been selected to match the viscosity (rather than the diffusion) of real gases.

For the linear model the integrals $A^{(\ell)}$ are, from Equation (4.7),

$$A^{(1)} = \left(\frac{1}{2} - \frac{2}{\pi^2}\right) z_o^2$$

$$A^{(2)} = z_o^2/4$$

$$A^{(3)} = \left(\frac{1}{2} - \frac{14}{9\pi^2}\right) z_o^2$$

$$A^{(4)} = \frac{5}{16} z_o^2$$

If we set $A^{(2)}$ for this model equal to $A^{(2)}$ calculated for the inverse power potential, the two models have the same viscosity cross-section when the values of a and α are the same. This sets the cut-off impact parameter

$$z_o^2 = 4A^{(2)}_{I.P.}$$

Figure 4.3 shows the deflection angle as a function of z for the inverse power potential for a range of α compared with the linear approximation which gives the same viscosity. It is apparent that for α in the range 8 to 14 (which is appropriate for most gases) that the linear approximation is quite close to the actual deflection angle. The

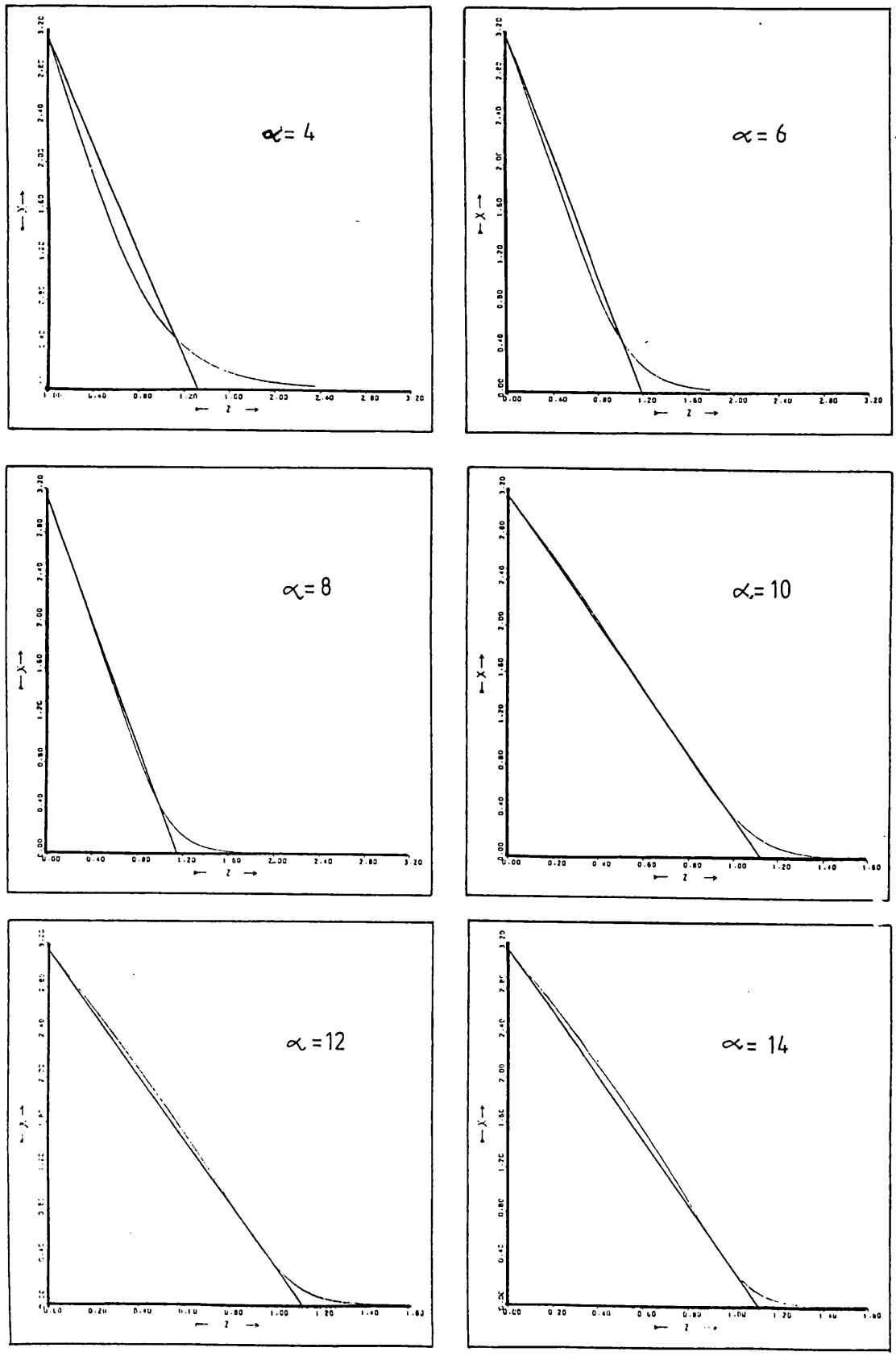


Fig. 4.3 DEFLECTION ANGLE CURVES - INVERSE POWER AND LIP APPROXIMATION.

momentum ratio R(13.51) for this LIP model is 0.94. Since $z_o^2 = 4A^{(2)}$ the collision cross-section, given by Equation (4.17), is exactly twice the viscosity cross-section, given by Equation (4.6). Like the inverse power potential the collision cross-section is not the same as the viscosity cross-section or the momentum cross-section.

To test further whether it is more important to match viscosity or momentum cross-sections we sought an approximate collision model where the relative values of the $A^{(\ell)}$ are different. A natural choice was a collision model where the scattering was determined by the simple hard sphere potential but the total cross-section $\pi d^2(g)$ was the same function of relative velocity as for the LIP model. Thus

$$\pi\, d^2(g) = \pi\, z_o^2 \quad (a\alpha/m^*g^2)^{2/\alpha} \,.$$

This 'variable diameter hard sphere' has been independently proposed by a number of authors in a variety of forms (see Chapter 2) and we follow Bird (1981) in calling it the VHS model. For hard spheres the deflection angle is easily calculated from geometric considerations as

$$\chi = 2 \arccos (b/d)$$

or, substituting for d and using Equation (4.4),

$$\chi(z) = \arccos (z/z_o) \qquad (4.18)$$

The collision integrals are

$$A^{(1)} = \tfrac{1}{2} z_o^2$$

$$A^{(2)} = \tfrac{1}{3} z_o^2$$

$$A^{(3)} = \tfrac{1}{2} z_o^2$$

$$A^{(4)} = \tfrac{2}{5} z_o^2$$

Again we can select z_o by matching the viscosity to the inverse power potential so that

$$z_o^2 = 3A^{(2)}_{I.P.}$$

Like the hard sphere molecule, the VHS model has a momentum cross-section equal to the actual cross-section for all values of g. The momentum ratio R(13.51) is 1.18. The deflection curve for this model is compared in Figure 4.4 with the LIP and the inverse power potential for a high value of α.

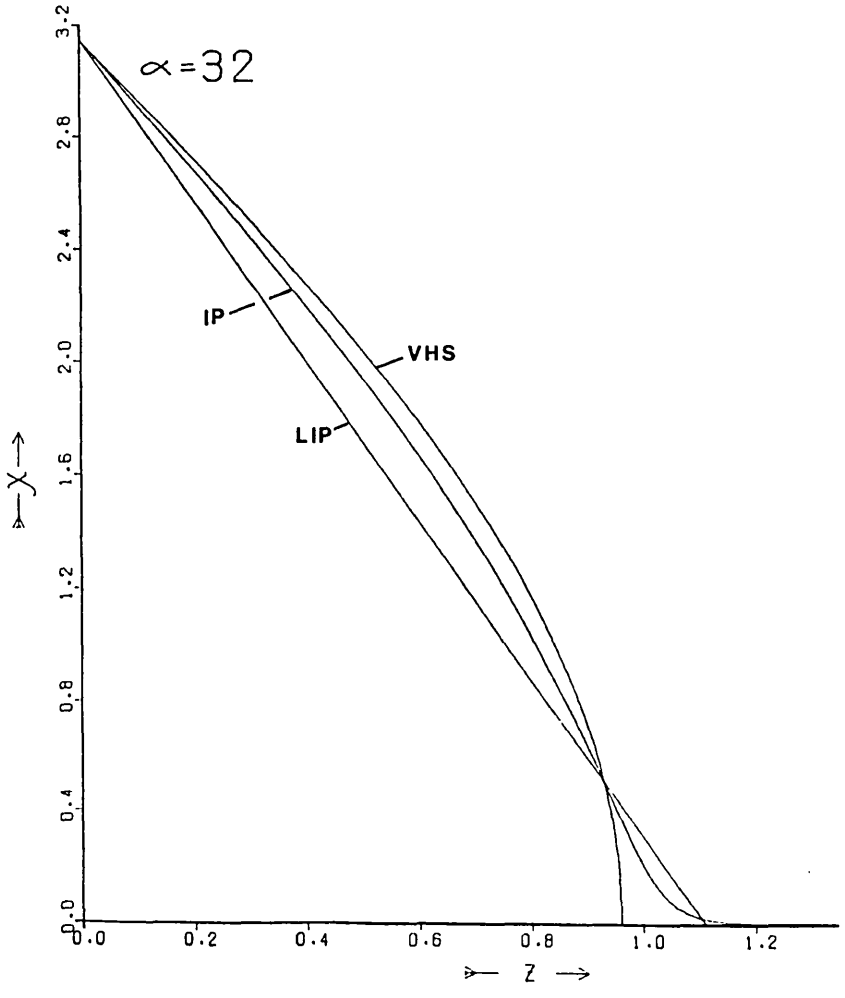


Fig. 4.4 DEFLECTIONS FOR THREE COLLISION MODELS

It is evident, by comparing these curves with those in Figure 4.3, that as α increases the scattering from the inverse power potential approaches that from this variable diameter hard sphere.

Another invented model which we have used has the deflection angle given by

$$\chi = \pi(1 - (z/z_o)^2)$$

which is particularly simple in that, since $(z/z_o)^2$ is randomly selected for each collision, the deflection angle may be selected as

$$\chi = \pi R_f \tag{4.20}$$

The collision integrals for this model are

$$A^{(1)} = \tfrac{1}{2} z_o^2$$
$$A^{(2)} = \tfrac{1}{4} z_o^2$$
$$A^{(3)} = \tfrac{1}{2} z_o^2$$
$$A^{(4)} = \tfrac{5}{16} z_o^2$$

so that by matching viscosity it has the same cross-section as the LIP model. This also has a momentum cross-section equal to the cut-off cross-section and the momentum ratio R(13.51) is 1.58.

Unknown to the author Krook and Wu (1977) had used a collision model which turns out to be the same as this model with $\alpha = 4$. They refer to it as an 'isotropic scattering' model since the deflection in the collision plane is isotropic. This is not the same as isotropic scattering in three dimensions in the centre of mass frame arising from the hard sphere collision model. We will use their term and refer to it as the ISO model. They found a particular solution to the Boltzmann equation but it seems that they have not so far found any

solutions corresponding to different values of α. They do however extend the solution to any distribution of the deflection angle in the collision plane and find the different relaxation rate for the different scattering. All the collision models presented here correspond with $\alpha = 4$, to their arbitrary collision models.

To assess whether or not it is necessary to model accurately the collision process we have tested as an extreme case a model which has only one single angle of deflection χ_c in every encounter.

The collision integrals are given by

$$A^{(\ell)} = (1 - \cos \ell \chi_c) \ \tfrac{1}{2} z_o^2$$

A cut-off cross-section must be chosen arbitrarily. By selecting the cross-section the same as the VHS model we find that $\chi_c = 54.74^\circ$ or 125.26° will give the same viscosity as the inverse power molecule (or VHS model). The momentum ratios R(13.51) are 0.42 and 1.60 respectively.

In Chapter 7 we use these collision models to determine the structure of a plane shock and are able to assess the relative importance of the viscosity and momentum cross-sections.

CHAPTER 5

COLLISION MODELS - II

5.0 Introduction

In this chapter we consider the Morse potential and the phenomenological exchange schemes of Borgnakke and Larsen. The variable-ϕ extension of these methods, developed by Pullin and Davis (Davis 1978), modifies the phenomenological description of the exchange process in an attempt to retain some features of a 'realistic' collision model. Davis (1978) has shown that this collision model, combined with the Morse potential, gives good results for the leading edge flat plate flow (see figure 3.3(a)).

It does have some disadvantages however. The deflection angle for the Morse potential must be pre-calculated and stored in an array as a function of b and g. Consequently there is an unsatisfactory and arbitrary cutoff on the range of relative velocities for which a collision can be calculated (Pullin and Harvey 1976). Secondly, the statistical exchange schemes had not been combined with the Morse potential in the most appropriate manner. The statistical models are derived for the inverse power potential and apparently it was assumed that they could be transferred directly to the Morse potential. This was not true and as a consequence the departure from equipartition at equilibrium will be greater for the Morse potential compared to the inverse power potential.

Since the Morse potential, variable-ϕ combination in its original form has often been used we have tested its relaxation behaviour to determine the difference between it and the inverse power potential, variable-ϕ combination. In doing so we discovered some errors in the

derivation of the equation itself. They are not large and the approximate nature of the model itself probably makes them even less important. However, the dimensional variable-ϕ equation was derived for a particular choice of the constant a and α which define the inverse power potential. If the method is to be used with different constants, to match viscosity for a different temperature range perhaps, then it must be rederived. It is useful therefore to review the method.

5.1 Scattering Cross-Section for the Morse Potential

Figure 5.1 shows the deflection angle for various values of b^* ($= b/\sigma$) and $g^*(=g\sqrt{(}m/4kT')^{\frac{1}{2}})$ calculated by Pullin (1974). For low energy collisions the particles may be held in a mutual orbit by the

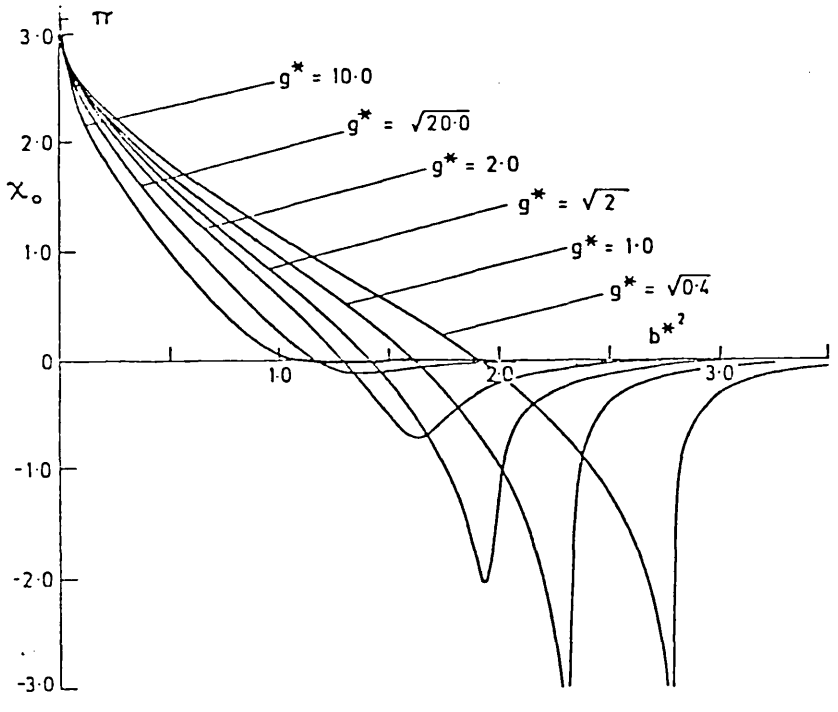


Fig. 5.1 MORSE POTENTIAL DEFLECTION ANGLE (PULLIN 1974)

attractive force, giving a negative singularity in the deflection angle at a particular miss distance. For large values of b the

deflection tends towards zero and a cutoff collision cross-section πb_o^2 must be defined. The deflection angle for a range of b^{*2} from 0 to $b_o^{*2}(g)$ can be calculated and stored as one row of the deflection array $\chi(g^*, (b/b_o)^2)$ and the deflection for any b and g is found by a simple interpolation. The interpolation across the singularity arbitrarily truncates the negative deflection angle. The bounds on the relative velocity for which deflection angles are stored are g_{min} and g_{max}.

Originally the program ignored collisions outside the range of the array. It is relatively safe to ignore low energy collisions since these are extremely rare and presumably unimportant, since little energy or momentum is available to be redistributed, but it can be seriously wrong to ignore higher relative velocities. A high velocity particle may be continually rejected for collisions since its velocity relative to other particles is greater than g_{max}. These high energy particles will continue unimpeded until, perhaps, they hit a surface, distorting the heat transfer and drag to that surface. It is precisely these particles which should have the greatest probability of collision. One way to avoid this problem is to make the value of g_{max} so large that no collisions are ignored. For the flat plate flow Pullin (1974) used $g^*_{min} = 0.1$ and $g^*_{max} = 10.0$ and few collisions were ignored. However for blunt body flows, where many particles are reflected back into the approaching stream, collisions at very high velocities are more frequent. Since the operator may have little prior knowledge of the details of the flow field, g_{max} has to be set arbitrarily higher. Extending the range of g will increase the amount of storage needed for the deflection array if the same accuracy is to be achieved.

Another approach is to take advantage of the similarities between the high energy scattering for the Morse and inverse power potentials. These similarities are accentuated by plotting the Morse deflections as a function of the dimensionless impact parameter z which completely collapses the inverse power deflection curves. The curves $\chi(g^*,z)$ for

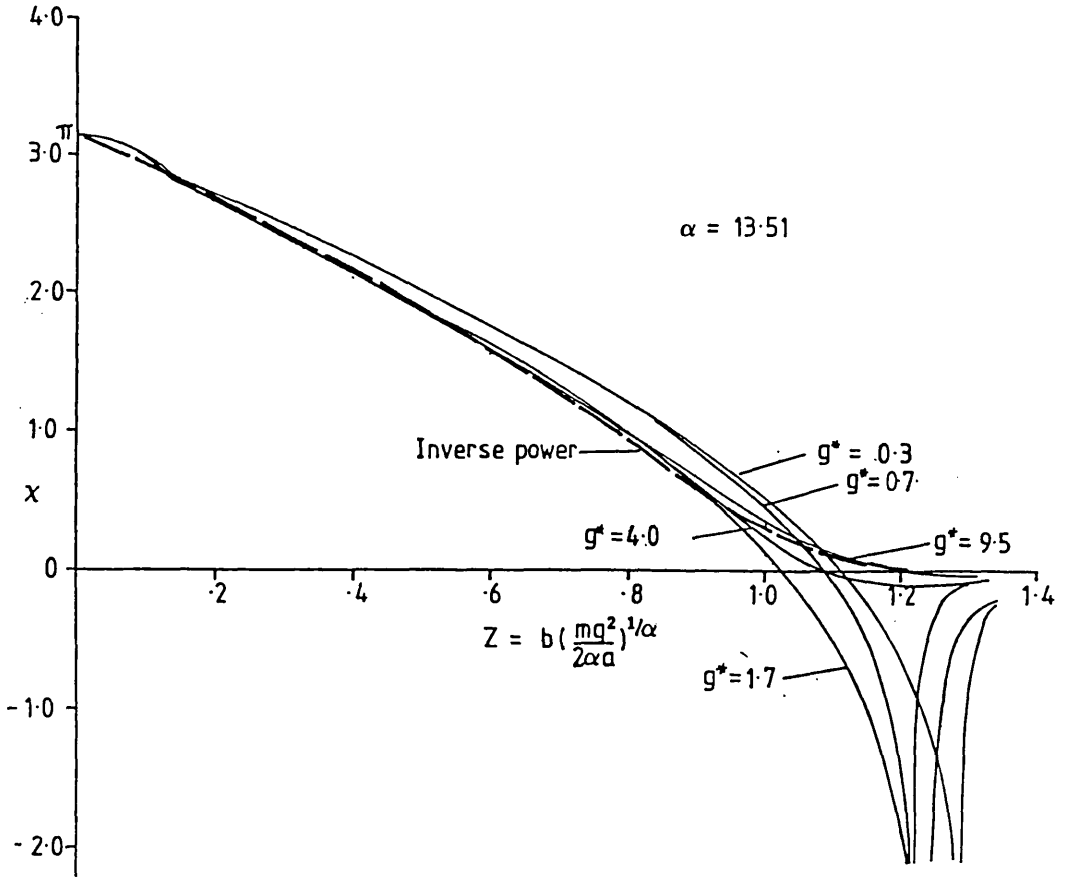


Fig. 5.2 DEFLECTIONS FOR MORSE AND INVERSE POWER POTENTIALS

the Morse potential are shown in figure 5.2. The constants a and α are those which gave a good fit with the nitrogen viscosity at high temperatures. At high relative velocities the deflection angle as a function of z is almost independent of g and is similar to the deflection curve for the inverse power potential. The row of the deflection array for g_{max} can be used with small error to calculate the deflection angle as a function of z. The row for g_{min} can be used, with less accuracy, to calculate the relatively rare collisions for which $g < g_{min}$.

A maximum impact parameter of z = 1.386 is used to define the collision cross-section for the Morse potential. It can be seen from figure 5.2 that this includes the large negative deflections which must be included if this potential is preferred to the inverse power. The cutoff deflection angle is not constant and it is slightly larger than that for the inverse power potential for the very low energy collisions. With the collision cross-section for the Morse potential based on the dimensionless impact parameter it is possible to make the collision selection routines identical for the inverse power and Morse potential. Appendix B gives details of this and the method of advancing the collision time counters.

5.2 Statistical Exchange Schemes

We consider first the inelastic part of the two-class exchange scheme (Borgnakke and Larsen 1975) in which the post-collision energies are distributed according to the local centre of mass equilibrium distribution. In order that the statistical exchange schemes satisfy the detail balance condition, the distribution of the pre-collision relative velocities at equilibrium must be that arising from a variation of the collision cross-section proportional to $1/g^{1-4/\alpha}$. The total pre-collision internal energy is $e_I = e_1 + e_2$ where e_1 and e_2 are the internal energies of the two particles stored in ξ degrees of freedom in each particle. The post-collision internal energy is, using Pullin's (1975) notation,

$$e_I' = s_2 e_{cm} \tag{5.1}$$

where $e_{cm} = e_t + e_I$, $e_t = \frac{1}{4}mg^2$ and s_2 is a random fraction chosen from the beta distribution with indices $i = \xi$ and $j = 2 - 2/\alpha$. The beta distribution is defined by

$$dB[s/i,j] = s^{i-1}(1 - s)^{j-1} ds / B[i,j]$$

where B[i,j] is the beta function $\int_0^1 x^{i-1}(1-x)^{j-1}dx$. The total post collision internal energy is divided between the two particles as

$$e_1' = s_1 e_I' \text{ and } e_2' = (1 - s_1)e_I' \tag{5.2}$$

where s_1 is chosen from the beta distribution with indices $i = j = \xi/2$. The post-collision translational energy follows from the conservation of energy.

When Pullin used this exchange shceme in his hybrid model he used the same indices $i = 2$, $j = 2 - 2/13.5$ which were used with the inverse power potential. The hybrid model incorporated a constant inelastic cross-section $\pi\sigma^2$ so the distribution of energy in the inelastic collisions at equilibrium is not the same as the distribution of energy in all the collisions, since the latter distribution depends on the variable total collision cross-section. Thus the 'statistical fraction' of the inelastic collisions, like the 'classical fraction', cannot satisfy the principle of detail balance.

5.3 Restricted Exchange

The restricted exchange scheme (Larsen and Borgnakke 1974) was based on the inelastic collision defined in equations (5.1) and (5.2). A fraction $1 - \phi$ of the pre-collision energy is 'frozen' and the remaining fraction is distributed between translational and internal energies. The total post collision internal energy is given by

$$e_I' = (1 - \phi)e_I + s_3\phi\, e_{cm} \tag{5.3}$$

The post-collision energies are selected from the equilibrium distribution of these quantities as though the number of degrees of freedom were reduced to the fraction ϕ of the normal values; that is, s_3 is chosen from the beta distribution with indices $i = \phi\xi$ and $j = \phi(2 - 2/\alpha)$. The internal energy is distributed between the two

particles according to equation (5.2) and the translational energy is calculated such that energy is conserved.

Pullin (1975) has shown that this model does not satisfy the principle of detail balance. The relative speed is changed to g' by an inelastic collision and the total number of collisions with relative speed g is different from the total number of collisions with speed g'. To make the forward and inverse collision rates equal the amount of energy available for transfer must be slightly different for the forward and inverse collisions to compensate for the different total collision rates. Perhaps the condition is expressed best by saying that the 'area' of internal energy space (surrounding the point e_I) in which the point e_I' can lie must be different for the forward and inverse collisions so that the density of scattered points is the same in each direction. Since the amount of energy exchanged is usually small ($g' \doteqdot g$), the error in detail balance in the original scheme should be small, but it may show up as a failure to achieve equipartition at equilibrium.

Pullin (1975) found a corrected version satisfying detail balance in which the post-collision internal energy is given by

$$e_I' = (1 - s_I)e_I + s_3 e_{act} \tag{5.4}$$

where s_3 and the division into e_1' and e_2' are the same as before. The 'active' energy available for exchange is not the constant ϕe_{cm} as before but

$$e_{act} = s_t e_t + s_I e_I \tag{5.5}$$

The fractions s_t and s_I are chosen from the beta distributions with indices $i = (2 - 2/\alpha)$, $j = (1 - \phi)(2 - 2/\alpha)$ and $i = \phi\xi$, $j = (1 - \phi)\xi$ respectively.

By analogy with Parker's diatomic molecule an inelastic cross-section smaller than the total cross-section was defined for the phenomenological schemes (Pullin, Davis and Harvey 1977). For the inverse power potential no exchange of energy was calculated if $z > 1$. This inelastic cross-section has the same dependence on g as was assumed in the derivation of equation (5.1). Thus, at equilibrium, the pre-collision distribution of energies in inelastic collisions will be the same as the post-collision distribution of energies in these collisions and the principle of detail balance will be satisfied as far as possible.

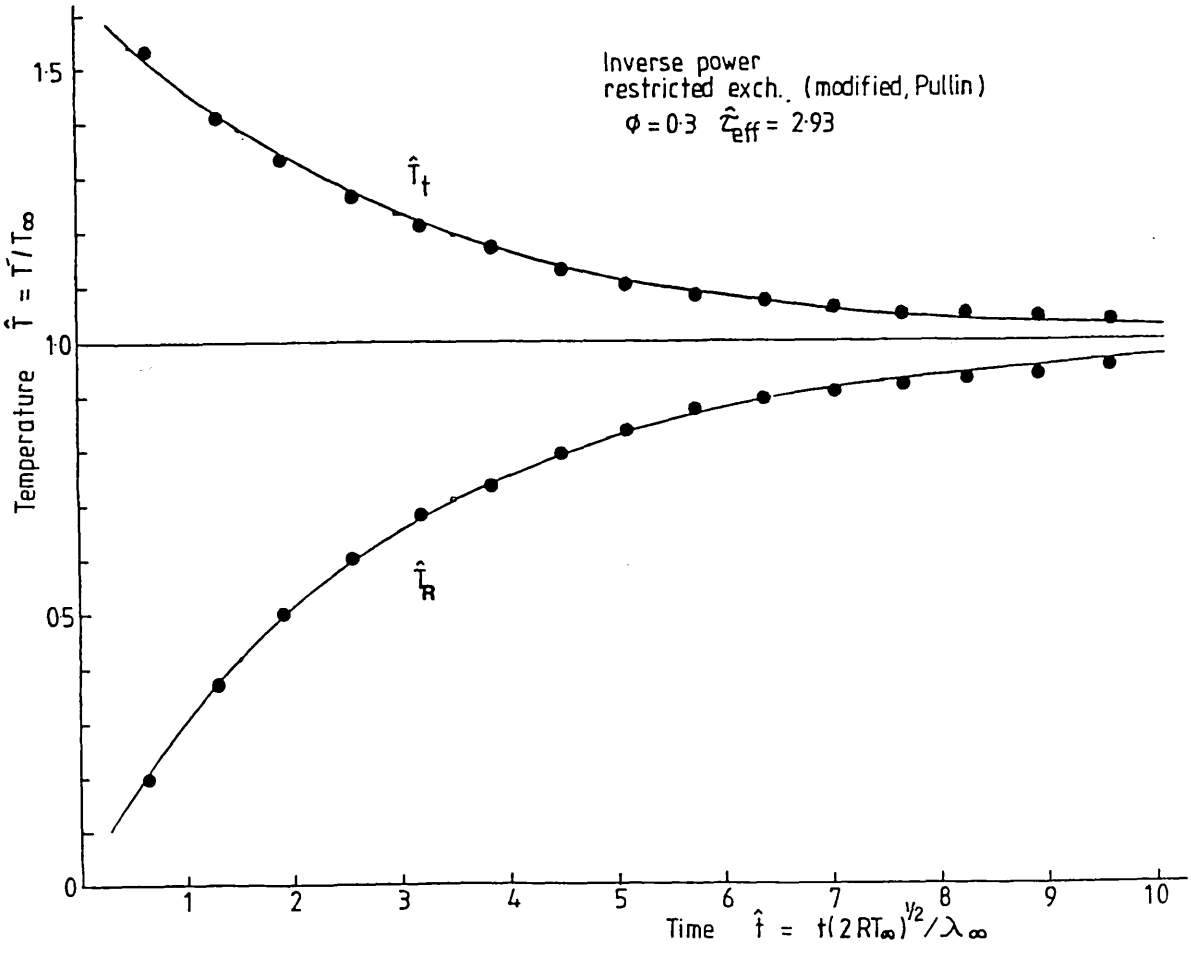


Fig. 5.3 CONSTANT ϕ RELAXATION TEST

Figure 5.3 shows a typical result for the rotational relaxation with this modified restricted exchange scheme and a constant value of ϕ. Initially the particles have no rotational energy and the same

speed with the velocity vectors randomly distributed over the unit sphere. Both the translation temperature T_t and the rotational temperature T_R approach an equilibrium temperature T_∞ according to the relaxation equation

$$(T_t - T_R) = (T_t - T_R)_{initial} \exp(-t/\tau_{eff}) \qquad (5.6)$$

The relaxation time τ_{eff} is only 3/5 the relaxation time τ required for the rotational temperature alone to approach a constant equilibrium temperature (Herzfeld and Litovitz 1959).

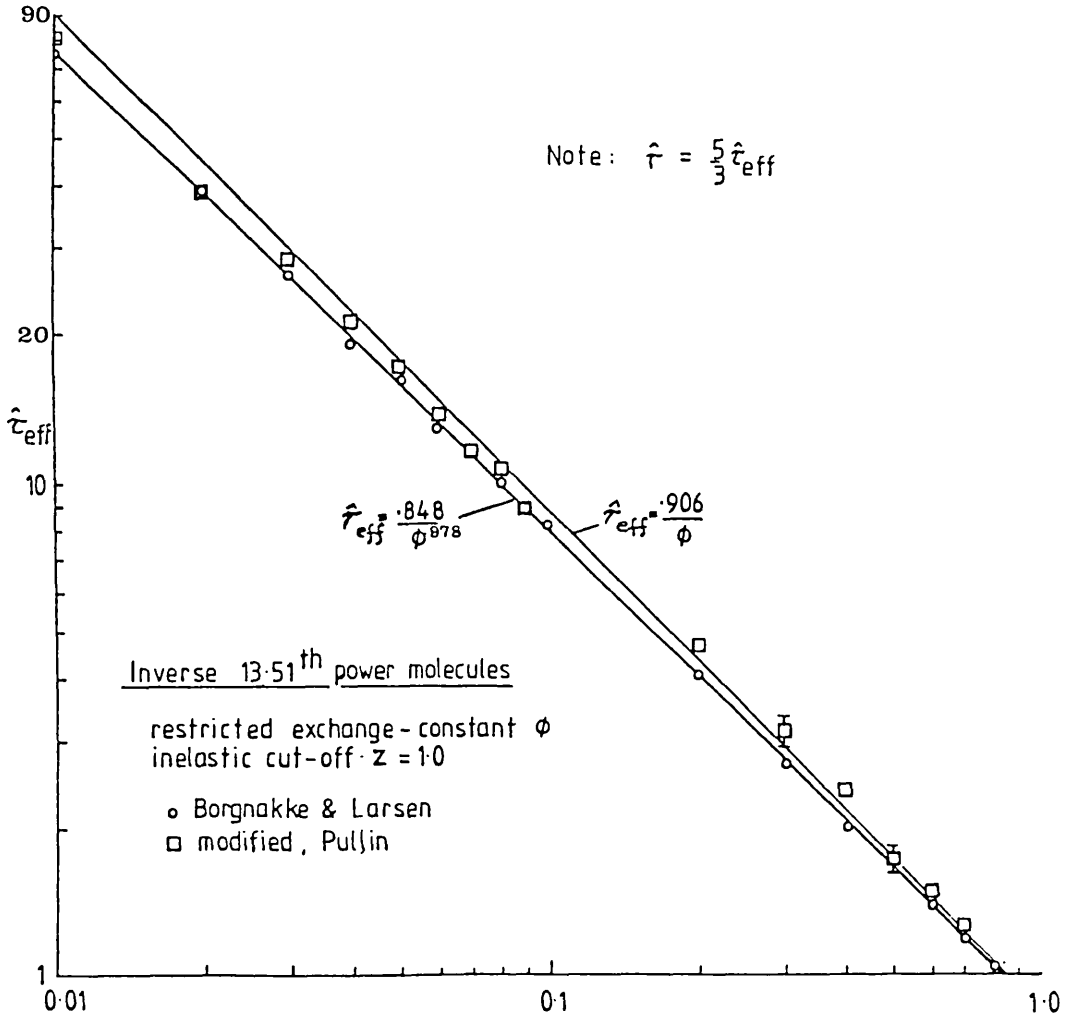


Fig. 5.4 RELAXATION RATE FOR CONSTANT ϕ

By fitting a curve of the form of (5.6) to the simulation results for constant ϕ the function $\tau_{eff}(\phi)$ can be determined. Figure 5.4 shows the normalised effective relation time $\hat{\tau}_{eff} = \tau_{eff}(2RT)^{\frac{1}{2}}/\lambda$ as a function of ϕ. The results for the original scheme are well fitted by the equation

$$\hat{\tau}_{eff} = 0.848/\phi^{0.978} \qquad (5.7)$$

Pullin (1975) found there was little difference between the relaxation rates for the original and the corrected versions of the restricted exchange scheme when he used hard sphere cross-sections. There is also little difference for these calculations.

The rotational collision number Z_R is the average number of collisions per molecule in the relaxation time τ, given by

$$Z_R = 4\tau p/\pi\mu \qquad (5.8)$$

where a collision rate based on the viscosity of the gas has been used. The experimental values of Z_R are derived, indirectly, from relaxation times and the measured viscosity of the gas. This viscosity is not necessarily the same at all temperatures as the theoretical viscosity used to normalise the simulation relaxation time (see figure 3.1).

5.4 Empirical Derivation of Variable-ϕ Equation

To reproduce the variation of Z_R with temperature measured for nitrogen by Carnevale et al. (1967) and shown in figure 3.6, Pullin and Davis (Davis 1978) proposed that the value of ϕ should vary for each collision. Pullin (1975) showed that his corrected exchange scheme would still satisfy detail balance if ϕ was a function of any property which was the same for the forward and inverse collisions. The centre of mass collision energy is one such invariant and the deflection angle is another. For the inverse power potential with energy exchange imposed, the deflection angle is a function of z which is thus the same for the inverse and forward collisions. As a first step then they proposed that ϕ vary with e_{cm} and the inelastic

cross-section $z < 1$ was used. Since the average collision energy varies with temperature the average value of ϕ and hence the relaxation rate will also vary with temperature.

We have reduced the experimental results of Carnevale et al. (1967) to values of τp, using the viscosity of nitrogen used by the experimenters, and the results are summarised in Table 5.1 and are shown in Figure 5.5.

Table 5.1 Relaxation Data
(from Carnevale et al. 1967)

T(K)	Z_R	$\mu \times 10^5$ kg/ms	$\tau p \times 10^5$ kg/ms
300	4.45	1.786	6.24
400	5.48	2.199	9.46
500	6.51	2.570	13.14
600	7.28	2.913	16.66
700	8.09	3.212	20.41
800	8.77	3.490	24.04
900	9.42	3.752	27.76
1000	9.97	4.000	31.32
1100	10.53	4.233	35.00
1200	11.04	4.454	38.62
1300	11.56	4.663	42.15

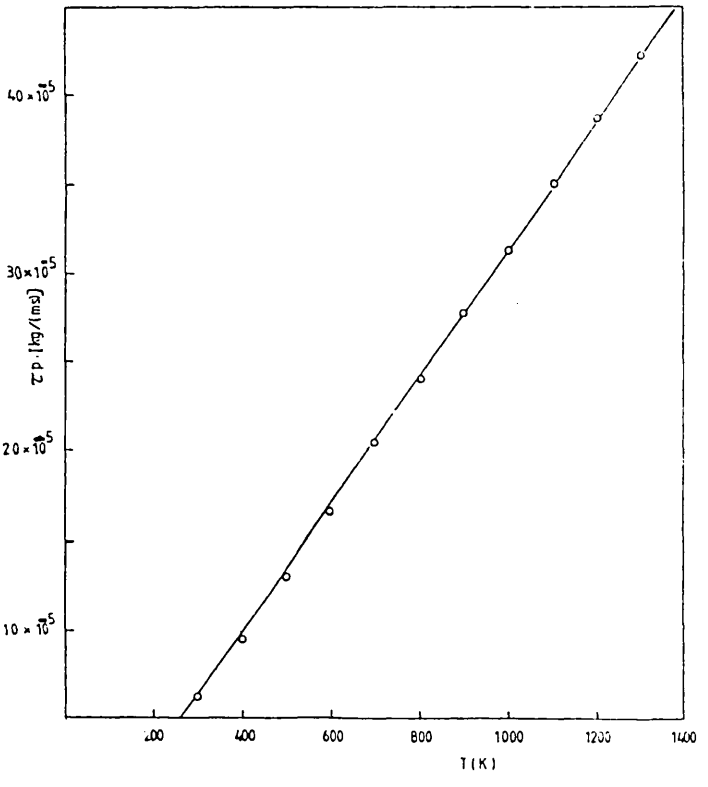


Fig. 5.5 ROTATIONAL RELAXATION TIME FOR NITROGEN

These results are closely fitted by a straight line

$$\tau p = (0.03586T - 4.518) \times 10^{-5} \text{ kg/ms} \qquad (5.9)$$

The value of τp in the relaxation calculations is derived from the measured values of $\hat{\tau}_{eff}$ as

$$\tau p = \frac{5}{3} \hat{\tau}_{eff} p\lambda/(2RT)^{\frac{1}{2}}$$

Expressing the time unit $\lambda/(2RT)^{\frac{1}{2}}$ in terms of the theoretical viscosity for the inverse power potential $\mu(IP) = \mu_o(T/T_o)^{\frac{1}{2}+2/\alpha}$, where the μ_o is a reference viscosity at T_o, we get

$$\tau p = 8/(3\pi^{\frac{1}{2}})\tau_{eff}(T/T_o)^{\frac{1}{2}+2/\alpha}$$

The high temperature ($\alpha = 13.51$) theoretical viscosity shown in figure 3.1 passes through the point ($T_o = 300K$, $\mu_o = 1.786 \times 10^{-5}$ kg/ms). Thus

$$\tau p = .0566T^{0.648}/\phi^{0.978} \times 10^{-5} \text{ kg/ms}$$

which in conjunction with equation (5.9) yields

$$\phi^{0.978} = \frac{.0566T^{0.648}}{0.0358T - 4.518} \qquad (5.10)$$

If ϕ is a function $\phi(e_{cm})$ the average value $\langle\phi\rangle$ at a particular temperature will be approximately equal to $\phi(\langle e_{cm}\rangle)$ where $\langle e_{cm}\rangle$ is the mean collision energy in a gas at equilibrium at temperature T. The relaxation rate at this temperature should be given approximately by $Z_R(\langle\phi\rangle)$ where $Z_R(\phi)$ is derived for constant ϕ.

The distribution of the centre of mass energy in collisions in an equilibrium gas is given by Borgnakke and Larsen (1975) in the derivation of the statistical exchange schemes. The probability of a pair of values e_t and e_R is given by (see also Bird 1976, p.184)

$$f(e_t, e_R)de_t de_I \propto (1/kT)^{4-2/\alpha} e_t e_I \exp[-(e_t+e_I)/kT]de_t de_I$$

where $f(e_t,e_I)$ is the joint distribution function. Since $e_{cm} = e_t + e_I$ we can eliminate e_I, integrate over all values of e_t from 0 to e_{cm} and normalise so that $\int_0^\infty f(e_{cm})de = 1$, to get the distribution function for e_{cm} as

$$f(e_{cm}) = (e_{cm}/kT)^{3-2/\alpha} \exp(-e_{cm}/kT)/\Gamma(4-2/\alpha).$$

The average value of e_{cm} is

$$\langle e_{cm} \rangle = \int_0^\infty e_{cm} f(e_{cm}) de_{cm} = (4-2/\alpha)kT \qquad (5.11)$$

Since energy is normalised against $2KT_\infty$ in the calculations we may substitute $T = \hat{e}_{cm}T_\infty/(2-1/\alpha)$, where $\hat{e}_{cm} = e_{cm}/2KT_\infty$, into equation (5.10) to obtain the variable-ϕ equation (for $\alpha = 13.51$)

$$\phi^{0.978} = (\hat{e}_{cm}T_\infty)^{0.648}/(.503\ \hat{e}_{cm}T - 122.04)$$

In view of the empirical nature of these results the equation may be simplified to

$$\phi = (\hat{e}_{cm}T_\infty)^{0.648}/(0.5\ \hat{e}_{cm}T - 122) \qquad (5.12)$$

If $\phi > 1.0$, a completely inelastic collision is calculated.

5.5 Rotational Relaxation Tests for a Variable-ϕ Collision Model

In figure 5.6 the speed distributions near equilibrium derived from relaxation calculations using both the original and corrected version of the restricted exchange schemes, are compared with the Maxwellian distribution. As Davis (1978) has found, the restricted exchange scheme gives a reasonable approximation to the correct equilibrium distribution. As expected, the distribution for the corrected scheme is slightly closer to the theoretical distribution.

Figure 5.7 shows a typical temperature history of a variable-ϕ

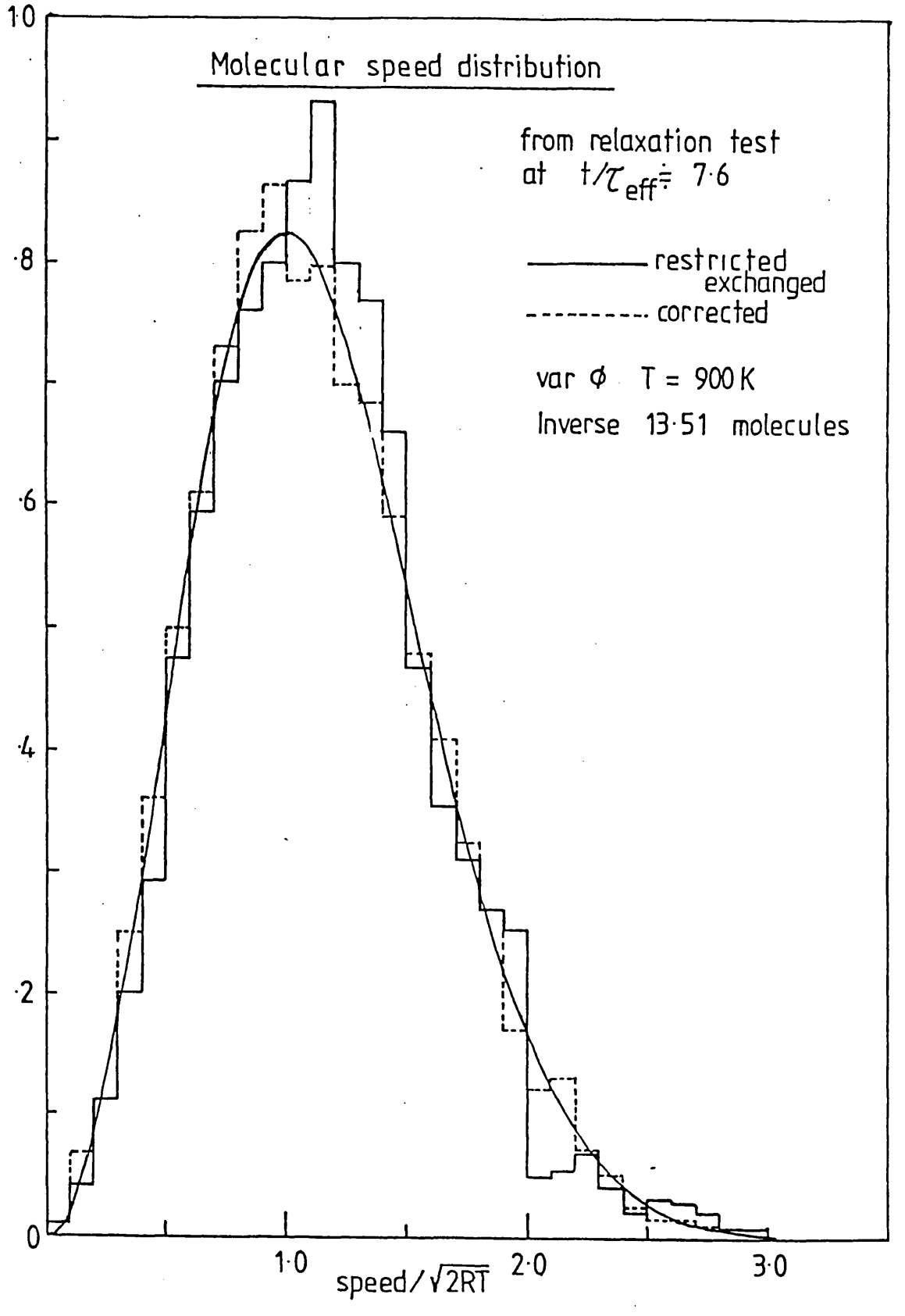


Fig. 5.6 NEAR-EQUILIBRIUM DISTRIBUTION OF MOLECULAR SPEED FOR TWO VARIABLE-ϕ COLLISION MODELS

relaxation calculation. Also shown is the average value of ϕ which changes during the simulation, making it difficult to fit an exponential curve to the results. A family of exponential curves, each of which has a different relaxation constant, passes through any chosen data point. Newton's method may be used to find the member of the family which gives the best fit. The process was repeated for various chosen points and $\hat{\tau}_{eff}$ was selected to give the best overall fit. The data point at t = 0 was neglected since these

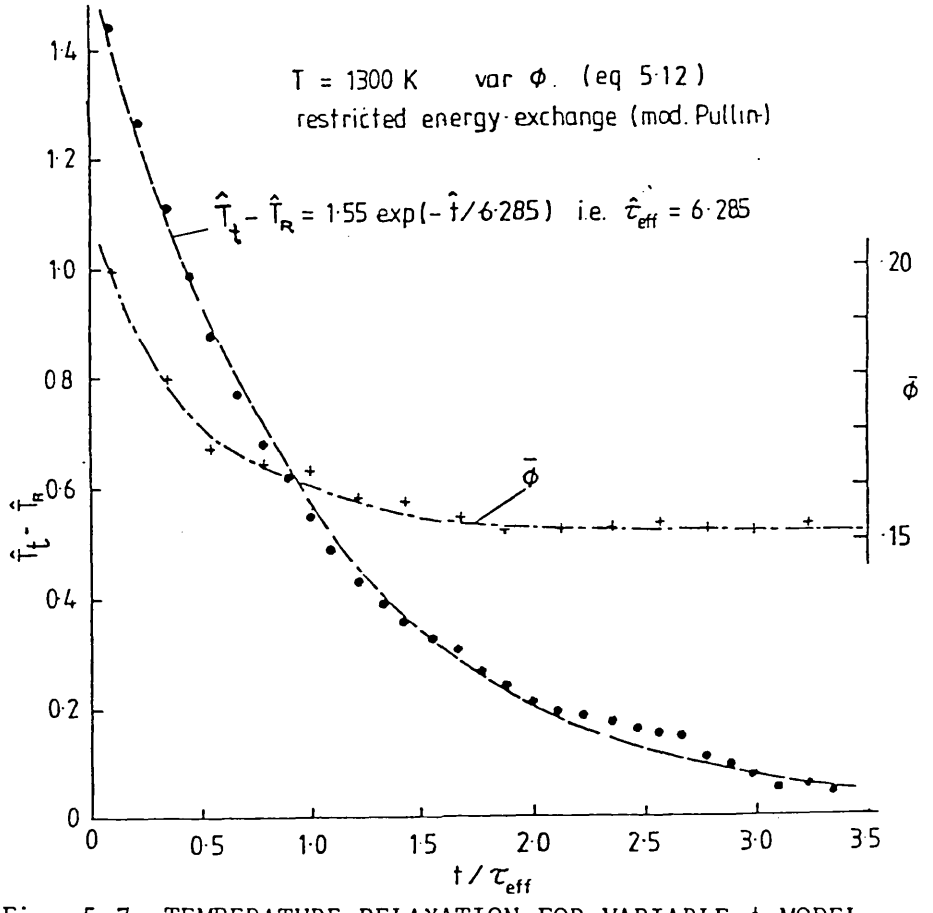


Fig. 5.7 TEMPERATURE RELAXATION FOR VARIABLE-ϕ MODEL

conditions were unrealistic. As equilibrium is approached there appears to be a periodic variation imposed on the temperature relaxation. Only those points for which $(T_t - T_R)/T_\infty > .05$ were used in the curve fitting. Each simulation used 3000 or 4000 particles, and at least two simulations were done for each temperature. The difference between the highest and the lowest estimate of $\hat{\tau}_{eff}$ was up to 10% of the average value.

When deriving Z_R from $\hat{\tau}_{eff}$ to compare with experiments care must be taken to use the same value of viscosity (i.e. assumed collision rate), as that used to convert the experimental measurements of relaxation time to Z_R. Converting the normalised relaxation time to a real time and using equation (5.8) we get

$$Z_R = (32/3\pi^{3/2})(\mu(IP)/\mu)\hat{\tau}_{eff}$$

Pullin (see Davis 1978), using his theoretical results (which we discuss later), derived a variable-ϕ equation intended to reproduce the variation of $Z_R(T)$ found by Carnevale et al. but has not given any details of this derivation. His equation is

$$\phi = 0.148 + 1.018 \exp(-1.722 \times 10^{-3}(K^{-1})\hat{e}_{cm}T_{\infty}) \qquad (5.13)$$

and this is compared with our empirically derived equation in figure 5.8. The values of $Z_R(T)$ obtained from relaxation calculations where ϕ is calculated for each collision from equation (5.12) or (5.13) are shown in figure 5.9. Equation (5.12) gives the best fit but has the fault that Z_R increases without limit. The minimum value of ϕ from equation (5.13) of 0.148, gives a maximum value of Z_R (assuming $\mu(IP)/\mu = 1$) as 10.5. The maximum theoretical value calculated by Parker (1959) was 15.6. The results using Pullin's equation are lower than the experimental values and it seems that Pullin, like Davis (1978), had taken the average value of e_{cm} to be 5kT rather than the correct value of 3.85kT for $\alpha = 13.51$. This result was checked in the relaxation calculation and it was found that as equilibrium was approached that the average value of $\hat{e}_{cm}$ was 3.80 ±.04.

The variable-ϕ equation (5.13) derived by Pullin has been used

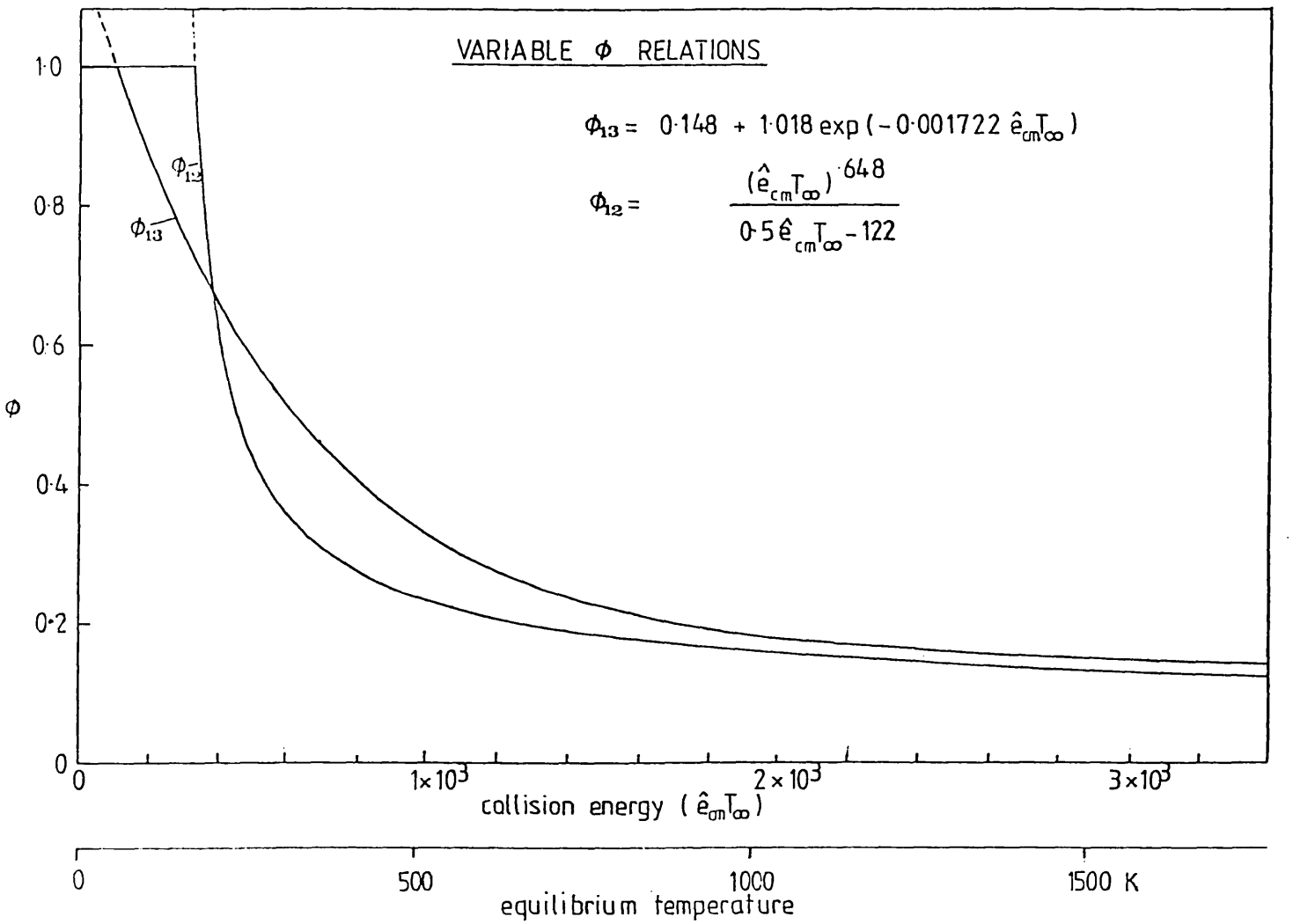


Fig. 5.8 TWO VARIABLE-ϕ EQUATIONS

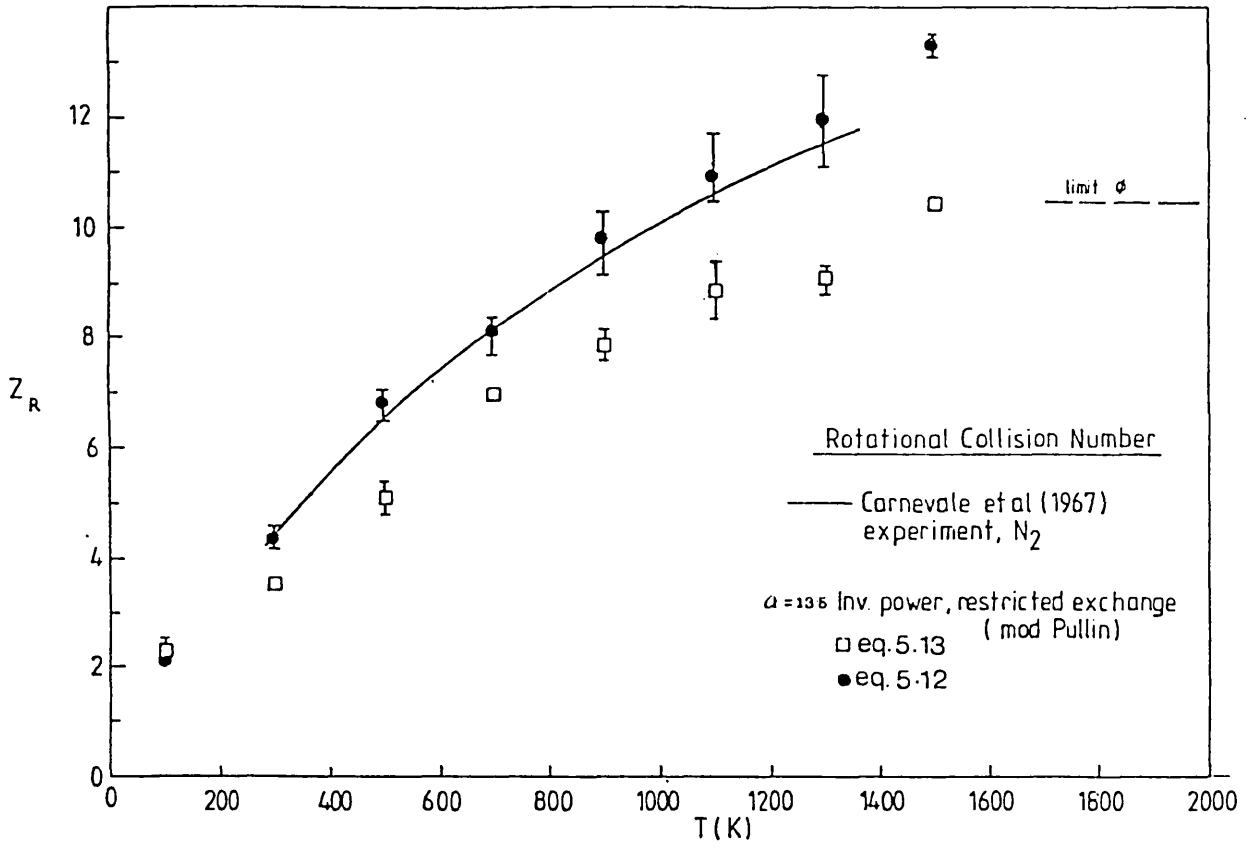


Fig. 5.9 VARIATION OF Z_R FOR VARIABLE-ϕ MODELS

for the calculation described in chapters 7 and 8 even though the values of Z_R are less than the experimental values. The measurements of $Z_R(T)$ by Carnevale et al. are the most comprehensive and agree reasonably well with the theoretical predictions of Parker (1959) and Lordi and Mates (1970), and particularly well with the predictions of Brau and Jonkman (1970). However, there are other measurements of $Z_R(T)$, for example those of Annis and Malinauskas (1971) and Butherus and Storvick (1974), which are derived by different methods and with different assumptions. The range of this data is greater than the differences found for the different variable-ϕ equations.

5.6 Theoretical Derivation of Variable-ϕ Equation

The Chapman-Enskog theory has been extended to polyatomic molecules by Wang-Chang and Uhlenbeck (see Hirschfelder et al. 1954, p.501). Pullin (1978) has applied these results to a particular version of his restricted exchange scheme to derive the transport properties. His model has two exchange restriction factors ϕ and ψ which represent the average fractions of translational and internal energy available for exchange. If $\psi = \phi$ the collision model is reasonably close to the original restricted exchange scheme. For this model, assuming two degrees of internal (rotational) freedom, the relaxation number is given by

$$Z_R = 4(3-2/\alpha)A^{(2)}(\alpha)/5\pi H \qquad (5.14)$$

where

$$H = \int_0^\infty zK(z)dz$$

$$K(z) = \int_0^\infty \phi/(4-2/\alpha)e^{5-2/\alpha}\exp(-e)de/\Gamma(6-2/\alpha)$$

and $e = e_{cm}/kT.$

For constant ϕ and an inelastic cross-section $z < 1$

$$Z_R = 8A^{(2)}(\alpha)(4-2/\alpha)(3-2/\alpha)/5\phi\pi$$

which with $\alpha = 13.51$ reduces to

$$Z_R = 1.736/\phi.$$

Converting Z_R to a normalised relaxation time (with $\mu(IP)/\mu = 1.0$) we get

$$\hat{\tau}_{eff} = 0.906/\phi.$$

This relation is shown in figure 5.4 and it is close to the empirically derived relation. Thus the more convenient theoretical results may be used to derive the variable-ϕ equation for the original re-

stricted exchange scheme.

Since the rotational-translational energy exchange decreases slowly for large miss distance a more sophisticated variable-ϕ equation might allow a continuous variation of ϕ with z. Suppose for each collision ϕ is given by

$$\phi = \phi_o(1 - z/z_{ex})$$

or

$$\phi = \phi_o(1 - (z/z_{ex})^2)$$

where ϕ_o is the maximum value of ϕ for each collision and z_{ex} defines the inelastic exchange cross-section (i.e. $\phi = 0$ for $z > z_{ex}$). If the LIP or ISO collision models proposed in chapter 4 were used with these equations and z_{ex} was set equal to z_o, then ϕ would be proportional to the deflection angle. Taking the first of these equations with $z_{ex} = 1.0$ it is found from equation (5.14) that the relaxation rate is halved compared with constant ϕ.

5.7 Morse Potential with Variable-ϕ Energy Exchange

When the Morse potential was first used with the variable-ϕ equation (Davis 1978) the inelastic cross-section was taken to be the same as for Pullin's hybrid model $\pi\sigma^2$ and it was erroneously assumed that the relaxation behaviour would be the same as for the inverse power potential. We have found that its relaxation behaviour at high temperature is different from that for the inverse power potential. The results were shown in figure 3.6. To make the relaxation rates the same (except for the differences arising from the different scattering) the same inelastic cross-section based on $z = 1.0$ should be used.

When combined with the Morse potential even the corrected restricted exchange scheme cannot satisfy the principle of detail balance. The inverse collisions have a relative velocity g' and a miss distance b' to give the same deflection angle as the forward collision. Pullin's corrected models were so arranged that the inverse collision rate (a function of g and the differential cross-section $2\pi bdb$) could be made dependent on z. For the inverse power potential the g' and b' are such that $z = z'$ but this is not so for the Morse potential. However, figure 5.2 shows that within the inelastic cross-section $z < 1$ the deflection for the Morse potential is nearly a function of z alone and the error should be small, and smaller than that expected if a constant inelastic cross-section were used. The figure suggests that a 'pseudo-Morse potential' might be constructed which replaced the deflection inside the inelastic cross-section with the inverse power deflections or the deflections from the one of the approximate models described in chapter 4. Outside the inelastic cross-section the Morse deflections could be retained or replaced by suitable approximations. The model would then satisfy detail balance when combined with Pullin's exchange schemes.

CHAPTER 6

A NEW COLLISION MODEL FOR POLYATOMIC MOLECULES

6.0 Introduction

In this chapter we present a collision model for polyatomic gases which may be considered to be intermediate between those that use a simple classical representation of the molecules and the statistical exchange schemes of Borgnakke and Larsen. The difficulty with the former approach is that it is not easy to devise simple classical models with the correct number of degrees of freedom. The rough sphere model, for example, is sufficiently simple but has three degrees of freedom for rotation. We propose that the energy exchange in collisions be calculated from a simplified, although rather abstract, representation of a collision. Any required number of degrees of freedom may be included but we present it for three translational and two internal degrees of freedom. Unlike the statistical exchange schemes, the post - collision 'state' is not selected from an equilibrium distribution for each collision but the equilibrium distribution is achieved for a large number of collisions.

The method is similar in some respects to the statistical schemes. An inelastic collision is defined in which energy is freely exchanged between internal and external energy and this may be used as part of a two class exchange scheme. The model may be easily extended to a restricted exchange scheme and has some computational advantages over the original methods when combined with a variable-ϕ equation. However, the method is not as versatile since in its basic form it only satisfies the detail balance condition for a Maxwell collision cross - section. The model can be used with any collision cross - section but to satisfy detail balance a slightly unsatisfactory modification must be made, which has little physical justification.

6.1 Equilibrium

Consider the equilibrium distribution of thermal velocities. The probability that a given molecule will have velocity in the range (v_1, v_2, v_3) to $(v_1 + dv_1, v_2 + dv_2, v_3 + dv_3)$ is

$$f(\underset{\sim}{v})\, dv_1\, dv_2\, dv_3 = \Phi(v_1)\, dv_1\, \Phi(v_2)\, dv_2\, \Phi(v_3)\, dv_3$$

where

$$\Phi(v_i) = \sqrt{\frac{m}{2\pi kT}} \exp(-mv_i^2/2kT).$$

Each component of thermal velocity is independently normally distributed. The Maxwell distribution is in fact the most probable distribution of velocities amongst the particles consistent with the conservation of the total energy. The proof, due to Jeans, applies to molecules with any internal structure for which the energy can be expressed as the sum of squared terms (Cowling 1950).

The method to be used in this collision model was suggested by Cowling's (1950, p. 104) interesting discussion of equipartition for a gas composed of N rotating rigid spheres having three degrees of translational freedom and three degrees of rotational freedom. He considers an 'equivalent' gas composed of 2N 'structureless' molecules having no internal energy. Half of these molecules have velocity components the same as the original molecules and the remainder have velocities such that their translational energy is equal to the rotational energy of a molecule in the original gas. The statistical theorems apply to this equivalent gas and he is able to deduce the rotational energy distribution in the original gas. In a similar manner we let each molecule have two internal energy components, v_j and v_k, which represent the rotational energy in each degree of freedom according to the rule

$$e_j = \tfrac{1}{2} m\, v_j^2 \qquad e_k = \tfrac{1}{2} m\, v_k^2$$

where $e_j + e_K$ is the total internal energy for one particle. The collision between molecules having translational and internal rotational energy will be represented by a collision in a five dimensional space between two ' pseudo particles' each having a five dimensional velocity representing the total energy. The statistical derivation of the equilibrium velocity and rotational energy distribution will still apply if these pseudo particles freely exchange energy in an arbitrary manner while conserving total energy.

By analogy with the monatomic collision in three dimensional velocity space we define the centre of mass velocity

$$v_{cm\ i} = \frac{1}{2}(v_i + v_i)$$

and the relative velocity of collision

$$g_i = (v_i - v_i)$$

in the five dimensional space (i = 1..5). The total energy of the two molecules is given by the same expression as in three dimensional space

$$\frac{1}{2}m\, \underset{\sim}{v}_{cm} \cdot \underset{\sim}{v}_{cm} + \frac{1}{4}m\, \underset{\sim}{g} \cdot \underset{\sim}{g}$$

and energy will be conserved if both $\underset{\sim}{v}_{cm}$ and $|\underset{\sim}{g}|$ are unchanged by the collision. The post- collision 'relative velocity' $\underset{\sim}{g}'$ will be the diameter of a 'hyper sphere' centered on $\underset{\sim}{v}_{cm}$. The post- collision 'velocity' points, which represent the state of the particles, cannot depart from $\underset{\sim}{v}_{cm}$ by more than $\frac{1}{2}\underset{\sim}{g}$ so there is a greater correlation between pre- and post- collision states than in the statistical exchange scheme. Perhaps more importantly the deflection angle in three dimensional space, which is a projection of the angle in five dimensional space between $\underset{\sim}{g}$ and $\underset{\sim}{g}'$, is linked to the amount of energy exchanged. Some sort of correlation like this exists for Parker's (1959) 'dumbbell' molecule and it may be that this classical

collision in three dimensional space can be mimicked by the present model.

6.2 Geometry of 5 Dimensional Euclidean Space

The following geometrical results are required for this collision model. These are derived by analogy with three dimensional geometry. Cylindrical coordinates for an increasing number of dimensions are indicated in figure 6.1. The Cartesian coordinates of a point a distance r from the origin in 3 space are

$$\begin{aligned} x_1 &= r \cos\theta_1 \\ x_2 &= r \sin\theta_1 \cos\theta_2 && 0 < \theta_1 < \pi \\ x_3 &= r \sin\theta_1 \sin\theta_2 && 0 < \theta_2 < 2\pi \end{aligned} \qquad (6.1)$$

where r, θ_1 and θ_2 are the cylindrical coordinates. In five space the Cartesian coordinates are

$$\begin{aligned} x_1 &= r \cos\theta_1 \\ x_2 &= r \sin\theta_1 \cos\theta_2 && 0 < \theta_1 < \pi \\ x_3 &= r \sin\theta_1 \sin\theta_2 \cos\theta_3 && 0 < \theta_2 < \pi \\ x_4 &= r \sin\theta_1 \sin\theta_2 \sin\theta_3 \cos\theta_4 && 0 < \theta_3 < \pi \\ x_5 &= r \sin\theta_1 \sin\theta_2 \sin\theta_3 \sin\theta_4 && 0 < \theta_4 < 2\pi \end{aligned} \qquad (6.2)$$

where r, θ_i , i = 1..4, are the 'hyper-cylindrical' coordinates.

The differential element of the area of the hyper sphere is

$$dA = r^2 \sin\theta_1 \, d\theta_1 \, d\theta_2 \qquad (6.3)$$

for three dimensions and

$$dA = r^4 \sin^3\theta_1 \, d\theta_1 \sin^2\theta_2 \, d\theta_2 \sin\theta_3 \, d\theta_3 \, d\theta_4 \qquad (6.4)$$

for five dimensions.

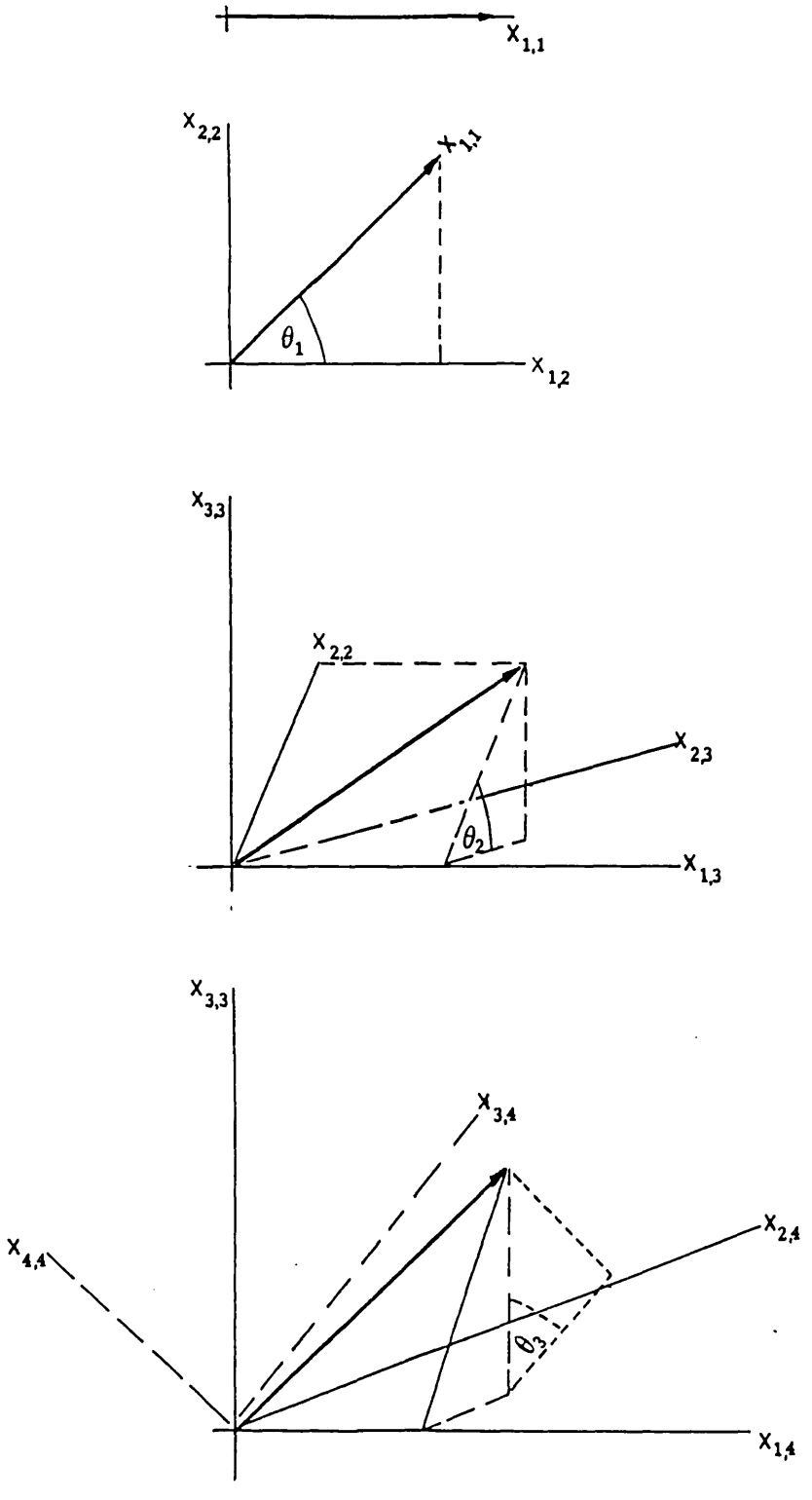


Fig. 6.1 CYLINDRICAL COORDINATES FOR INCREASING NUMBER OF DIMENSIONS

6.3 Collision Model in 5 Space

The simplest collision model in the five dimensional space is an extension of the hard sphere collision in three dimensional space. For hard sphere collisions, given that the impact parameters are randomly selected, the components of $\underset{\sim}{g}'$ may be selected directly and the method is given by Bird (1976, p. 131). For a large number of collisions with velocity $\underset{\sim}{g}$ the end points of the vectors $\underset{\sim}{g}'$ are uniformly distributed over the surface of the sphere in velocity space. The number of post - collision relative velocity vectors with cylindrical coordinates θ_1 and θ_2 in the range θ_1 to $\theta_1 + d\theta_1$ and θ_2 to $\theta_2 + d\theta_2$ is therefore proportional to the elemental area $\sin\theta_1 \; d\theta_1 \; d\theta_2$. Defining the distribution functions f_1 and f_2 for the cylindrical coordinates the number of these points in the elemental area is

$$f_1 \; d\theta_1 \; f_2 \; d\theta_2 = \sin\theta_1 \; d\theta_1 \; d\theta_2 .$$

The distribution of θ_2 is uniform so this coordinate can be selected directly from

$$\theta_2 = 2.0\,\pi \; R_f \qquad (6.5a)$$

The distribution of θ_1 is proportional to $\sin\theta_1$. Since $\sin\theta_1 \; d\theta_1 = -d(\cos\theta_1)$, the distribution of $\cos\theta_1$ is uniform and $\cos\theta_1$ may be selected directly from

$$\cos\theta_1 = 1.0 - 2.0 \; R_f \qquad (6.5b)$$

The components of $\underset{\sim}{g}'$ are calculated from equations (6.1) with $r = g$.

In five dimensional space the components of $\underset{\sim}{g}'$ may be calculated similarly from an assumed uniform distribution of the direction of $\underset{\sim}{g}'$. The distribution functions for each of the 'hyper cylindrical' coordinates are

$$f_1\ d\theta_1 \propto \sin^3\theta_1\ \ d\theta_1 \propto \sin^2\theta_1\ \ d(\cos\theta_1)$$

$$f_2\ d\theta_2 \propto \sin^2\theta_2\ \ d\theta_2 \propto \sin\theta_2\ \ d(\cos\theta_2)$$

$$f_3\ d\theta_3 \propto \sin\theta_3\ \ d\theta_3 \propto d(\cos\theta_3)$$

$$f_4\ d\theta_4 \propto d\theta_4.$$

The cosine of θ_1 is distributed proportional to $\sin^2\theta_1$ and the von Neumann technique is required to generate $\cos\theta_1$. The appropriate procedure is

repeat..

$$\cos\theta_1 := 1.0 - 2.0\ R_f$$

$$[\sin^2\theta_1] := 1.0 - \cos^2\theta_1$$

until.. $[\sin^2\theta_1] > R_f$. (6.5c)

The cosine of θ_2 is distributed proportional to $\sin\theta_2$ so the selection procedure is

repeat..

$$\cos\theta_2 := 1.0 - 2.0\ R_f$$

$$[\sin^2\theta_2] := 1.0 - \cos^2\theta_2$$

until.. $[\sin^2\theta_2] > (R_f)^2$. (6.5d)

The remaining coordinates θ_3 and θ_4 are selected in the same manner as in three dimensional space using equations (6.5a) and (6.5b). The five components of $\underset{\sim}{g}'$ are calculated from equations (6.2) with r = g. The final velocities and internal energies of both particles are determined from

$$\underset{\sim}{v}' = \underset{\sim}{v}_{cm} + \tfrac{1}{2}\underset{\sim}{g}'$$

$$\underset{\sim}{v}' = \underset{\sim}{v}_{cm} - \tfrac{1}{2}\underset{\sim}{g}' \qquad (6.6)$$

We can deduce the form of the 3 space scattering law which is incorporated into this model. Notice that if the coordinates i = 3 to 5 are the translational velocity components then the last three

equations of (6.2) have the same form as equations (6.1) with $r = g \sin\theta_1 \sin\theta_2$. In other words the deflection in three space is derived from the variable hard sphere collision dynamics with an altered relative velocity arising from the exchange of internal energy. The collision model can be combined with any scattering model in three dimensional space, whereby the deflection is calculated as usual from the pre- collision relative velocity and the randomly chosen impact parameters.

This collision model has been tested for stability and figure 6.2 shows a temperature history of a sample of 3000 particles. For simplicity a Maxwell cross - section was assumed so that pairs of molecules were selected for collision with equal probability independent of the relative velocity of collision. We later describe a modification which must be made if a different collision cross - section is used. It is not necessary to use time counters for these calculations and the time axis is marked in simulation collision time, i.e. collisions per particle, which can easily be converted to nominal collision time derived from viscosity by using equation (4.14). The initial velocity components (both translational and internal energy) were generated from the equilibrium distribution. Because of the finite sample size the initial translational temperature is about 2% greater than the equilibrium tempertaure, T_e, derived from the total energy but this difference was reduced by the action of collisions. This calculation was repeated a number of times and continued for up to 60 collision intervals. The translational temperature changed from above to below T_e many times and was usually within 1% and always within 2% of equilibrium.

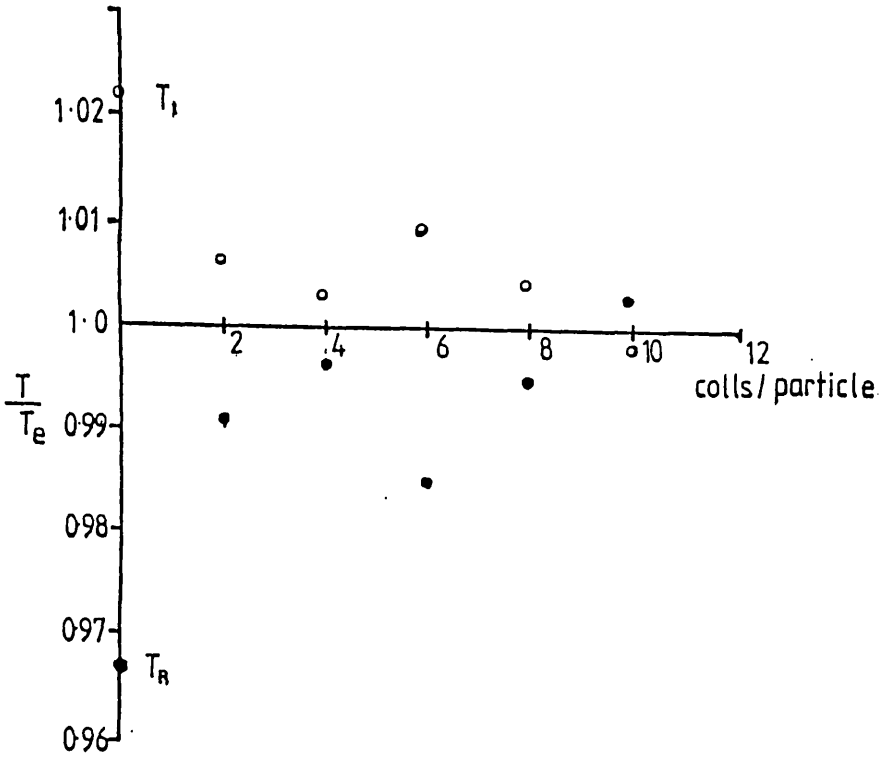
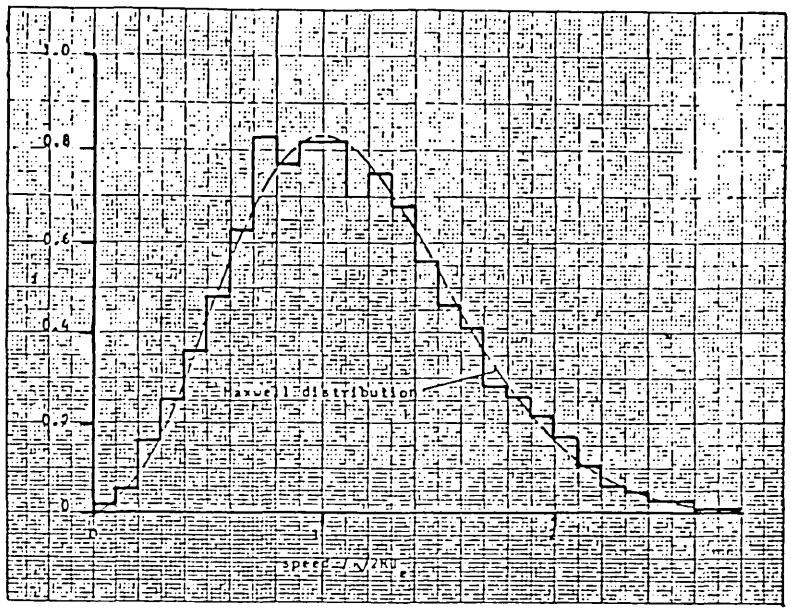


Figure 6.2 TEMPERATURE HISTORY : PSEUDO HARD SPHERE IN 5 SPACE

The distributions of speeds and internal energy after many collisions is compared with the theoretical distributions in figures 6.3 and 6.4. It is clear that the correct equilibriumdistributions are maintained. A similar stability test was made with the deflection angle in 3 space calculated using the LIP collision model described in chapter 4. These results are shown in figure 6.5 and are similar to those using hard sphere scattering.

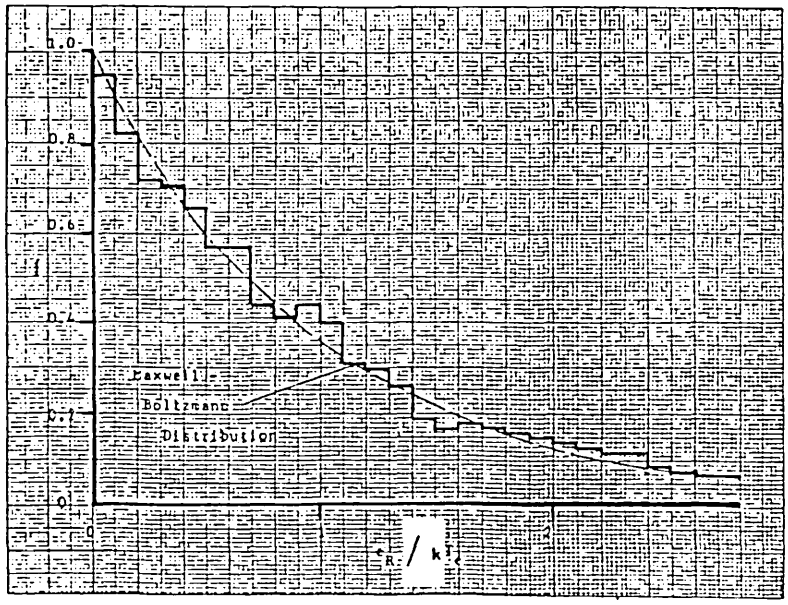
6.4 Restricted Exchange

It is easy in principle to restrict the amount of energy which is exchanged between internal and external modes in a collision. The



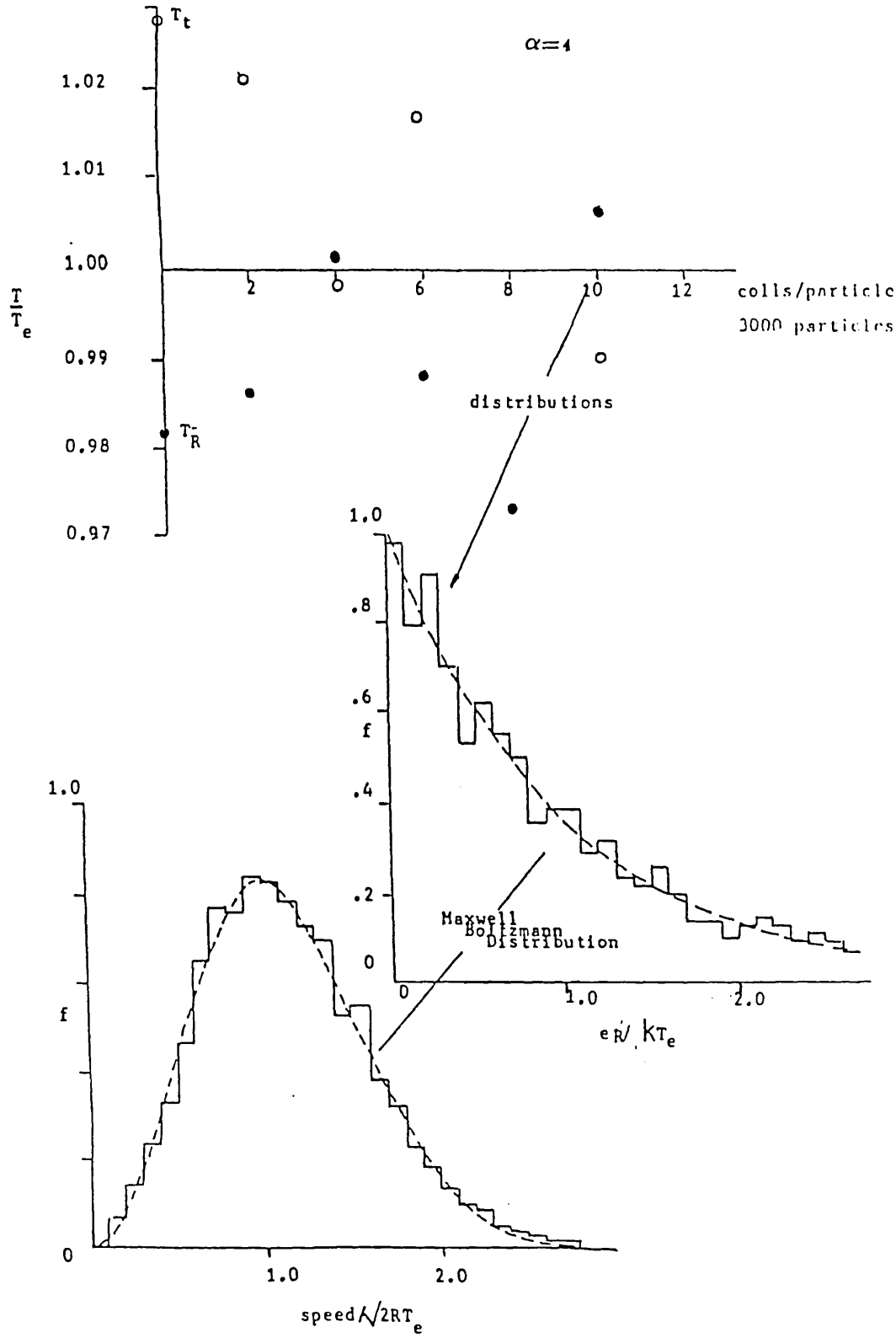
5-SPACE COLLISION MODEL : PSEUDO HARD SPHERE

Fig. 6.3 STABILITY TEST(a) MOLECULAR SPEED DISTRIBUTION



5-SPACE COLLISION MODEL : PSEUDO HARD SPHERE

Fig. 6.4 STABILITY TEST(a) INTERNAL ENERGY DISTRIBUTION

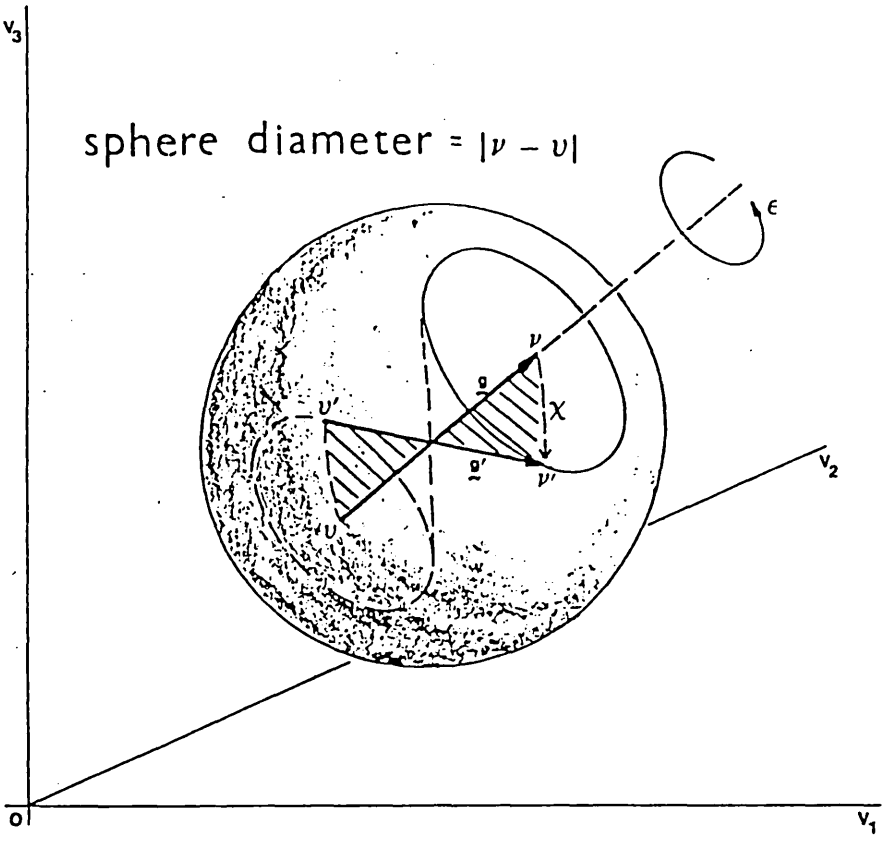


5-SPACE COLLISION MODEL

Fig. 6.5 STABILITY TEST(b) DEFLECTION FROM LIP MODEL

angle between the pre- and post- collision 5 vector g is the 'deflection angle in 5 space' and the greater this angle the greater will be the change in state across the collision. If this angle is limited to a value $\phi\pi$ the change in state is consequently limited.

It is useful to consider again the representation of a monatomic collision in three dimensional velocity space. If the deflection

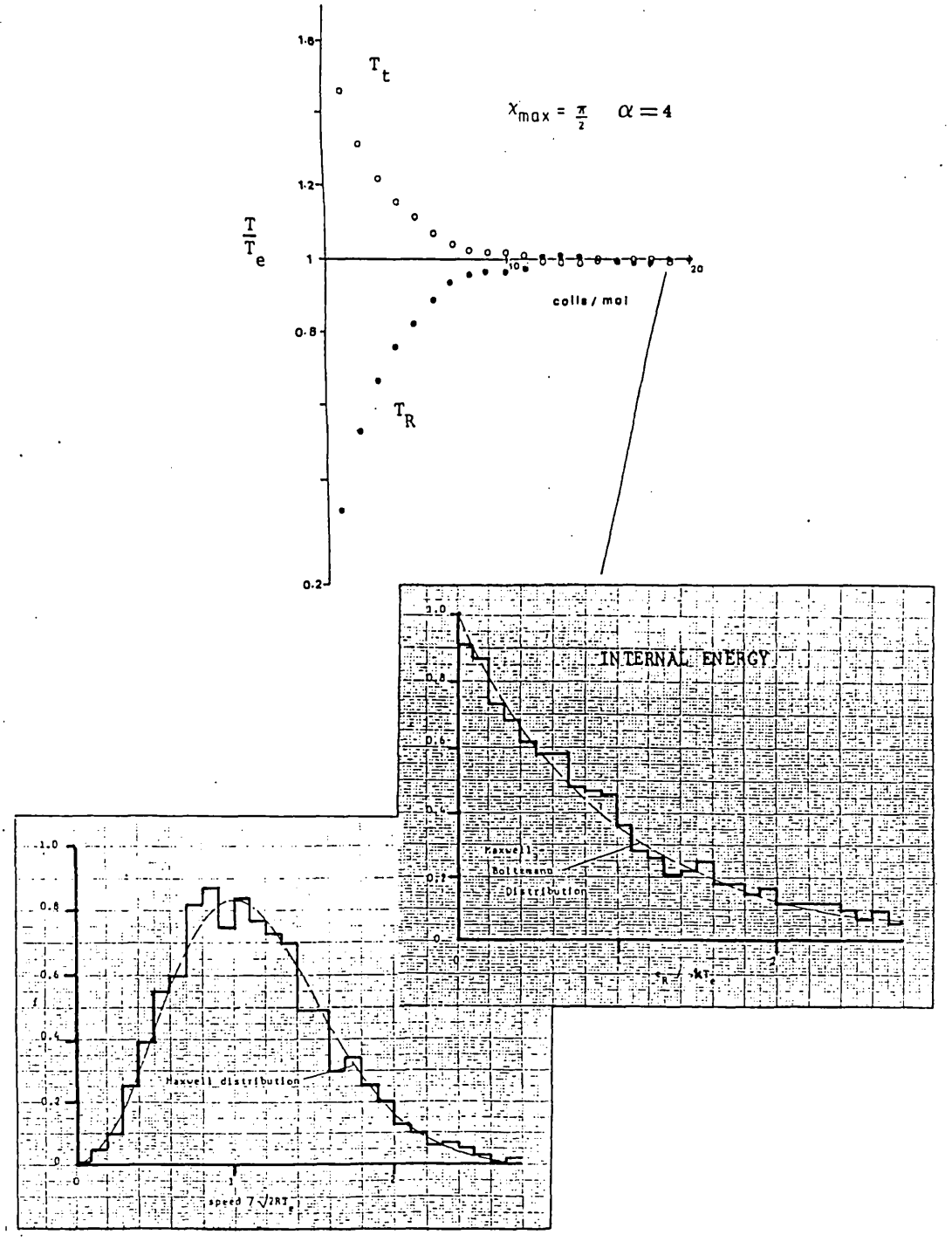


Collision in velocity 'space' $v\,v \rightarrow v'v'$

centre of mass velocity = $\frac{1}{2}(v + v)$

Figure 6.6 COLLISION IN VELOCITY SPACE

angle is limited, the direction of $\underset{\sim}{g}'$ must lie within a cone with half angle $\phi\pi$ and $\underset{\sim}{g}$ as the axis. The resulting distribution of post-collision velocity points on the surface of the sphere is axially symmetric about $\underset{\sim}{g}$. In five dimensional space the direction of $\underset{\sim}{g}'$ relative to $\underset{\sim}{g}$ is specified by the hyper cylindrical coordinates, g, θ_i (i = 2,3,4), selected from equation (6.6), and χ, where χ is the



VHS DEFLECTION IN THREE SPACE

Fig. 6.7 STABILITY TEST (c) 5-SPACE COLLISION MODEL: RESTRICTED EXCHANGE

restricted deflection angle $0 < \chi < \phi\pi$. The Cartesian components of $\underset{\sim}{g}'$ are then determined from these cylindrical coordinates and the orientation of $\underset{\sim}{g}$. The details are given in appendix C for three and five dimensions. The relaxation behaviour for ϕ = 0.5 is shown in figure 6.7 as well as the long time distributions of speeds and rotational energy. The scattering in 3 space was determined from the VHS model. The method works well and the equilbrium distribution is maintained.

6.5 Detail Balance

Unfortunately if the Maxwell cross - section is not used the method no longer satisfies the detail balance condition and equilibrium is not maintained. This is because the collision rates at different relative velocities are different for all but the Maxwell cross - section. The inverse of a collision with internal energy included has the same magnitude of the five dimensional 'relative velocity' vector (i.e. total energy) but not the same magnitude of the three dimensional relative velocity. Hence the inverse and forward collision rates are different. Detail balance can be satisfied if the collision probability depends on the magnitude of the 5 dimensional 'relative velocity' rather than the correct three dimensional velocity. In effect this adds a small perturbation, which depends on the internal energy, to the correct collision rate. Some classical models with internal energy behave in a similar, but not strictly analogous, way. For example, the different orientations of rotating dumbbell molecules as they collide will produce slight variations in the collision cross - section and the 'correct' collision rate for these molecules is not as well defined as for simple representations of monatomic molecules. The least satisfactory aspect of using the five dimensional 'velocity'

when selecting pairs of particles for collisions is that particles with no relative velocity in 3 space might be chosen. The only possible, and admittedly slight, justification for this would be to suppose that the long range attractive force between two molecules initially at rest produced the collision.

The theoretical distribution of relative velocities in collisions at equilibrium depends on the variation of the collision cross - section. The distribution of the dimensionless collision energy $E = mg^2/4kT$ for inverse power cross - sections is

$$f_E \; dE = 1/\Gamma(2 - 2/\alpha) E^{1-2/\alpha} \exp(-E)\, dE \qquad (6.7)$$

(see Bird 1976, p. 184 for example). To determine how far the collision rate for the modified model departs from the monatomic

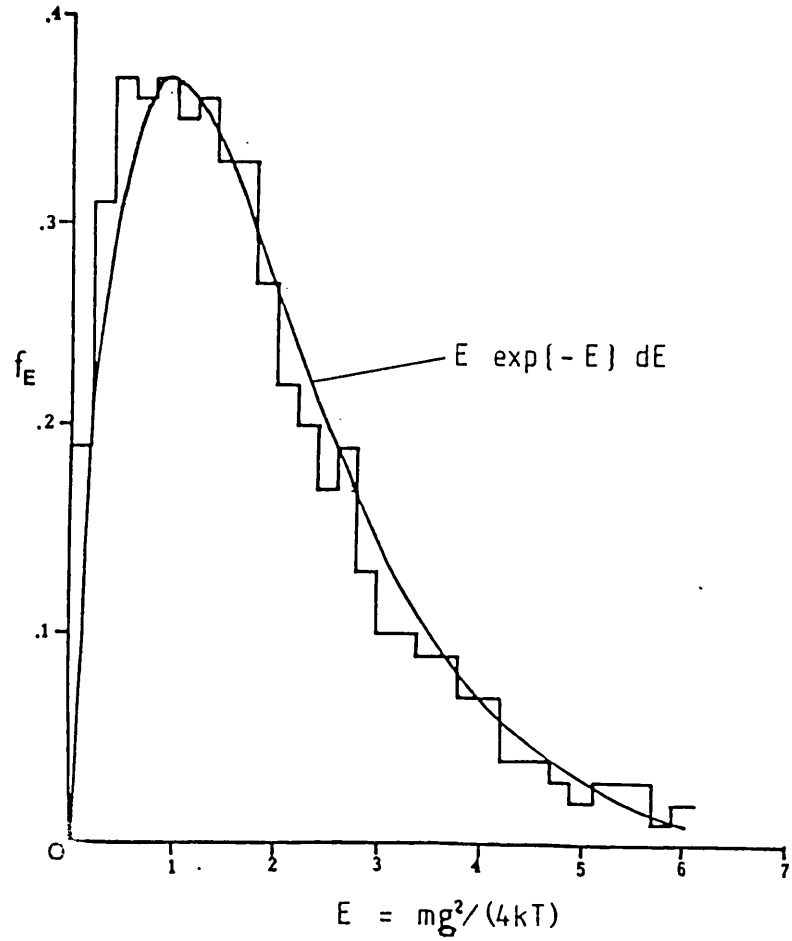
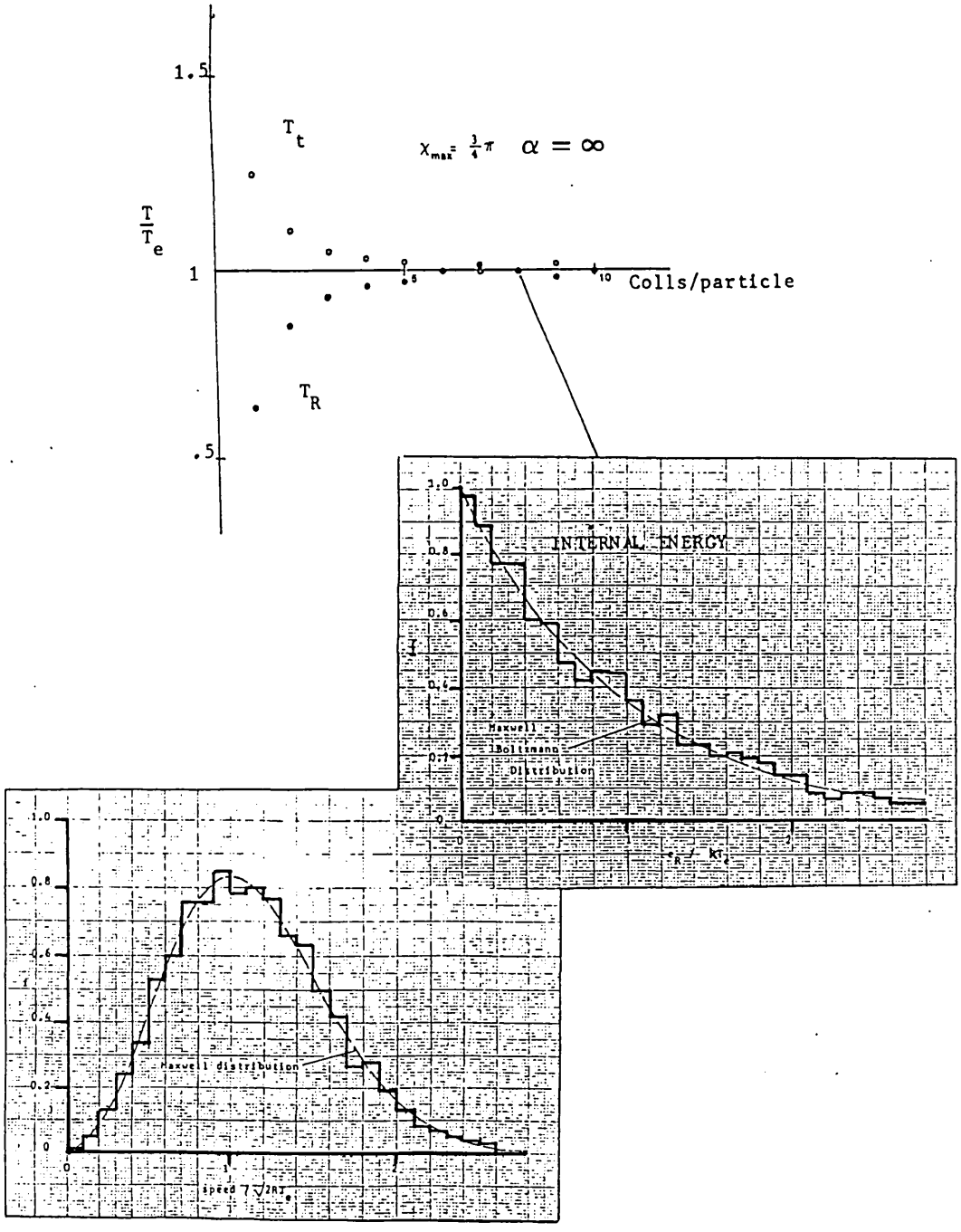


Figure 6.8 EQUILIBRIUM DISTRIBUTION OF COLLISION ENERGY IN SIMULATION

collision rate we have tested the collision model for hard sphere cross - sections ($\alpha = \infty$) where the relative probability of selecting a collision pair was made proportional to g in 5 space. The actual distribution of relative velocity in collisions using this modified collision probability was determined empirically from a simulation calculation and is compared with the correct distribution in figure 6.8. There is a slight shift in the relative frequencies towards the lower relative velocities but it does not appear to be a great distortion. Since the theoretical collision rate is derived from an idealised representation of the collision cross - section, it may be that this distortion of the relative collision rates is acceptable.

The relaxation behaviour with the modified collision probability is shown in figure 6.9. These results are better than for the Borgnakke and Larsen restricted exchange scheme which does not achieve detail balance (see for example Davis 1978, figure 29). It is possible that this 5-space model might be used in place of the restricted exchange scheme. When combined with a variable-ϕ equation the 5-space model executes 20% faster than the original scheme (see appendix D). This is in contrast to Pullin's (1978) modified restricted exchange which required twice as much machine time for each collision. However, a suggestion is given in appendix D which could make the original scheme up to 50% faster than the 5-space model with variable-ϕ. If this is so then the extra memory required for the 5-Space model (one element per particle) would certainly tip the balance in favour of the restricted exchange scheme, in spite of its small error in detail balance.



DEFLECTIONS FROM LIP MODEL

Fig. 6.9 STABILITY TEST (d): MODIFIED HARD SPHERE COLLISION PROBABILITY

CHAPTER 7

THE PLANE SHOCK

7.0 Introduction

In this chapter the new approximate collision models described in chapter 4 are tested by calculating a relatively simple flow, the one dimensional shock. Bird (1970a), Melville (1972), Alsmeyer (1976) and Sturtevant and Steinhilper (1974) have all used the Monte Carlo Direct Simulation method to calculate the structure of shocks. The method agrees well with the experimental results and the theoretical predictions for shock thickness using the Mott-Smith bimodal theory (Mott-Smith 1951). The shock structures for a monatomic gas using the ISO, VHS and constant deflection angle (CON) models have been calculated using the collision cross- sections derived from the inverse 11th power potential and the results are compared with experimental results for argon.

We also give results for a diatomic gas using the classical potentials and the LIP and ISO models. These calculations use the collision cross- sections based on the 13.51 inverse power potential and the results are compared with shock experiments in nitrogen.

7.1 Definitions

Figure 7.1 shows the plane shock in the frame of reference in which the shock is stationary. The conditions upstream are denoted by the subscript 1 and the downstream conditions by the subscript 2. The Mach number of the shock is $M = v_1 / (\gamma RT_1)^{\frac{1}{2}}$ where γ is the specific heat ratio. The velocity, temperature, pressure and density across the shock are related by the Rankine- Hugoniot equations (Liepmann and Roshko 1957).

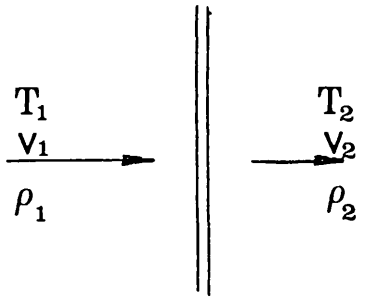


Fig. 7.1 THE PLANE SHOCK

Figure 7.2 shows typical temperature and density shock profiles which are normalised in the following manner

$$\overline{\rho} = (\rho - \rho_1)/(\rho_2 - \rho_1)$$
$$\overline{T} = (T - T_1)/(T_2 - T_1) \qquad (7.1)$$

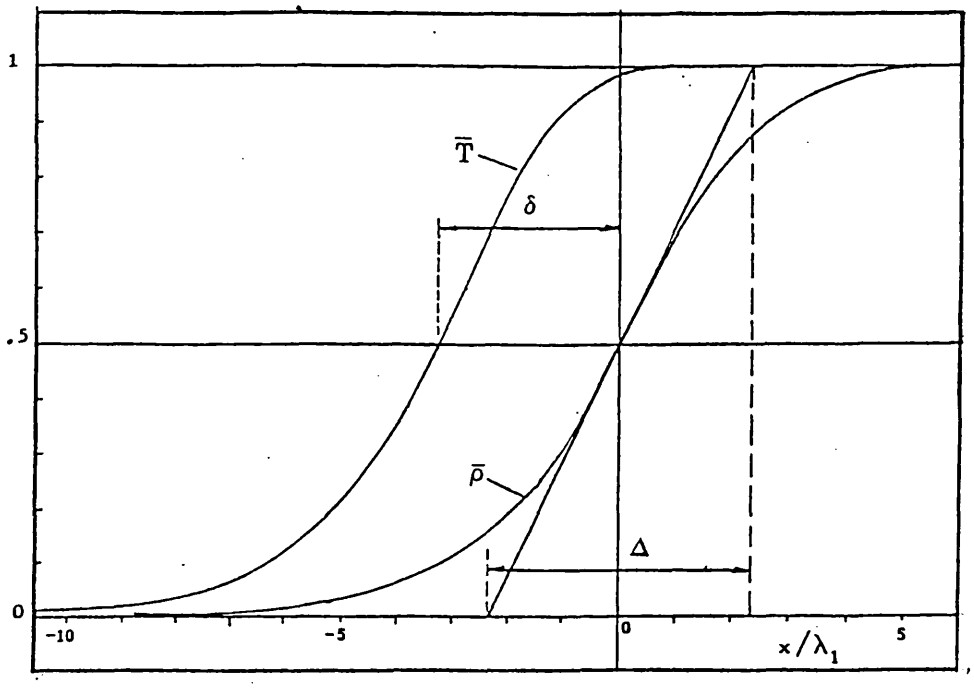


Fig. 7.2 TYPICAL SHOCK PROFILES

A representative thickness of the shock can be derived from the maximum slope of the density profile as follows

$$\Delta = (\rho_2 - \rho_1)/ \, d\rho/dx_{max} \, .$$

The maximum slope need not be at the point where $\bar{\rho} = 0.5$. The temperature rises ahead of the density and another measure of shock thickness is δ defined as the distance between the points where $\bar{T} = 0.5$ and $\bar{\rho} = 0.5$. The Mott-Smith theory predicts a symmetric density profile which is not seen in experiments, in spite of the fact that this theory gives good predictions of shock thickness Δ. Schmidt (1969) used the asymmetry factor

$$Q = \frac{\int_{-\infty}^{0} \bar{\rho}\, dx}{\int_{0}^{\infty} (1 - \bar{\rho})\, dx} \qquad (7.2)$$

to further define a shock profile. This quantity is extremely sensitive to the resolution of the up- and down- stream tails of the profile and is difficult to determine from the results of the simulation calculations.

The mean free path in the upstream gas is usually used to define the length scale for the shock. For collision models which have inverse power cross- sections the nominal mean free path is defined in equation (4.~~13~~12).

7.2 Method of Simulation

We have used a slightly different method to generate the shock than has been used previously (see Bird 1976, p. 183). We produce a 'stationary' shock with upstream and downstream boundaries at a constant distance from the shock. The upstream and downstream conditions were initially set from the Rankine- Hugoniot conditions with a sharp discontinuity within the flowfield representing the shock. While the particles were moved, specularly reflecting surfaces were moved at the upstream and downstream boundaries with the local theoretical mean speed. These surfaces correspond to the stationary

end wall and the moving piston in Bird's simulation of a moving shock. New particles were added to the upstream and particles were discarded in the downstream to keep the boundaries a constant distance from the shock. After a few decoupling intervals the initial discontinuity 'relaxed' into a reasonably smooth profile.

7.3 Computational Accuracy

The length and time intervals quoted in this section are in units of the nominal mean free path, λ_1, and the nominal collision time $\lambda_1/(2RT_1)^{\frac{1}{2}}$. The number of particles in each simulation at any one time varied from 3000 - 7000 and the minimum number of particles in any cell was about 30. The 'time-counter' method of establishing the collision rate was used which should be accurate for the large number of particles per cell in these simulations. Larsen's modification whereby the last collision at each time step is not always calculated was used in some simulations and not in others with no detectable effect. The normalised de-coupling interval was 0.1 for all simulations. The actual collision time is ≈ 0.5 in the upstream and $\approx$ 0.18 in the downstream so the decoupling interval ranged from about 0.2 to 0.6 of the mean time between collisions. The cell width was 0.4 or 0.5 which is usually about 1/10 of the shock thickness.

Successive samples were taken at time intervals of 1.0. After steady conditions were assumed to exist, 20 - 30 samples were added to get a shock profile. If the Rankine- Hugoniot conditions are not exactly maintained, so that the shock is not stationary in our reference frame, the profile will be distorted. It is important to know whether there is a systematic difference between the shock speed and the theoretical value. Since $\gamma = (5 + \xi)/(3 + \xi)$ where ξ is the number of degrees of freedom of internal energy, the stability of the

shock is a sensitive test of the accuracy of internal energy exchange scheme. It was found that a stationary shock could not be produced for the original restricted exchange scheme and that the translational and rotational temperatures approached different limits on the downstream side. A similar effect was found by Melville (1972) using an approximate classical model which violated the detailed balance condition. All diatomic calculations for these shocks were made using Pullin's (1975) corrected version of the restricted exchange scheme and the variable-ϕ equation.

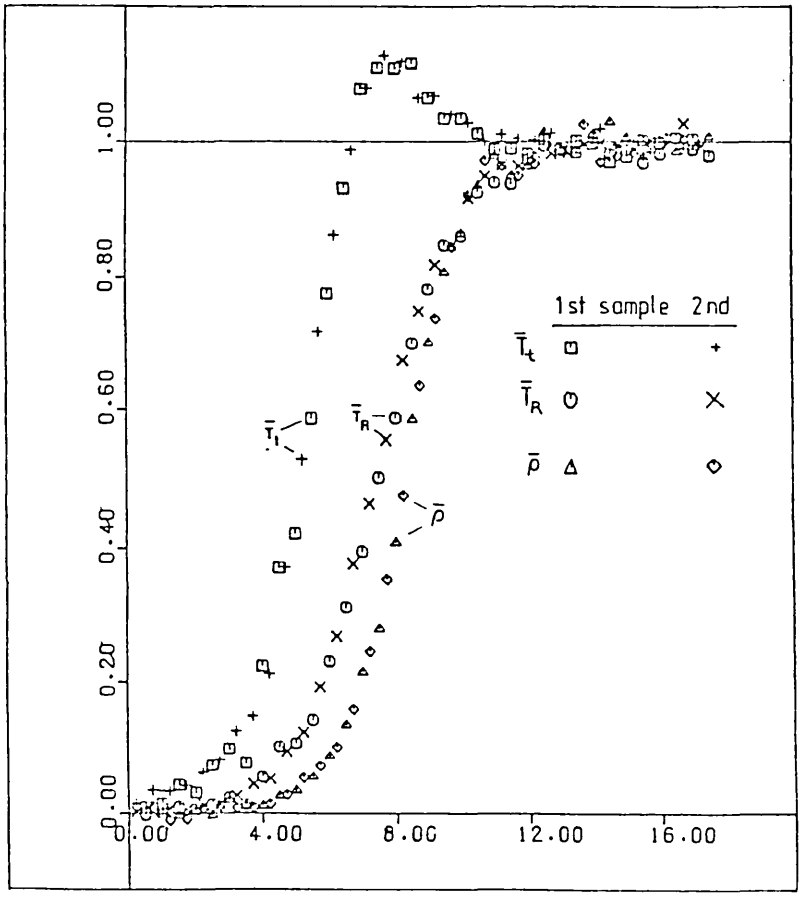


Fig. 7.3 SUCCESSIVE SHOCK PROFILES

Figure 7.3 is a typical example showing successive profiles of density, translational temperature and rotational temperature from the same calculation. The profiles are drawn so that the density profiles co-incide as closely as possible. The necessary shift was found by a simple least squares method and the 'drift' speed so determined was

$\approx 1\%$ of the theoretical speed for this Mach 5 shock. It was found that there was no systematic error in the shock speed, the drift being apparently random in size and direction for different runs and always within 2% of the Rankine value. However in any one simulation it was found that the profiles might slowly drift upstream or downstream and this means that the profiles taken from succesive samples will be slightly distorted, particularly in the extremes of the up- and downstream tails.

7.4 Mean Free Path Across Shock

Muckenfuss (1962) has applied the Mott-Smith bimodal method to the shock problem for a variety of inter-molecular potentials. An interesting result is that the average number of collisions suffered by a molecule when travelling across the shock quickly approaches an upper limit for high Mach numbers. A mean free path between collisions for an upstream particle moving through a cloud of downstream particles can be calculated. The shock thickness should be an approximately constant multiple of this mean free path. For simplicity we ignore the random thermal velocities and assume that all upstream particles have the same velocity and all downstream particles have the same velocity. Taking the collision cross- section $K_i \pi (2\alpha a/mg^2)^{2/\alpha}$ (see equation 4.8) and using the continuity condition $n_1 v_1 = n_2 v_2$ we get the mean free time as

$$v_2/[n_1 \pi K_i v_1 g (2\alpha a/mg^2)^{2/\alpha}]$$

where $g = (v_1 - v_2)$. The corresponding mean free path is the distance travelled by the upstream molecule relative to the stationary shock in this interval and is

$$\lambda_{12}/\lambda_1 = A^{(2)}(\alpha)\Gamma(4-2/\alpha) \quad \hat{v}_2/[2^{\frac{1}{2}+\frac{2}{\alpha}} \hat{g}^{1-\frac{4}{\alpha}} K_1] \qquad (7.3)$$

where $\hat{g}$ and $\hat{v}_2$ are in simulation units, and equation (4.12) has been used. According to this approximate analysis the downstream particles

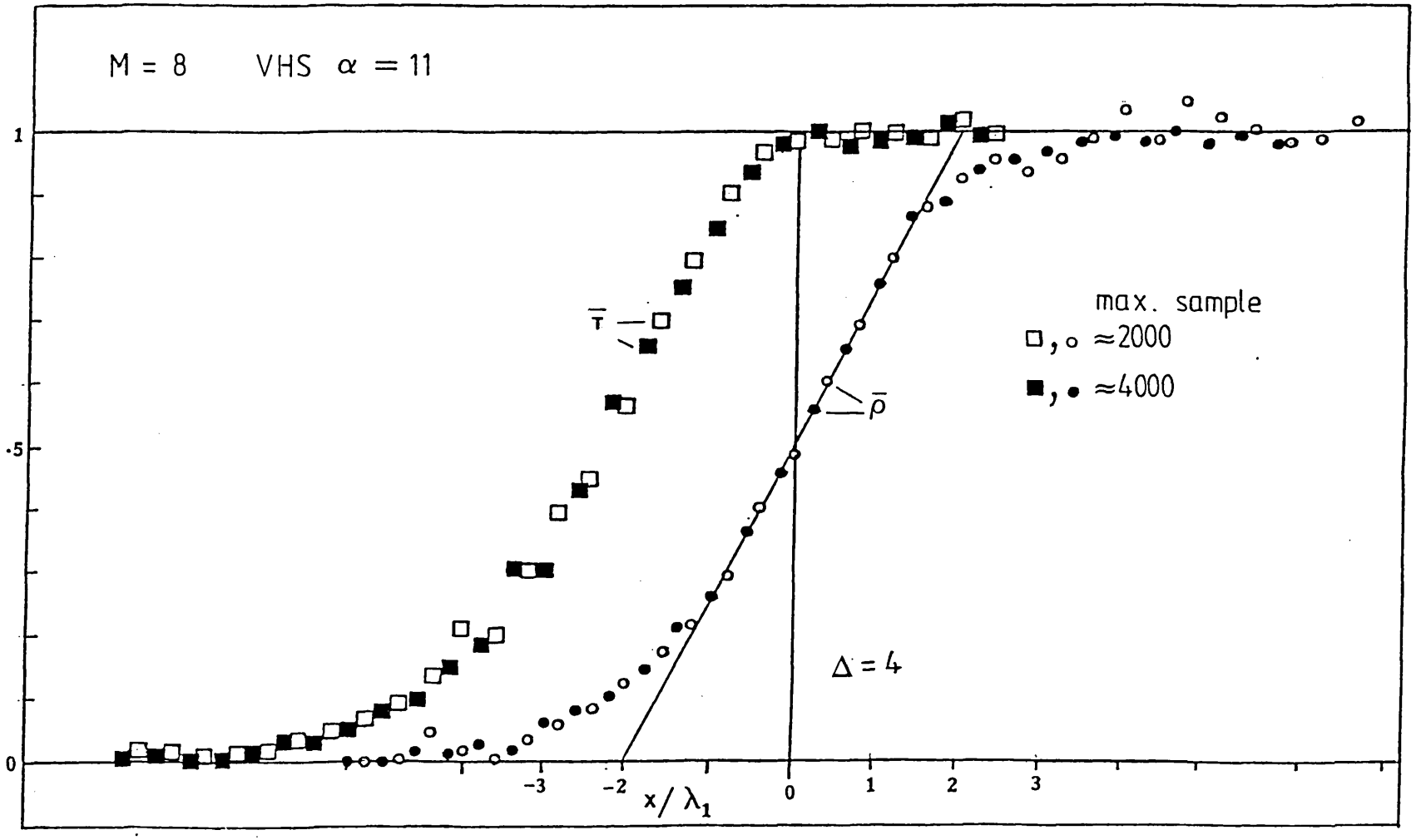


Fig. 7.4 DENSITY AND TEMPERATURE SHOCK PROFILES-VHS MODEL. MONATOMIC GAS

travel the same distance on average before being hit by the upstream molecules.

7.5 Comparison with Experiment

Figure 7.4 shows the shock profiles derived from two independent simulation calculations using the VHS collision model. For a larger sample size it is expected that the scatter is reduced proportional to $\sqrt{N}$ and it is clear that the two profiles are consistent with each other.

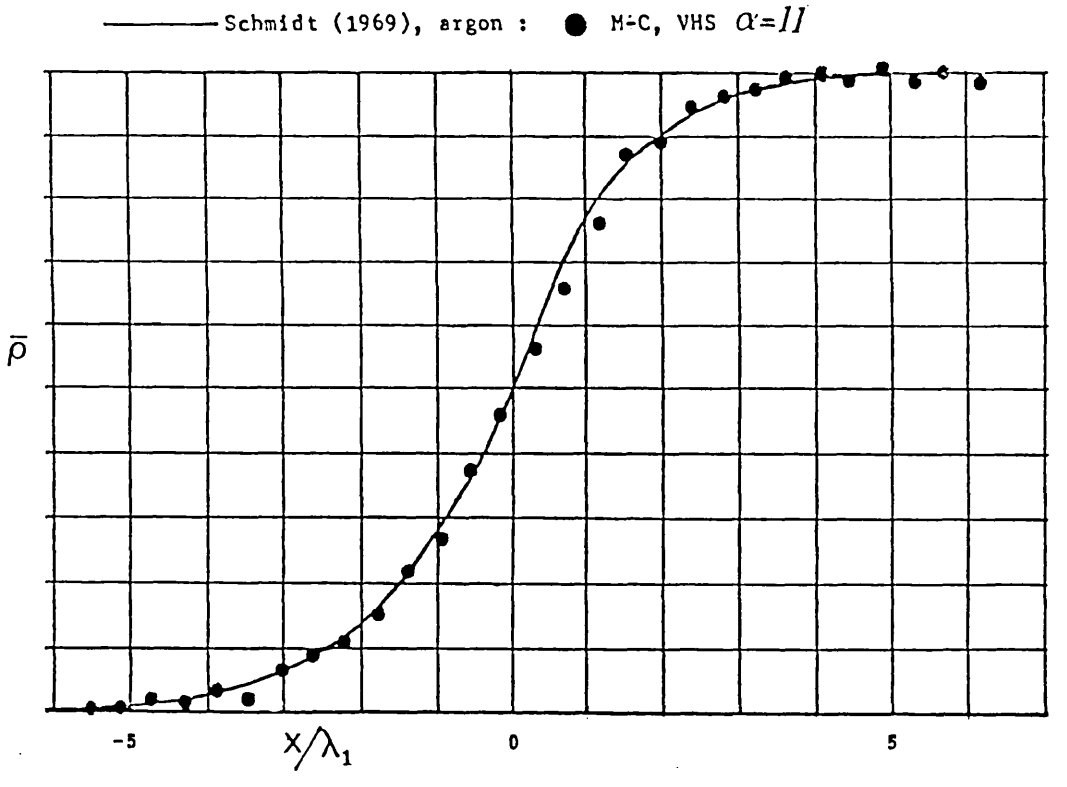


Fig. 7.5 DENSITY PROFILE FOR VHS MODEL COMPARED WITH EXPERIMENT

In figure 7.5, the density profile, for the larger sample sizes, is compared with Schmidt's measured profile for argon. The agreement is very close for most of the curve but not as good as that obtained by Bird with the inverse 11th power potential.

It is obviously difficult to determine the maximum slope of the density curves from these results. The best way seemed to be to fair a smooth curve to the points and to lay off the tangent to this curve by hand. An error of ± 5% was estimated by repeating the process at different times. The faired curve was also used to calculate the asymmetry factor Q.

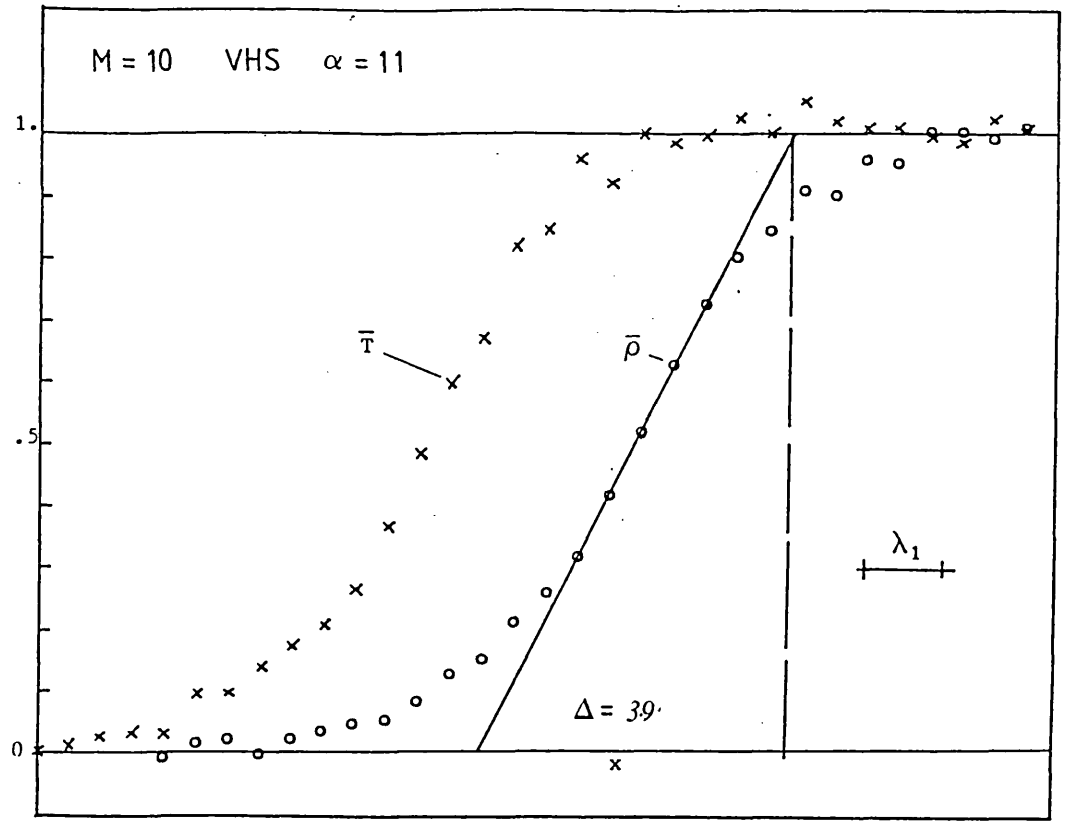
Table 7.1

Shock Thickness

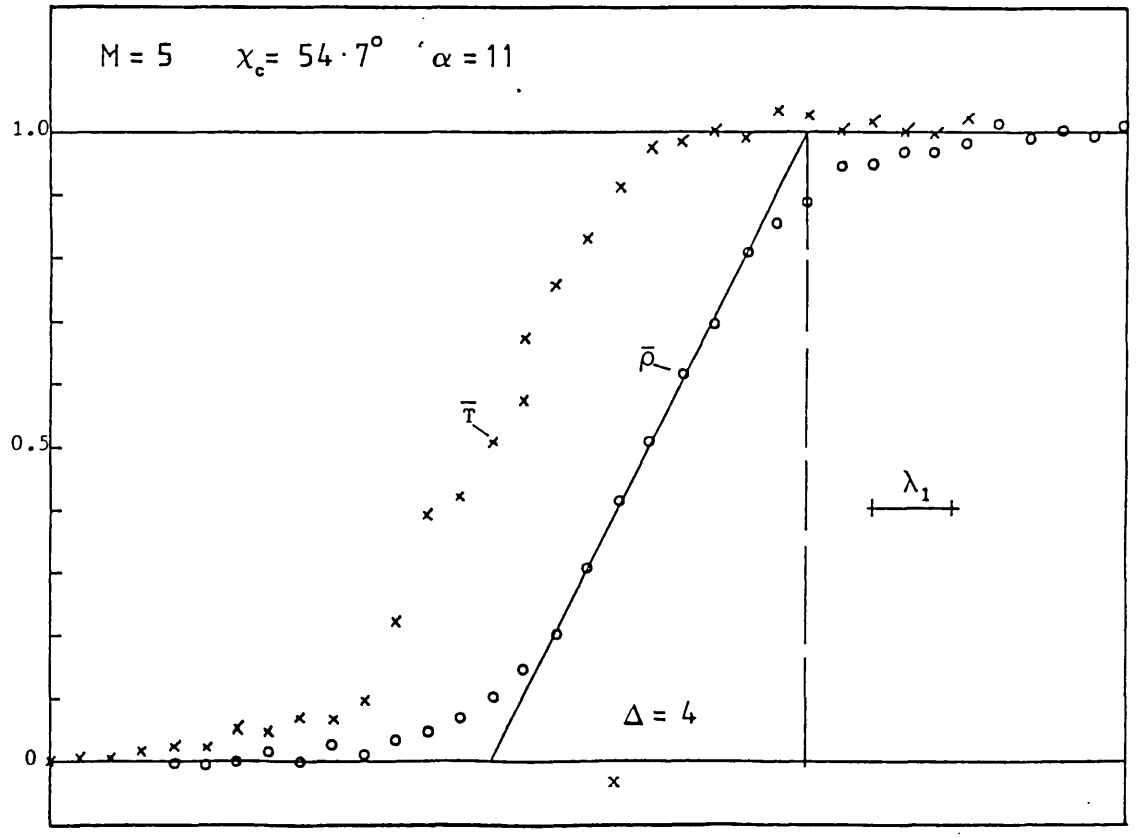
α = 11

Model	M	Δ/λ_1	δ/λ_1	λ_μ/λ_1	λ_m/λ_1	Δ/λ_μ	Δ/λ_m	δ/λ_μ
CON	5	4.0	2.1	.896	1.415	4.46	2.83	2.34
ISO	7	3.7	2.2	.948	.474	3.90	7.81	2.32
ISO	8	4.3	2.5	.978	.488	4.40	5.12	2.56
VHS		4.0	2.4	.978	.651	4.09	6.14	2.45
CON		4.2	2.4	.978	1.543	4.09	2.59	2.45
ISO	10	4.0	2.5	1.040	.521	3.85	7.68	2.40
VHS		3.9	2.6	1.040	.694	3.75	5.59	2.50
					mean	4.08	5.39	2.43
					standard deviation	0.25	1.93	0.08

Table 7.1 shows the shock thickness derived from a number of simulations for a monatomic gas with α= 11 for the various collision models. The normalised mean free path across the shock is given for two cross- sections as follows: λ_μ/λ_1 for $K_i = 2\,A^{(2)}$ (11) (viscosity cross- section) and λ_m/λ_1 for $K_i = 2\,A^{(1)}$ (11) (momentum cross- section). The standard deviations of the ratios Δ/λ_μ and Δ/λ_m



DENSITY AND TEMPERATURE SHOCK PROFILES-VHS MODEL. MONATOMIC GAS



DENSITY AND TEMPERATURE SHOCK PROFILES-CONSTANT DEFLECTION MODEL. MONATOMIC GAS

Fig. 7.6 SHOCK PROFILES FOR TWO COLLISION MODELS

indicate that, for these collision models, it is the viscosity cross-section, rather than the momemtum cross- section which correlates the shock thickness. The ratio of the viscosity to the momentum cross-section is nearly the same for most realistic potentials and either cross- section could have been important. The most startling results are for the crude collision model denoted CON in which the deflection angle is the same in every collision. Figure 7.6 shows profiles for this model and for the VHS model for different Mach numbers. The density profiles for the CON model look plausible even though the momentum cross- section for this model is vastly different from those for the other collision models. However the unrealistic deflections do increase the scatter in the temperature profile in the non-equilibrium 'centre' of the shock.

The results for shock thickness in table 7.1 are compared in figure 7.7 with those measured in argon by Schmidt (1969) and Alsmeyer (1976). Also shown is a curve for $\Delta / \lambda_{\mu} = 4.07$ which is a reasonable fit to Schmidt's data except at Mach 5, and two results calculated by Bird (1969 1970a) using the inverse power potential. Bird's 1969 result is that compared favourable with the measured values by Schmidt (1969). Bird's 1970 figure does not agree so closely with the experimental values. The shock thickness is perhaps misprinted in Bird's 1970 paper since a thickness scaled from the shock profile given in that paper is closer to the 1969 result. Alsmeyer (1976) found that using an inverse 9th power potential in the Direct Simulation method gave good agreement with his own measured profiles in argon for a range of Mach numbers. These profiles were slightly different from Schmidt's at Mach 8. Alsmeyer notes that $\alpha = 9$ gives a better fit to the viscosity data for argon for the temperatures in his experiments than does $\alpha = 11$. Alsmeyer's results

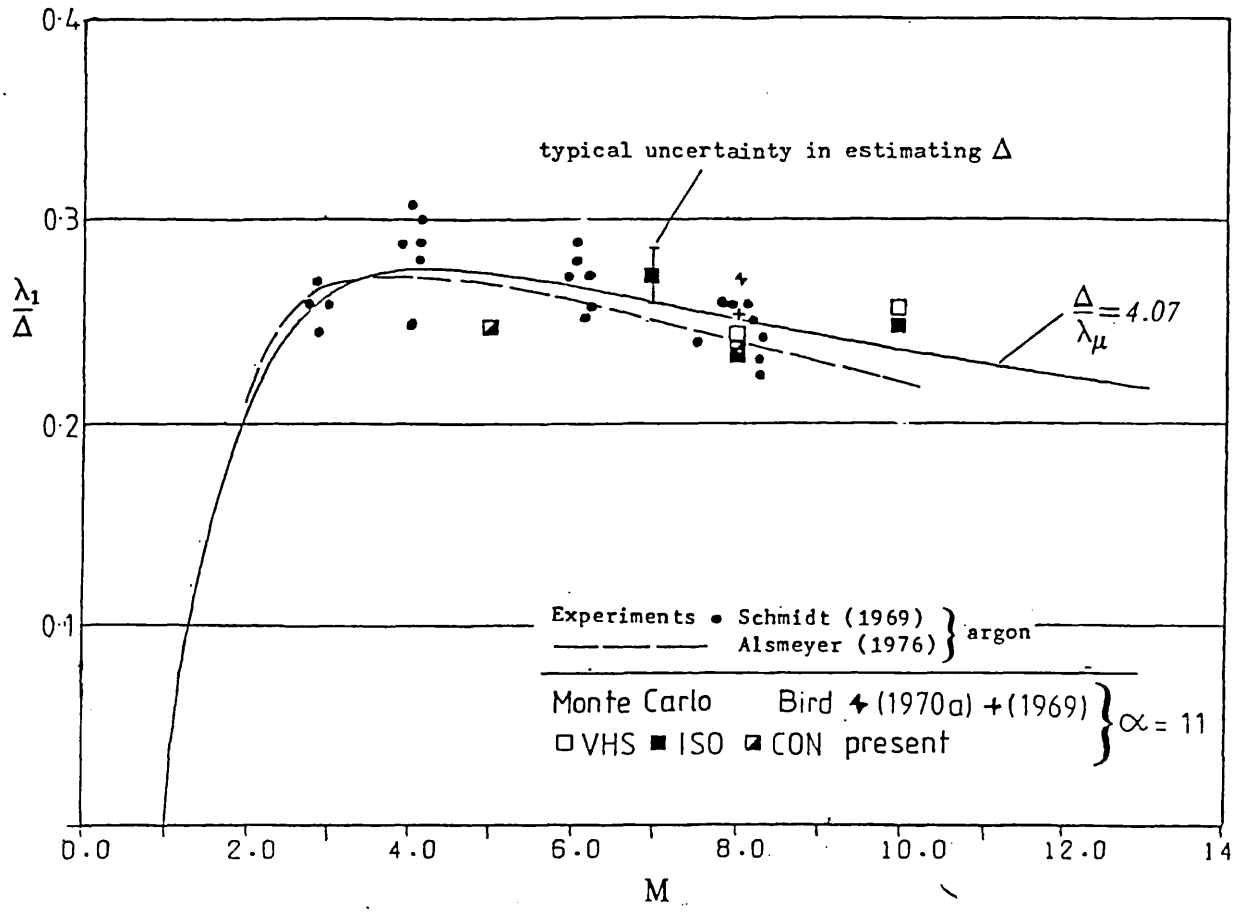


Fig. 7.7 SHOCK THICKNESS FOR ARGON

for shock thickness for Mach 3 to 9 give Δ/λ_μ = 4.0 to 4.15 when λ_μ is calculated for α = 9. The lowest Mach numbers give this ratio as $\approx$ 4.48. That this ratio is reasonably constant, more so than for α = 11, tends to support Alsmeyer's choice of α.

The asymmetry of the calculated profiles is compared with the experimental results of Schmidt and Alsmeyer in figure 7.8. In general these computations give profiles which are more skewed than the profiles determined in experiments. The present Monte Carlo results follow the trend assumed by Schmidt, shown as a solid line in the figure, of unlimited increase of Q with Mach number. Alsmeyer's Q for Mach 10 is not much greater than that for Mach 7.5 and he assumed the trend was towards a constant Q for high Mach number. The shock

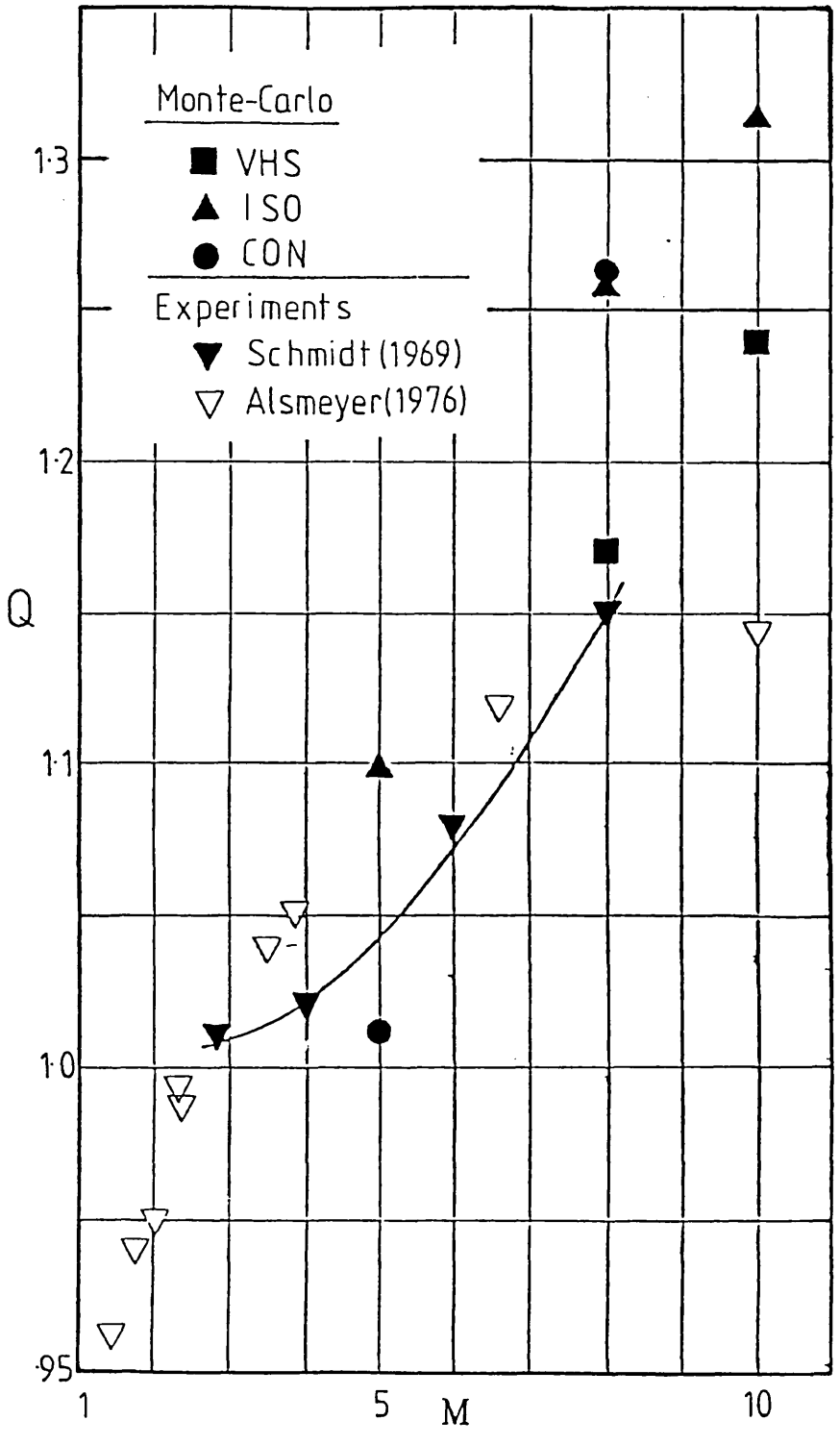


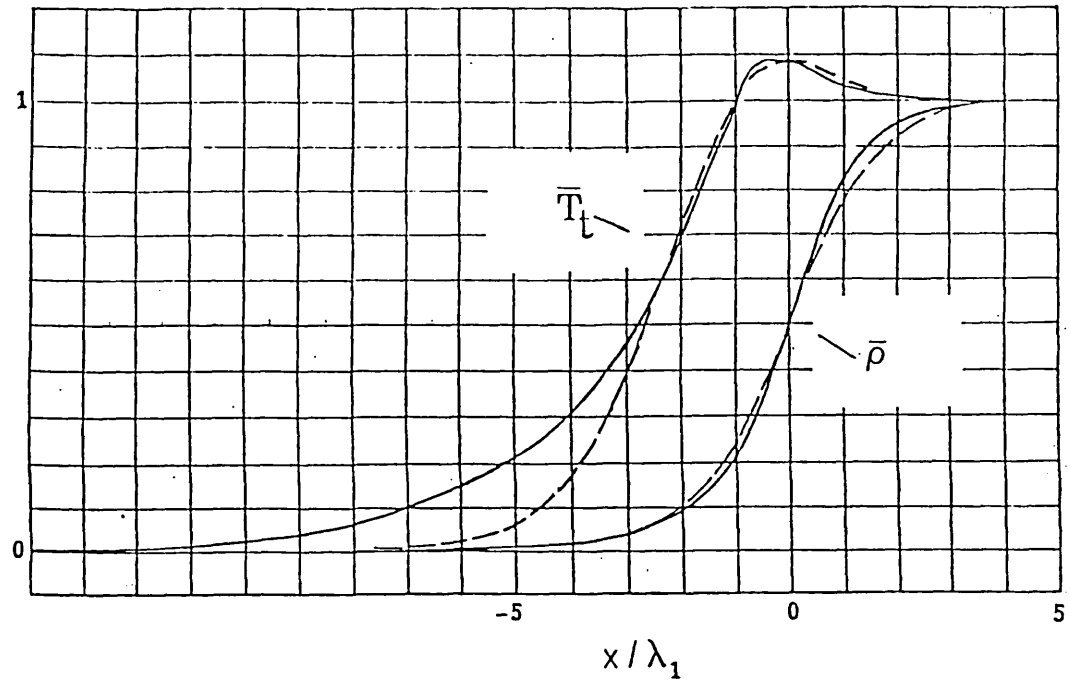
Fig. 7.8 ASYMMETRY OF DENSITY PROFILES FOR ARGON

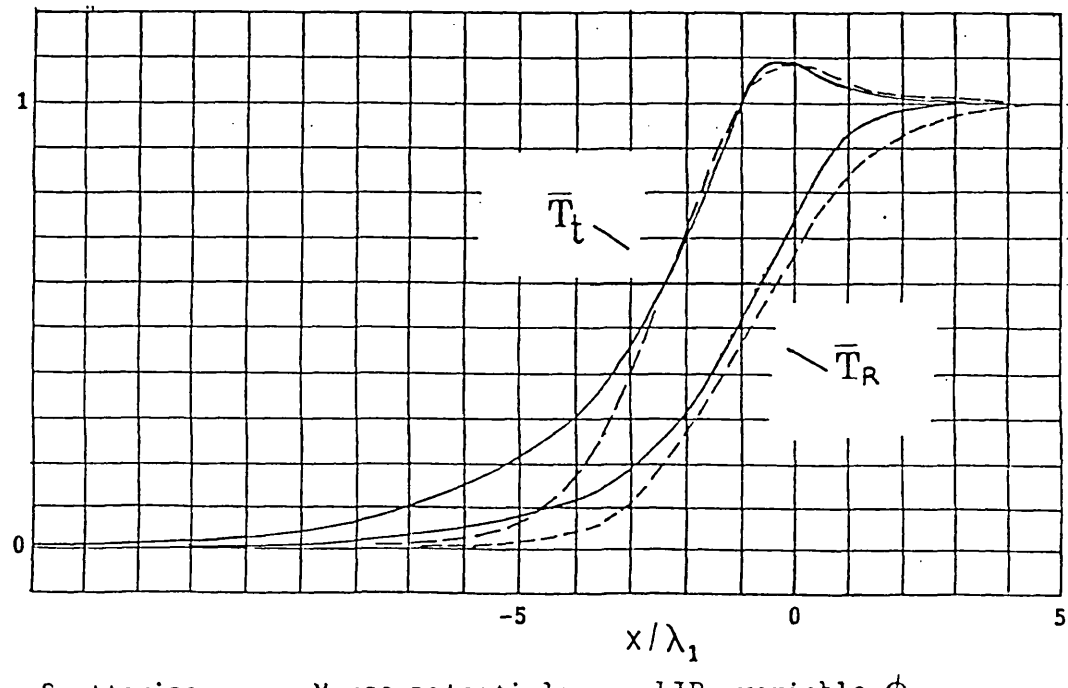
thickness and asymmetry for these few results indicate that the VHS model is better than the ISO model.

7.6 Diatomic Gas

Shock profiles calculated using the Morse potential and the LIP approximate collision model are shown in figure 7.9. All the parameters for the Morse potential and the variable-ϕ equation have been chosen to match nitrogen as closely as possible. The LIP model has been chosen to match the high temperature viscosity of nitrogen (α = 13.51). In retrospect, we note that this was not a good choice for the range of temperatures (80 K - 464 K) in this shock. Alsmeyer (1976) found that calculations using an inverse 8th power potential gave the best agreement with his measured density profiles in nitrogen. The mean free path in the upstream gas for the present LIP model will be larger than that for the Morse potential, since this is where the viscosity curve for α = 13.51, shown in figure 3.1, does not match the experimental values. In spite of this there is only a small difference in the density profiles. However, the translational temperature profiles are vastly different in the upstream gas. A similar effect is noticed in the shock in front of a blunt body when using this collision model (see chapter 8). Note that if we change the scale of the LIP calculations to make the density profiles match more closely (effectively by changing the viscosity to make it closer to that for the Morse potential in the upstream) then the differences between the translational temperature profiles will be greater.

The shock thicknesses, Δ , derived from simulation calculations using the variable-ϕ scheme, with various scattering models, are shown in figure 7.10 and are tabulated in Appendix E. Also shown are





Scattering: ——— Morse potential; ----LIP. variable-ϕ

Fig. 7.9 DENSITY AND TEMPERATURE PROFILES FOR MACH 5 SHOCK (NITROGEN)

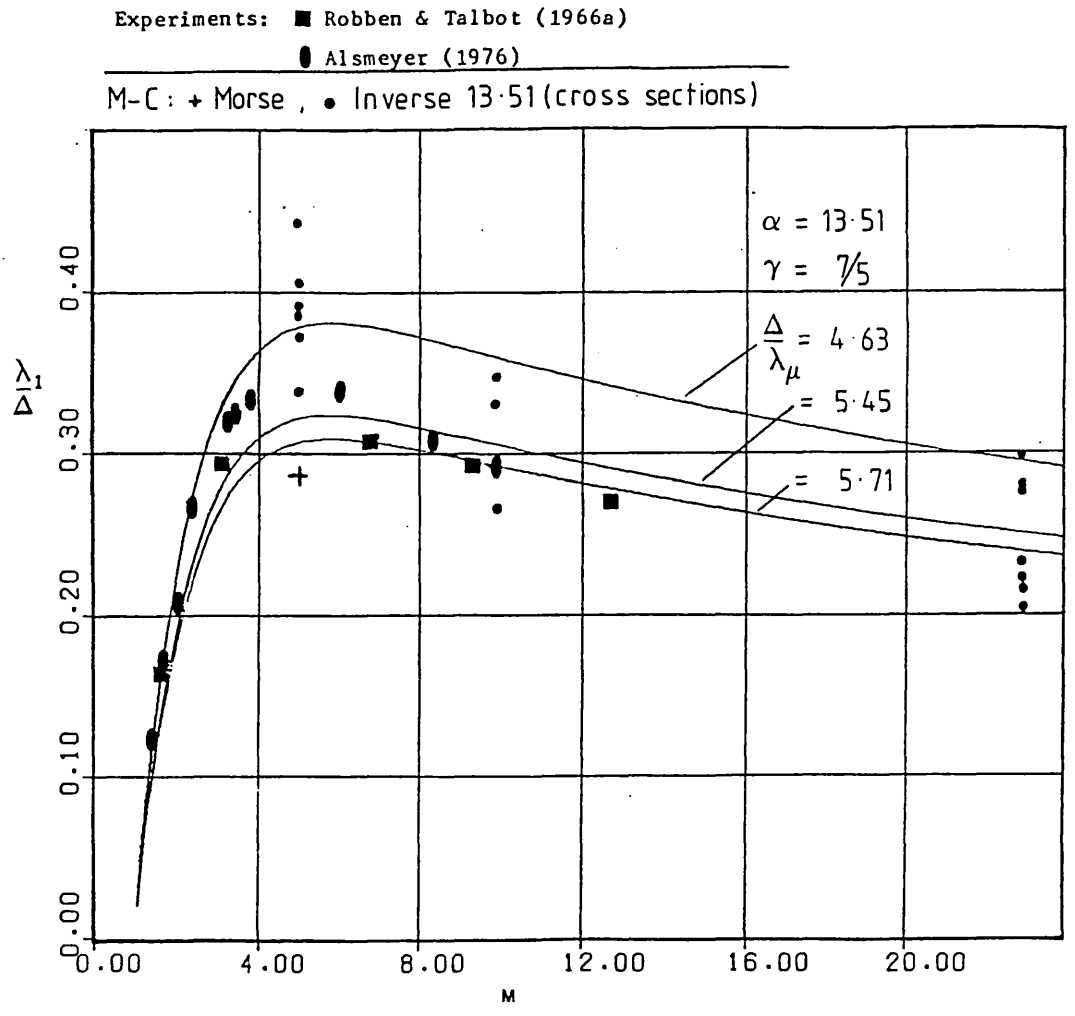


Fig. 7.10 SHOCK THICKNESS Δ FOR NITROGEN

the experimental results of Robben and Talbot (1966a) and Alsmeyer (1976). Robben and Talbot presented their results as L^*/Δ where L^* is a length unit derived from a high temperature, characteristic of the stagnation temperature of the flow. They did this because T_1 was in the range 9 K - 189 K and they did not wish to guess the viscosity of nitrogen at low temperatures. To compare these results with the result calculated using the Morse potential, we have converted their data to λ_1/Δ by calculating λ_1 for the Morse potential and the results are in reasonable agreement with Alsmeyer's results. When Alsmeyer presented Robben and Talbot's results he found that they were vastly different from his own measurements. He does not explain how he

converted the data. We have presented our method of converting this data in Appendix E.

Since the viscosity of nitrogen is not correctly matched in the α = 13.51 calculations the shock thickness cannot be compared unambiguously with experimental results. The diatomic calculations using the variable-ϕ equation are dimensional and the same length unit, the nominal mean free path in the upstream gas derived from the viscosity for the Morse potential, was chosen for all these calculations. For the collision models based on the inverse power cross- section (z_0 = constant) various collision cross- sections were used. The inelastic cross- section, given by z = 1.0, was the same in all calculations. The results in figures 7.10 and 7.11 are calculated for λ_1 derived for the inverse 13.51 power potential.

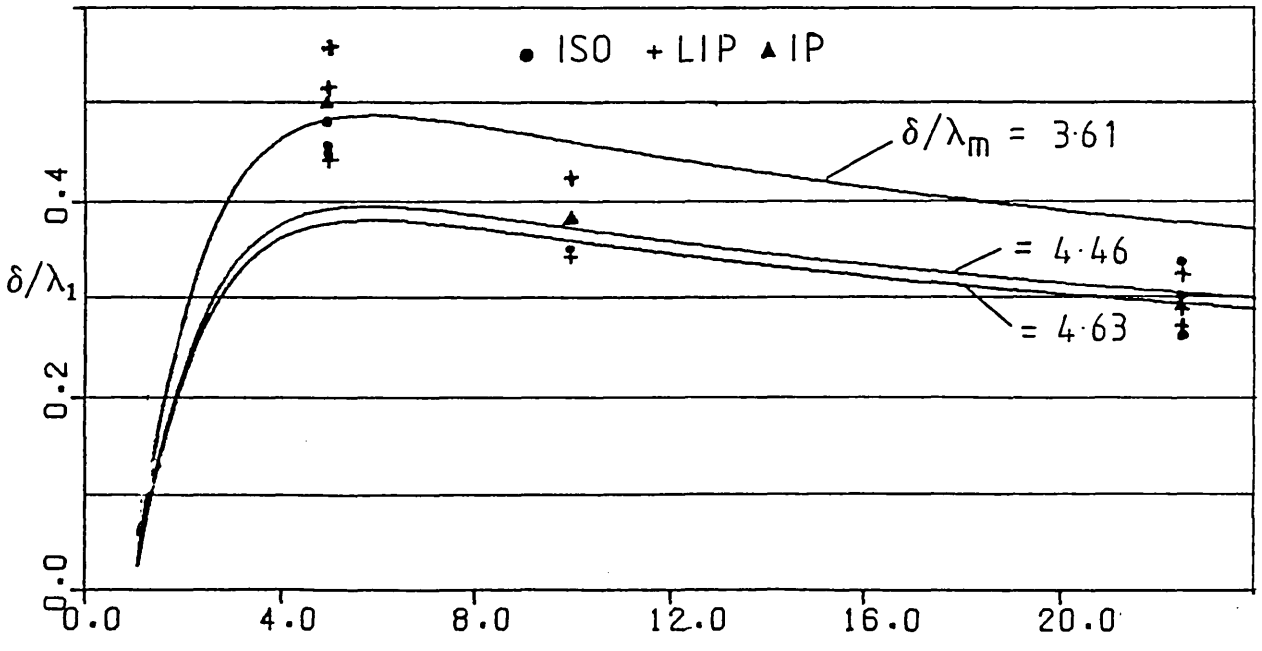


Fig. 7.11 CALCULATED SHOCK THICKNESS δ FOR DIATOMIC GAS

The shock thickness δ for these calculations is shown in figure 7.11. The results are badly scattered, as are those for Δ, even though it would seem that δ could be obtained more reliably from the calculated profiles. The method of normalisation (i.e. making the viscosity the same in all calculations) effectively changes both the collision cross- section and the inelastic cross- section. Hence the effective values of rotational collision number $Z_R(T)$ are changed. It is probable that this change in Z_R, which can be as much as 30%, is responsible for some of the scatter of these calculations. In addition the actual mean collision time, which is a function of the cut-off cross- section, varied for these calculations so there are different accuracies associated with the de-coupling interval. The 'correct' way to make inverse power calculations for nitrogen is to choose the exponent wisely and then rederive the variable-ϕ calculation for the particular cross- section (see chapter 5).

Appendix E contains some results for the asymmetry of the density profiles in these simulations. This asymmetry has not been reported for any experiments in a diatomic gas but we have traced the profiles given by Robben and Talbot (1966a 1966b) and Alsmeyer (1976). There are a few anomalous results for the calculated asymmetries but these could be attributed to the extra scatter in the diatomic calculations, discussed above, which makes it particularly difficult to determine Q. Appendix E also contains the results for some calculations for a monatomic gas with α = 13.51.

CHAPTER 8

APPLICATIONS IN RAREFIED HYPERSONIC FLOWS

8.0 Introduction

In this chapter we test some of the collision models in 'engineering' applications of hypersonic flows around three different body shapes. The first body is a circular cylinder with its flat end facing into the flow. This produces a rapid compression of the gas and a rapid rise of temperature. R. G. Dominy has measured density profiles and rotational temperatures in the compression region in front of a blunt cylinder for Mach numbers of $\sim$20 - 25. The flow conditions are known accurately and calculations have been made for conditions corresponding to those in the experiments. The second body is a sharp cone where the viscous effects would be expected to dominate the flow in the transition between the free molecular and continuum inviscid limits. Finally the flow about a blunt cone is examined.

The Lennard-Jones viscosity formulation has been used to calculate the freestream Knudsen and Reynolds numbers quoted in this chapter.

8.1 Blunt Cylinder

8.1.1 Flowfield

In supersonic flow at high Reynolds numbers a blunt body generates a strong nearly plane shock wave ahead of its front face. Behind this shock there is a region of subsonic radial outflow which is essentially inviscid and a thin viscous layer adjacent to the surface. A sonic line extends from the corner of the body to the shock and beyond this line there is a rapid supersonic expansion of the fluid as

it flows from the front face down the sides of the cylinder. As the Reynolds number is reduced the viscous layer and the shock thicken until eventually the two merge in front of the body producing a continuous compression up to the front face.

Figure 8.1 shows density contours taken from a representative example of the flow fields calculated using the variable-ϕ , Morse potential model. The steady rise in density ahead of the front face and the expansion around the corner are both evident. Near-axis

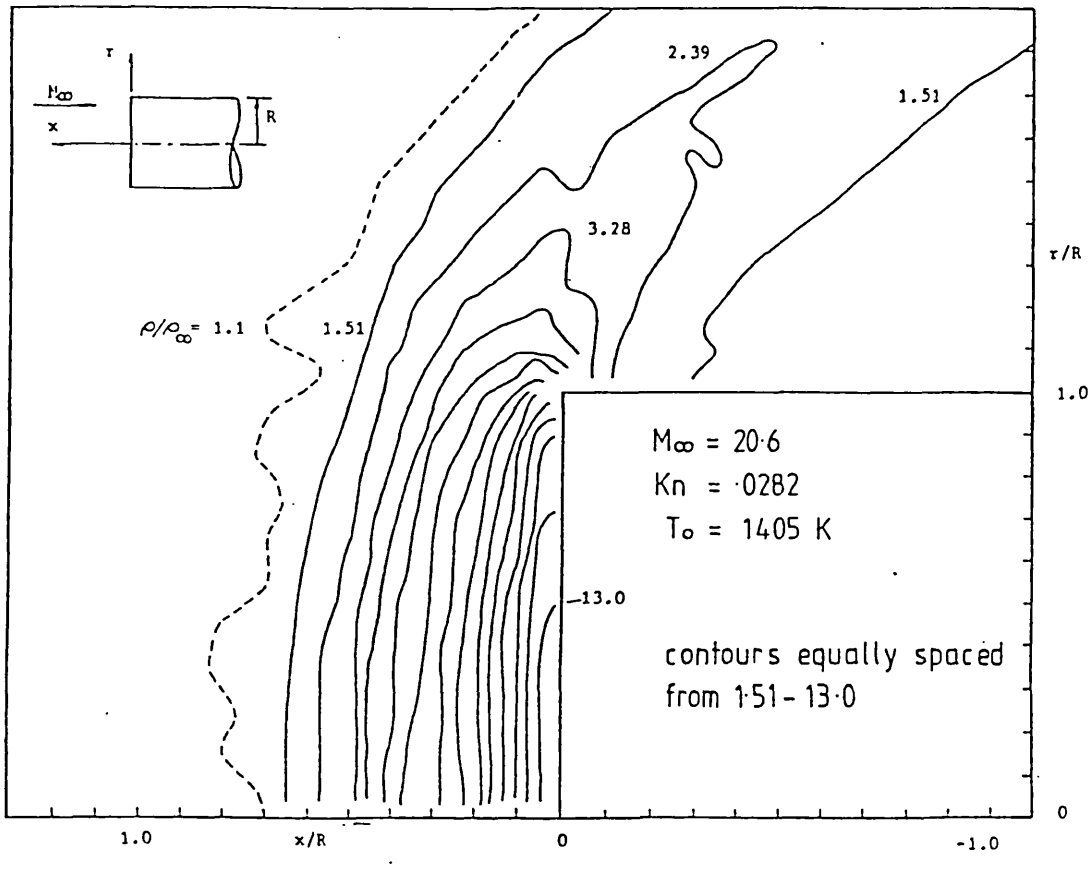


Fig 8.1 DENSITY CONTOURS AHEAD OF BLUNT CYLINDER

streamwise density and temperature profiles calculated for a range of Knudsen numbers, based on the cylinder radius R, are presented in figures 8.2 (a) and 8.2 (b). The density rises steadily until it is more than twice the value for the equivalent continuum inviscid flow.

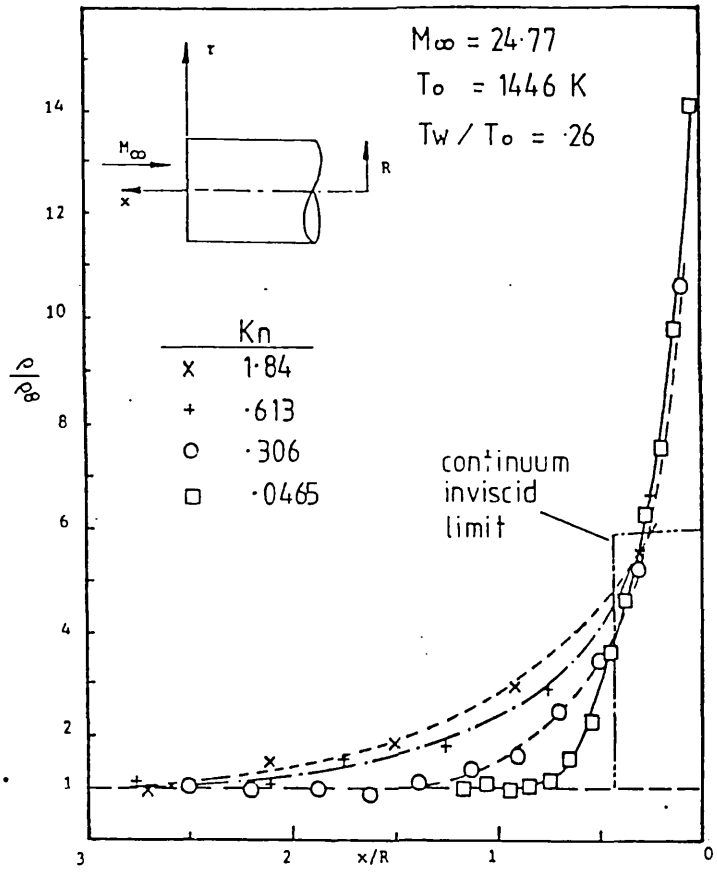


Fig. 8.2 (a) DENSITY PROFILES AHEAD OF BLUNT CYLINDER FOR VARIOUS KNUDSEN NUMBERS

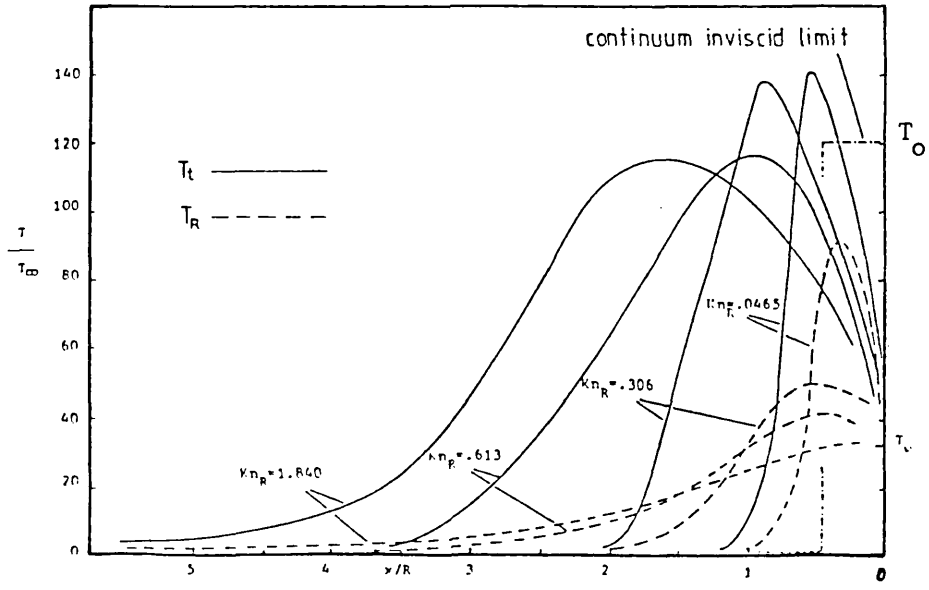


Fig. 8.2 (b) TEMPERATURE PROFILES AHEAD OF BLUNT CYLINDER FOR VARIOUS KNUDSEN NUMBERS

There is a rapid rise in the translational temperature characteristic of a shock which occurs further from the body than the shock stand-off distance predicted for an inviscid continuum flow (Vinokur 1959) and before any appreciable rise in density. For the most rarefied flows the particles reflected from the surface interfere with the shock so that the temperature never rises to the Rankine value T_2 behind the shock. For the denser flows the range of influence of the wall reflected particles is less and this, combined with the slow rise in rotational temperature, allows the translational temperature to rise above the continuum value for a diatomic gas before dropping towards the surface temperature near the body.

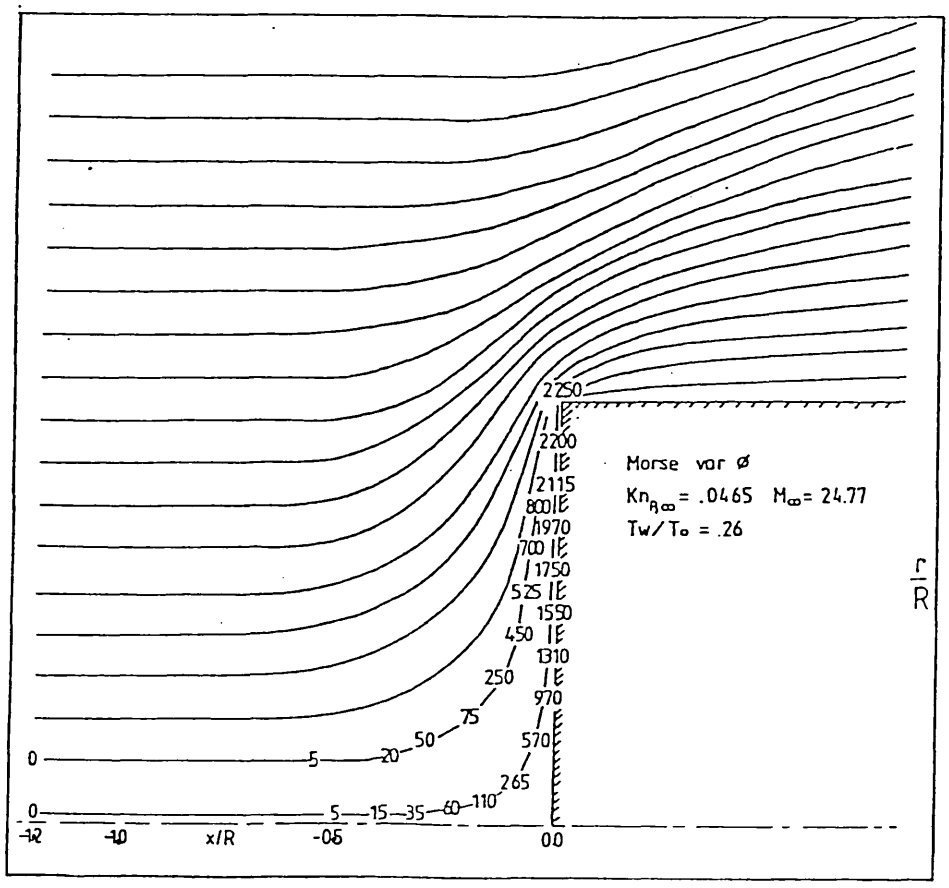


Fig. 8.3 NUMBER OF COLLISIONS ALONG STREAMLINES

To check if vibrational relaxation could be affecting the experimental results near the stagnation line, collision rates were

estimated from the simulation results. This estimate was based on the cutoff cross-section for the Morse potential and would include all those collisions likely to release vibrational energy. Figure 8.3 shows streamlines derived from the simulation and the approximate accumulative number of collisions for a molecule travelling along the streamlines close to the stagnation line. The expected number of collisions for a molecule travelling through the 'shock' and along the front face of the cylinder is approximately 2000. The vibrational collision number at the stagnation temperature of these experiments (1200-2000 K) is approximately 10^5 (Vincenti and Kruger 1965, P. 205). Hence vibrational energy is essentially frozen and cannot play an important role in determining the flow field.

8.1.2 Comparision with experiment

Streamwise density profiles in the stagnation region measured by Dominy (Dominy, Macrossan and Harvey 1981) for different radial positions are presented in figure 8.4. A line has been faired through each set of measured points which show very little scatter. Numerically predicted values of density for each collision model are plotted as points. For much of the flow field there is close agreement between the measured and computed values and the variable-ϕ , inverse power model gives the most accurate prediction. In these calculations for the Morse potential the inelastic cross-section was set equal to the total collision cross-section $z_o = 1.386$. We note in retrospect that this was not a good choice for two reasons. Firstly, this reduced the rotational collision number at any temperature to 52% of the value for the inelastic cross-section $z = 1$ used with the inverse power calculations to derive the variable-ϕ equation. Secondly, it is probable that this cutoff increased the error in achieving detail balance, since the portion of the cross-section for which $z > 1$

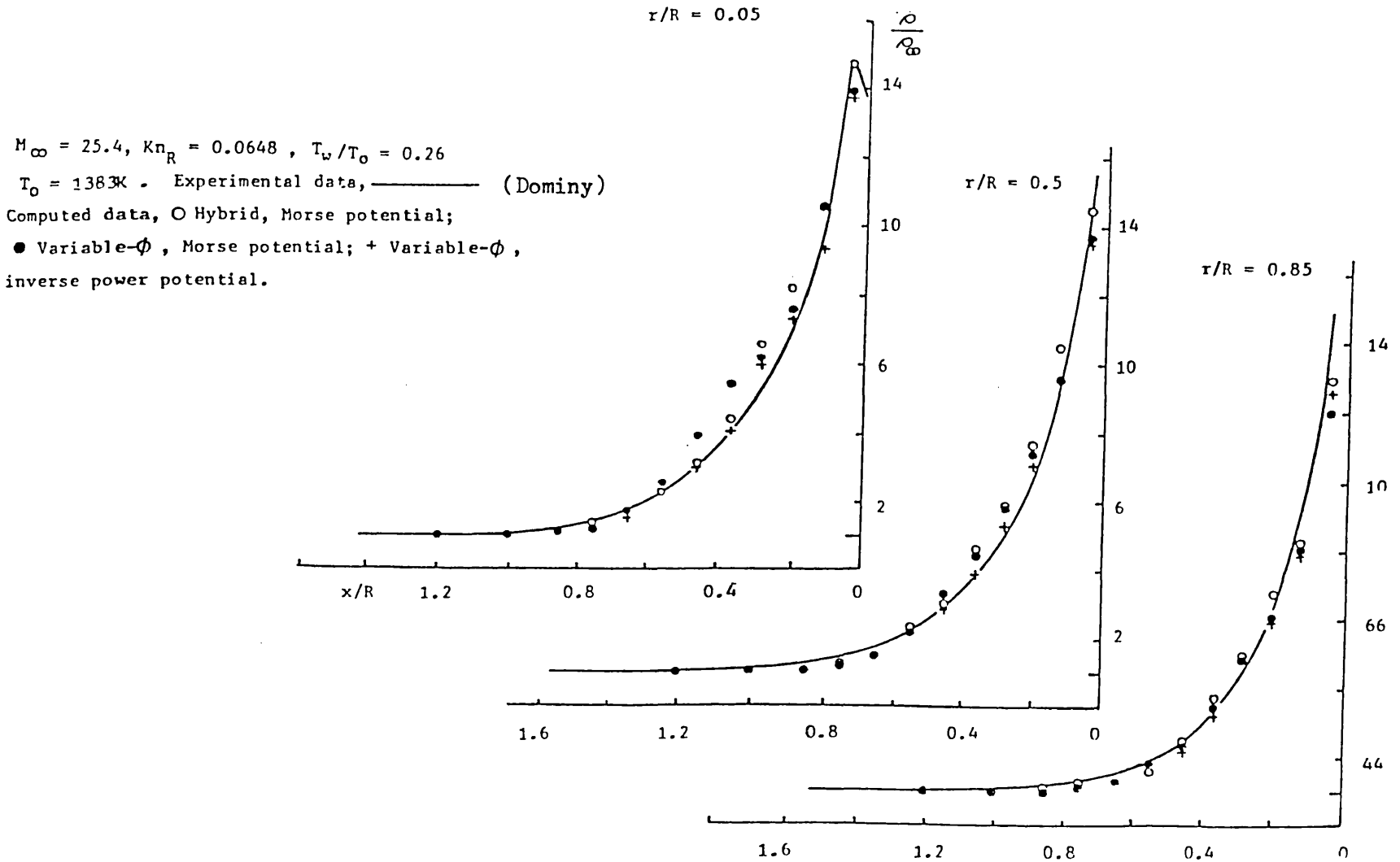


Fig. 8.4 COMPUTED DENSITY PROFILES AHEAD OF BLUNT CYLINDER COMPARED WITH MEASURED PROFILES

includes those grazing collisions where the deflections for the Morse potential are most different from the inverse power deflections (see figure 5.2).

Calculations for slightly different freestream conditions, corresponding to Dominy's second set of experimental results (Davis, Dominy, Harvey and Macrossan 1983), were made using the inverse power and Morse potentials with the same inelastic cutoff ($z = 1.0$). The near stagnation line density profiles are shown in figure 8.5. In contrast to the results in figure 8.4 the densities calculated with the Morse potential are generally less than those calculated with the inverse power potential. The differences between the profiles for the two scattering models are smaller than before. Thus it can be concluded that the rotational relaxation has a substantial effect on the density field. The more realistic Morse potential seems to have had relatively little, if any, advantage over the inverse power potential. In this flow the collisions between freestream and body reflected particles should have the greatest influence on the flow. For these high energy collisions the attractive part of the intermolecular force has little effect and the two potentials produce similar deflections (see figure 5.2). These conclusions must be taken cautiously since a further unquantifiable error is present. The maximum value of the relative velocity which could be calculated using the Morse potential was set too low and about 0.15% of the total number of collisions in the whole flowfield were ignored. In the stagnation region the percentage would be higher since most of the high energy collisions are in this region. These neglected collisions would be expected to have a disproportionate influence on the results of these calculations.

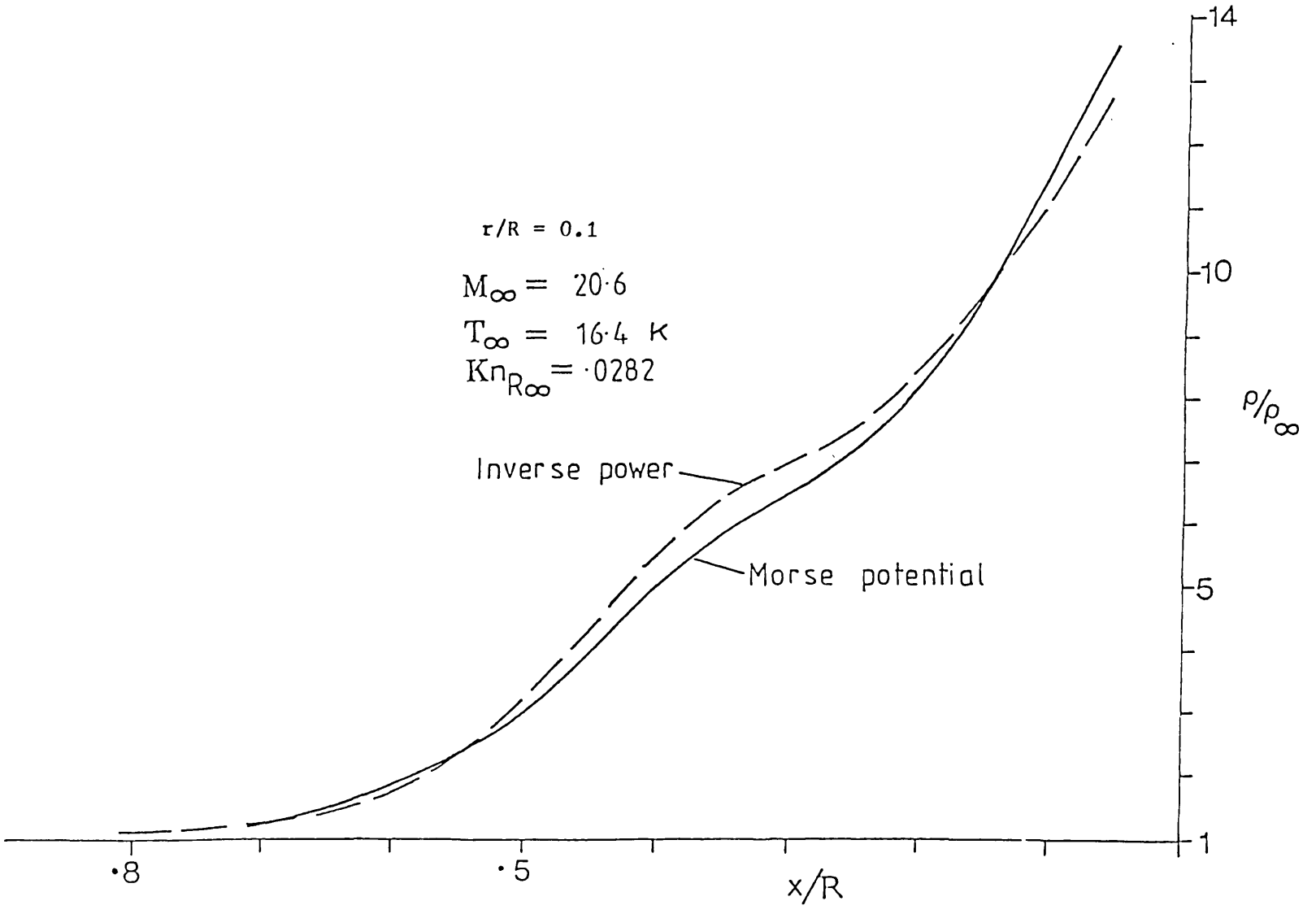


Fig. 8.5 DENSITY PROFILES FOR TWO COLLISION MODELS

The computed density profiles in figures 8.4 and 8.5 show the beginnings of a discrete shock appearing at x/R ~•4. A similar effect for low Knudsen numbers in a Mach 10 flow about a blunt cylinder was found by Pullin, Davis and Harvey (1977). There is no indication of this in the experimental density profiles. Figures 8.1 and 8.4 both indicate that the effect is reduced away from the axis.

The near-axis rotational temperature $\overset{S}{\wedge}$ measured by Dominy (Davis et al. 1983) are shown in figure 8.6 (a). Calculated rotational temperature profiles agree well with the measured values. Figure 8.6 (b) shows the corresponding translational temperature profiles and it can be seen that each scattering model gives a different stand-off distance for the temperature 'shock'. The translational temperatures could not be measured so we cannot judge the relative merits of the scattering potentials from this. The difference between the translational and rotational temperatures is a measure of the amount of energy which is available to be transferred from translational to rotational modes by collisions. If Z_R were constant, that is if the average amount of energy transferred were independent of the energy of collision, we would expect the rotational temperature profiles to differ where they rise rapidly, their spacing echoing that of the translational temperature profiles. Thus the variations in Z_R have compensated in some way for the variation in position of the thermal shock. When the inelastic cross-sections were different for the Morse and inverse power potentials the rotational temperature profiles calculated with each model were quite different (Dominy et al. 1981). It seems from this that a constant ϕ scheme would not have worked as well here.

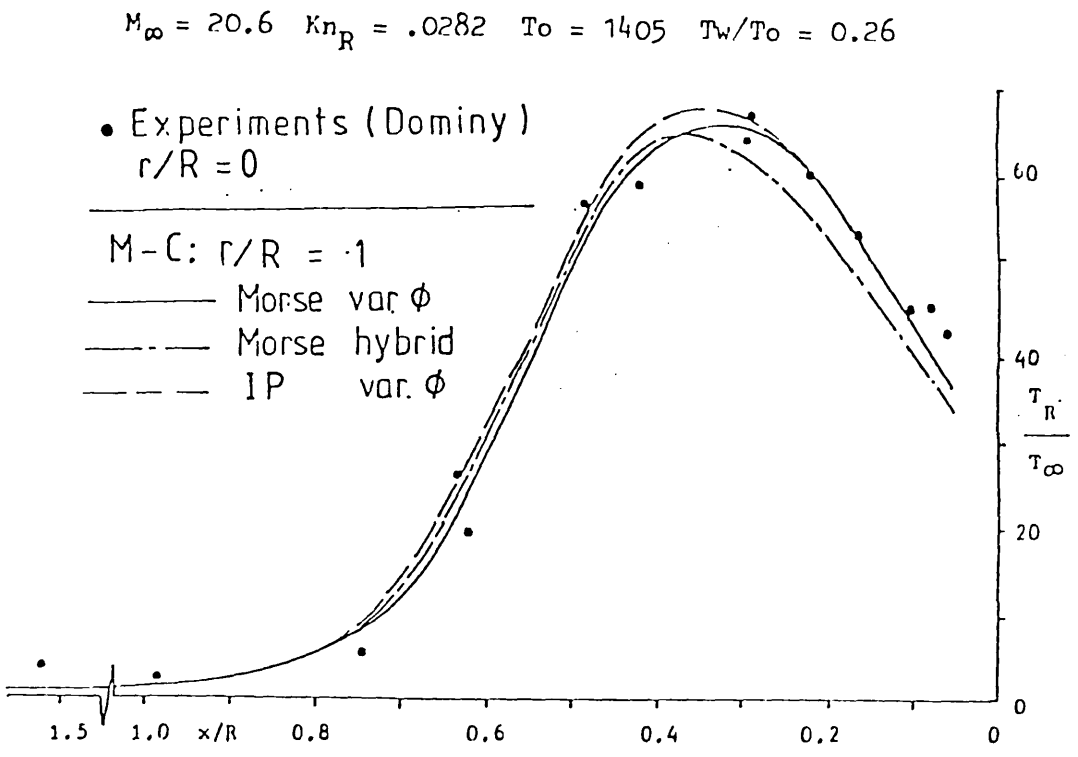


Fig. 8.6 (a) STREAMWISE ROTATIONAL TEMPERATURE PROFILES NEAR STAGNATION LINE AHEAD OF BLUNT CYLINDER

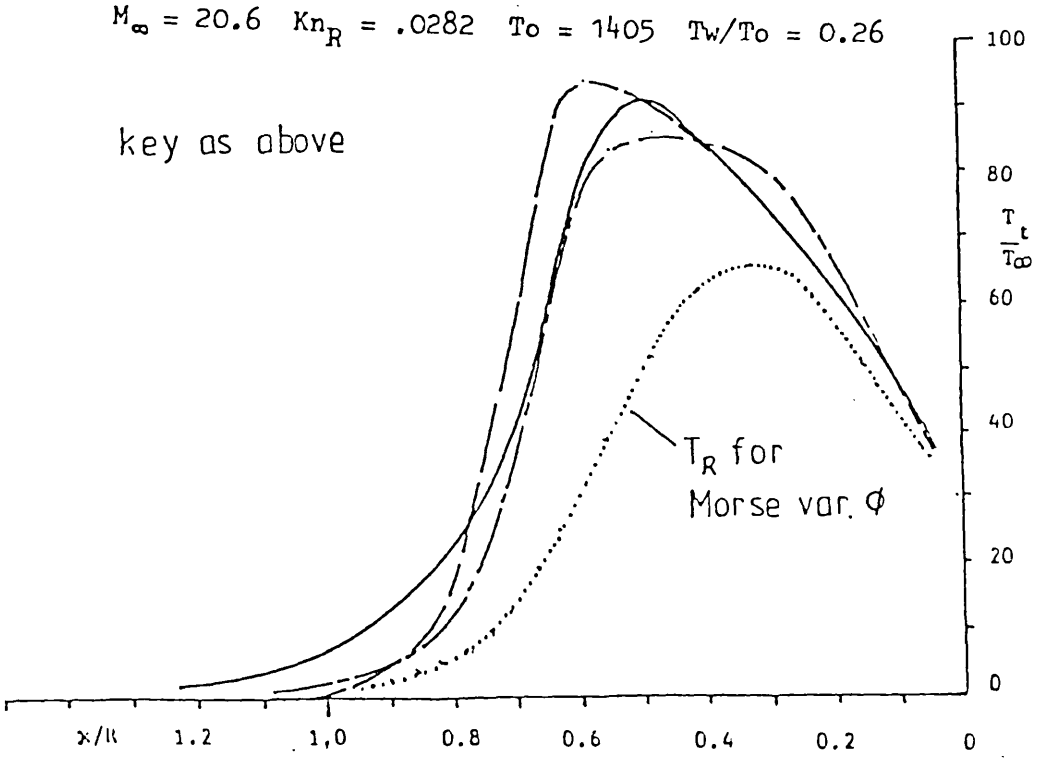


Fig. 8.6 (b) STREAMWISE TRANSLATIONAL TEMPERATURE PROFILES NEAR STAGNATION LINE AHEAD OF BLUNT CYLINDER

The translational temperature profile calculated with the Morse potential and the hybrid scheme is quite different from that calculated with the same potential and the variable-ϕ scheme. Figure 8.6 (b) shows that the temperature rises further from the body for the variable-ϕ scheme. The calculations for a lower density (Dominy et al. 1981) showed that the temperature disturbance for the hybrid scheme extended further ahead of the face of the cylinder. This discrepancy may have been caused by the different inelastic cutoff conditions used in the earlier calculations.

8.1.3 Heat transfer to blunt cylinder

Heat transfer to the body has been calculated and expressed as Stanton number, i.e.

$$C_h = \frac{\dot{q}}{\rho_\infty U_\infty (H_o - H_w)} \doteq \frac{\dot{q}}{\frac{1}{2}\rho_\infty U_\infty^3 (1 - T_w/T_o)} \qquad (8.1)$$

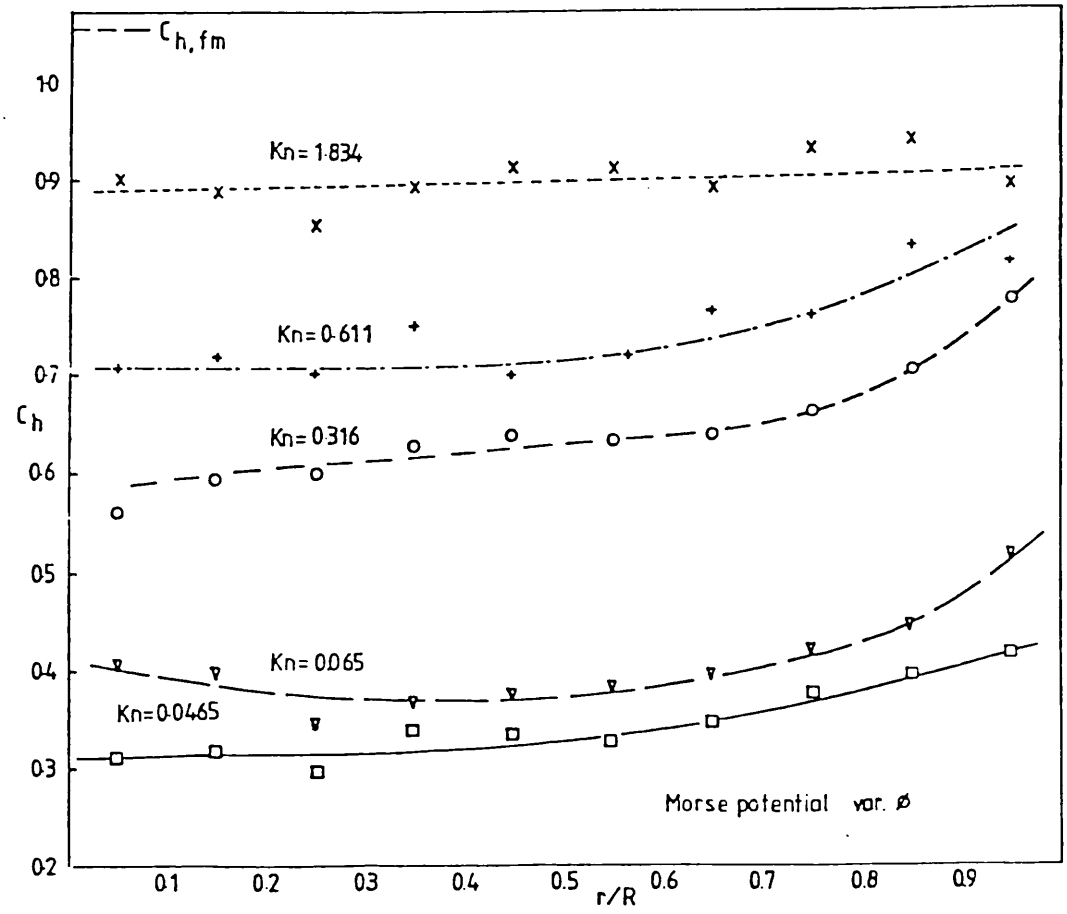


Fig. 8.7 VARIATION OF HEAT TRANSFER ACROSS FRONT FACE OF CYLINDER

The heat transfer distribution across the front face of the cylinder using the Morse potential, variable-ϕ model, for various Knudsen numbers is shown in figure 8.7. For the most rarefied conditions the heat transfer is virtually uniform despite the scatter, but still below the free molecular limit. As the flow density increases the total heat transfer falls and the distribution approaches the shape of the inviscid predictions of Vinokur (1962) for which the heat transfer increases further from the axis.

Coleman, Metcalf and Berry (1977) have measured the heat transfer to the front face of a blunt cylinder for Mach numbers of 7.5 to 14.0. To correlate the heat transfer results for different Mach numbers, stagnation temperatures and wall temperatures they used Cheng's (1961) rarefaction parameter

$$K_r^2 = p_\infty \; R \; / \; \mu_\infty U_\infty \; C^* \qquad (8.2)$$

where $C^* = \mu^* \; T_\infty \; / \; \mu_\infty \; T^*$ and μ^* is the vicosity at the temperature $T^* = \frac{1}{2}(T_2 + T_w)$ characteristic of the region between the nominal shock and the blunt body. The rarefaction parameter is related to the Knudsen number by

$$K_r^2 = 8/5 \; (\pi\gamma/2)^{\frac{1}{2}} M_\infty \; C^* \; Kn_{r\infty}$$

where

$$C^* = \frac{\Omega^{(22)*}(T_\infty)}{\Omega^{(22)*}(T^*)} \sqrt{\frac{T_\infty}{T^*}}$$

and $\Omega^{(22)*}$ is the collision integral used to define the viscosity.

The calculated average heat transfer rates to the whole front face of the cylinder for various flows, including the Mach 10 flow calculated by Pullin et al (1977), are plotted against K_r^2 in figure 8.8. The parameter correlates this data very well. The results for the

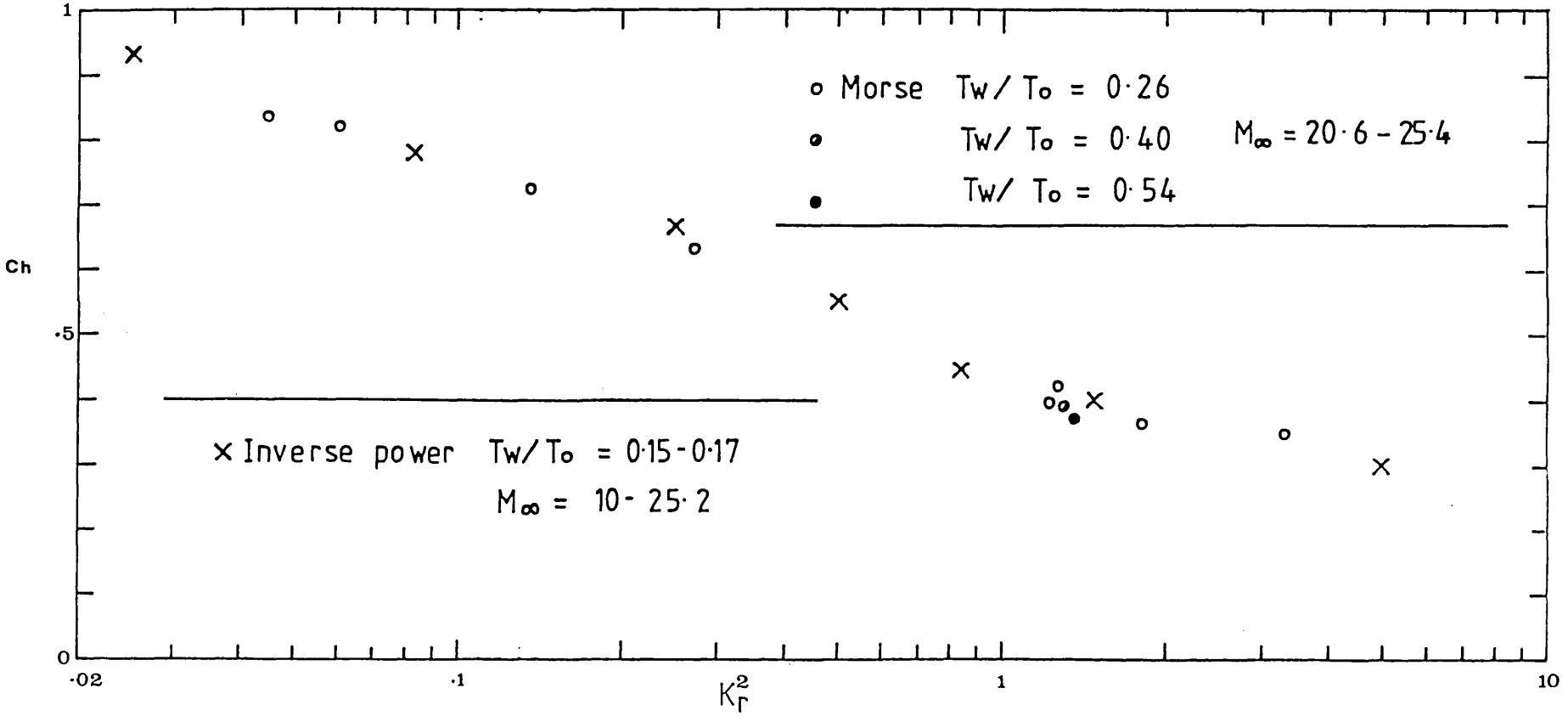


Fig. 8.8 CORRELATION OF CALCULATED HEAT TRANSFER TO FRONT FACE OF BLUNT CYLINDER USING CHENG'S PARAMETER K_r^2

Morse potential appear to show a small dependence on the ratio of wall temperature to stagnation temperature. When some of these calculations are repeated using the inverse power potential rather than the Morse potential, the heat transfer is found to be consistently lower (see figure 8.9), despite the scatter, and the high values for the Morse potential are almost certainly a result of the insufficient size of the deflection array which was used. When calculations made with the inverse power and Morse potentials are compared, this error tends to mask the probable small dependence of C_h on T_w/T_o.

The calculated heat transfer rates are compared with the experimental results of Coleman et al (1977) and Dolman (1980) in figure 8.9. The experimental results have been converted from stagnation point values to average front face values using the

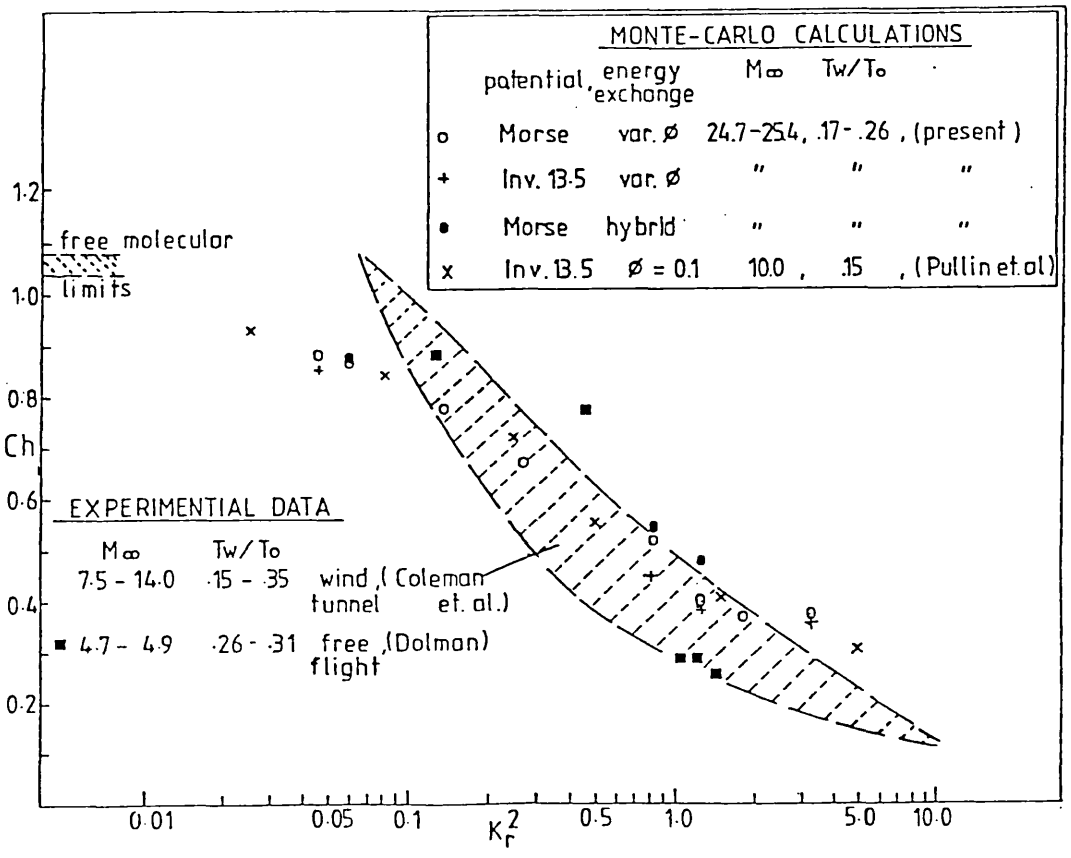


Fig. 8.9 HEAT TRANSFER TO BLUNT CYLINDER COMPARED WITH EXPERIMENTS

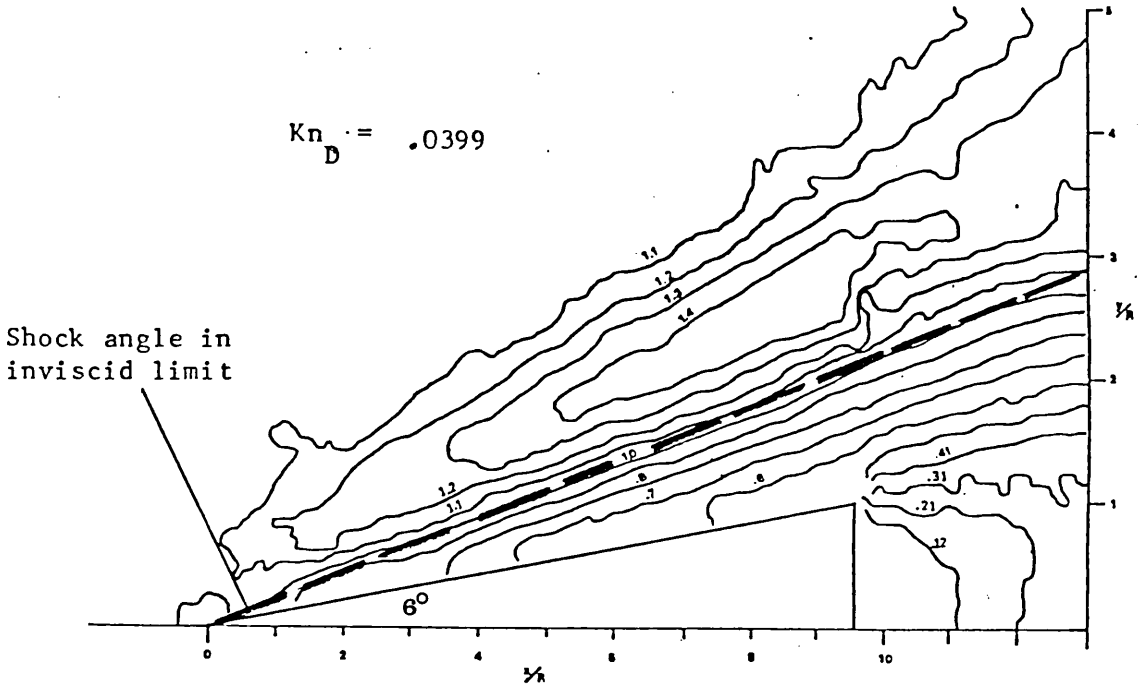
relationship given by Metcalf, Coleman and Berry (1974). The calculated heat transfer agrees with the experimental values in the range $0.1 < K_r^2 < 2.0$ although, because of the scatter in the experimental values, this is not a severe test. The measured values approach and overshoot the free molecular limit while the calculated results are always lower than this limit. For calculations at higher densities (higher K_r^2) the decoupling interval becomes large compared with the mean free time between collisions near the wall, an error which is in practice unavoidable. Too many particles reach the wall because the collisions which would have diverted some of them are ignored. These 'extra' particles will tend to have large velocities, so the heat transfer is artificially increased. The different rotational relaxation rates arising from the two inelastic cross-sections used in the Morse, variable-ϕ calculations had little effect on the heat transfer in spite of the different division of energy in the flow into rotational and translational forms.

A summary of the Monte Carlo results in figures 8.8 and 8.9 is given in appendix F.

8.2 Sharp Cones

8.2.1 Flowfield

Hickman (1967) has used an electron beam to measure density and rotational temperature profiles in a Mach 9.4 flow around a sharp cone. Our calculations were for lower Mach numbers and a slightly different cone angle but the general features of the flow are the same. The surface temperature of the cone is equal to the stagnation temperature of the flow (the 'adiabatic wall' condition). Figure 8.10 shows the density contours for two freestream densities. The corresponding translational and rotational temperature fields are



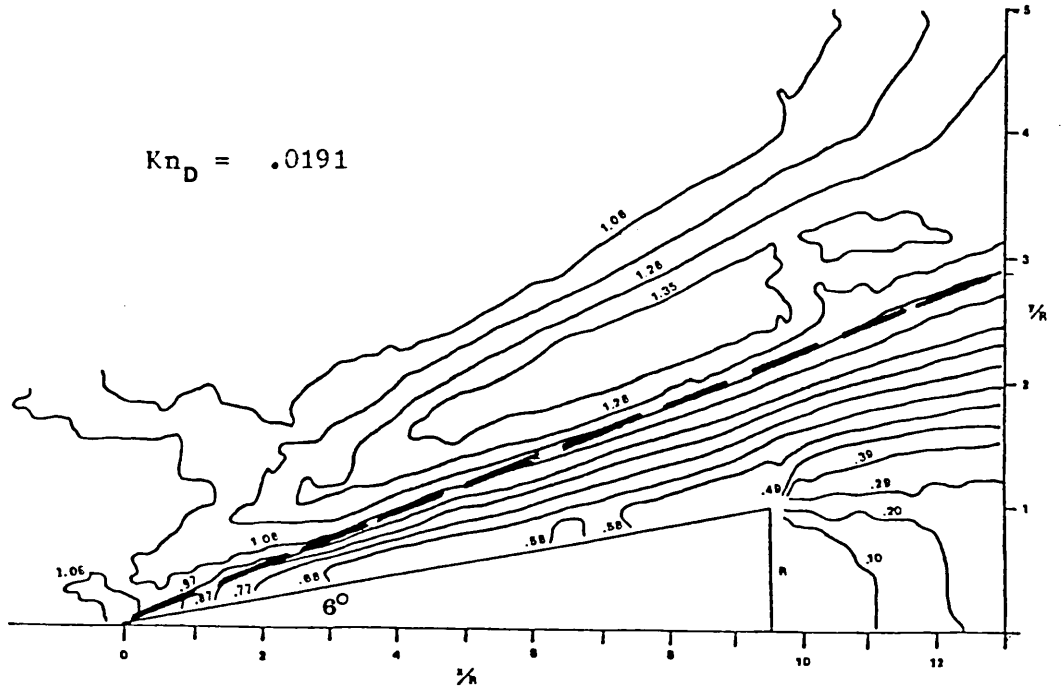
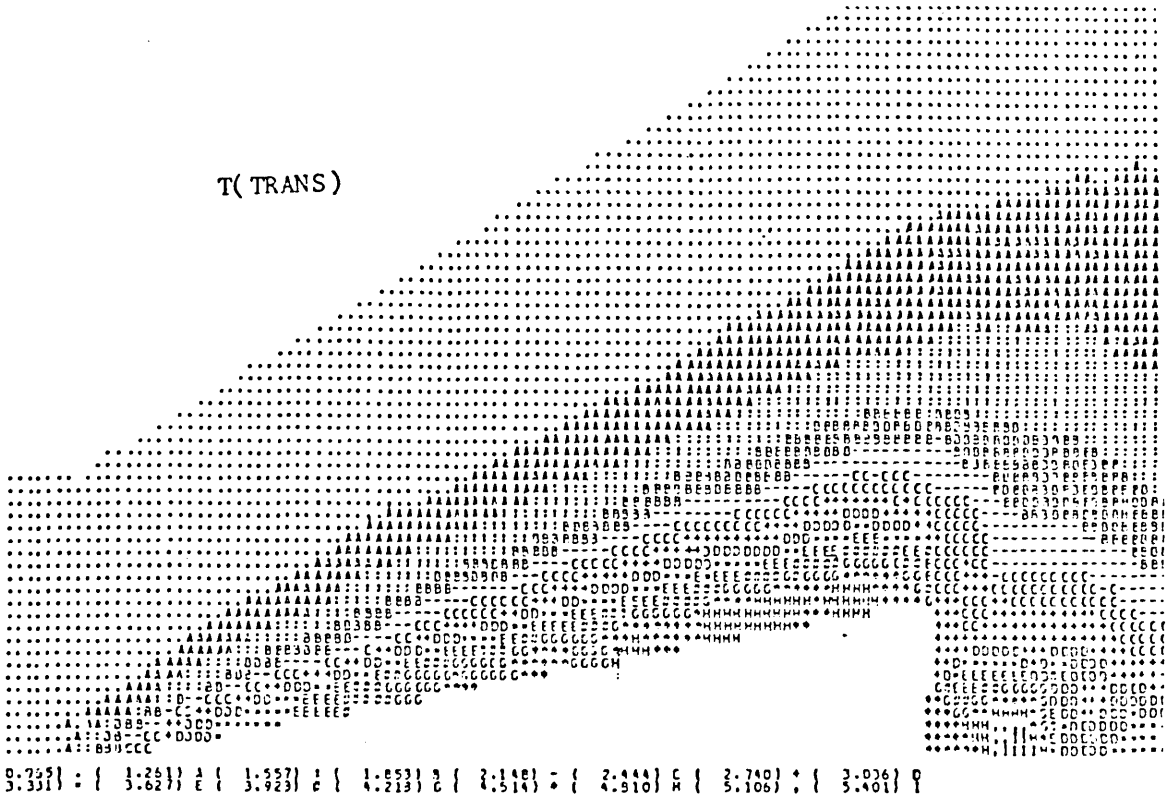
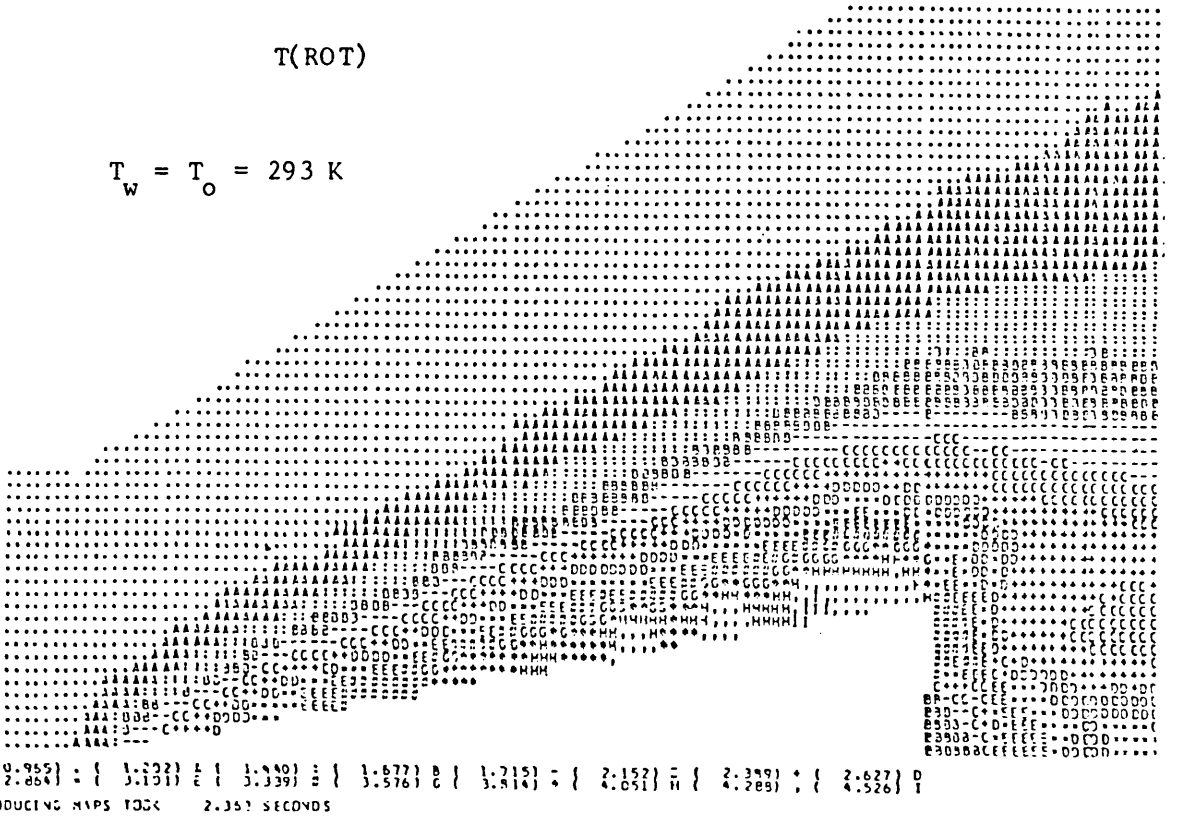


Fig. 8.10 DENSITY ρ/ρ_∞ CONTOURS. SHARP CONES $M_\infty = 5.095$ $T_\infty = 47.1$

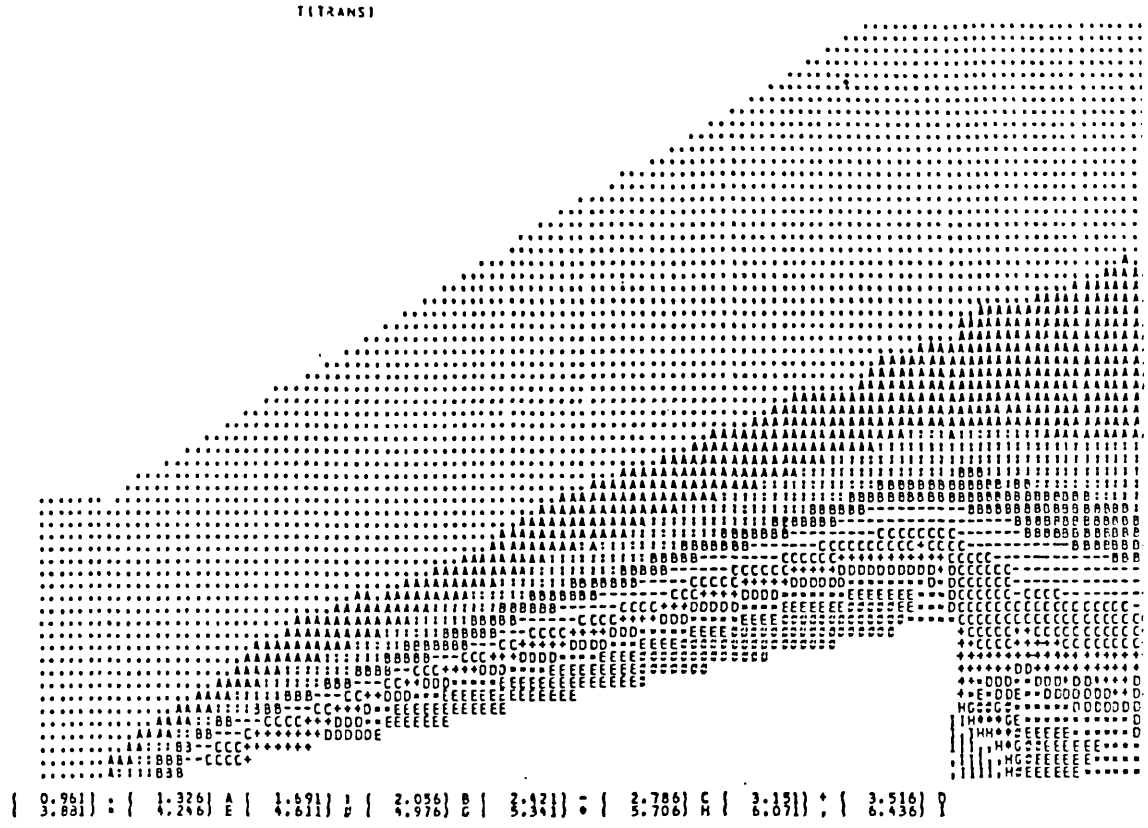


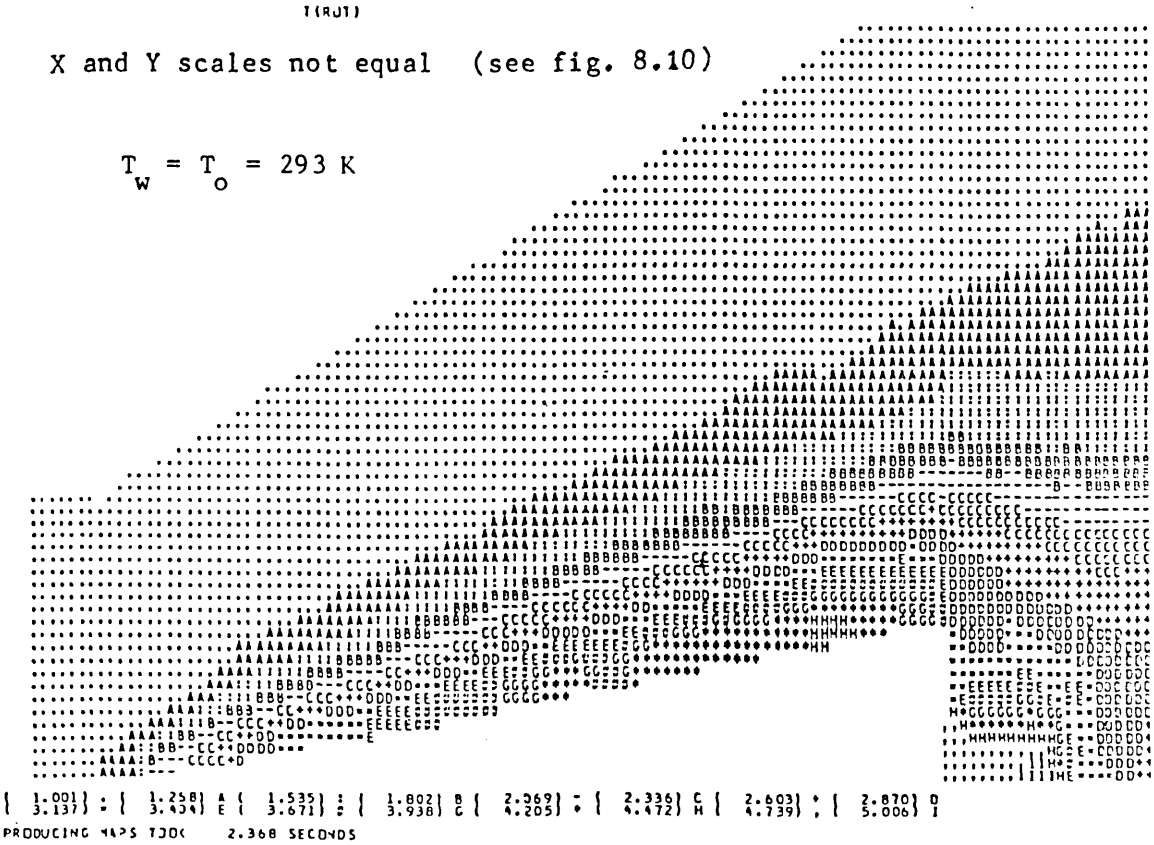
x and y scales not equal (see fig. 8.10)



6° HALF ANGLE. $M_\infty = 5.095$ $T_\infty = 47.1$ $Kn_\infty = .0399$

Fig. 8.11 FLOWFIELD TEMPERATURE ABOUT SHARP CONE





X and Y scales not equal (see fig. 8.10)

$T_w = T_o = 293$ K

6° HALF ANGLE. $M_\infty = 5.095$ $T_\infty = 47.1$ $Kn_\infty = .0191$

Fig. 8.12 FLOWFIELD TEMPERATURE ABOUT SHARP CONE

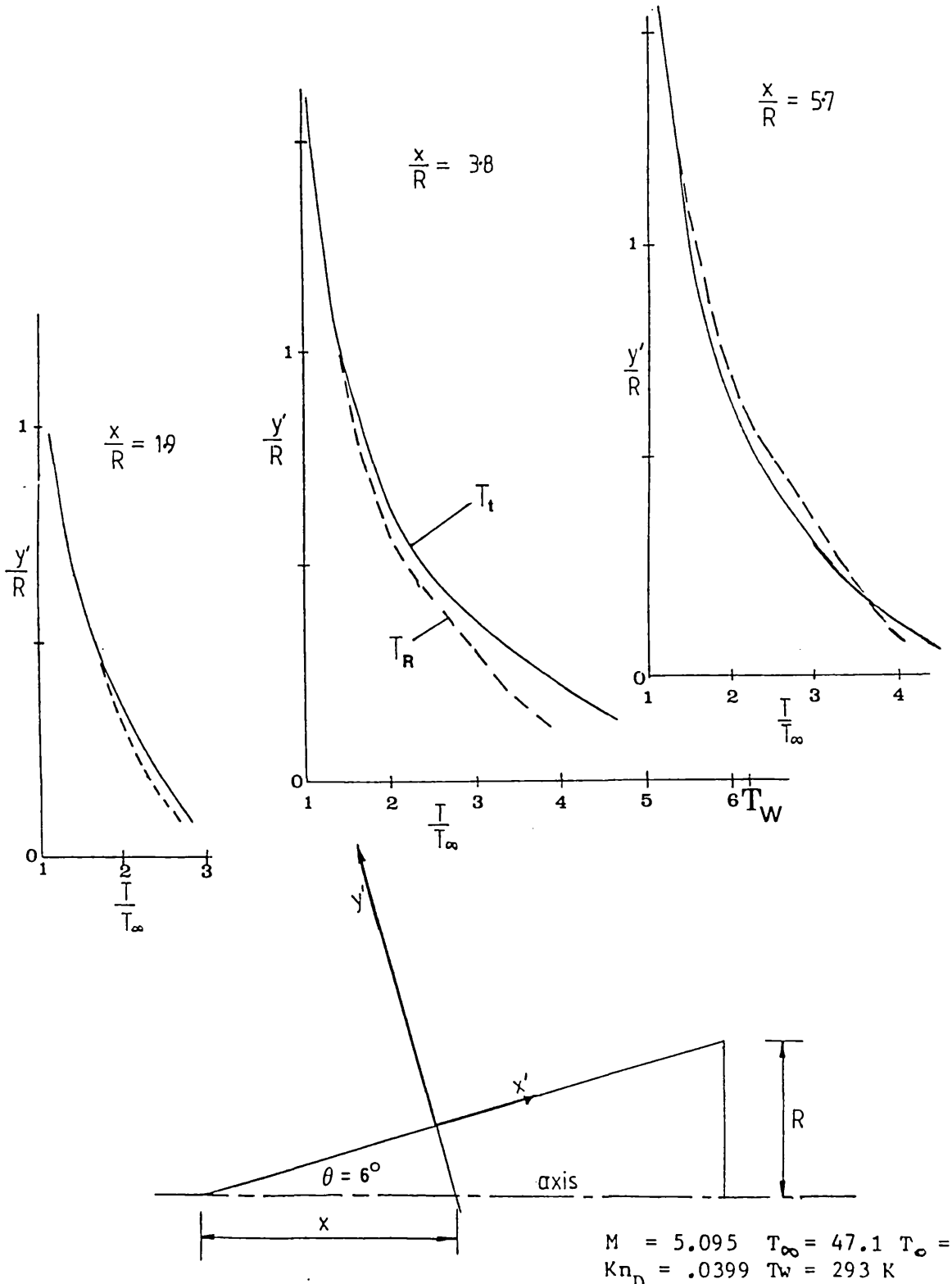


Fig. 8.13 TEMPERATURE PROFILES- SHARP CONE

shown in figures 8.11 and 8.12. These are taken directly from the computer output and each point in the field is obtained from a linear interpolation from the values at three close centroids of the simulation cells. The density contours in figure 8.10 were traced from a similar line printer plot of density.

A weak 'density shock' and a region of low density between it and the body can be seen. The weak shock is displaced by the boundary layer and is further from the cone than the shock for an inviscid flow. A number of temperature profiles, derived from figure 8.11, are shown in figure 8.13. The temperature increases smoothly from the freestream towards the cone surface with no indication of a temperature shock. In some parts of the flow the rotational temperature, is a little above the translational temperature. Since it appears that the temperature rises monotonically along the streamlines this is probably the result of the errors in the energy exchange scheme. Hickman found that the steepest rotational temperature gradients were near the tip of the cone, while in these calculations they are further along the body.

8.2.2 Comparison with experiments

Figure 8.14 shows a number of experimental results for the cone drag coefficient, Cd, in air and nitrogen. The drag is normalised between the free molecular and inviscid limits (denoted by the subscripts 'fm' and 'i' respectively) by

$$C' = (Cd - Cd_i)/(Cd_{fm} - Cd_i).$$

which is plotted against the freestream Knudsen number. This normalisation tends to collapse the data for different cone angles and Mach numbers for adiabatic walls. The drag decreases smoothly from the free molecular towards the inviscid limit as the density increases.

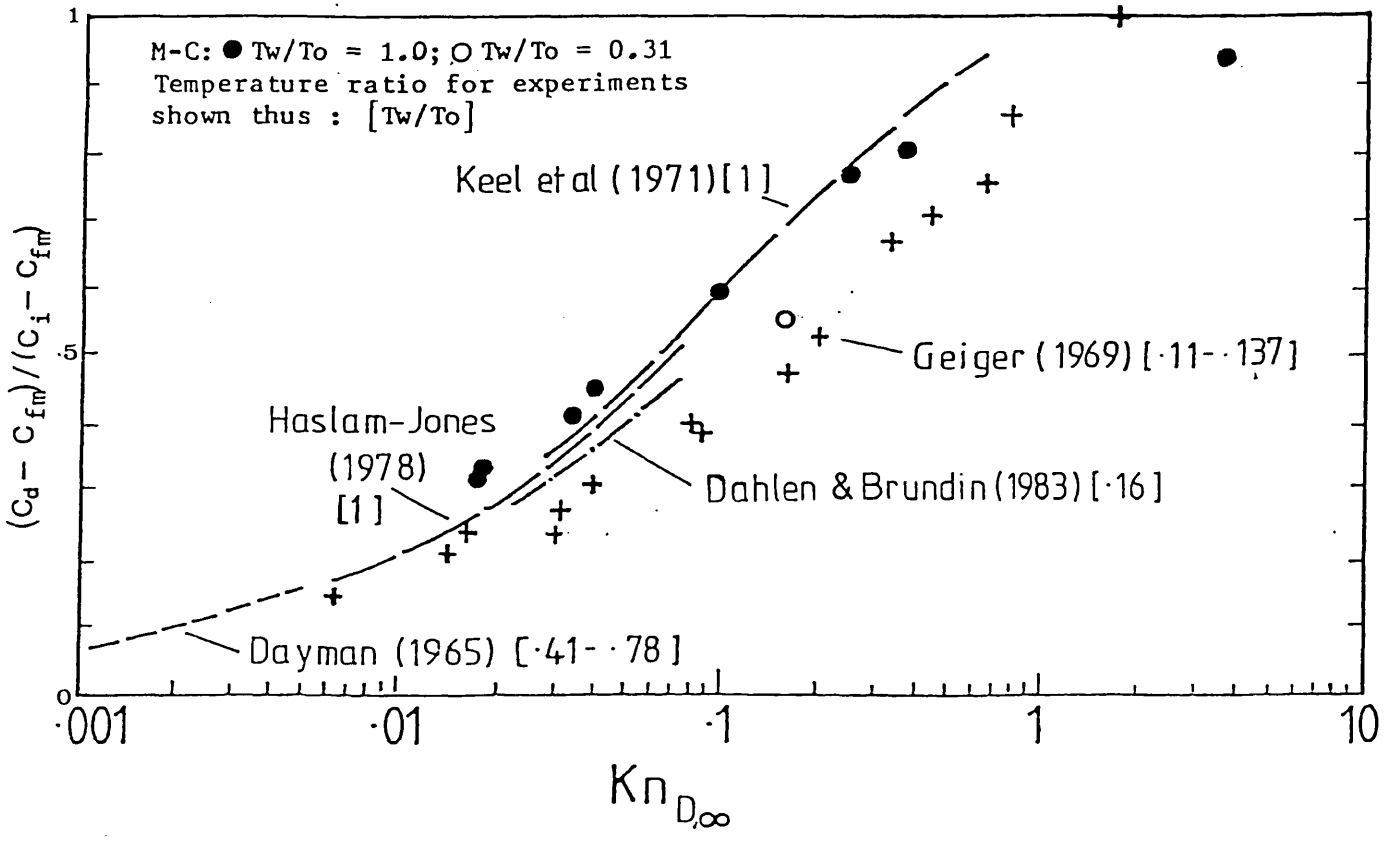


Fig. 8.14 CONE DRAG VS. FREESTREAM KNUDSEN NUMBER (LENNARD-JONES VISCOSITY)

For cold walls ($T_w/T_o \ll 1$) the drag is reduced below that for adiabatic walls and the data of Geiger (1969) for high Mach numbers ($\sim$22) and high stagnation temperatures (1500 - 2000 K) and that of Dahlen and Brundin (1983) for relatively low Mach numbers ($\sim$5) and low stagnation temperatures (523 K) are shown.

The values of Cd for an adiabatic wall derived from Monte-Carlo calculations (denoted M-C in the figure) agree well with the experimental values in the transition region. At each extreme of Knudsen number, however, the calculated and measured values deviate in the same way as did the heat transfer results for the blunt cylinder. The calculations for low Knudsen numbers were for conditions virtually identical to those in Haslam-Jones's (1978) experiments. The calculations are for nitrogen while the experiments were in air, which may account for some small differences, but it is more likely that the calculations suffer from the errors associated with the finite decoupling interval. These calculations were made with the Morse and inverse 13.51 power potentials with the variable-ϕ equation and there is little to choose between them. In these calculations the problem of the finite size of the deflection array for the Morse potential had been overcome as decribed in chapter 5. No collisions were ignored so the drag should not be artificially increased for the Morse potential compared with the inverse power potential in the way that the heat transfer to the blunt cylinder was.

Bird (1983) has calculated the drag on a sharp cone using Borgnakke and Larsen's two-class exchange scheme. He found that the calculated drag was relatively insensitive to the chosen constant rotational relaxation rate. We have made a single calculation for a cold wall (T_w/T_o = 0.31) using the VHS model with α = 8.33 and a

constant value of ϕ. The calculated drag is intermediate between those for $T_w/T_o = 1.0$ and the experimental results for $T_w/T_o \sim 0.1$. It has been suggested (e.g. Hamel and Cooper 1969, Whitfield 1973, Pullin et al. 1977) that the heat transferred to and the drag force on bodies in near free molecular flow will depend on the mean free path λ_{bf}. This is the average distance between collisions for a particle reflected from the wall and moving through a cloud of freestream particles. Whitfield (1973) gives succesive approximations to λ_{bf} for hard sphere molecules reflected from a surface which is at an arbitrary angle to the freestream flow direction. A correlation parameter which is proportional to his zero and first order expressions for λ_{bf} for a surface parallel to the flow is

$$K_{bf} = 1/\sqrt{2}\, n_\infty \pi\, \sigma^2 D\, S_w \qquad (8.3)$$

where

$$S_w = S_\infty \sqrt{T_\infty / T_w}$$

The constants in this expression have been chosen so that the parameter may be calculated conveniently from the freestream Knudsen number. Thus

$$K_{bf} = Kn_\infty \Omega^{(22)*}(T_\infty) / S_w$$

where the collision cross-section $\pi\sigma^2$ has been used. It is easily shown that $K_{bf} \propto \Omega^{(22)*}(T_\infty) / Re_\infty \sqrt{T_\infty / T_w}$ and the parameter $Re_\infty \sqrt{T_\infty / T_w}$ has been used for correlating hot and cold wall drag (Geiger 1969). The factor $\Omega^{(22)*}(T_\infty)$ gives the departure of the viscosity used to calculate the freestream Reynolds number from the theoretical viscosity for hard sphere molecules of diameter σ. Also $K_{bf} / \Omega^{(2,2)*}(T_w)$ is proportional to $Re_\infty\, \mu_\infty / \mu_w$, which is the 'wall Reynold's number' used by Potter (1967) to correlate a variety of data in the transition regime. It is proportional to λ_{bf} calculated with a collision cross-section equal to an average cross-section for collisions in a near equilibrium gas at temperature T_w. For

temperatures above 300 K, $\Omega^{(2,2)*}$ is a slowly decreasing function of T.

Hot and cold wall drag coefficients plotted against K_{bf} are shown in figure 8.15. The parameter tends to bring together the data in the

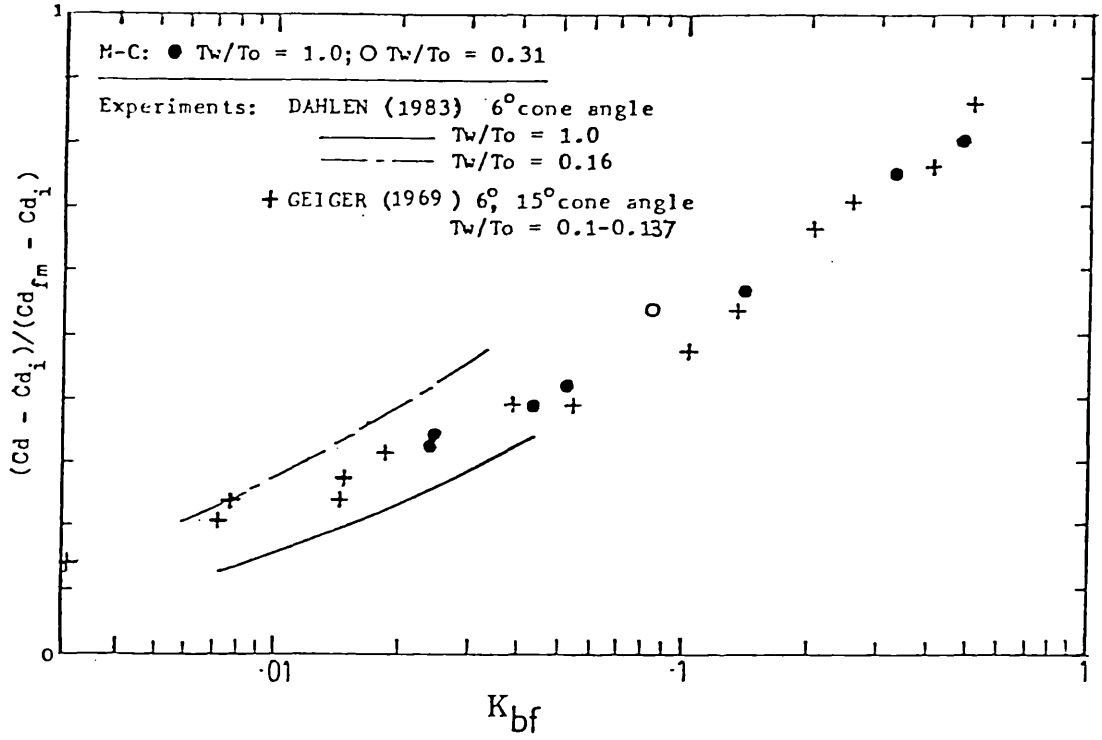


Fig. 8.15 HOT AND COLD WALL CONE DRAG

near free molecular limit as expected but it 'over corrects' the data for higher densities. Following Pullin (1974) by using a viscosity cross-section $\pi\sigma^2 Q^{(2)*}(g)$, which is only a slowly varying function for large relative velocities, is little better. This correlation is shown in figure F.2 (appendix F). It can be seen in figure F.1 (appendix F) that Whitfield's parameter based on his first order result for λ_{bf} for a blunt body, does not correlate the heat transfer to the blunt cylinders as well as Cheng's rarefaction parameter does.

8.3 Blunt Cones

8.3.1 Flowfield

A few calculations have been made for flows about a 6° cone with a blunt nose. Density contours for two Mach 5 flows are shown in figure 8.16 and the temperature fields are shown in figures 8.17 and 8.18. Ahead of the cone is a stagnation region showing characteristics similar to those of the flow ahead of the blunt cylinder. The same sort of weak density shock which was seen for the sharp cone is seen here. The maximum density contours are roughly parallel to a line drawn at an angle of 17° to the freestream from the imaginary tip of a sharp cone. This corresponds to a shock about a sharp cone with half angle 12° in an inviscid flow. The distributions of normal and shear stress for three different densities are shown in figure 8.19. As the density is reduced the shear stress increases while there is relatively little change in the normal pressure.

8.3.2 Comparison with experiments

The calculated drag coefficients are compared with experimentally determined coefficients in figure 8.20. The experiments were performed by T. Haslam-Jones in the Oxford low density wind tunnel (personal communication 1981) and his results for a 6° cone and a Mach 5 flow are shown. The drag calculated with the Morse potential is in excellent agreement with the experimental results. This is a better result than that obtained for the sharp cones for similar Knudsen numbers and for this more complex flow there is a greater difference for different collision models. The calculations using the inverse power potential and VHS model predict drag coefficients which are higher than those measured.

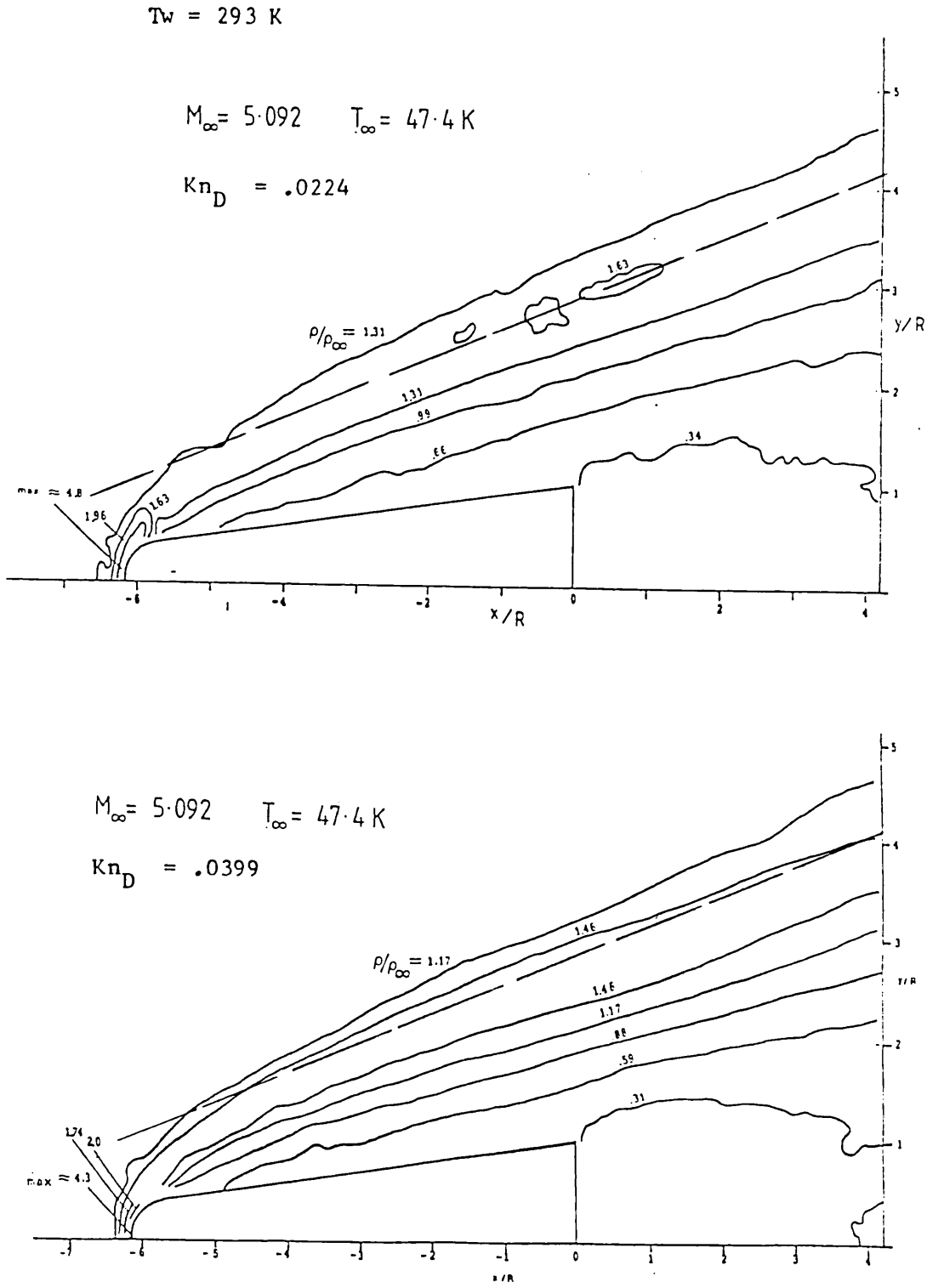
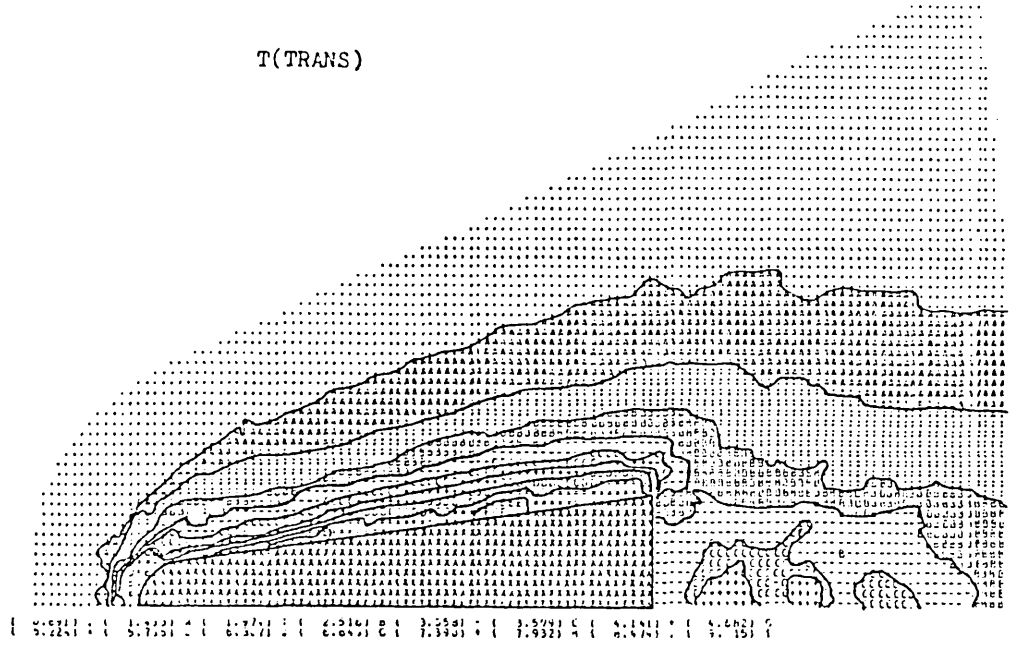


Fig. 8.16 DENSITY CONTOURS- BLUNT CONES



M = 5.092 T = 47.4 K To = Tw = 293 K Kn_D = .0399

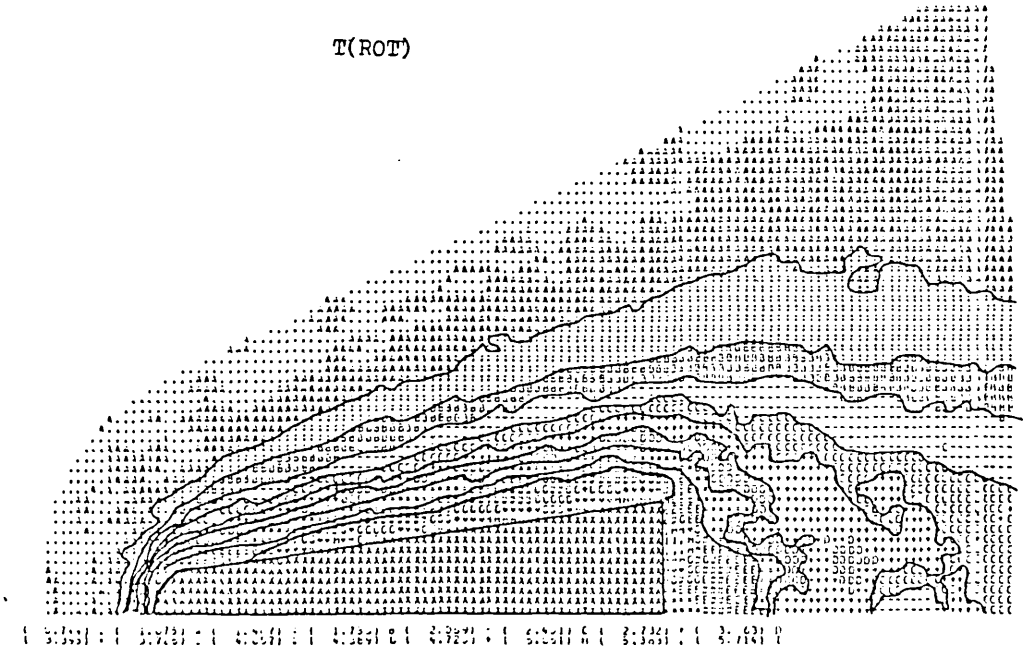


Fig. 8.17 FLOWFIELD TEMPERATURE ABOUT BLUNT CONE

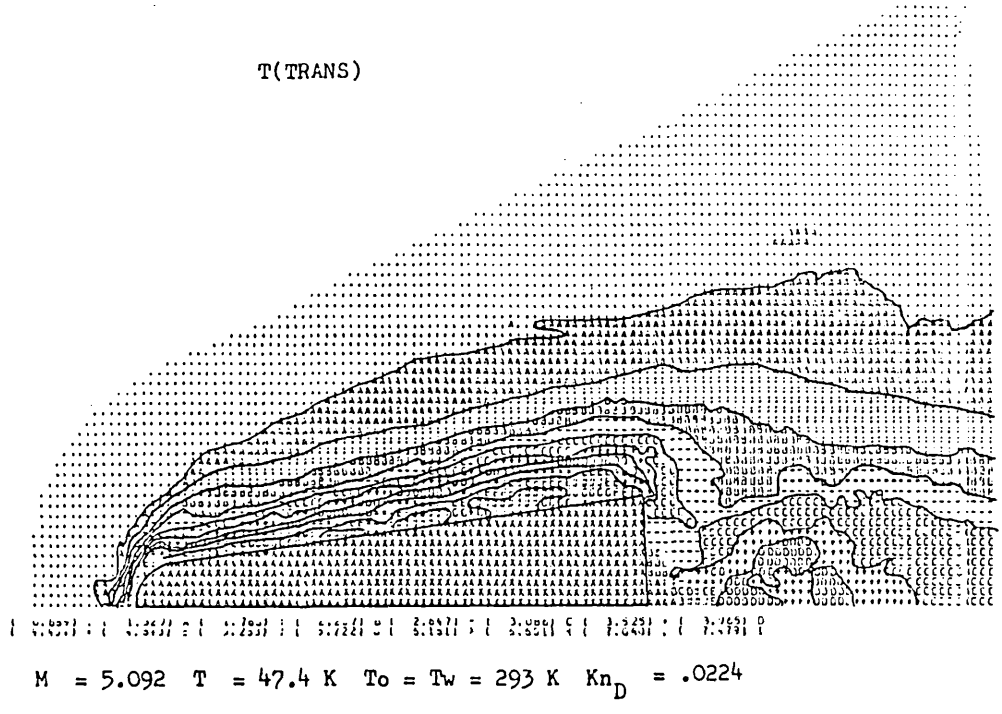


Fig. 8.18 FLOWFIELD TEMPERATURE ABOUT BLUNT CONE

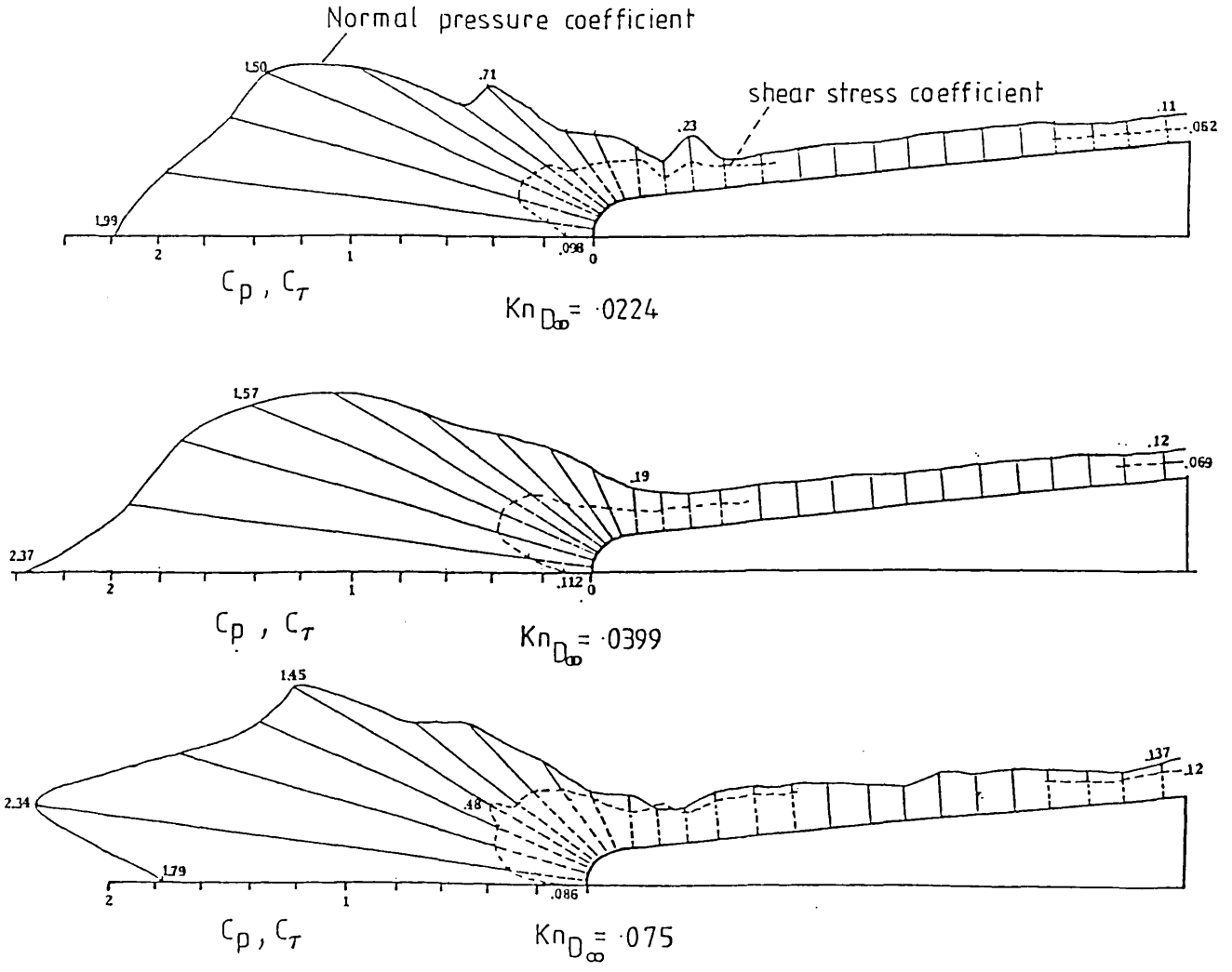


Fig. 8.19 PRESSURE AND STRESS ON BLUNTED CONE $M_\infty = 5.092$ $T_w = T_o = 293$ K

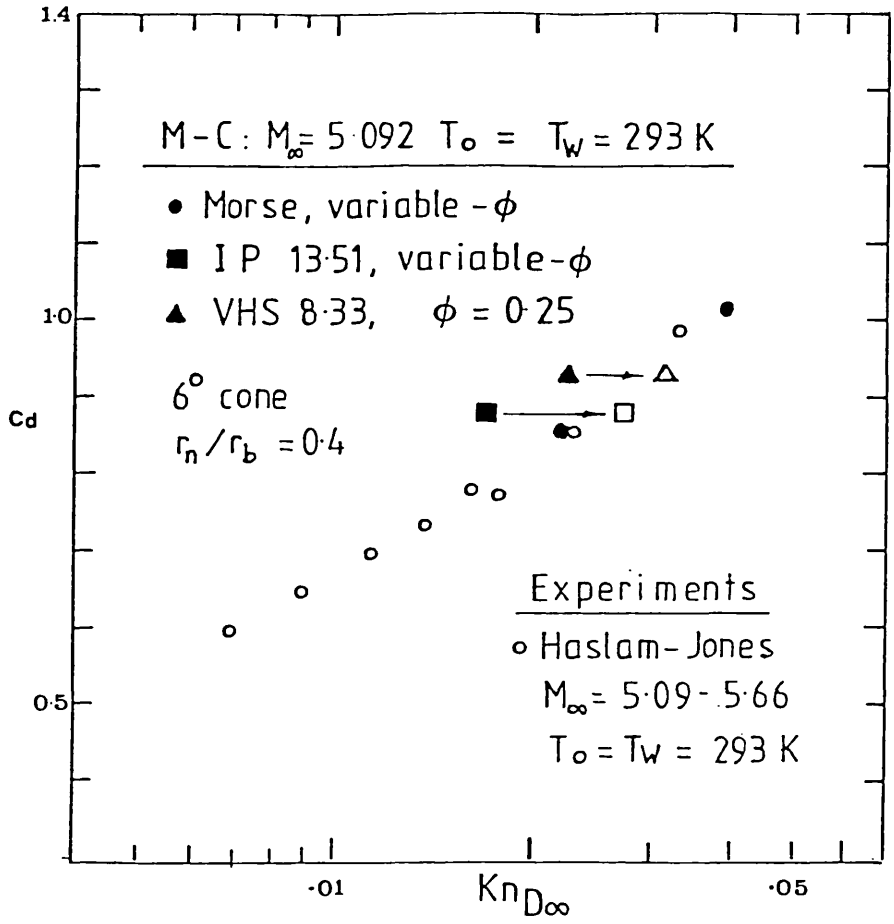


Fig. 8.20 DRAG ON BLUNT CONES

The surface stress distributions for the Morse and VHS models at the same freestream density are compared in 8.21. The increased drag for the VHS calculations is a result of the increased shear stress and is an indication of the greater viscosity for the VHS model at low temperatures. Figure 8.20 shows the data points for the inverse power and VHS collision model displaced to the point where the Knudsen number is that calculated by increasing the size of the molecular model until the viscosity in the freestream is equal to the viscosity calculated for the Lennard-Jones potential. This is the same renormalisation which was shown for Davis's (1978) flat plate calculations in figure 3.3 and which improved the inverse power predictions for part of the flow. Exact agreement with the experimental results would require a molecular size somewhere between these limits.

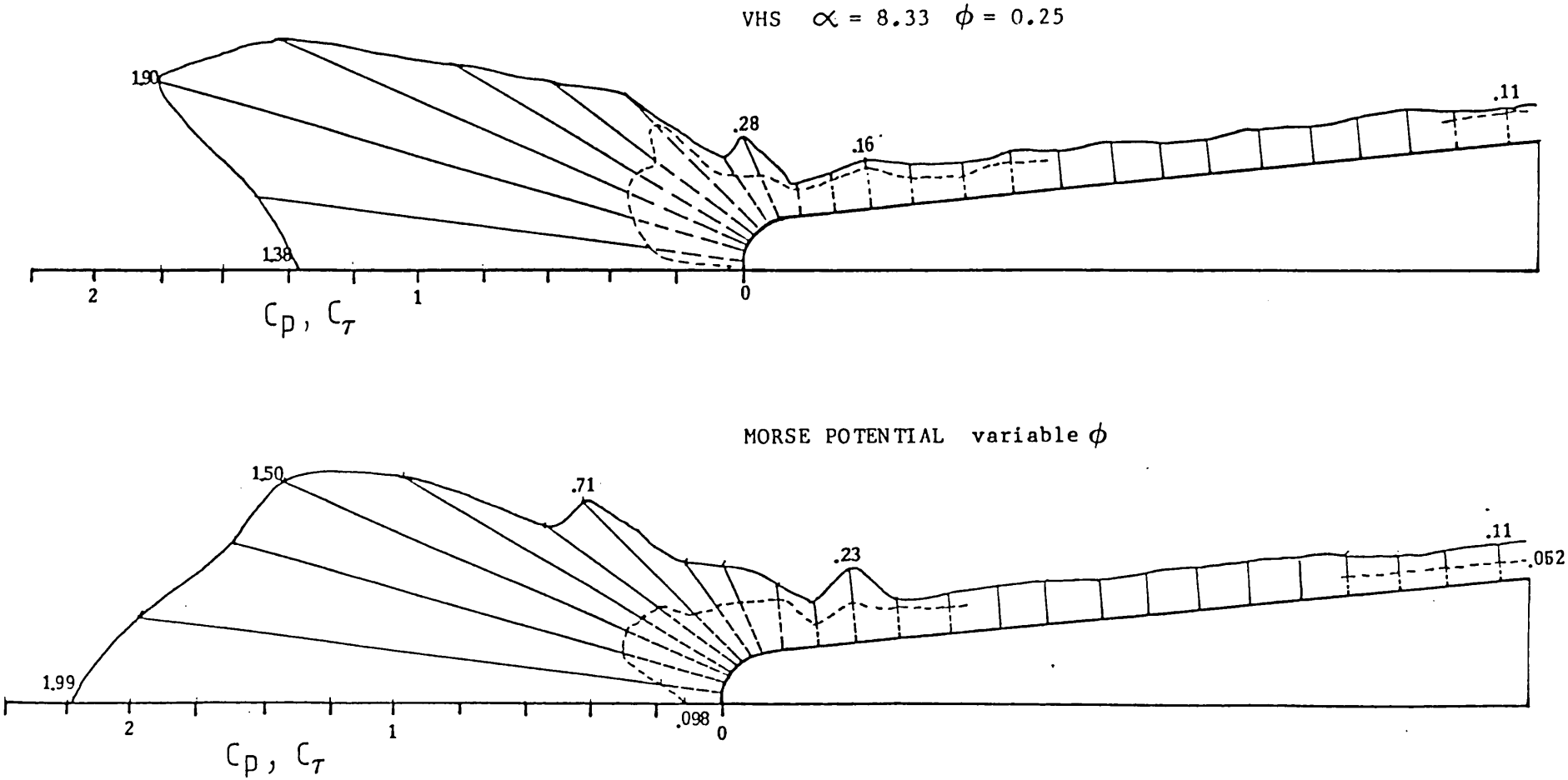


Fig. 8.21 PRESSURE AND STRESS ON BLUNTED CONE FOR TWO COLLISION MODELS M_∞ = 5·092 $Kn_{D\infty}$ ·0224 $T_o = T_w$ = 293 K

It is surprising that for this flow, and not the flow about the sharp cone, the viscosity near the freestream temperature appears to be more important than that near the stagnation temperature. One would expect the opposite since the flow about the blunt cone has a definite 'stagnation region' which would produce an 'enthalpy layer' shielding the surface from the freestream. However this may be an indication that for flows about more complex body shapes the molecular trajectories become more important. If this is so then the exact details of the deflections produced during the collision calculations will also be important, rather than those average effects of the deflections on which the theoretical viscosity depends.

8.4 Conclusions

The collision models tested in this chapter have all given reasonable predictions of the integrated force on and heat transfered to bodies in flows in the transition region between the free molecular and inviscid limits. These results show that with some care in selecting the exponent α the simplest collision models, such as the VHS or inverse power potential, can give estimates of these quantities which are useful for 'engineering' purposes. It is apparently more important that the viscosity of the model gas is correctly scaled than the rotational relaxation rate is correct. Calculations with constant ϕ (Pullin et al. 1977) predicted the heat transfer to the cylinder as accurately as the present variable-ϕ calculations. In part this will be because for the present calculations the value of ϕ varies little for the high energy collisions in the stagnation region. However, a 53% change in the relaxation rate, which altered the densities in the flowfield markedly, hardly changed the heat transfer. Thus the simplest of Borgnakke and Larsen's exchange schemes, which takes no

account of the variation of rotational relaxation rate may be used with some success.

Without prior knowledge that any particular flow is insensitive to the molecular model it is safer to use the more sophisticated collision models. It is only by including the attractive intermolecular forces that the theoretical viscosity will match the viscosity of the gas over a wide range of temperature. The collision model based on the Morse potential, adjusted to give good viscosity predictions, has been shown here to give good results for a variety of flows. If the details of the distribution of translational and kinetic energy throughout the flowfield are taken as the tests of accuracy of a collision model, then the simplest methods may be inadequate. Earlier work by Davis (1978) indicated that density profiles for the flat plate flow, for example, were affected by the rotational relaxation rate. He found that the classical modelling of rotational-translational energy exchange in the hybrid model gave some better results than did the calculations using the phenomenological exchange scheme with constant ϕ . The variable-ϕ collision model gave results similar to those for the hybrid scheme. This has been confirmed here where the variable-ϕ and hybrid calculations gave accurate predictions of the rotational temperatures ahead of the blunt cylinder.

CHAPTER 9

SUMMARY AND CONCLUSIONS

Bird's Monte-Carlo direct simulation method has been reviewed in the light of a number of recent criticisms. No fatal objections have been raised and the generally good results have verified the method in practice. The methods by which it may be extended to the near continuum regime have been discussed and we have suggested ways in which its performance in this area may be improved.

A number of collisions models suitable for use in the simulation method have been reviewed and developed. The methods of selecting collision models for different applications are discussed. The most promising models have been tested in practical applications of rarefied hypersonic flow about both blunt and slender axisymmetric bodies at zero angle of attack. A first test of the usefulness of these models is how well they predicted the drag on these bodies and the heat transfer to these bodies. Unfortunately, the scatter of most experimental data for these quantities in hypersonic flows makes this a not very sensitive test of the different collision models. In addition, because of the low freestream temperatures encountered in some high Mach number flows, the freestream conditions are not always known to an accuracy sufficient to test critically the different collision models. A more exacting test is to compare the details of the flowfields with precise experimental measurements. Dominy's experiments in the Imperial College hypersonic nitrogen wind tunnel in which the freestream conditions are accurately known have been used for this purpose.

Calculations dealing with flight through the atmosphere require a diatomic collision model. For diatomic collisions both the scattering and the exchange of rotational energy with energy of translational motion must be calculated. The scattering models considered here may be used for calculations of flows in a monatomic gas. We have investigated a number of new scattering models all derived from the classical inverse power potential. These are the 'linear inverse power', (LIP) model; the 'isotropic scattering' (ISO) model; and the 'variable diameter hard sphere' (VHS) model which has been proposed before under different names. An unlimited number of similar collision models may be constructed. We have examined the relation between the various theoretical collision cross-sections and the cutoff cross-section used in the simulation calculations. The new collision models are presented in a dimensionless form to highlight their relation to that inverse power potential which has the same theoretical viscosity.

With a suitable choice of inverse power exponent these scattering models can give good results. When used to calculate the structure of a plane shock these new collision models gave reasonable agreement with experiments when the theoretical viscosity of the model gas was matched to the experimentally determined viscosity law for the range of temperatures in the shock. For this flow the inverse power potential was little better than the simpler models.

For more complex flows, especially where shocks and viscous boundary layers interact, the details of the scattering can be important, rather than those average scattering effects measured by

the viscosity. Davis (1978) had found that the scattering produced by the more realistic Morse potential improved the detailed predictions of densities in the flow over a flat plate. We have found also that this model gave results generally better than those obtained with the inverse power potential. Some practical difficulties, associated with a finite computer memory, were encountered when this collision model was originally developed by Pullin (1974). Thus a number of details of the 'computer model' were unsatisfactory or theoretically unsound. Most of these defects have been eliminated and the model is now as simple to use as the inverse power potential.

We have reviewed some simplified rotational-translational energy exchange models suitable for calculations dealing with a diatomic gas. The most useful are the statistical models proposed by Borgnakke and Larsen; in particular their 'restricted exchanged scheme' (Larsen and Borgnakke 1974). An extension of this model called the 'variable-ϕ' collision model was proposed by Pullin and Davis (Davis 1978). We have examined the construction of this model and have shown how it may be combined with the Morse potential to best effect. We have shown how an idea originally used by Pullin (1974), whereby the amount of energy exchanged in a collision is in effect correlated to the deflection, may be extended in this model and may be easily be adapted for the simpler statistical exchange models.

We have considered briefly Pullin's (1975) modified restricted exchange scheme which avoids a small error found in Borgnakke and Larsen's method. This model has been used to calculate the structure of a plane shock for a diatomic gas. We have presented a new inelastic

exchange scheme, called the 'five-space collision model' which satisfies the detail balance condition for Maxwell collision cross-sections. The model has some computational advantages over the statistical schemes. However, for useful collision cross-sections it must be modified in a manner which makes the collision rates slightly different from the theoretical collision rates derived for a spherical inverse power potential.

The hypersonic flow ($\sim$Mach 20) of nitrogen about a blunt cylinder has been calculated. Details of the flowfield and the heat transfer are presented. Density and rotational temperature profiles in the stagnation region ahead of the cylinder have been compared with experiments. We have found that the variable-ϕ scheme works well. The differences between the calculated and experimental results are smaller than the expected experimental errors (Davis et al. 1983). The results of calculations for flows (Mach 5 and 10) about sharp and blunted cones are presented. Some details of the temperatures and density in the flow are given, as are surface stresses and the drag on the cones. The calculated drag has been compared with experimental measurements. These results show that the variable-ϕ scheme coupled with the Morse potential is the most versatile but that the simpler collision models may be adequate in particular cases.

This study has shown that Bird's Monte-Carlo direct simulation method is a powerful and accurate method for calculating the rarefied hypersonic flow of a diatomic gases about different body shapes.

APPENDIX A

COLLISION INTEGRALS

Equation (4.5) for the deflection angle for inverse power molecules may be written as

$$\chi = \pi - 2\int_0^{y_m}\left[1 - y^2 - \frac{2}{\alpha}\left(\frac{y}{z}\right)^{\alpha}\right]^{-\frac{1}{2}} dy \qquad A.1$$

where $y = b/r$, and $y_m = b/r_m$ is found from the relation

$$1 - y_m^2 - \frac{2}{\alpha}\left(\frac{y_m}{z}\right)^{\alpha} = 0 \qquad A.2.$$

Using the change of variable

$$x^2 = 1 - y/y_m$$

and equation (A.2) the deflection angle is

$$\chi = \pi - \int_0^1\left[(2-x^2) - \frac{1}{x^2}\left(\frac{1}{y_m^2} - 1\right)\{1-(1-x^2)^{\alpha}\}\right]^{-\frac{1}{2}} dx \qquad A.3$$

This integration to determine the deflection angle for a value of z was done with an IBM SSP library procedure (SUBROUTINE DQG24). This uses the integration formulae for Gaussian 24 point quadrature from Krylov (1962), pp. 100-111 and pp. 337-340. The integration to find an approximate value of $A^{(\ell)}$ (equation 4.7), that is,

$$A^{(\ell)} = \frac{1}{2}\int_0^{z_m^2}[1 - \cos^{\ell}\chi]\, dz^2 \qquad A.4$$

was done with the adaptive integration algorithms from the standard NAG library (FUNCTION D01AHF). The cut-off value z_m was increased until successive results were identical when rounded to 4 decimal places.

The integrals $A^{(\ell)}$ for various values of α are shown in table A.1. The value of $A^{(1)}(\alpha = 13) = .3895$ is different from the value .3905

given by Nanbu and Watanabe (1981) . We have checked this result using double precision arithmetic with the same program that calculated all the other results. Their other values of $A^{(1)}$ and $A^{(2)}$ agree with the values given here.

Table A.1 Collision Integrals for Inverse Power Potential

α	$A^{(1)}$	$A^{(2)}$	$A^{(3)}$	$A^{(4)}$
3.0	.4940	.5608	.7494	.7987
4.0	.4219	.4362	.5852	.5971
5.0	.3959	.3840	.5188	.5131
6.0	.3854	.3567	.4856	.4690
7.0	.3815	.3407	.4670	.4426
8.0	.3808	.3304	.4558	.4254
8.33	.3810	.3278	.4531	.4211
9.0	.3817	.3235	.4488	.4137
10.0	.3834	.3187	.4444	.4052
11.0	.3856	.3153	.4416	.3990
12.0	.3880	.3128	.4398	.3943
13.0	.3895	.3110	.4389	.3910
13.51	.3918	.3103	.4385	.3892
14.0	.3931	.3096	.4383	.3879
16.0	.3980	.3079	.4383	.3839
18.0	.4026	.3070	.4391	.3813
20.0	.4069	.3066	.4402	.3796
24.0	.4144	.3066	.4429	.3778
28.0	.4208	.3071	.4457	.3771
32.0	.4262	.3078	.4484	.3770
∞	1/2	1/3	1/2	2/5

Viscosity Cross - Section

The viscosity cross - section for a single component inverse power gas is

$$Q^{(2)} = 2\pi A^{(2)}[\alpha] \left(\frac{2\alpha a}{m g^2}\right)^{\frac{2}{\alpha}} \qquad A.5$$

where $A^{(2)}$ as a function of alpha is given above. For the Morse and Lennard - Jones potentials the viscosity cross - section is conveniently normalised as

$$Q^{(2)*}(g^{*2}) = \frac{Q^{(2)}}{2/3\pi\sigma^2} \qquad A.6$$

where $\frac{2}{3}\pi\sigma^2$ is the viscosity cross - section for a hard sphere molecule of diameter σ, and $g^* = g/(4kT'/m)^{\frac{1}{2}}$.

The values of $Q^{(2)*}$ as a function of g^{*2}, shown in table A.2, were calculated by Pullin (1974) for the Morse potential. The values for the Lennard - Jones (6-12) potential are taken from figure 8.4-4 of Hirschfelder, Curtiss and Bird (1954). For high and low relative velocities approximate equations are given.

Table A.2 Collision Integral $Q^{(2)*}$

	Morse	Lennard - Jones
g^{*2}	$Q^{(2)*}$	$Q^{(2)*}$
0.2-1.0	$2.02-0.92 \log(g^{*2})$	
1.0	2.02	2.75
2.0	1.78	2.10
3.0	1.54	1.60
4.0	1.33	1.40
5.0	1.23	1.20
6.0	1.15	1.10
7.0	1.11	1.05
8.0	1.07	1.02
9.0	1.04	1.00
10.0	1.02	0.98
20.0	0.91	0.80
>20.0	$0.91-0.17 \log(\frac{g^{*2}}{20})$	

Viscosity Integrals

The viscosity integral $\Omega^{(22)}$ is conveniently normalised against the constants σ and T' by dividing by the hard sphere value,

$$\Omega^{(22)*} = \frac{\Omega^{(22)}\sqrt{\frac{\pi m}{4kT}}}{\pi\sigma^2} \qquad A.7$$

Values of the viscosity integral $\Omega^{(22)*}$, as a function of the reduced temperature $T^* = T/T'$, calculated by Pullin (1974) for the Morse potential, are as shown in table A.3.

Table A.3 Viscosity integral for Morse potential

T^*	.01	.02	.03	.04	.05	.06	.07	.08	.09
$\Omega^{(2,2)*}$	3.44	3.11	2.93	2.80	2.71	2.64	2.57	2.53	2.47

T^*	0.1	0.2	0.3	0.4	0.5	0.6	0.7	0.8	0.9	1.0
$\Omega^{(2,2)*}$	2.43	2.16	2.00	1.89	1.79	1.70	1.63	1.56	1.50	1.44

T^*	1.4	2.0	3.0	4.0	5.0	6.0	7.0	8.0	9.0	10.0
$\Omega^{(2,2)*}$	1.28	1.15	1.04	0.98	0.95	0.93	0.90	0.88	0.87	0.85

For low T the viscosity integral is well approximated by

$\Omega^{(2,2)*} = m \log T^* + C.$

The viscosity integral for the Lennard- Jones potential in the range $0.1 < T^* < 0.3$ was approximated by such an extrapolation of the results of Hirschfelder et al. (1954). For $T^* < 0.1$ the viscosity was assumed to decrease linearly to zero at $T^* = 0.0$.

It is sometimes useful to have the viscosity integral for the inverse power potential reduced in the same way. It is

$$\Omega_{IP}^{(22)*} = \frac{A^{(2)}[\alpha]\,\Gamma[4 - 2/\alpha]}{2\sigma^2}\left(\frac{\alpha_s}{2kT}\right)^{\frac{2}{\alpha}} \qquad A.8$$

APPENDIX B

THE COLLISION TIME COUNTER

The local non-equilibrium collision rate is established through the time-counter method (see Chapter 2). We give here the value to be added to the time counter for each collision in a form matching that used in the computer program.

When weighting factors are used each simulator may represent a different number of molecules in the real gas and equation (2.14) for the time counter increment must be slightly modified. Pullin (1974, Appendix A) gives the result

$$\Delta t_c = \frac{2}{Nwpn_s g\overline{A(g)}} \tag{B.1}$$

where N = number of simulators in cell

w = relative weighting factor of simulators in cell

p = number of molecules represented by each unit weight simulator

n_s = local number density of simulators

g = relative velocity of collision

$A(g) = \pi b_0^2(g)$ = total collision cross-section for relative velocity g.

The collision rate depends on the local density of the gas, the local velocity distribution, through the distribution of g, and the cut-off cross-section πb_0^2 (itself a function of g).

In the simulations all these quantities are made dimensionless by dividing by some convenient values. The usual unit temperature is the freestream temperature T_∞, the usual speed unit is the most probable thermal speed in the freestream $(2kT_\infty/m)^{\frac{1}{2}}$ and it is convenient

for the length unit to be a body dimension, D.

The freestream number density, n_∞, is chosen as the unit and it is specified in the calculation through the nominal mean free path calculated from the equation

$$\lambda_\infty = \frac{5\pi\mu(T_\infty)}{32mn_\infty\langle c\rangle} \quad . \tag{B.2}$$

For the Lennard-Jones or Morse Potential the nominal mean free path is conveniently written as

$$\lambda_\infty = 1/[\sqrt{2}n_\infty\pi\sigma^2\Omega^{(2,2)^*}(T_\infty)] \quad . \tag{B.3}$$

This mean free path in normalised units is λ_∞/D which is the Knudsen number, Kn. The time unit, derived from the velocity and length units, is $\lambda_\infty/[Kn(2kT_\infty/m)^{\frac{1}{2}}]$. For calculations with no body dimension, such as those for temperature relaxation, the mean free path itself is chosen as the length unit and the following expressions apply with Kn = 1. The actual mean free path based on the cut-off cross-section is approximately half the nominal mean free path (see equation 4.13). The decoupling interval should be small compared to the free time so in normalised units $\delta\hat{t}_m < Kn/2$. The increase of density in some parts of the flow means that $\delta\hat{t}_m$ should be taken even smaller (or vary throughout the flow-field).

The normalised increment added to the time counter is

$$\hat{\Delta t}_c = \frac{2\sqrt{2}\Omega^{(2,2)^*}(T_\infty)Kn}{Nw(pn_s/n_\infty)\hat{g}\ b_o^{*2}} \tag{B.5}$$

where

$$b^* = b/\sigma$$

$$\hat{g} = g/(2kT_\infty/m)^{\frac{1}{2}}$$

and pn_s/n_∞ is the local gas number density in normalised units. This density may be expressed in terms of the local simulator density N/V, where V is the cell volume in simulation units, and the freestream simulator density n_o. Therefore the cell time counter is incremented by an amount

$$\Delta\hat{t}_c = \frac{2\sqrt{2}n_o\Omega^{(2,2)^*}(T_\infty)KnV}{N^2w\hat{g}b_o^{*2}} .$$

Let the cut-off cross-section be based on a maximum value of the impact parameter z_o. The collision partners are selected with a probability proportional to gb_o^2. Using the definition of z from equation (4.4) we find

$$\hat{g}b_o^{*2} = (z_o/\sigma)^2(a\alpha/kT_\infty)^{2/\alpha}\hat{g}^{1-4/\alpha}$$

and equation (2.13) for the condition that a pair be accepted for a collision becomes

$$[\hat{g}^{1-4/\alpha}]/[\hat{g}^{1-4/\alpha}]_{max} > R_f.$$

The increment per collision becomes

$$\Delta\hat{t}_c = \frac{2\sqrt{2}n_o\sigma^2\Omega^{(2,2)^*}(T_\infty)KnV}{z_oN^2w\hat{g}^{1-4/\alpha}}\left(\frac{a\alpha}{kT_\infty}\right)^{-2/\alpha} . \qquad (B.6)$$

The constants z_o, σ, k, α and a are all contained in the program. The values of α and a have been chosen as those which, when used in the inverse power potential, gave a good fit for the viscosity of nitrogen at high temperatures. These are $\alpha = 13.51$ and $a = 1.11677 \times 10^{-148}$ in MKS units. For lower temperatures the theoretical viscosity for $\alpha = 8.33$ and $a = 9.91167 \times 10^{-100}$, gives a closer approximation to the experimentally determined viscosity of nitrogen.

For the inverse power potential a different expression may be used. The nominal mean free path, $\lambda(I)$, at the freestream temperature is given in equation 4.12. The length unit is $D = \lambda(I)/Kn(I)$ and the normalised collision time increment is

$$\Delta\hat{t}_c = \frac{2^{1/2-2/\alpha} A_{(2)}(\alpha)\Gamma(4-2/\alpha) n_o Kn(I) V}{z_o'^2 N^2 w \hat{g}^{1-4/\alpha}} \qquad (B.7)$$

where we have written z_o' to indicate the cut-off value of the impact parameter chosen for this potential.

It is important to note that in Bird's (1976) presentation of the method the mean free path is used to define both the freestream density and the constant a. This constant does not appear in equation B.7 (c.f. equation B.6) and need not be specified directly since the viscosity used to calculate the mean free path effectively establishes its value. To ensure that the same value of a is used in different calculations the theoretical viscosity with the constants a and α should be used to calculate the nominal mean free path specified to the program. The measured viscosity at the freestream may be different since the inverse power potential is unable to match viscosity data over the complete temperature range.

To standardise the input to the program for all collision models we can choose to specify the freestream number density of the real gas through the mean free path calculated for the Lennard-Jones potential. This has the advantage of emphasizing that the nominal Knudsen number merely defines the freestream density and is independent of the collision model assumed in the program. Let $\lambda(LJ)$ be the mean free path in the freestream calculated from the Lennard-Jones potential and equation (B.3). This mean free path must be

specified to the program through the Knudsen number $Kn(LJ) = \lambda(LJ)/D$. Since

$$[Kn\Omega^{(2,2)*}(T_\infty)](LJ) = [Kn\Omega^{(2,2)*}(T_\infty)](M),$$

where the notation (M) denotes these quantities calculated for the Morse Potential, the expression for $\Delta\hat{t}_c$ in equation (B.6) is unchanged by using the Lennard-Jones values of Kn and $\Omega^{(2,2)*}(T_\infty)$. The same applies to the inverse power potential and equation (B.6) can also be used for this potential if we specify the mean free path derived from the Lennard-Jones potential. This can be verified as follows. The reduced collision integral, $\Omega^{(2,2)*}(T)(I)$, for the inverse power potential is given in Appendix A. Substituting $\Omega^{(2,2)*}(T)(I)$ and $Kn(I)$ into equation (B.6) we obtain an equation of the same form as (B.7) for the normalised collision time increment. Since the product $\Omega^{(2,2)*}(T_\infty)Kn$ is the same for all collision models, the Lennard-Jones values may be used.

It might appear natural to specify the freestream number density directly rather than through the nominal mean free path. Bird (1981) recommends this for 'engineering' calculations and this has the advantage of making it clear that the calculations are truly dimensional. However there is some advantage in our method. The Knudsen number is usually required in any case to compare the simulation results with experimental results. In addition the theoretical viscosity for the Lennard-Jones potential is very close to the experimental values. The Knudsen number specified to the program can be calculated directly from viscosity data and the program can supply the function $\Omega^{(2,2)*}(T)(LJ)$. When the product $[\Omega^{(2,2)*}(T_\infty)Kn](LJ)$ is used in equation (B.6) the collision rate in the simulation will be correct. This approach is perhaps best for one unfamiliar with the details of the method.

It should be emphasized that the time and length units are arbitrary and different choices might be more convenient for different applications. For example the length unit might be chosen as the nominal mean free path defined in equation (B.2) with 1/2 in place of $5\pi/32$ and the velocity unit might be chosen as the mean thermal speed. With these choices the unit time in the simulation would be exactly equal to the nominal mean collision time used to define Z_R. Hence, these would be convenient speed and length units for temperature relaxation calculations.

APPENDIX C

FIVE SPACE COLLISION MODEL

The collision model in five space is derived as an extension of the methods used in three space. We first consider, in three space, how the components of $\underset{\sim}{g}'$ are calculated when $\underset{\sim}{g}$, the deflection angle and, ε, the orientation of the collision plane, are known.

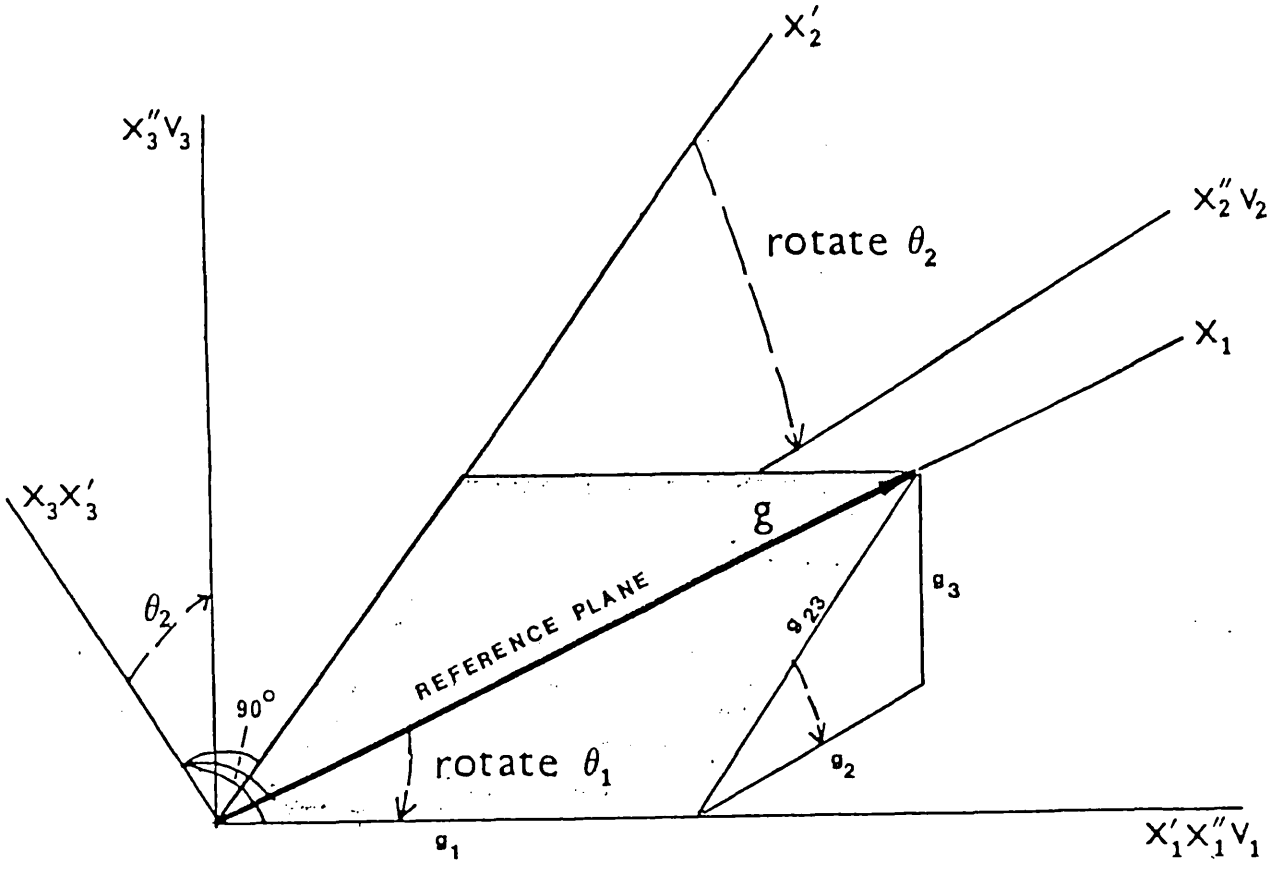


Fig. C.1 COLLISION COORDINATE SYSTEMS

Consider the Cartesian coordinate system (x_1, x_2, x_3) in velocity space (v_1, v_2, v_3) which is shown in figure C.1. The x_1 axis is directed along $\underset{\sim}{g}$ and the x_3 axis is perpendicular to plane containing $\overset{v_1}{\cancel{x_1}}$ and $\underset{\sim}{g}$, marked as the reference plane. The angle

ε is assumed to be measured from this plane. The cylindrical coordinates of $\underset{\sim}{g}'$ relative to (v_1, v_2, v_3) are g, θ_1, θ_2 where

$$\begin{aligned} \cos\theta_1 &= g_1/g \\ \sin\theta_1 &= g_{23}/g \\ \cos\theta_2 &= g_2/g_{23} \\ \sin\theta_3 &= g_1/g_{23} \end{aligned} \tag{C.1}$$

and where

$$g_{23} = (g_2^2 + g_3^2)^{\frac{1}{2}} .$$

The coordinate system (x_1, x_2, x_3) is transformed into the laboratory reference system (v_1, v_2, v_3) by two rotations:

(1) Rotation about the x_3 axis by an angle θ_1 until the x_1' and v_1 axes coincide, i.e.

$$\underset{\sim}{x}' = R\underset{\sim}{x}$$

where

$$\underset{\sim}{x}^T = (x_1 \; x_2 \; x_3)$$

$$\underset{\sim}{x}'^T = (x_1' \; x_2' \; x_3')$$

and

$$R = \begin{bmatrix} \cos\theta_1 & -\sin\theta_1 & 0 \\ \sin\theta_1 & \cos\theta_1 & 0 \\ 0 & 0 & 1 \end{bmatrix}$$

(2) Rotation about the x_1' axis by the angle θ_2 until x_2'' and x_3'' coincide with v_2 and v_3, i.e.

$$\underset{\sim}{v} = \underset{\sim}{x}'' = R'\underset{\sim}{x}'$$

where

$$\underset{\sim}{v}^T = (v_1 \; v_2 \; v_3) = (x_1'', x_2'', x_3'')$$

and

$$R' = \begin{bmatrix} 1 & 0 & 0 \\ 0 & \cos\theta_2 & -\sin\theta_2 \\ 0 & \sin\theta_2 & \cos\theta_2 \end{bmatrix}$$

The complete transformation is

$$\underset{\sim}{v} = R'R\underset{\sim}{x} . \tag{C.2}$$

The cylindrical coordinates of $\underset{\sim}{g}'$ relative to (x_1, x_2, x_3) are g, χ and ε, the Cartesian components are

$$x_1 = g \cos\chi$$
$$x_2 = g \sin\chi \cos\varepsilon$$
$$x_3 = g \sin\chi \sin\varepsilon$$

and these may be substituted into equation (C.2) to give the components of $\underset{\sim}{g}'$ in the laboratory frame of reference.

In five dimensional space a similar transformation is required. The components of $\underset{\sim}{g}'$ relative to a coordinate system directed along $\underset{\sim}{g}$ are found from equations (6.2) as

$$x_5 = g \cos\chi$$
$$x_4 = g \sin\chi \cos\varepsilon_4$$
$$x_3 = g \sin\chi \sin\varepsilon_4 \cos\varepsilon_3$$
$$x_2 = g \sin\chi \sin\varepsilon_4 \sin\varepsilon_3 \cos\varepsilon_2$$
$$x_1 = g \sin\chi \sin\varepsilon_4 \sin\varepsilon_3 \sin\varepsilon_2 \qquad \text{(C.3)}$$

where we have chosen for later convenience to renumber the axes from 5 down to 1. The angle χ is the restricted deflection angle chosen as

$$\chi = \phi\pi R_f$$

and the remaining angles (hyper orientation angles ε_i) are chosen so that the direction of $\underset{\sim}{g}'$ is isotropic within the hyper cone with half angle χ, i.e.

ε_4 is selected via equation (6.5d)

ε_3 is selected via equation (6.5b)

ε_2 is selected via equation (6.5a).

The components (C.3) must be resolved into the global coordinate asystem. The coordinate system directed along $\underset{\sim}{g}$ must be successively rotated through the angles θ_5, θ_4, θ_3 and θ_2 and each

rotation θ_n alters only the two Cartesian components x_n and x_{n-1}. The complete transformation is

$$\underset{\sim}{v} = R''' R'' R' R\underset{\sim}{x} \tag{C.4}$$

where

$$R = \begin{bmatrix} \cos\theta_5 & -\sin\theta_5 & 0 & 0 & 0 \\ \sin\theta_5 & \cos\theta_5 & 0 & 0 & 0 \\ 0 & 0 & 1 & 0 & 0 \\ 0 & 0 & 0 & 1 & 0 \\ 0 & 0 & 0 & 0 & 1 \end{bmatrix}$$

$$R' = \begin{bmatrix} 1 & 0 & 0 & 0 & 0 \\ 0 & \cos\theta_4 & -\sin\theta_4 & 0 & 0 \\ 0 & \sin\theta_4 & \cos\theta_4 & 0 & 0 \\ 0 & 0 & 0 & 1 & 0 \\ 0 & 0 & 0 & 0 & 1 \end{bmatrix}$$

$$R'' = \begin{bmatrix} 1 & 0 & 0 & 0 & 0 \\ 0 & 1 & 0 & 0 & 0 \\ 0 & 0 & \cos\theta_3 & -\sin\theta_3 & 0 \\ 0 & 0 & \sin\theta_3 & \cos\theta_3 & 0 \\ 0 & 0 & 0 & 0 & 1 \end{bmatrix}$$

$$R''' = \begin{bmatrix} 1 & 0 & 0 & 0 & 0 \\ 0 & 1 & 0 & 0 & 0 \\ 0 & 0 & 1 & 0 & 0 \\ 0 & 0 & 0 & \cos\theta_2 & -\sin\theta_2 \\ 0 & 0 & 0 & \sin\theta_2 & \cos\theta_2 \end{bmatrix}$$

The angles θ_5 to θ_2 are just the hyper cylindrical coordinates of g relative to the global reference frame. The elements of the rotation matrices are

$$\cos\theta_5 = g_5/G_5 \quad \sin\theta_5 = G_4/G_5$$
$$\cos\theta_4 = g_4/G_4 \quad \sin\theta_4 = G_3/G_4$$
$$\cos\theta_3 = g_3/G_3 \quad \sin\theta_3 = G_2/G_3$$
$$\cos\theta_2 = g_2/G_2 \quad \sin\theta_2 = G_1/G_2$$

where

$$G_n = \left[\sum_{j=1}^{n} g_j^2 \right]^{\frac{1}{2}}$$

and the g_j are the global Cartesian coordinates of g. Substituting equation (C.3) for $\underset{\sim}{x}$ into (C.4) gives expressions for the components of $\underset{\sim}{g}'$ and equation (6.6) then defines the post-collision state of each particle. Notice that the deflection angle in three space and the energy exchange are intricately connected in this collision model.

It is probably more useful to separate the energy exchange and the deflection calculation so that any scattering in 3 space may be used. This is easily done by retaining only the rows of the matrix equation (C.4) which correspond to the two components of internal energy. These are

$$\begin{aligned} g_5' &= g_5 \cos\theta_5 - G_4 \sin\theta_5 \cos\theta_5 \\ g_4' &= g_4(\cos\theta_5 + g_5 \sin\theta_5 \cos\theta_4/G_4) \\ &\qquad - G_5 G_3 \sin\theta_5 \sin\theta_4 \cos\theta_3/G_4 \,. \end{aligned} \tag{C.5}$$

The three components of translational relative velocity (g_3', g_2', g_1') can be calculated in the normal way for any deflection angle in 3 space.

APPENDIX D

EXECUTION TIMES OF EXCHANGE MODELS

The execution speeds for the 5-space (5-S) collision models and Borgnakke and Larsen's (B+L) statistical exchange schemes were measured on two machines. The CDC FORTRAN (FTN5) compiler has various levels of optimisation from OPT=0 (no optimisation) to OPT=3 (maximum optimisation). The following versions of the compiler were used:

a) The ICCC batch system with OPT=0. With no optimisation the relative speeds might be similiar to that for a mini computer.

b) The ICCC time sharing system with (OPT=2). This is a representative type of compiler: DO loops are quick and the registers are extensively used so that intermediate results are not stored in memory. The machine itself is rather slow.

c) The ULCC 7600 batch processing system with the FTN5 compiler. There was no difference in speed between the second (OPT=2) and third (OPT=3) optimising levels.

Compiler (a) was only tested for the completely inelastic collision. Borgnakke and Larsen's method was 1.31 times faster than the 5-space collision model. This is presumably because of the time needed to calculate with an extra variable representing internal energy. In addition the DO loops in the 5-space model make it slower for this compiler than the B+L model for which explicit expressions for each of the three velocity components are written. The optimising compilers will reduce this penalty and the length of these DO loops (five iterations) is about that where it is better to use loops rather

than explicit expressions.

The execution times include only the basic calculation of the collision and not the time consuming collision selection procedures. Collisions between the same two particles were calculated a large number of times (1000 - 50000). Energy was conserved (to less than .004 % deviation) in all tests. Each execution speed, expressed as collisions/CPU seconds, was derived from at least three and usually more than 5 different tests. There was very little difference in the execution times for the runs which differed in the sequence of random numbers used. In the B+L scheme a randomly distributed beta variable must be chosen for each collision. The method is the acceptance - rejection technique and is given in the appendix of I.C. Aero Report (75-10) (Pullin 1975). To reduce the iterations the maximum value of the random variable must be known and is calculated from the indices of the beta distribution. Wherever possible this maximum is calculated once only. All calculations with the B+L schemes were for two internal degrees of freedom.

Table D.1

Execution speeds for exchange schemes-compilers (b) and (c).

	two class scheme		restricted exchange			
	$\phi = 1$		constant ϕ		variable-ϕ	
Model	(b)	(c)	(b)	(c)	(b)	(c)
B+L	1480	26480	1480	26480	1087	14520
5-S	1920	28240	1215	17600	1215	17600

Notes: For the constant ϕ calculations the speeds of each model have been deduced from other cases. For the B+L model the speed is virtually the same as for the completely inelastic collisions and should differ only because a random number is selected from a different distribution. For the 5-S model the execution time should be virtually the same as for variable-ϕ except for the time required to calculate the different value of ϕ for each collision.

The Borgnakke and Larsen restricted exchange scheme suffers with variable-ϕ since the indices of the beta distribution are not known in advance but are different for every collision. The maximum of the beta distribution is a function involving powers of the fractional indices . This maximum value must be calculated for each collision and this is a time consuming operation. A step function for $\phi(e_{cm})$ might be used to reduce the computing time for the B+L variable-ϕ calculations. In this case the maximum of the beta variable for each ϕ could be calculated once only. This 'step variable-ϕ' calculation should execute nearly as fast as the constant ϕ calculations.

When used in simulations the number of collisions calculated per CPU second is less than that given above since the time for moving the particles and selecting collision pairs must be included. For the relatively simple one-dimensional shock the collision rate was 8000 - 13000 colls/CPU sec for compiler (c). For two-dimensional calculations the execution rate depends on the geometry, the Knudsen number and the various ratios of the moving, sampling and printing intervals. The rate is reduced to 1500 - 4000 colls/CPU sec

APPENDIX E

SHOCK THICKNESS

The tables give the shock thickness and the mean free paths in simulation length units. This unit length was the nominal mean free path in the upstream gas, i.e.

$$\lambda_1 = [\sqrt{2}\ n_1 \pi \sigma^2\ \Omega^{(2,2)^*}]^{-1}$$

where $\Omega^{(2,2)^*}$ for the Morse potential was used. The temperature in the upstream and the value of $\Omega^{(2,2)^*}$ used to calculate the mean free path are given in each case. The collision cross - sections were based on z_o for α = 13.51 and the appropriate value of 'a' given in appendix B. The mean free path λ_o shown in the table is based on this cross - section and is calculated for the upstream conditions.

(a) Monatomic calculations

Table E.1

M = 5.0 : T_1 = 80.0 K : T_2 = 694.4 K : $\Omega^{(2,2)^*}$ = 1.515

Model	z_o	λ_o	Δ	δ	λ_μ	λ_m	Δ/λ_μ	δ/λ_μ
ISO	0.965	.740	5.6	3.8	1.480	0.740	3.78	2.57
IP+	1.212	.469	3.9	2.2	1.110	1.465	3.51	1.98
						mean	3.65	2.28

Table E.2

M = 10.0 : T = 40.0 K : T = 1284.9 : $\Omega^{(2,2)^*}$ = 1.85

Model	z_o	λ_o	Δ	δ	$\lambda\mu$	λ_m	$\Delta/\lambda\mu$	$\delta/\lambda\mu$
LIP	1.212	.572	4.1	2.9	1.142	0.960	3.59	2.54
ISO	0.964	.902	6.9	3.3	1.804	0.902	3.82	1.83
	1.212	.572	5.1	2.7	1.142	0.571	4.47	2.36
IP	1.212	.572	5.0	3.3	1.354	1.071	3.69	2.44
IP+	1.212	.572	5.3	3.2	1.354	1.787	3.91	2.36
						mean	3.89	2.31
						s.d.	0.34	0.27

Note: IP+ indicates that the deflections were calculated for the inverse power potential but restricted to the range $0 < \chi' < \frac{\pi}{2}$ (see chapter 4).

Table E.3

M = 22.5 : T = 12.71 K : T = 2022 K : $\Omega^{(2,2)^*}$ = 2.29

Model	z_o	λ_o	Δ	δ	$\lambda\mu$	λ_m	$\Delta/\lambda\mu$	$\delta/\lambda\mu$
LIP	1.114	.878	7.7	4.4	1.756	1.476	4.38	2.51
	1.212	.742	6.6	4.0	1.484	1.248	5.29	2.70
ISO	0.964	1.170	9.6	5.8	2.340	1.170	4.10	2.48
	1.212	.742	6.2	3.8	1.480	0.742	4.19	2.57
IP	1.212	.742	7.3	4.6	1.756	1.391	4.15	2.62
						mean	4.42	2.58
						s.d.	0.50	0.09

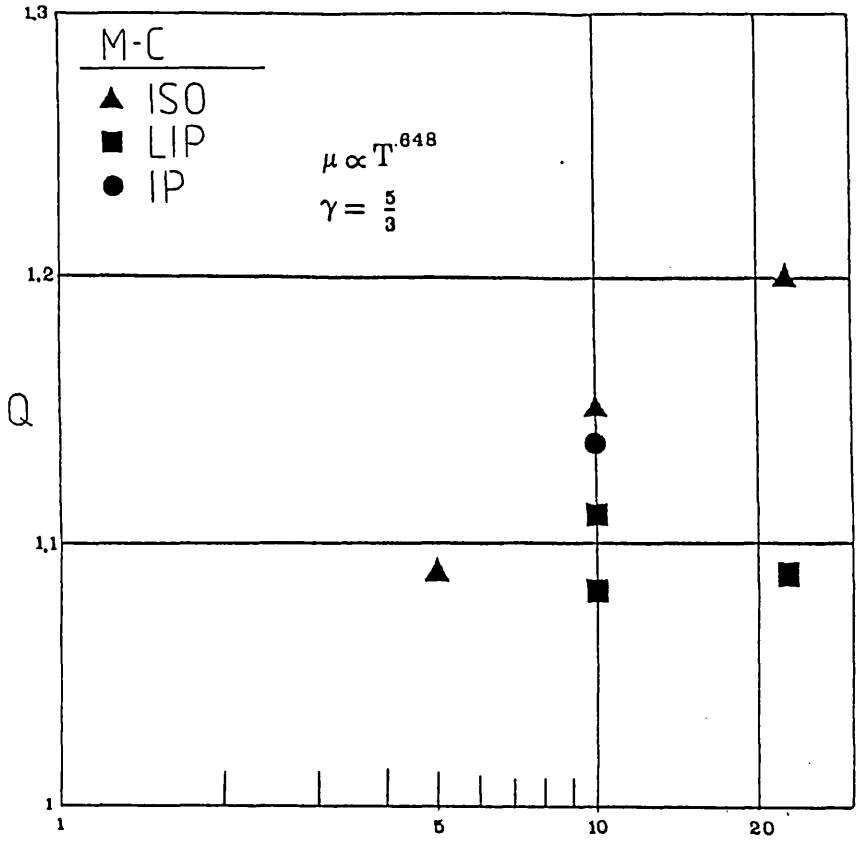


Fig. E.1 ASYMMETRY OF CALCULATED SHOCK PROFILES (MONATOMIC GAS)

(b) Diatomic calculations

Table E.4

M = 5.0 : T_1 = 80.0 K : T_2 = 464 K : $\Omega^{(2,2)^*}$ = 1.515

Model	z_o	λ_o	Δ	δ	$\lambda\mu$	λ_m	$\Delta/\lambda\mu$	$\delta/\lambda\mu$
LIP	1.114	.359	3.2	2.6	.717	.604	4.46	3.63
	1.250	.285	2.6	2.2	.570	.479	4.56	3.86
	1.386	.232	2.4	1.8	.464	.391	5.17	3.88
ISO	0.965	.478	3.8	3.0	.956	.485	3.97	3.14
	1.083	.380	3.3	2.6	.760	.380	4.34	3.42
	1.386	.232	2.4	1.8	.464	.232	5.17	3.88
IP	1.212	.303	3.4	2.5	.717	.570	4.74	3.49
						mean	4.63	3.61
						s.d.	0.44	0.26

Table E.5

M = 10.0 : T_1 = 40.0 K : T_2 = 815.5 K : $\Omega^{(2,2)^*}$ = 1.85

Model	z_o	λ_o	Δ	δ	λ_μ	λ_m	Δ/λ_μ	δ/λ_μ
LIP	1.212	.351	4.0	3.3	0.702	.590	5.70	4.70
ISO	0.964	.555	5.3	4.4	1.110	.555	4.77	3.96
	1.212	.351	4.4	3.4	0.702	.351	6.27	4.84
IP	1.212	.351	4.2	3.6	0.831	.658	5.05	4.33
						mean	5.45	4.46
						s.d.	0.67	0.34

Table E.6

M = 22.5 : T_1 = 12.71 K : T_2 = 1261 K : $\Omega^{(2,2)^*}$ = 2.29

Model	z_o	λ_o	Δ	δ	λ_μ	λ_m	Δ/λ_μ	δ/λ_μ
LIP	0.964	.708	8.8	5.7	1.416	1.190	6.21	4.03
	1.114	.531	4.9	4.8	1.060	.893	4.62	4.53
	1.386	.343	4.4	3.6	0.686	.577	6.41	5.25
ISO	0.964	.708	7.0	5.9	1.416	.708	4.94	4.17
	1.165	.486	5.8	4.5	0.972	.486	5.97	4.63
	1.386	.343	4.7	3.5	0.686	.343	6.85	5.10
IP	1.212	.448	5.3	5.0	1.060	.840	5.00	4.72
						mean	5.71	4.63
						s.d.	0.85	0.41

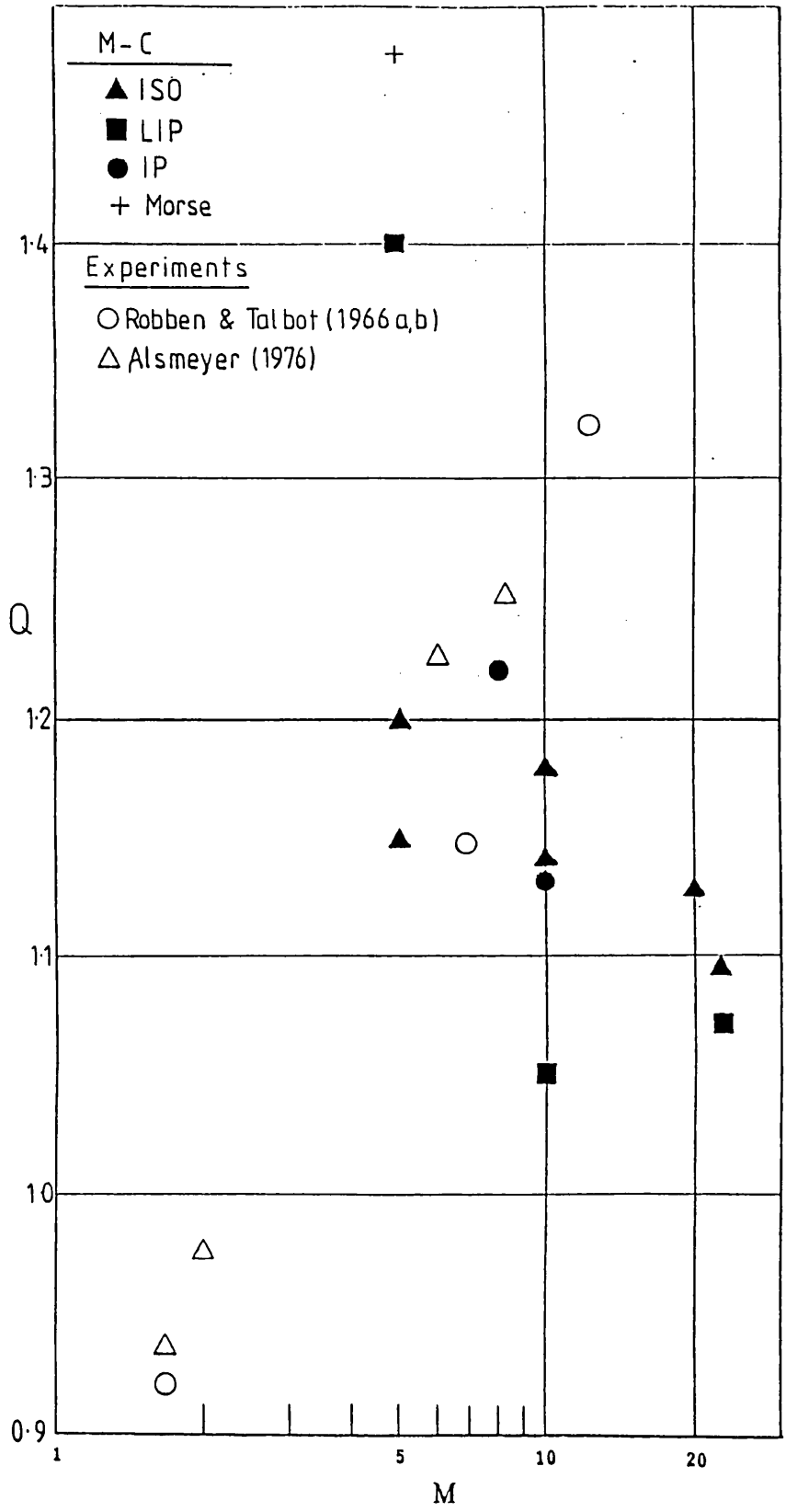


Fig.E.2 ASYMMETRY OF DENSITY PROFILES FOR NITROGEN

(c) Reduction of Experimental data

Robben and Talbot (1966a) present shock thickness as L^*/Δ where

$$L^* = \mu(T^*)/\rho\, v = \mu(T^*)/\rho_1 v_1 \qquad (E.1)$$

and $T^* = 2T_o/(\gamma + 1)$ is a reference temperature derived from the stagnation temperature T_o. To convert to the mean free path in the upstream equation (E.1) should be multiplied by $32\, v_1 \mu(T_1)/5\pi\mu(T^*)\langle c\rangle$ where $\langle c\rangle = (8kT_1/\pi m)^{\frac{1}{2}}$ is the mean thermal speed in the upstream. Hence

$$\frac{\lambda_1}{\Delta} = \frac{16}{5} M\sqrt{\frac{\gamma T_1}{2\pi T^*}}\,\frac{\Omega^{(22)*}(T^*)}{\Omega^{(22)*}(T_1)}$$

where the relation $\mu(T) \propto \sqrt{T}\ /\ \Omega^{(2,2)*}(T)$ has been used. Table E.7 presents a few results converted to λ_1/Δ. The viscosity integral for the Morse potential has been used.

Table E.7

T_o = 297 K

T^* = 247.5 K $\quad \Omega^{(2,2)*}(247.5\ K) = 1.07$

M	1.69	3.1	6.87	9.4	12.7
T_1(K)	189	102	28.4	15.9	8.93
$\Omega_1^{(2,2)*}$	1.14	1.39	1.99	2.21	2.44
L^*/Δ	.080	.128	.162	.168	.170
λ_1/Δ	.167	.295	.306	.294	.271

APPENDIX F

CALCULATED HEAT TRANSFER AND DRAG

The freestream mean free paths quoted in the tables have been calculated from the viscosity predictions for nitrogen derived for the Lennard- Jones potential (figure 3.5), and are given as a Knudsen number based on the cylinder radius R and the cone diameter D. The Reynold's number can be calculated from the Knudsen number used here as

$$Re = 3.2(\gamma/2\pi)^{\frac{1}{2}} \quad M_\infty / Kn_\infty$$

In addition to the parameters K_r^2 and K_{bf} defined in chapter 8 the following parameters based on the mean free path λ_{bf} are given in the tables:

$$\bar{K} = Kn_\infty \Omega^{(22)*}(T_\infty)/[\sqrt{\pi}\, S_W + 1] \qquad F.1$$

and

$$K'_{bf} = Kn_\infty \Omega^{(22)*}(T_\infty)/[Q^{(2)*}(\varepsilon)\, S_W] \qquad F.2$$

where

$$g^2 = (U_\infty + c_w \sin\theta_c)^2 + c_w^2 \cos^2\theta_c$$

and θ_c is the cone half angle.

The parameter $\bar{K}$ is given by Whifield (1973) without the term $\Omega^{(22)*}$. If the freestream Knudsen number is derived from a hard sphere viscosity law, with a diameter chosen to fit the high temperature viscosity data, which is extrapolated to low temperatures, then this factor may be omitted. However it is usual to derive the Knudsen number from the viscosity data (or the Lennard- Jones extrapolation for low temperatures) which means that, in effect, a different hard sphere cross- section is used for every freestream

temperature. The factor $\Omega^{(2,2)*}$ gives the ratio of this cross-section to the cross-section $\pi\sigma^2$.

Diffuse scattering fully accommodated to the surface temperature has been assumed when calculating the free molecular limits of heat transfer and drag. Four collision models were used in these calculations and are denoted

M Morse potential, variable-ϕ

IP inverse 13.5, variable-ϕ

H Morse potential, hybrid exchange scheme

VHS α = 8.33 and constant ϕ = 0.25.

F.1 HEAT TRANSFER TO BLUNT CYLINDER

The average heat transfer to the front face, $\dot{q}$, is used to calculate Ch.

Table F.1

M_∞ = 20.6 Tw = 364 K Ch_{fm} = 1.062

To = 1405 K T_∞ = 16.4 K

Kn	$\bar{K}$	K_r^2	Ch	$\dot{q}/\dot{q}_{fm}$	
.0282	.0126	3.325	.367	.345	M
			.348	.328	IP
			.349	.329	H

Table F.2

M_∞ = 24.77 Tw = 375 K Ch_{fm} = 1.058

To = 1446 K T_∞ = 11.7 K

Kn	$\bar{K}$	K_r^2	Ch	$\dot{q}/\dot{q}_{fm}$	
1.840	.916	.045	.887	.838	M
			.885	.836	IP
1.382	.868	.060	.868	.820	M
			.872	.824	H
0.613	.305	.136	.768	.726	M
0.306	.152	.271	.670	.633	M
.0656	.0326	1.27	.424	.400	M
.0465	.0231	1.79	.364	.344	M

Table F.3

M_∞ = 25.17 Tw = 396 K Ch_{fm} = 1.038

To = 2271 K T_∞ = 17.8 K

Kn	$\bar{K}$	K_r^2	Ch	$\dot{q}/\dot{q}_{fm}$	
.1603	.058	.84	.521	.502	M
			.450	.434	IP
			.558	.538	H

Table F.4

M_∞ = 25.4 Tw = 364 K Ch_{fm} = 1.059

To = 1383 K T_∞ = 10.6 K

Kn	$\bar{K}$	K_r^2	Ch	$\dot{q}/\dot{q}_{fm}$	
.0648	.0335	1.25	.397	.375	M
			.385	.364	IP
			.474	.448	H

Table F.5

M_∞ = 25.4 Tw = 550 K Ch_{fm} = 1.103

To = 1383 K T_∞ = 10.6 K

Kn	$\bar{K}$	K_r^2	Ch	$\dot{q}/\dot{q}_{fm}$	
.0648	.0400	1.305	.393	.356	M

Table F.6

M_∞ = 25.4 Tw = 750 K Ch_{fm} = 1.178

To = 1383 K T_∞ = 10.6 K

Kn	$\bar{K}$	K_r^2	Ch	$\dot{q}/\dot{q}_{fm}$	
.0648	.0455	1.356	.376	.319	M

Table F.7

M_∞ = 10.0 Tw = 300 K Ch_{fm} = 1.077

To = 2000 K T_∞ = 95.2 K

Kn	$\bar{K}$	K_r^2	Ch	$\dot{q}/\dot{q}_{fm}$
7.66	1.277	.025	.93	.86
2.30	.383	.083	.84	.78
.766	.128	.250	.72	.67
.383	.0639	.500	.55	.51
.128	.0213	1.50	.40	.37
.0383	.00639	5.00	.30	.28

Note: These results were calculated using the inverse 13.5 power potential with constant ϕ = 0.1 (Pullin et al. 1977)

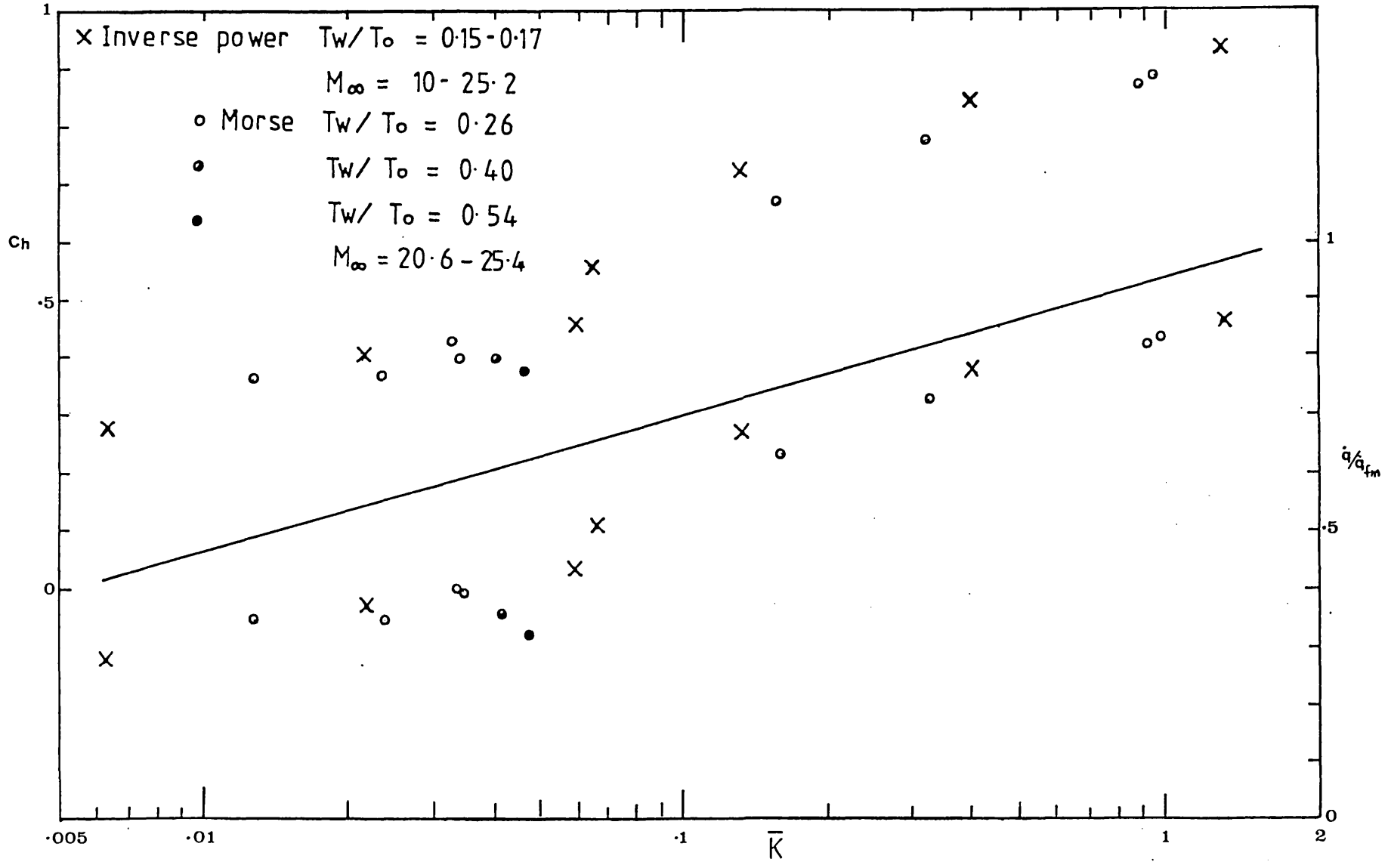


Fig. F.1 HEAT TRANSFER TO BLUNT CYLINDER - CORRELATION WITH WALL MEAN FREE PATH

F.2 DRAG ON SHARP CONES

Drag co-efficients marked thus (*) are a weighted average from several runs with identical conditions. The individual values, listed below the average value, were weighted according to the duration of the sampling interval. The drag co-efficient in the inviscid limit, Cd_i , was calculated using Hui's (1975) method.

F.2.1 Half Angle = 6

Table F.8

M_∞ = 5.095 Tw = 293 K T_∞ = 47.1 K

Cd_{fm} = 2.6861 Cd_i = .0306

Kn	K_{bf}	K'_{bf}	Cd	C'	
.0191	.0249	.0234	*.948	.345	M
			.918		
			.956		
.0334	.0435	.0409	1.060	.388	M
.0399	.0520	.0489	1.149	.421	M
.3755	.489	.460	*2.154	.800	M
			2.147		
			2.157		

Table F.9

M_∞ = 5.526 Tw = 293 K T_∞ = 40.9 K

Cd_{fm} = 2.5955 Cd_i = .0297

Kn	K_{bf}	K'_{bf}	Cd	C'	
3.688	5.071	5.071	2.448	.943	M

Table F.10

M_∞ = 5.536 Tw = 293 K T_∞ = 40.9 K

Cd_{fm} = 2.5931 Cd_i = .0297

Kn	K_{bf}	K'_{bf}	Cd	C'	
.0181	.0248	.0234	.867	.327	
.1000	.137	.1294	1.486	.568	

F.2.2 Half angle = 12

Table F.11

M_∞ = 5.095 Tw = 293 K T_∞ = 47.1 K

Cd_{fm} = 2.3537 Cd_i = .1029

Kn	K_{bf}	K'_{bf}	Cd	C'	
.2500	.326	.306	1.800	.754	M

Table F.12

M_∞ = 10.0 Tw = 500 K T_∞ = 75.0 K

Cd_{fm} = 2.1299 Cd_i = .0943

Kn	K_{bf}	K'_{bf}	Cd	C'	
.1500	.0814	.0993	1.193	.540	VHS

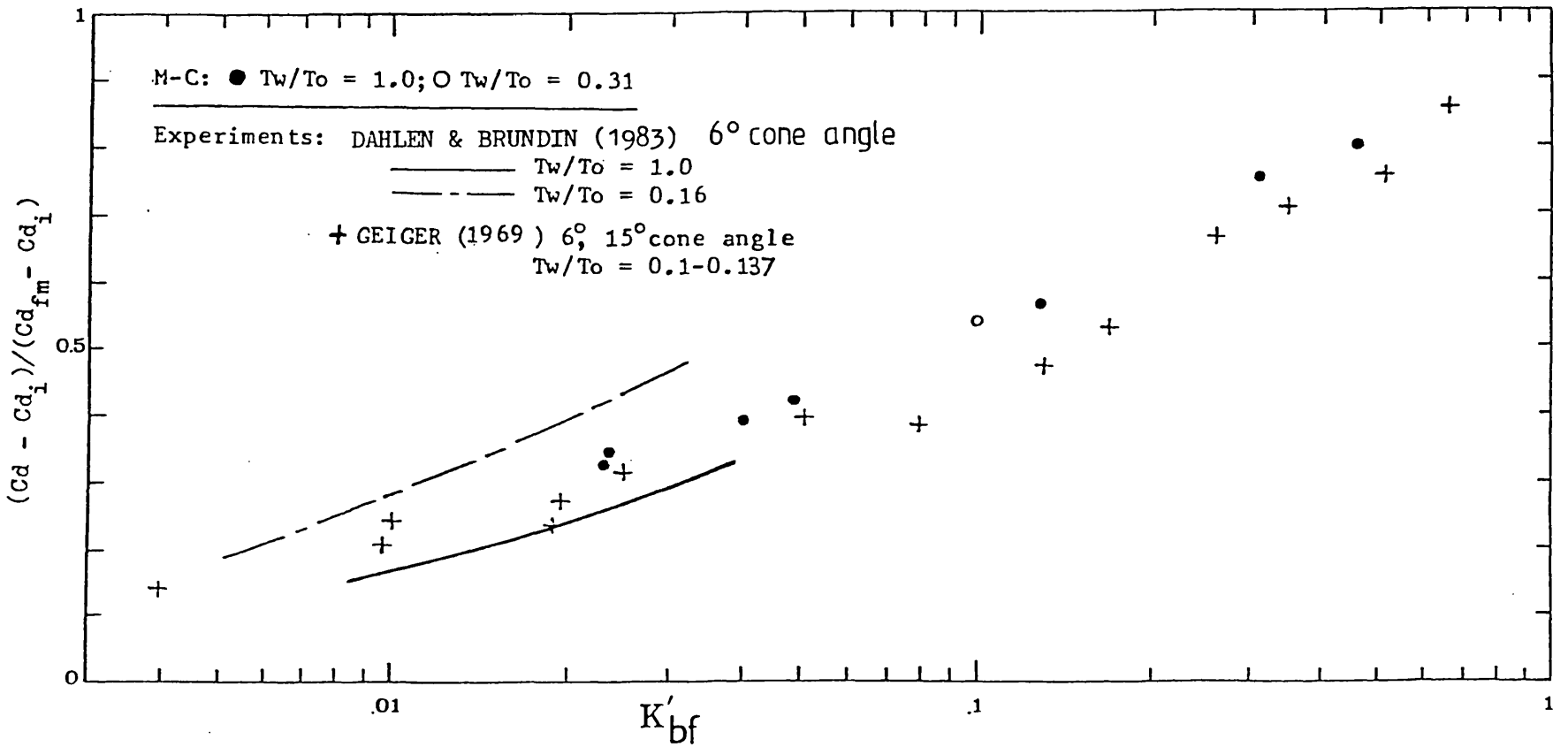


Fig. F.2 CONE DRAG VS. WALL MEAN FREE PATH (VARIABLE CROSS-SECTION)

F.3 DRAG ON BLUNT CONE

F.3.1 Half angle = 6, r_n/r_b = 0.4

Table F.13

M_∞ = 5.092 Tw = 293 K T_∞ = 47.4 K

Kn	Cd		Kn	Cd		Kn	Cd	
.0004	.605	M	.0165	*.889	IP	.0224	.925	VHS
.0224	*.856	M		.879				
	.834			.895				
	.862			.899				
.0399	1.018	M						
.0750	1.527	M						

REFERENCES

Alder, B.J. and T. Wainwright (1958): 'Studies in Molecular Dynamics I. General Method', J. Chem. Phys., 31, p. 459

Alsmeyer, H. (1976): 'Density Profiles in Argon and Nitrogen Shock Waves Measured by the Absorption of an Electron Beam', J. Fluid Mech., 74, p.497

Annis, B. K. and A. P. Malinauskas (1971): 'Temperature Dependence of Rotational Collision Numbers from Thermal Transpiration', J. Chem. Phys., 54, p. 4763

Belotserkovskiy, O. M. and V. Y. Yanitsky (1978): 'Statistical Modelling of Flows of Ideal Monatomic Gases', Fluid Mech. Soviet Res., 7, p. 42

Bhatnagar, P. L. , E. P. Gross and M. Krook (1954): 'A Model for Collision Processes in Gases I. Small Amplitude Processes in Charged and Neutral One-Component Systems', Phys. Rev., 94, p. 511

Bird, G. A. (1963): 'Approach to Translational Equilibrium in a Rigid Sphere Gas', Phys. Fluids, 6, p. 1518, Academic Press

Bird, G. A. (1965): 'Shock Wave Structure in a Rigid Sphere Gas', Rarefied Gas Dynamics, 4th. Symposium (ed. de Leeuw), part I, p. 216

Bird, G. A. (1969): 'Direct Simulation Monte Carlo Method', Rarefied Gas Dynamics, 6th. Symposium (ed. Trilling & Wachman), part I, p. 85, Academic Press

Bird, G. A. (1970a): 'Aspects of the Structure of Strong Shock Waves', Phys. Fluids, 13, p. 1172

Bird, G. A. (1970b): 'Direct Simulation and the Boltzmann Equation', Phys. Fluids, 13, p. 2676

Bird, G. A. (1970c): 'Breakdown of Translational and Rotational Equilibrium in Gaseous Expansions', A.I.A.A. Jour., 8, p. 1998

Bird, G. A. (1973): 'Near Continuum Impact of an Underexpanded Jet Plume on a Wall', Proc. A.I.A.A Computational Fluid Dynamics Conf. 1973, p. 103

Bird, G. A. (1976): 'Molecular Gas Dynamics', Clarendon Press, Oxford

Bird, G. A. (1979): 'Simulation of Multi-Dimensional and Chemically Reacting Flows', Rarefied Gas Dynamics , 11th Symposium, (ed. Camprague), part I, p. 365, C.E.A. (Paris)

Bird, G. A. (1981): 'Monte-Carlo Simulation in an Engineering Context', Rarefied Gas Dynamics (ed. Fisher), 12th. Symposium, Part I, p. 239, (Progress in Astronautics and Aeronautics, 74, A.I.A.A)

Bird, G. A. (1983): 'Rarefied Hypersonic Flow Past a Slender Cone', to be published in Rarefied Gas Dynamics, 13th. Symposium

Borgnakke, C. and P. S. Larsen (1973): 'Statistical Collision Model for Monte-Carlo Simulation of Polyatomic Gas', Dept. of Fluid Mechanics, Technical University of Denmark, Lyngby, Denmark, AFM 73-08

Borgnakke, C. and P. S. Larsen (1975): 'Statistical Collision Model for Monte-Carlo Simulation of Polyatomic Gas Mixture', J. Comp. Phys., 18, p. 405

Brau, C. A. and R. M. Jonkman (1970): 'Classical Theory of Rotational Relaxation in Diatomic Gases', J. Chem. Phys., 52, p. 477

Butherus, T. F. and T. S. Storvick (1974): 'Rotational Collision Numbers and the Heat Conductivity of Nitrogen Gas from Thermal Transpiration Measurements to 1250 K', J. Chem. Phys., 60, p. 321

Carnevale, E. H., C. Cary and G. Larsen (1967): 'Ultrasonic Determination of Rotational Collision Numbers and Vibrational Relaxation Times of Polyatomic Gases at High Temperatures', J. Chem. Phys., 47, No. 8, p. 2829

Chahine, M. T. (1963): 'The Shock Structure According to the Krook Collision Model', Rarefied Gas Dynamics (ed. Laurmann), 3rd. Symposium, Part I, p. 260, Academic Press

Chapman, S. and T. G. Cowling (1952): 'The Mathematical Theory of Non-Uniform Gases', 2nd edn., (3rd edn. 1970), Cambridge University Press

Cheng, H. K. (1961): 'Hypersonic Shock-Layer Theory of the Stagnation Region at Low Reynolds Number', Proc. of the 1961 Heat Transfer and Fluid Mechanics Institute

Coleman, G. T., S. C. Metcalf and C. J. Berry (1977): 'Heat transfer to Hemishere Cylinders and Bluff Cylinders Between Continuum and Free Molecular Limits', Rarefied Gas Dynamics, 10th Symposium (ed. Potter), part I, p. 393, (Progress in Astronautics and Aeronautics, 51, A.I.A.A)

Cowling, T. G. (1950): 'Molecules in Motion', Hutchinson's University Library

Dahlen, G. A. and C. L. Brundin (1983): 'Wall Temperature Effects on Rarefied Hypersonic Cone Drag', to be published in Rarefied Gas Dynamics, 13th. Symposium

Davis, J. (1978): 'An Experimental Study to Evaluate and Develop the Direct Simulation Method as Applied to Rarefied Hypersonic Flow Fields', Dept. of Aero., Imperial College, Ph. D. Thesis

Davis, J., R. G. Dominy, J. K. Harvey, and M. N. Macrossan (1983): 'The Evaluation of Some Collision Models Used for the Monte-Carlo Calculation of Rarefied Hypersonic Flows', J. Fluid Mech., 135, p. 355

Dayman, B. (1965): 'Hypersonic Viscous Effects on Free-Flight Slender Cones', A.I.A.A. Jour., 3, p. 1391

Deiwert, G.S. and K. K. Yoshikawa (1975): 'Analysis of a Semi-Classical Model for Rotational Transition Probabilities', Phys. Fluids, 18, p. 1085

Deshpande, S. M., P. V. Subba Raju and N. Ramani (1979): 'A Comparative Study of the Time Counter and Random Collision Number Strategies Used in Monte Carlo Simulation', Rarefied Gas Dynamics, 11th Symposium (ed. Campragué), part I, p. 435, C.E.A. (Paris)

Dolman, K. A. (1980): 'Heat Transfer to a Hemisphere-Cylinder and a Bluff Cylinder in High Altitude Flight', R.A.E., Tech. Memo. Aero. 1819

Dominy, R. G., M. N. Macrossan and J. K. Harvey (1981): 'Rarefied Hypersonic Flow about a Blunt-Ended Circular Cylinder', Dept. of Aero., Imperial College, Rep. No. 81-01

Erofeev, A. I., and V. A. Perepukhov (1979): 'Hypersonic Rarefied Flow about a Flat Plate by the Direct Simulation Method', Rarefied Gas Dynamics, 11th Symposium (ed. Campragué), Part I, p. 417, C.E.A. (Paris)

Geiger, R. E. (1969): 'Slender Cone, Zero Angle of Attack Drag in Continuum and Non-Continuum Flow', A.I.A.A. paper 69-711

Hamel, B. B. and A. L. Cooper (1969): 'A First Collision Theory of the Hyperthermal Leading Edge Problem', Rarefied Gas Dynamics, 6th. Symposium (ed. Trilling & Wachman), part I, p. 443, Academic Press

Harvey, J. K., R. W. Jeffery and D. C. Uppington (1971): 'The Imperial College Graphite Heated Hypersonic Wind Tunnel', British A.R.C., R. & M. 3701

Haslam-Jones, T. F. (1978): 'Measurements of the Drag of Slender Cones in Hypersonic Flow at Low Reynolds Numbers Using a Magnetic Suspension and Balance', Dept. of Eng. Sci., Univ. of Oxford, Rep. No. 1235/78

Haviland, J. K. (1963): 'Determination of Shock-Wave Thickness by the Monte Carlo Method', Rarefied Gas Dynamics (ed. Laurmann), 3rd. Symposium, Part I, p. 274, Academic Press

Herzfeld K. F. and T. A. Litovitz (1959): 'Absorption and dispersion of Ultrasonic Waves', Academic Press

Hickman, R. S. (1967): 'An Experimental Study of a Hypersonic Rarefied Flow over a 10° Cone', Rarefied Gas Dynamics, 5th. Symposium (ed. Brundin), Part II, p. 1067, Academic Press

Hirschfelder, J. O., C. F. Curtiss and R. B. Bird (1954): 'Molecular Theory of Gases and Liquids', (2nd. edn. 1965), Wiley

Huang, K. (1963): 'Statistical Mechanics', Wiley

Hui, W. H. (1975): 'Simple Formulae for Supersonic Flow Past a Cone', Aeronautical Quarterly, 26, p. 11

Itikawa, Y. and K. K. Yoshikawa (1975): 'Monte-Carlo Calculations of Diatomic Molecule Gas Flows', NASA, Ames Research Centre, TND, 8100

Jeffery, R. W. (1975): 'The Aerodynamics of Wings in Low-Density Hypersonic Flow', Dept. of Aero., Imperial College, Ph. D. thesis

Keel, A. G., L. G. Kraige, R. D. Passmore and R. N. Zapata (1971): 'Hypersonic Low Density Cone Drag', A.I.A.A. paper 71-133

Keeler, R. N., M. Van Theil and B. J. Alder (1965): 'Corresponding States at Small Interatomic Distances', Physica, 31, p. 1437

Krook, M. and T. T. Wu (1977): 'Exact Solution of the Boltzmann Equation', Phys. Fluids, 20, p. 1589

Krylov, V. I. (1962): 'Approximate Calculation of Integrals', Macmillian

Larsen, P. I. and C. Borgnakke (1974): 'Statistical Collision Model for Simulating Polyatomic Gas with Restricted Energy Exchange', Rarefied Gas Dynamics, 9th Symposium (ed. Becker & Fiebig), paper A7, DFVLR Press (Göttingen)

Larsen, P. I. (1976): 'Monte Carlo Simulation of a Homogeneous Dissociating Gas', Arch. Mech., 28, p. 719

Leipman H. W., R. Narasimha and M. T. Chahine (1962): 'Structure of a Plane Shock Layer', Phys. Fluids, 5, p. 1313, (for errata see 8, p. 551)

Leipman H. W. and A. Roshko (1957): 'Elements of Gasdynamics', Wiley

Lengrand, J-C, and M. Raffin and J. Allègre (1981): 'Monte Carlo Simulation Method Applied to Jet Wall Interactions under Continuum Flow Conditions', Rarefied Gas Dynamics (ed. Fisher), 12th. Symposium, Part II, p. 994, (Progress in Astronautics and Aeronautics, 74, A.I.A.A)

Lordi, J. A. and R. E. Mates (1970): 'Rotational Relaxation in Nonpolar Diatomic Gases', Phys. Fluids, 13, No. 2, P. 291

Macpherson, A. K. (1969): 'Shock Collision at a Molecular Level', J. Fluid Mech., 39, p. 849

Macpherson, A. K. (1971): 'Rotational Temperature Profiles of Shock Waves in Diatomic Gases', J. Fluid Mech., 49, Part 2, p. 337

Macrossan, M. N. (1981): 'Improvements of the Algorithms Used for Monte-Carlo Direct Simulation Computations', Dept. of Aero., Imperial College, Rep. No. 81-03

Melville, W. K. (1972): 'The Use of the Loaded Sphere Molecular Model for Computer Simulation of Diatomic Gases', J. Fluid. Mech., 51, p. 571

Merkle, C. L., H. W. Behrens and R. D. Hughes (1981): 'Application of the Monte Carlo Simulation Procedure in the Near Continuum Regime', Rarefied Gas Dynamics (ed. Fisher), 12th. Symposium, Part I, p. 256, (Progress in Astronautics and Aeronautics, 74, A.I.A.A)

Metcalf, S. C., G. T. Coleman and C. J. Berry (1974): 'Heat Transfer to Bluff Faced and Hemispherical Faced Cylinders between Continuum and Free Molecular Limits', Rarefied Gas Dynamics, 9th Symposium (ed. Becker & Fiebig), paper D16, DFVLR Press (Gottingen)

Monchick, L. and E. A. Mason (1961): 'Transport Properties of Polar Gases', J. Chem. Phys., 35, No. 5, p. 1676

Morse, P. M. (1929): 'Diatomic Molecules According to the Wave Mechanics II. Vibrational Levels', Phys. Rev., 34, p. 51

Mott-Smith, H. M. (1951): 'The Solution of the Boltzmann Equation for a Strong Shock Wave', Phys. Rev., 82, p. 885.

Muckenfuss, C. (1962): 'Some Aspects of Shock Structure According to the Bimodal Model', Phys. Fluids, 5, p. 1325

Nanbu, K. (1980a): 'Direct Simulation Scheme Derived from the Boltzmann Equation. I. Monocomponent Gases', J. Phys. Soc. Japan, 49, p. 2042

Nanbu, K. (1980b): 'Direct Simulation Scheme Derived from the Boltzmann Equation. II. Multicomponent Gas Mixtures', J. Phys. Soc. Japan, 49, p. 2050

Nanbu, K. (1980c): 'Direct Simulation Scheme Derived from the Boltzmann Equation. III. Rough Sphere Gases', J. Phys. Soc. Japan, 49, p. 2055

Nanbu, K. (1981a): 'Direct Simulation Scheme Derived from the Boltzmann Equation. IV. Correlation of Velocity', J. Phys. Soc. Japan, 50, p. 2829

Nanbu, K. (1981b): 'Slowing Down of Energetic Molecules in a Spatially Uniform Gas', Rep. Inst. High Speed Mech., Tohoku Univ., Japan, 43, Rep. No. 335

Nanbu, K. (1982a): 'Direct Simulation Scheme Derived from the Boltzmann Equation. V. Effects of Sample Size, Number of Molecules, Step Size, and Cut-Off Angle upon Simulation Data', Rep. Inst. High Speed Mech., Tohoku Univ., Japan, 45, Rep. No. 348

Nanbu, K. (1982b): 'Direct Simulation Scheme Derived from the Boltzmann Equation. VI. Velocity Correlation in a Model Cell', J. Phys. Soc. Japan, 51, p. 59

Nanbu, K. (1982c): 'Direct Simulation Scheme Derived from the Boltzmann Equation. VIII. Velocity Correlation Relevant to Boundary Conditions', J. Phys. Soc. Japan, 51, p. 1763

Nanbu, K. (1982d): 'Applicability of the Random Walk Model to Free Molecular Motion in the Direct Simulation Method', Rep. Inst. High Speed Mech., Tohoku Univ., Japan, 45, Rep. No. 350

Nanbu, K. and Y. Watanabe (1981): 'Relaxation Rates of Inverse-Power and Rigid-Sphere Molecules', Rep. Inst. High Speed Mech., Tohoku Univ., Japan, 43, Rep. No. 334

Neyland, C. (1967): 'Rotational Relaxation of Homonuclear Diatomic Molecules', J. Chem. Phys., 46, p. 63

Nordsieck, A. and B. L. Hicks (1967): 'Monte Carlo Evaluation of the Boltzmann Collision Integral', Rarefied Gas Dynamics, 5th. Symposium (ed. Brundin), Part I, p. 695, Academic Press

Parker, J. G. (1959): 'Rotational and Vibrational Relaxation in Diatomic Gases', Phys. Fluids, 2, p. 449

Pearson, W. E. and C. F. Hansen (1974): 'Collision Induced Rotational Transition Probabilities', Rarefied Gas Dynamics, 8th Symposium (ed. Karamcheti), p. 167, Academic Press

Potter, J. L. (1967): 'The Transitional Rarefied-Flow Regime', Rarefied Gas Dynamics, 5th. Symposium (ed. Brundin), Part II, p. 881, Academic Press

Pullin, D. I. (1974): 'Rarefied Leading Edge Flow of a Diatomic Gas', Dept. of Aero., Imperial College, Ph.D. Thesis

Pullin, D. I. (1975): 'Model Kinetic Equations for Structureless Polyatomic Molecules with Phenomenological Energy Exchange', Dept. of Aero, Imperial College, Rep. No. 75-10

Pullin, D. I. (1978): 'Kinetic Models for Polyatomic Molecules with Phenomenological Energy Exchange', Phys. Fluids, 21, p. 209

Pullin, D. I. (1980): 'Direct Simulation Methods for Compressible Inviscid Ideal-Gas Flow', J. Comp. Phys., 34, p. 231

Pullin, D. I., J. Davis and J. K. Harvey (1977): 'Monte-Carlo Calculations of the Rarefied Transition Flow Past a Bluff Faced Cylinder', Rarefied Gas Dynamics, 10th Symposium (ed. Potter), part I, p. 379, (Progress in Astronautics and Aeronautics, 51, A.I.A.A)

Pullin, D. I. and J. K. Harvey (1976): 'A Numerical Simulation of the Rarefied Hypersonic Flat-Plate Problem', J. Fluid Mech., 78, p. 689

Robben, F. and L. Talbot (1966a): 'Measurements of Shock Wave Thickness by the Electron Beam Fluorescence Method', Phys. Fluids, 9, p. 633

Robben, F. and L. Talbot (1966b): 'Measurements of the Rotational Distribution Function of Nitrogen in a Shock Wave', Phys. Fluids, 9, p. 653

Schmidt, B. (1969): 'Electron Beam Density Measurements in Shock Waves', J. Fluid Mech., 39, 36

Sturtevant, B. and E. A. Steinhilper (1974): 'Intermolecular Potentials from Shock Structure Experiments', Rarefied Gas Dynamics, 8th Symposium (ed. Karamcheti), p. 159, Academic Press

Tolman, R. C. (1938): 'The principles of Statistical Mechanics', Oxford University Press

Vincenti, W. G. and C. H. Kruger (1965): 'An Introduction to Physical Gas Dynamics', Wiley, New York

Vinokur, M. (1959): 'Hypersonic Flow Around Bodies of Revolution which are Generated by Conic Sections', 6th. Midwestern Conferenec on Fluid Mechanics, University of Texas

Vinokur, M. (1962): 'Laminar Heat-Transfer Distribution on Oblate Ellipsoidal Noses in Hypersonic Flow', J. Aerosp. Sci., 29, p. 113

Watanabe, Y. and K. Nanbu (1982): 'Direct Simulation Scheme Derived from the Boltzmann Equation. VII. Ergodicity of Simulation Solutions', Rep. Inst. High Speed Mech., Tohoku Univ., 45, Rep. No. 349

Whitfield, D. L. (1973): 'Mean Free Path of Emitted Molecules and Correlation of Sphere Drag Data', A.I.A.A. Jour., 11, p. 1666

Wooley, H. W. (1956): 'Thermodynamic Properties of Gaseous Nitrogen', NACA TN 3271

Wu, T-Y and T. Ohmura (1962): 'The Quantum Theory of Scattering', Prentice-Hall

Yen, S. M., F. G. Tcheremissine (1981): 'Monte-Carlo Solutions of the Nonlinear Boltzmann Equation', Rarefied Gas Dynamics, 12th. Symposium (ed. Fisher), Part I, p. 287, (Progress in Astronautics and Aeronautics, 74, A.I.A.A)

Yen, S. M., W. P. Walters, W. Ng and J. R. Flood (1974): 'Solutions of the Non-Linear Boltzmann Equation for Shock Waves in a Maxwellian Gas', Rarefied Gas Dynamics, 8th Symposium (ed. Karamcheti), p. 137, Academic Press